Cover Page

Universiteit Leiden

The handle http://hdl.handle.net/1887/30206 holds various files of this Leiden University dissertation.

Author: Rabe, Martin
Title: Coiled-coils on lipid membranes : a new perspective on membrane fusion
Issue Date: 2014-12-18

COILED-COILS ON LIPID MEMBRANES:

A NEW PERSPECTIVE ON MEMBRANE FUSION

MARTIN RABE

Coiled-coils on lipid membranes:
A new perspective on membrane fusion

Proefschrift

ter verkrijging van
de graad van Doctor aan de Universiteit Leiden,
op gezag van Rector Magnificus prof.mr. C.J.J.M. Stolker,
volgens besluit van het College voor Promoties
te verdedigen op donderdag 18 december 2014
klokke 11.15 uur

door

Martin Rabe
geboren te Jena, Germany, 1984

Promotiecomissie:

Promoter:	Prof. dr. ir. J. G. E. M. Fraaije
Copromotor:	Dr. A. Kros
Thesis Comissie:	Prof. dr. J. Brouwer
	Dr. G. Schneider
	Prof. dr. T. J. Aartsma
	Prof. dr. A. Böker, RWTH Aachen University

ISBN: 978-83-60391-23-5

Layout and printing: Lovebird design & printing solutions

To my family

TABLE OF CONTENTS

CHAPTER I	General Introduction	**9**
CHAPTER II	Determination of Oligomeric States of Peptide Complexes Using Thermal Unfolding Curves	**23**
CHAPTER III	Interactions of Fusogenic Coiled-Coil Lipopeptides with Zwitterionic Lipid Monolayers: Implications for Lipopeptide Mediated Vesicle Fusion	**47**
CHAPTER IV	Insertion of an amphipathic coiled-coil peptide in lipid vesicles: Molecular details revealed by tryptophan fluorescence spectroscopy	**81**
CHAPTER V	The interplay between membrane interaction and homo-coiling of coiled-coil peptides on the membrane studied by temperature dependent FTIR and CD spectroscopy	**101**
CHAPTER VI	Can one methylene group make a difference? Influence of lysine snorkeling on the activity of fusogenic coiled-coil peptides	**127**
CHAPTER VII	Summary and Perspectives	**153**
	Samenvatting	**161**
	Zusammenfassung	**163**
	List of symbols	**165**
	List of abbreviations	**167**
	Curriculum Vitae	**169**
	List of publications	**170**

Chapter I

General Introduction

NATURAL AND ARTIFICIAL MEMBRANE FUSION

Membrane fusion, i.e. the merging of two initially separate lipid bilayers into one continuous bilayer is a key process in all living systems. It ranges in its versatility from fusion of enveloped viruses with cells, to fusion of vesicles with the synaptic membrane upon neurotransmitter release, and to the fusion of cells, for instance myoblasts during the formation of muscular tissue. However all these processes sha*re* the same basic procedure at the membrane level starting with the approach, followed by merging of the bilayers and finalized with opening and expansion of the fusion pore.[1] During these processes, the lipids in the bilayers have to rearrange which involves intermediate states that might be non-bilayer structures and are unfavorable as they require high local curvatures (Figure **1**A-D). Therefore, spontaneous vesicle fusion does not take place in biological systems and fusion proteins are employed to guide this process.[1-4]

One of the most studied protein complexes that plays a central role in intracellular and neuronal vesicle fusion consists of the SNARE (soluble NSF attachment protein receptor) proteins.[5] These proteins are known to dock vesicles to the target membrane by the formation of a 4-helix coiled-coil complex (Figure 1E).[6,7] However, especially in neuronal vesicle fusion the SNARE proteins are not the only proteins involved, other

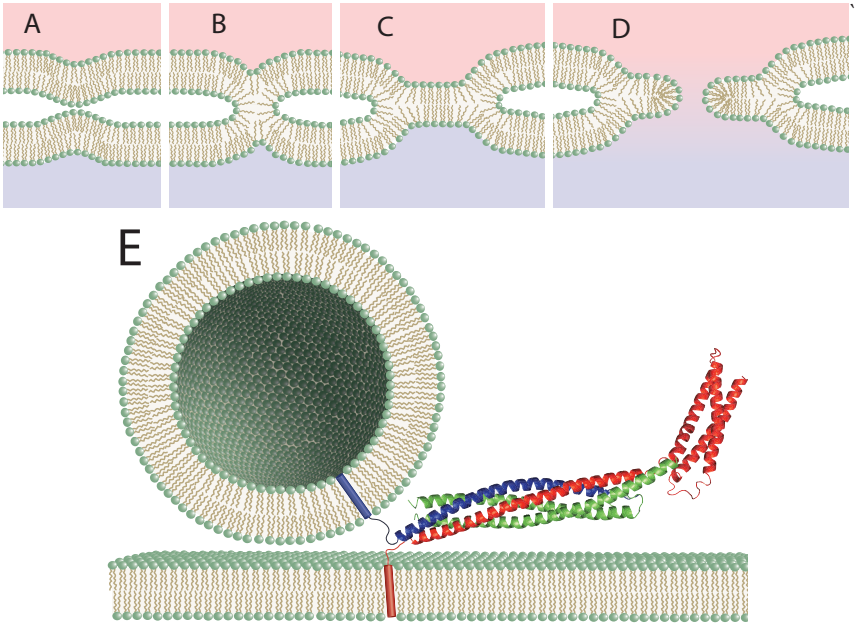

Figure 1. Intermediate states of lipid reorientation during membrane fusion: (A) point-like protrusions, (B) stalk, (C) hemifusion diaphragm, (D) fusion pore opening. (E) Illustration of the cis-SNARE complex with syntaxin (red), synaptobrevin (blue), and SNAP-25 based on X-ray structures of the SNARE complex PDB-ID: 1SFZ;[6] and N-terminal segment of syntaxin (red) PDB-ID: 1BR0.[7]

important proteins for instance SM (Sec1/Munc18-like), complexin, and the calcium sensor syntaxin assemble to a complex protein machinery that enables specific, quick Ca^{2+} triggered fusion.[8-10] Although, most of the involved proteins are known, the precise series of molecular events that results in intracellular fusion are a matter of ongoing debate.

In their important review, Chernomordik and Kozlov[1] summarized and analyzed the different tasks fusion proteins have to fulfill in order to enable full fusion of membranes. First, the membrane compartments that are supposed to fuse must be brought together; this process requires a high degree of specificity. In SNARE mediated fusion this specificity is achieved due to the fact that complementary SNARE proteins are specifically incorporated in the vesicles (v-SNAREs) or the target membrane (t-SNAREs).[5] Next, the lipid interfaces must be brought into close proximity; almost zero distance, which is hindered by strong intermembrane repulsions. Several mechanisms have been proposed for how proteins might accomplish this task. It was proposed that a force is generated and transferred to the membrane via the SNARE linker regions resulting in the membranes being pulled together.[8,9,11] This force might also create a bulge in the membrane.[12,13] Likewise bulges, point like protrusions, or fluctuations in the prefusion membranes might be caused by incorporation of synaptogagmins C2B domain and this promotes the lipid interface approximation (Figure 1A).[12-16] Subsequently, the first connection between the two membranes is obtained in the fusion stalk (Figure 1B).[17,18] In this intermediate state the monolayers are strongly bent and lipids have to tilt and splay to prevent vacuum voids. Negative spontaneous curvature promotes this intermediate, thus for DOPE the stalk was predicted to be energetically favourable, while for DOPC energy has to be expended, which might be curvature strain generated by the fusion proteins.[1] Next, the stalk extends into a hemifusion diaphragm in which the acyl chains of the distal lipid monolayers are in contact (Figure 1C). Finally, a fusion pore has to open in the hemifusion diaphragm to allow the mixing of the two initially separated aqueous compartments (Figure 1D). Chernomordik and Kozlov hypothesized that in these stages the task of fusion protein might be the generation of a pulling force that increases the diameter of the hemifusion diaphragm, as this would increase the probability of a spontaneous fusion pore opening.[1] Other models suggested the existence of complex proteinaceous fusion pores, i.e. a bridging of the intermembrane gap by protein channels.[17,19] However, these models circumvent the hemifusion diaphragm intermediate which has been observed experimentally for instance in SNARE mediated fusion.[20-22]

The hallmark of biological membrane fusion, meaning the specific content mixing between two different enclosed compartments without leakage, makes this process an interesting target for supramolecular and biomaterials chemists as it opens a route to applications in biotechnology and drug delivery. Consequently,

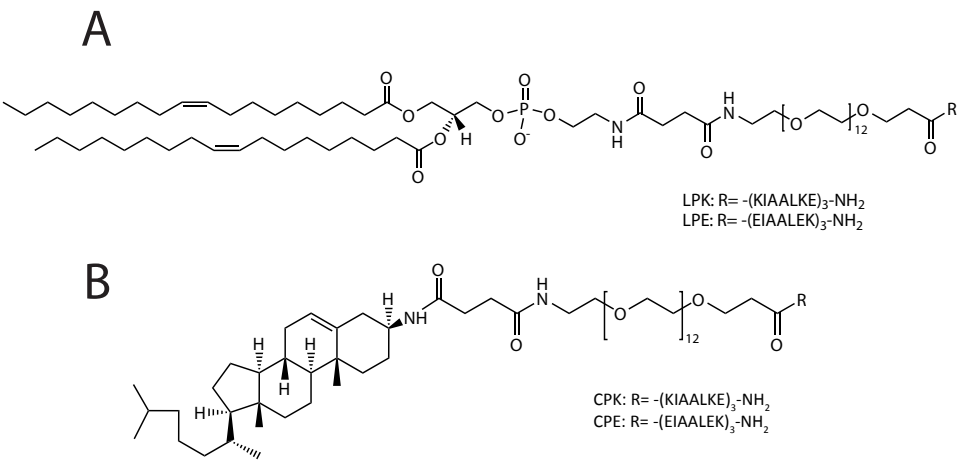

Figure 2. Chemical structures of (A) LPE and LPK, (B) CPE and CPK.

simple model systems have been designed with the aim to enable membrane fusion by means of simple, synthetic molecules.[23,24] Despite the immense efforts in this field, the creation of a targeted, and effective model system that shows lipid mixing and non-leaky content mixing remains a challenge. One system showing these properties was inspired by the SNARE proteins and designed in the Kros laboratory.[25] In the original system two heterodimeric coiled-coil forming peptides, termed E and K are covalently linked to lipid membrane anchors via a polyethyleneglycol (PEG_{12}) linker, yielding the lipopeptides LPE and LPK (Figure 2A). Incorporated into DOPC : DOPE : Cholesterol (2 : 1 : 1) vesicles of ~100 nm diameter these lipopeptides initiated efficient lipid- and content mixing, upon combination of the vesicles (Figure 3).[25,26] The E/K coiled coil formation is thought to be responsible for the specific molecular recognition and the vesicle docking. Further semi-rational improvement of the system showed that using a cholesterol anchored version of the lipopeptides CPE and CPK, permits a post modification of preformed vesicles and yields efficient membrane fusion (Figure 2B).[27] Studies on the peptide molecular recognition units of the lipopeptides revealed that the binding orientation has no influence on the fusion,[28] while an increase of the binding strength was reported to increase fusion efficiency.[29] The systems was also shown to enable the specific targeting of living cells and zebrafish skin.[30]

In light of the challenging tasks demanded from fusion proteins, the effective lipid and content mixing displayed by these systems appears astonishing. The simple docking model as proposed by Marsden et. al.[25,26] gives no answer to the question of what promotes the lipid reorientation (Figure 3), hence a further role of the lipopeptides LPE and LPK beyond molecular recognition and vesicle docking

appears reasonable. This role is to date unknown and is the central study of this thesis. It is expected that a detailed understanding of the mechanism of lipopeptide mediated membrane fusion will help to rationally improve this system.

COILED COILS

The term coiled-coil refers to several interacting peptide helices winding around each other. These structures are an abundant motif for protein oligomerization domains and can be found in proteins with different functions such as DNA transcription factors,[31,32] ion transporters,[33] viral fusion proteins,[34,35] or intracellular fusion proteins.[6] The underlying sequence motif termed the heptad repeat, consists of seven polar (*p*) or hydrophobic (*h*) amino acids in the pattern *hpphppp*. The positions in this pattern are usually denoted *abcdefg*. Hydrophobic interactions between the *a* and *d* positions of adjacent peptide chains leads to a tight knobs-into-hole packing of these side chains (Figure 4). Furthermore electrostatic interactions between the *e* and *g* positions contribute to the binding and stability of these peptide oligomers.

The amino acid sequence of coiled-coils determines their oligomeric state, orientation and stability and analysis of natural sequences has led to sets of design rules that enable the de novo design of coiled coils.[36] For instance the de novo design of specific heterodimeric coiled coil pairs based on leucine residues in the *d* position and glutamic acid and lysine residues in the *e*, *f*, and *g* positions were reported by Litowski and Hodges.[37] Amongst the studied peptides the pair with only three heptad repeats of IAAL in the *a-d* positions was found to form conformationally stable, fully helical, specific, and dimeric hetero coiled coils. The two resulting peptides $(EIAALEK)_3$ and $(KIAALKE)_3$ are denoted as peptides E and K within this thesis. Fletcher et al. reported the targeted design of a basis set of peptide oligomers with defined oligomeric states from dimer up to a tetramer, of which the trimer CC-Tri-N13 is studied, amongst others, in C*hapter II*.[38]

PEPTIDE MEMBRANE INTERACTIONS

The interactions of peptides with lipid membranes are manifold in terms of the effects in biological systems. One can for instance distinguish antimicrobial, cell penetrating, or cytolytic peptides.[39-42] The property of many of these peptides to induce leakage or lysis of lipid membranes has been explained with different models including the carpet-, barrel stave- or torroidal pore mechanisms.[43,44] All these mechanisms describe the disruption of the membrane integrity as the result of the concerted action of folded membrane-bound peptides. A common principal in these models is that, prior to the joint peptide action, a threshold concentration of lipid bound peptides has to be exceeded.

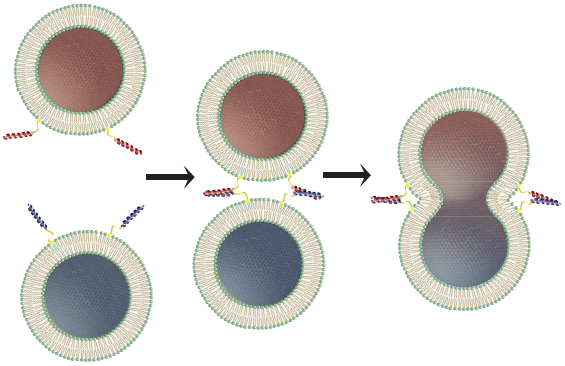

Figure 3. Model of vesicle fusion mediated by lipopeptides LPE and LPK as proposed by Marsden et. al.[25]

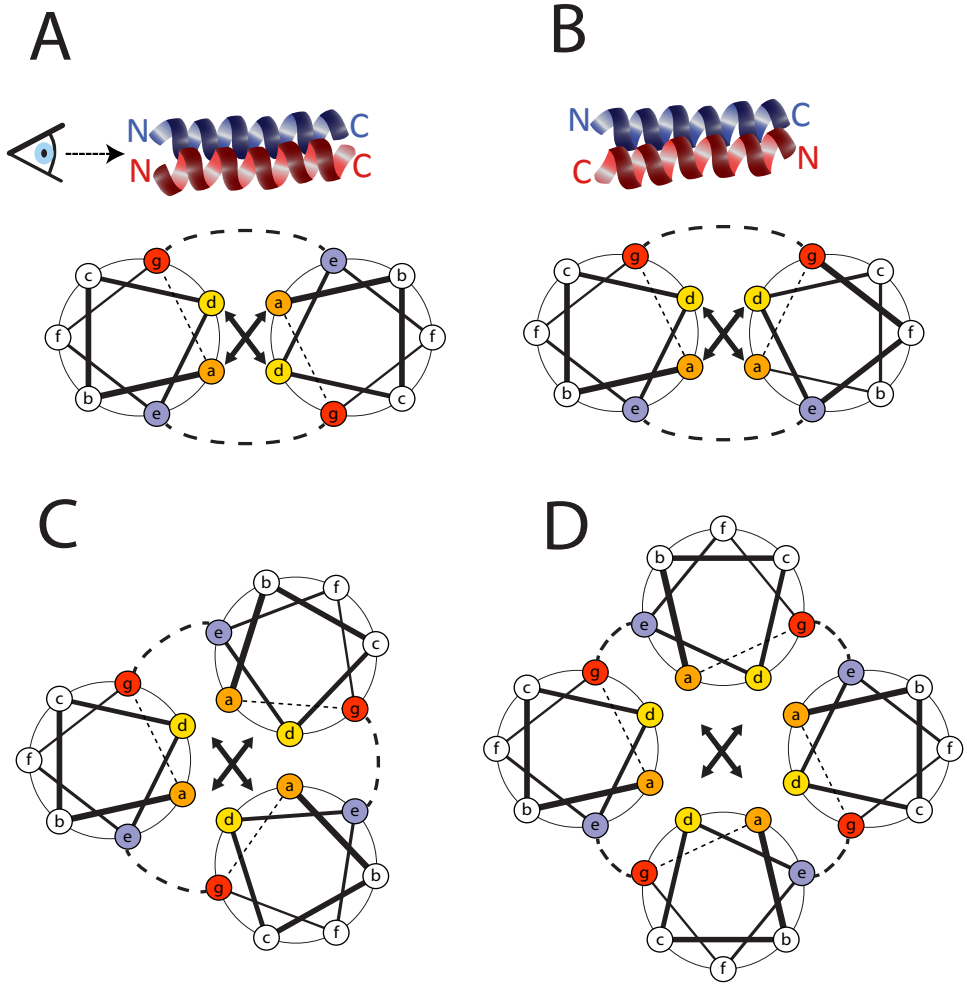

Figure 4. Positions of heptad repeat *abcdefg* projected in helicel wheels of coiled coil complexes. (A) Parallel dimer; (B) antiparallel dimer; (C) parallel trimer; and (D) parallel tetramer. Hydrophobic interactions are highlighted with arrows, salt bridges with dashed lines.

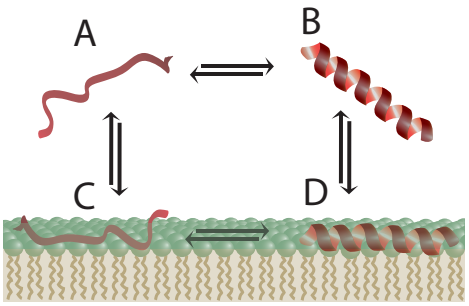

Figure 5. Illustration of equilibria in partitioning-folding coupling. Peptide are in (A) solvated, unfolded; (B) solvated, (C) folded; membrane bound, unfolded (C); and (D) membrane bound, folded states.

The initial step, the peptide binding to the membrane, is relatively well understood and depends on the specific equilibrium between hydrophobic and electrostatic interactions. Some examples of peptides exist that bind to membranes in an unordered state as in the case of strongly positively charged cell penetrating peptides[42] interacting with negatively charged lipid membranes or very short tryptophan and proline rich peptides.[45] However, a majority of peptides fold into a distinct structure upon membrane binding and unfold upon membrane unbinding, which is generally referred to as partitioning-folding coupling (Figure 5).[46-50] In this case, the membrane bound structures are amphipathic in nature, i.e. they comprise a spatial separation of hydrophobic and polar amino acid residues which are partitioned in the amphipathic membrane environment. The separation of hydrophobic and polar residues results in a hydrophobic moment in the peptide molecule.[51,52]

White and coworkers studied the thermodynamics of peptides that exhibit partitioning-folding coupling in detail.[48-50] They found that binding of unstructured peptides to membranes is usually very weak because the energetic costs for partitioning of solvated peptide bonds into the hydrophobic environment exceed the Gibbs energy gained from partitioning of the hydrophobic side chains (state C in Figure 5).[48] Compared to that, the energetic costs of partitioning a hydrogen bonded peptide bond of a folded peptide into the bilayer is drastically reduced (state D in Figure 5). Thus, the formation of hydrogen bonds between peptide bonds poses the strongest Gibbs free energy contribution to the folding process and hence drives the membrane binding of the peptide.[48-50,53]

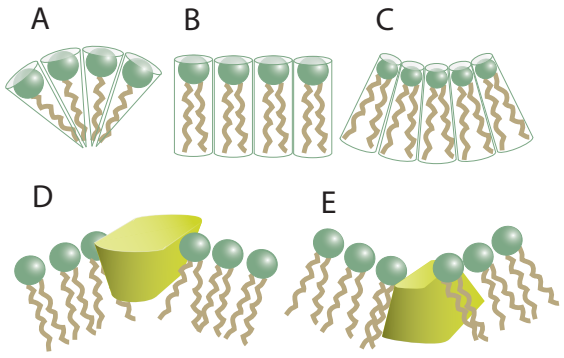

Figure 6. Illustration of spontaneous curvature of lipid interfaces. (A) Positive curvature from inverted cone shaped lipids such as lyso-PCs; (B) planar interface from cylindrically shaped lipids such as PCs; (C) negative curvature from inverted, truncated cone shaped lipids such as PEs. (D) Models of wedge like insertion into monolayers: (E) positive curvature caused by preferential insertion in headgroup region and negative curvature from preferential insertion in acyl chain region.

AMPHIPATHIC α-HELICES

One common structural motif in membrane active peptides, as well as in membrane associated proteins is the amphipathic α-helix (AH).[54-56] In these structures the regular arrangement of the hydrophobic and polar amino acids on separate faces of the helix results in a hydrophobic moment perpendicular to the helical axis. In 1990 Segrest et. al. proposed a classification of naturally occurring AHs in proteins based on the analysis of the hydrophobic moment and the distribution of the amino acids on the helical wheels of these peptides.[55] The membrane interacting AH were divided in classes A: apolipoproteins; H: polypeptide hormones; L: lytic polypeptides; and M: transmembrane helices. These peptides generally have positive charges on the polar face, but differ in the size of the hydrophobic face, the charge distribution, and the charge density. Further classes were defined for AHs that prefer protein-protein interactions, such as class G: globular proteins; K: calmodulin-regulated protein kinases; and C: coiled-coil proteins. Such a classification comes in useful for the identification of AHs in databases, their computational analysis, and the discovery of an intriguing effect, the so called 'Snorkel' mechanism in class A AHs.[46,55-58] However, the boundaries between the different classes are blurred and often a distinct helix can show hallmarks of different classes at the same time.[56] Also, recent views on membrane proteins include a more dynamic picture with different equilibria between multiple membrane associated and soluble states, which renders a too rigid classification inconvenient.[59] A new type of AH, the so called ALPS motif (ArfGAP1 lipid packing sensor) with polar but uncharged serine and threonine residues on the polar face was reported from the Antonny group.[60,61] The ALPS motifs have the remarkable property of being able to bind preferably, strongly curved membranes as found in small vesicles. Although it was already known that the interaction of AHs with membranes can create curvature strain, this sensing ability was a new perspective.

CURVATURE IN MEMBRANE INTERACTIONS

The effects that peptide interactions have on the global properties of membranes are manifold and depend also on the studied membrane system. For instance cell lysis and vesicle leakage,[62,63] pore formation in bilayer stacks,[64,65] tubulation from vesicles or supported lipid bilayers,[66,67] or stabilization of vesicles[63] have been reported. However, most often a common effect is employed to explain these observations: the induction of curvature strain that is a direct consequence of peptide insertion into the bilayer.[40,54,63-69]

By general convention, lipid interfaces curved towards the acyl chains are termed positively curved, while curving towards the headgroup is termed negative. The spontaneous curvature of a lipid interface as well as the distinctive lipid mesophase

behavior is determined by the intrinsic molecular shape of the lipids (Figure 6).[70,71] Inverted cone shaped molecules prefer positively curved interfaces and micelles, while more cylindrical ones tend to form planar bilayers, and truncated cones tend to form negatively curved interfaces (Figure 6A-C). These intrinsic parameters can influence the global and the local properties of lipid mixtures. For instance DOPC/DOPE mixtures form globally small unilamellar vesicles (SUV) upon sonication, with the more cylindrically shaped DOPC enriched in the outer leaflet and DOPE with an inverted cone shape enriched in the inner leaflet.[72] An example for a local curvature effect is the enrichment of DOPC in highly curved lipid tubules pulled from giant unilamellar vesicles (GUV) made of DOPC, brain sphingomyelin and cholesterol.[73]

Several reasons are generally considered to cause the creation of curvature strain by peptides in bilayers: hydrogen bonding, electrostatic repulsion, monolayer surface area, and lateral pressure.[40] AHs are thought to employ the two latter principles which can be understood by the concept of molecular shapes (Figure 6D-E). An incorporation of a wedge with a cone-shaped or inverted cone-shaped cross section into a monolayer results in different lateral pressures on lipid headgroup and acyl chain regions which can cause positive or negative curvature of the lipid interface.[63] A more general, but nonetheless representative, model assumes that the incorporation into one leaflet of an elastic lipid bilayer can increase the area of this monolayer, to avoid the creation of empty volumes between the two leaflets the bilayer reacts by creation of curvature.[74,75] The multiple incorporation of several wedges in a close proximity is known to create local areas of very high curvature and can for example cause membrane bulging and vesicle budding in cells.[12,13,74,75]

AIMS AND GENERAL OUTLINE OF THIS THESIS

Starting with the working hypothesis that the docking of vesicles by LPE and LPK is not sufficient to yield full membrane fusion, the work reported here aims to study the properties of the lipopeptides LPE and LPK as well as similar systems in detail, and to develop reasonable hypotheses regarding modes of action of these lipopeptides that enable fusion, and to elaborate methods to test the hypotheses. These peptides are able to form amphipathic helices, thus detailed studies of the peptide-peptide and peptide-membrane interactions in different membrane model systems are conducted for this purpose. Initially a new tool is developed to study peptide-peptide interaction by means of spectroscopic unfolding curves in *Chapter II*. The thermodynamics of folding of coiled coil complexes of any oligomeric state in aqueous environment can be investigated by this method. It will prove useful in the characterization of newly designed variants of the original peptides E and K, in the following chapters. Next, the interaction of lipopeptides LPE, LPK and the

free peptides E and K with lipid monolayers are studied in *Chapter III*. The insights and hypothesis gained from the simplified monolayer system are extended towards bilayers, in the form of vesicles and tested experimentally in *Chapter IV* and *Chapter V*. The data collected in these chapters indicate that distinctive peptide membrane interactions might promote the lipopeptide mediated fusion. To test this hypothesis a targeted inhibition of these interactions is attempted in *Chapter VI*. Based on the collected data and the conclusions a summary and perspectives for further research on this topic are given in *Chapter VII*.

REFERENCES

(1) Chernomordik, L. V.; Kozlov, M. M., Protein-lipid interplay in fusion and fission of biological membranes. *Annu. Rev. Biochem.* **2003**, *72*, 175.

(2) Söllner, T. H., Intracellular and viral membrane fusion: a uniting mechanism. *Curr. Opin. Cell Biol.* **2004**, *16*, 429.

(3) Jahn, R.; Lang, T.; Südhof, T. C., Membrane Fusion. *Cell* **2003**, *112*, 519.

(4) Martens, S.; McMahon, H. T., Mechanisms of membrane fusion: disparate players and common principles. *Nat. Rev. Mol. Cell Biol.* **2008**, *9*, 543.

(5) Weber, T.; Zemelman, B. V.; McNew, J. A.; Westermann, B.; Gmachl, M.; Parlati, F.; Söllner, T. H.; Rothman, J. E., SNAREpins: Minimal Machinery for Membrane Fusion. *Cell* **1998**, *92*, 759.

(6) Sutton, R. B.; Fasshauer, D.; Jahn, R.; Brunger, A. T., Crystal structure of a SNARE complex involved in synaptic exocytosis at 2.4[thinsp]A resolution. *Nature* **1998**, *395*, 347.

(7) Fernandez, I.; Ubach, J.; Dulubova, I.; Zhang, X.; Südhof, T. C.; Rizo, J., Three-Dimensional Structure of an Evolutionarily Conserved N-Terminal Domain of Syntaxin 1A. *Cell* **1998**, *94*, 841.

(8) Jahn, R.; Fasshauer, D., Molecular machines governing exocytosis of synaptic vesicles. *Nature* **2012**, *490*, 201.

(9) Südhof, T. C.; Rothman, J. E., Membrane fusion: grappling with SNARE and SM proteins. *Science* **2009**, *323*, 474.

(10) Südhof, T. C., The Molecular Machinery of Neurotransmitter Release (Nobel Lecture). *Angew. Chem. Int. Ed.* **2014**.

(11) Stein, A.; Weber, G.; Wahl, M. C.; Jahn, R., Helical extension of the neuronal SNARE complex into the membrane. *Nature* **2009**, *460*, 525.

(12) Kozlov, M. M.; McMahon, H. T.; Chernomordik, L. V., Protein-driven membrane stresses in fusion and fission. *Trends Biochem. Sci.* **2010**, *35*, 699.

(13) McMahon, H. T.; Kozlov, M. M.; Martens, S., Membrane Curvature in Synaptic Vesicle Fusion and Beyond. *Cell* **2010**, *140*, 601.

(14) Hui, E.; Johnson, C. P.; Yao, J.; Dunning, F. M.; Chapman, E. R., Synaptotagmin-Mediated Bending of the Target Membrane Is a Critical Step in Ca^{2+}-Regulated Fusion. *Cell* **2009**, *138*, 709.

(15) Martens, S.; Kozlov, M. M.; McMahon, H. T., How Synaptotagmin Promotes Membrane Fusion. *Science* **2007**, *316*, 1205.

(16) Wu, Z.; Schulten, K., Synaptotagmin's Role in Neurotransmitter Release Likely Involves Ca^{2+}-induced Conformational Transition. *Biophys. J.* **2014**, *107*, 1156.

(17) Chernomordik, L. V.; Kozlov, M. M., Membrane Hemifusion: Crossing a Chasm in Two Leaps. *Cell* **2005**, *123*, 375.

(18) Kozlovsky, Y.; Kozlov, M. M., Stalk Model of Membrane Fusion: Solution of Energy Crisis. *Biophys. J.* **2002**, *82*, 882.

(19) Jackson, M. B.; Chapman, E. R., The fusion pores of Ca^{2+}-triggered exocytosis. *Nat Struct Mol Biol* **2008**, *15*, 684.

(20) Reese, C.; Heise, F.; Mayer, A., Trans-SNARE pairing can precede a hemifusion intermediate in intracellular membrane fusion. *Nature* **2005**, *436*, 410.

(21) Giraudo, C. G.; Hu, C.; You, D.; Slovic, A. M.; Mosharov, E. V.; Sulzer, D.; Melia, T. J.; Rothman, J. E., SNAREs can promote complete fusion and hemifusion as alternative outcomes. *The Journal of Cell Biology* **2005**, *170*, 249.

(22) Wang, T.; Smith, E. A.; Chapman, E. R.; Weisshaar, J. C., Lipid Mixing and Content Release in Single-Vesicle, SNARE-Driven Fusion Assay with 1–5 ms Resolution. *Biophys. J.* **2009**, *96*, 4122.

(23) Marsden, H. R.; Tomatsu, I.; Kros, A., Model systems for membrane fusion. *Chem. Soc. Rev.* **2011**, *40*, 1572.

(24) Ma, M. M.; Bong, D., Controlled Fusion of Synthetic Lipid Membrane Vesicles. *Acc. Chem. Res.* **2013**, *46*, 2988.

(25) Robson Marsden, H.; Elbers, Nina A.; Bomans, Paul H. H.; Sommerdijk, Nico A. J. M.; Kros, A., A Reduced SNARE Model for Membrane Fusion. *Angew. Chem. Int. Ed.* **2009**, *48*, 2330.

(26) Robson Marsden, H.; Korobko, A. V.; Zheng, T.; Voskuhl, J.; Kros, A., Controlled liposome fusion mediated by SNARE protein mimics. *Biomaterials Science* **2013**, *1*, 1046.

(27) Versluis, F.; Voskuhl, J.; van Kolck, B.; Zope, H.; Bremmer, M.; Albregtse, T.; Kros, A., In Situ Modification of Plain Liposomes with Lipidated Coiled Coil Forming Peptides Induces Membrane Fusion. *J. Am. Chem. Soc.* **2013**, *135*, 8057.

(28) Versluis, F.; Dominguez, J.; Voskuhl, J.; Kros, A., Coiled-coil driven membrane fusion: zipper-like vs. non-zipper-like peptide orientation. *Faraday Discuss.* **2013**, *166*, 349.

(29) Zheng, T. T.; Voskuhl, J.; Versluis, F.; Zope, H. R.; Tomatsu, I.; Marsden, H. R.; Kros, A., Controlling the rate of coiled coil driven membrane fusion. *Chem. Commun.* **2013**, *49*, 3649.

(30) Zope, H. R.; Versluis, F.; Ordas, A.; Voskuhl, J.; Spaink, H. P.; Kros, A., In vitro and in vivo supramolecular modification of biomembranes using a lipidated coiled-coil motif. *Angew Chem Int Ed Engl* **2013**, *52*, 14247.

(31) Lavigne, P.; Crump, M. P.; Gagné, S. M.; Hodges, R. S.; Kay, C. M.; Sykes, B. D., Insights into the mechanism of heterodimerization from the ^{1}H-NMR solution structure of the c-Myc-Max heterodimeric leucine zipper. *J. Mol. Biol.* **1998**, *281*, 165.

(32) Glover, J. N. M.; Harrison, S. C., Crystal structure of the heterodimeric bZIP transcription factor c-Fos-c-Jun bound to DNA. *Nature* **1995**, *373*, 257.

(33) Eshaghi, S.; Niegowski, D.; Kohl, A.; Molina, D. M.; Lesley, S. A.; Nordlund, P., Crystal Structure of a Divalent Metal Ion Transporter CorA at 2.9 Angstrom Resolution. *Science* **2006**, *313*, 354.

(34) Bullough, P. A.; Hughson, F. M.; Skehel, J. J.; Wiley, D. C., Structure of influenza haemagglutinin at the pH of membrane fusion. *Nature* **1994**, *371*, 37.

(35) Chan, D. C.; Fass, D.; Berger, J. M.; Kim, P. S., Core Structure of gp41 from the HIV Envelope Glycoprotein. *Cell* **1997**, *89*, 263.

(36) Woolfson, D. N. In *Adv. Protein Chem.*; David, A. D. P., John, M. S., Eds.; Academic Press: 2005; Vol. Volume 70, p 79.

(37) Litowski, J. R.; Hodges, R. S., Designing heterodimeric two-stranded alpha-helical coiled-coils. Effects of hydrophobicity and alpha-helical propensity on protein folding, stability, and specificity. *J. Biol. Chem.* **2002**, *277*, 37272.

(38) Fletcher, J. M.; Boyle, A. L.; Bruning, M.; Bartlett, G. J.; Vincent, T. L.; Zaccai, N. R.; Armstrong, C. T.; Bromley, E. H.; Booth, P. J.; Brady, R. L.; Thomson, A. R.; Woolfson, D. N., A basis set of de novo coiled-coil peptide oligomers for rational protein design and synthetic biology. *ACS Synth Biol* **2012**, *1*, 240.

(39) Wimley, W.; Hristova, K., Antimicrobial Peptides: Successes, Challenges and Unanswered Questions. *J Membrane Biol* **2011**, *239*, 27.

(40) Koller, D.; Lohner, K., The role of spontaneous lipid curvature in the interaction of interfacially active peptides with membranes. *Biochimica et Biophysica Acta (BBA) - Biomembranes* **2014**, *1838*, 2250.

(41) Madani, F.; Lindberg, S.; Langel, U.; Futaki, S.; Graslund, A., Mechanisms of Cellular Uptake of Cell-Penetrating Peptides. *Journal of Biophysics* **2011**, *2011*.

(42) Magzoub, M.; Gräslund, A., Cell-penetrating peptides: small from inception to application. *Quarterly Reviews of Biophysics* **2004**, *37*, 147.

(43) Yeaman, M. R.; Yount, N. Y., Mechanisms of Antimicrobial Peptide Action and Resistance. *Pharmacological Reviews* **2003**, *55*, 27.

(44) Sanderson, J. M., Peptide-lipid interactions: insights and perspectives. *Organic & Biomolecular Chemistry* **2005**, *3*, 201.

(45) Ladokhin, A. S.; Selsted, M. E.; White, S. H., Bilayer Interactions of Indolicidin, a Small Antimicrobial Peptide Rich in Tryptophan, Proline, and Basic Amino Acids. *Biophys. J.* **1997**, *72*, 794.

(46) Hristova, K.; Wimley, W. C.; Mishra, V. K.; Anantharamiah, G. M.; Segrest, J. P.; White, S. H., An amphipathic α-helix at a membrane interface: a structural study using a novel X-ray diffraction method. *J. Mol. Biol.* **1999**, *290*, 99.

(47) Hristova, K.; Dempsey, C. E.; White, S. H., Structure, Location, and Lipid Perturbations of Melittin at the Membrane Interface. *Biophys. J.* **2001**, *80*, 801.

(48) Wimley, W. C.; Hristova, K.; Ladokhin, A. S.; Silvestro, L.; Axelsen, P. H.; White, S. H., Folding of β-sheet membrane proteins: a hydrophobic hexapeptide model. *J. Mol. Biol.* **1998**, *277*, 1091.

(49) Almeida, P. F.; Ladokhin, A. S.; White, S. H., Hydrogen-bond energetics drive helix formation in membrane interfaces. *Biochimica et Biophysica Acta (BBA) - Biomembranes* **2012**, *1818*, 178.

(50) Ladokhin, A. S.; White, S. H., Folding of amphipathic α-helices on membranes: energetics of helix formation by melittin. *J. Mol. Biol.* **1999**, *285*, 1363.

(51) Phoenix, D. A.; Harris, F., The hydrophobic moment and its use in the classification of amphiphilic structures (Review). *Molecular Membrane Biology* **2002**, *19*, 1.

(52) Zasloff, M., Antimicrobial peptides of multicellular organisms. *Nature* **2002**, *415*, 389.

(53) Wieprecht, T.; Apostolov, O.; Beyermann, M.; Seelig, J., Thermodynamics of the α-helix-coil transition of amphipathic peptides in a membrane environment: implications for the peptide-membrane binding equilibrium. *J. Mol. Biol.* **1999**, *294*, 785.

(54) Drin, G.; Antonny, B., Amphipathic helices and membrane curvature. *FEBS Lett.* **2010**, *584*, 1840.

(55) Segrest, J. P.; De Loof, H.; Dohlman, J. G.; Brouillette, C. G.; Anantharamaiah, G. M., Amphipathic helix motif: Classes and properties. *Proteins: Structure, Function, and Bioinformatics* **1990**, *8*, 103.

(56) Segrest, J. P.; Jones, M. K.; Mishra, V. K.; Anantharamaiah, G. M. In *Curr. Top. Membr.*; Sidney A. Simon, T. J. M., Ed.; Academic Press: 2002; Vol. Volume 52, p 397.

(57) Mishra, V. K.; Palgunachari, M. N.; Segrest, J. P.; Anantharamaiah, G. M., Interactions of synthetic peptide analogs of the class A amphipathic helix with lipids. Evidence for the snorkel hypothesis. *J. Biol. Chem.* **1994**, *269*, 7185.

(58) Segrest, J. P.; Jones, M. K.; De Loof, H.; Brouillette, C. G.; Venkatachalapathi, Y. V.; Anantharamaiah, G. M., The amphipathic helix in the exchangeable apolipoproteins: a review of secondary structure and function. *J. Lipid Res.* **1992**, *33*, 141.

(59) Bechinger, B., A dynamic view of peptides and proteins in membranes. *Cell. Mol. Life Sci.* **2008**, *65*, 3028.

(60) Bigay, J.; Casella, J. F.; Drin, G.; Mesmin, B.; Antonny, B. *ArfGAP1 responds to membrane curvature through the folding of a lipid packing sensor motif*, 2005; Vol. 24.

(61) Drin, G.; Casella, J.-F.; Gautier, R.; Boehmer, T.; Schwartz, T. U.; Antonny, B., A general amphipathic α-helical motif for sensing membrane curvature. *Nat Struct Mol Biol* **2007**, *14*, 138.

(62) Dathe, M.; Schumann, M.; Wieprecht, T.; Winkler, A.; Beyermann, M.; Krause, E.; Matsuzaki, K.; Murase, O.; Bienert, M., Peptide helicity and membrane surface charge modulate the balance of electrostatic and hydrophobic interactions with lipid bilayers and biological membranes. *Biochemistry* **1996**, *35*, 12612.

(63) Tytler, E. M.; Segrest, J. P.; Epand, R. M.; Nie, S. Q.; Epand, R. F.; Mishra, V. K.; Venkatachalapathi, Y. V.; Anantharamaiah, G. M., Reciprocal effects of apolipoprotein and lytic peptide analogs on membranes. Cross-sectional molecular shapes of amphipathic alpha helixes control membrane stability. *J. Biol. Chem.* **1993**, *268*, 22112.

(64) Matsuzaki, K.; Sugishita, K.-i.; Ishibe, N.; Ueha, M.; Nakata, S.; Miyajima, K.; Epand, R. M., Relationship of Membrane Curvature to the Formation of Pores by Magainin 2†. *Biochemistry* **1998**, *37*, 11856.

(65) Hallock, K. J.; Lee, D.-K.; Ramamoorthy, A., MSI-78, an Analogue of the Magainin Antimicrobial Peptides, Disrupts Lipid Bilayer Structure via Positive Curvature Strain. *Biophys. J.* **2003**, *84*, 3052.

(66) Arouri, A.; Kiessling, V.; Tamm, L.; Dathe, M.; Blume, A., Morphological Changes Induced by the Action of Antimicrobial Peptides on Supported Lipid Bilayers. *J. Phys. Chem. B* **2011**, *115*, 158.

(67) Varkey, J.; Isas, J. M.; Mizuno, N.; Jensen, M. B.; Bhatia, V. K.; Jao, C. C.; Petrlova, J.; Voss, J. C.; Stamou, D. G.; Steven, A. C.; Langen, R., Membrane Curvature Induction and Tubulation Are Common Features of Synucleins and Apolipoproteins. *J. Biol. Chem.* **2010**, *285*, 32486.

(68) Bechinger, B., Rationalizing the membrane interactions of cationic amphipathic antimicrobial peptides by their molecular shape. *Current Opinion in Colloid & Interface Science* **2009**, *14*, 349.

(69) Epand, R. M.; Shai, Y.; Segrest, J. P.; Anantharamiah, G. M., Mechanisms for the modulation of membrane bilayer properties by amphipathic helical peptides. *Biopolymers* **1995**, *37*, 319.

(70) Cullis, P. R.; De Kruijff, B., Lipid polymorphism and the functional roles of lipids in biological membranes. *Biochimica et Biophysica Acta (BBA) - Reviews on Biomembranes* **1979**, *559*, 399.

(71) Israelachvili, J. N.; Marčelja, S.; Horn, R. G., Physical principles of membrane organization. *Quarterly Reviews of Biophysics* **1980**, *13*, 121.

(72) Op den Kamp, J. A. F., Lipid Asymmetry in Membranes. *Annu. Rev. Biochem* **1979**, *48*, 47.

(73) Roux, A.; Cuvelier, D.; Nassoy, P.; Prost, J.; Bassereau, P.; Goud, B. *Role of curvature and phase transition in lipid sorting and fission of membrane tubules*, 2005; Vol. 24.

(74) Campelo, F.; Fabrikant, G.; McMahon, H. T.; Kozlov, M. M., Modeling membrane shaping by proteins: Focus on EHD2 and N-BAR domains. *FEBS Lett.* **2010**, *584*, 1830.

(75) Campelo, F.; McMahon, H. T.; Kozlov, M. M., The hydrophobic insertion mechanism of membrane curvature generation by proteins. *Biophys. J.* **2008**, *95*, 2325.

Chapter II

Determination of Oligomeric States of Peptide Complexes Using Thermal Unfolding Curves

ABSTRACT

In their native form peptides are often found as oligomeric complexes, meaning that they consist of more than one peptide chain. Coiled coils and helical bundles are common examples of such complexes. Their oligomeric state needs to be known precisely as this tremendously influences their biochemical and biophysical properties. The extensive analysis of circular dichroism spectroscopic data is commonly used to investigate the thermodynamics of binding and folding of these complexes. Here we present *FitDis!* an easy-to-use programme which fits the most common two-state unfolding transition to the measured thermal unfolding curves of any oligomer of any stoichiometry. Beyond this we demonstrate, with simulated and experimental examples, that the comparison of different stoichiometric models fitted to the same dataset reveals the oligomeric states of these complexes along with detailed thermodynamic information. This method will significantly ease the analysis of, and increase the amount of information gained from, the thermal unfolding curves of peptide complexes.

INTRODUCTION

A majority of natural proteins fold into oligomers meaning they are composed of multiple polypeptide chains, which has broad implications for their functionality.[1-4] One important class of oligomers is the coiled coil, a protein folding motif comprising of two or more α-helices wound around each other to form a left-handed supercoil.[5,6] These folding motifs can for instance be found in DNA regulatory proteins or ion channels maintaining the functional form of the protein.[7-12] Coiled coils play crucial roles in directing dynamic processes such as viral or neuronal membrane fusion,[14-16] and are promising targets in the *de novo* design of peptides and materials chemistry.[5,6,17-22] Coiled coils are identified by the so-called heptad repeat, a recurring sequence of seven hydrophobic (h) and polar (p) amino acids in the pattern *hpphppp*. This regular arrangement of amino acids leads to a specific packing regime and therefore specific interactions in these complexes, making them easily identifiable. The purposeful utilization of these principles has led to the ability to design synthetic complexes with defined binding affinities and predictable oligomeric states.[13,18,19,23-25] The detailed characterization of these complexes in solution and under different conditions is of substantial importance for their specific application and the detailed understanding of their role in protein function.

Commonly used techniques for the oligomeric state determination of coiled coils include analytical ultracentrifugation (AUC), x-ray crystallography, or size exclusion chromatography combined with light scattering (SEC MALS).[26,27] Naturally, each of these techniques has advantages and disadvantages, both AUC and x-ray crystallography for instance require expensive, specialized equipment, while SEC MALS is generally only suitable for macromolecules with large size differences. Needless to say, that crystal structures can provide spectacular insights into the structural details of peptides and proteins. Although the conditions under which crystallization succeeds can be very distinct from native conditions and a crystal structure does not necessarily represent the solution structure. A combination of several techniques will always be preferable in order to gain information regarding a specific complex under different conditions and to overcome the limitations of one single method.

Spectroscopic techniques, such as circular dichroism (CD), are widely used to study peptide and protein folding.[9,10,25,28-33] Samples can be analyzed over a broad peptide concentration range and conditions such as pH, salt concentration, and solvent composition can be easily varied. An extension of the analysis methods to gain structural information from spectroscopic data would be a facile, fast, and convenient strategy for researchers as it omits the necessity to purchase new equipment or to conduct time-consuming experiments.

The thermodynamics of peptide folding are often analyzed using denaturants or temperature dependent CD spectroscopy.[30-32] For the latter, typically the thermal unfolding curve of the peptide complex is fitted by a model assuming a two-state transition. For this purpose a distinct set of formulae for each possible stoichiometric model is often used.[25,31-33] In contrast, here we use a formalism that allows the unified treatment of the two-state transitions of all peptide complexes of any number of binding peptides *An* with the stoichiometric parameters v_n of the form $A1_{v1}A2_{v2}\ldots$ A freely accessible programme, called *FitDis!* was developed, which allows the easy to use application of this formalism to fit any model to the experimental or simulated data. We show that the study of thermal unfolding curves at different concentrations can yield datasets that allow the determination of the oligomeric state additional to the determination of the thermodynamic binding parameters. The general applicability of this approach is tested by means of simulated data sets. Finally, real coiled-coil peptide complexes are employed to prove the practical relevance of the method.

THEORETICAL BACKGROUND

The unfolding of most oligomeric proteins and peptides proceeds via a two-state transition.[3,4,34] Similar to a formalism described by Marky and Breslauer,[35,36] this process can be described using the equilibrium constants of folding K_F, or unfolding K_U, by the general chemical equilibrium between folded oligomers and unfolded monomers (Figure 1, eq. (1)):

$$A1_{v_1}A2_{v_2}\ldots \overset{K_{U/F}}{\longleftrightarrow} v_1A1 + v_2A2 + \ldots \tag{1}$$

This generalized treatment covers homo- and hetero-oligomers of any oligomeric number n ($n = \Sigma\, v_i$). The thermal unfolding of these molecules can be described with the Gibbs-Helmholtz equation:

$$\Delta G = \Delta H° + \Delta C_P(T - T°) - T\left(\frac{\Delta H°}{T°} + \Delta C_P \ln\left(\frac{T}{T°}\right)\right) \tag{2}$$

The parameters ΔC_P is the change in heat capacity upon unfolding, $\Delta H°$ and T° are the enthalpy and the temperature where $\Delta G = 0$ and $K_U = K_F = 1$ (Supplementary Note 1).[4,31,36,37] Once the correct model parameters v_i are known, the unfolded fraction β can be calculated at every temperature by solving equation (3):

$$a\beta^n + \beta - 1 = 0 \tag{3}$$

The parameter a depends on the complex concentration P_T, the folding constant K_F and the model parameters (Supplementary Note 1). In case of α-helical peptides,

the unfolded fraction β or the folded fraction α ($\alpha = 1 - \beta$) is accessible via the measurable mean residual ellipticity at 222 nm $[\theta]_{222nm}$:[31,32]

$$\alpha = \frac{[\theta]_{222nm} - \theta_U}{\theta_F - \theta_U} \tag{4}$$

Where θ_F and θ_u stand for the mean residue elliticity at 222 nm of the fully folded and fully unfolded state, respectively. These are thought to depend, in a linear fashion, on the temperature T, which is described by the baseline parameters θ_{F0}, $m_{F,}$ θ_{u0}, and m_U:

$$\theta_{F/U} = \theta_{F0/U0} + m_{F/U}T \tag{5}$$

Analytical solutions for equation (3) can be found for $n < 5$ only. We use numerical solutions instead, which can be found for any n by the iteration algorithm *zeroin* (Matlab function: *fzero*).[38,39] This was implemented in a global fitting algorithm which is easily controlled by a freely accessible programme named *FitDis!* (http://sbc.lic.leidenuniv.nl/software/fitdis). *FitDis!* can be used to fit any model described by the general equation (1) to experimental, or simulated spectroscopic thermal unfolding data.

Simulated melting curves, based on equations (1) - (5) are shown in Figure 1 to for two different concentrations of a homomeric dimer ($n = v_1 = 2$) to graphically elucidate the meaning of the parameters in these equations.

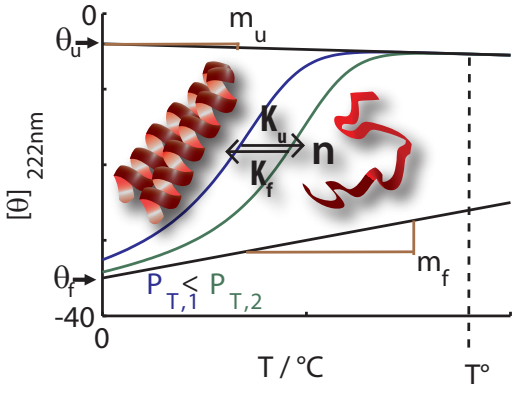

Figure 1. Graphical description of peptide complex unfolding and the parameters for formal description: Measured signal: mean molecular ellipticity at 222 nm $[\theta]_{222nm}$, equilibrium constants K_U and K_F, standard temperature T°, concentration PT, and baseline parameters θ_U, θ_F, m_U and m_F. For oligomeric complexes (n > 1) the apparent melting temperature depends on the concentration, i.e. the curve for the higher concentration ($P_{T,1}$; green line) is shifted to higher temperatures with respect to the lower concentration ($P_{T,2}$, blue line).

A consequence of equation (3) is the unique shape of a set of concentration-dependent melting curves for a distinct n. These differences enable the determination of the oligomeric state. The melting curves for different n differ in both the steepness and the distance of the concentration dependent curves (cf. Appendix, Figure A1).

Practically, thermal unfolding curves at different peptide concentrations are fitted with models of varying n and the model best describing the data yields the oligomeric number of the complex.

It should be noted that for $n = 1$, i.e. for the melting of a single folded peptide chain the thermal unfolding curves are independent of the peptide concentration and the parameter $T°$ equals the melting temperature T_m, where half of the peptide is folded ($\beta = 0.5$). This simple observation can already be practically used to differentiate a simple chain melting ($n = 1$) from an unfolding process involving multiple chains ($n > 1$). The procedure proposed here, using global fitting of thermodynamic models to concentration dependent unfolding curves, does differentiate between different n and can therefore be seen as a refinement of this facile approach.

RESULTS AND DISCUSSION

SIMULATIONS OF UNFOLDING CURVES

As a proof of principle, melting curves assuming different homomeric (GCN4-bzip[10], A_2 – A_6) and heteromeric models (A_1B_1 – A_3B_3) were simulated using equations A(1) – A(13) (cf. Appendix) with thermodynamic and baseline parameters typical for the thermal denaturation of coiled-coil complexes (cf. Appendix, Table A1 – A4).[4] Simulated concentration errors and measurement errors were added to the data, reflecting maximal errors in a state-of-the-art CD setup. In this manner 100 datasets per model were calculated and fitted, assuming different models n_{fit}, using the *FitDis!* regression algorithm. An example of one simulated dataset of the leucine zipper (GCN4-bzip) fitted with models of varying n_{fit} (2…4) is shown in Figure 2. The analysis of the residuals clearly shows the simulated data is best described by the model with the correct oligomeric number $n_{fit} = 2$, while higher values $n_{fit} = 3, 4…$ led to increasing deviations in the residuals.

The simulation and fit results of all datasets are compared when both coincide ($n_{fit} = n_{sim}$). Under this condition, the average of all fit parameters ($<\Delta H°_{fit}>$, $<T°_{fit}>$ and $<\Delta C_{P,fit}>$) coincides with the corresponding simulated values (cf. Appendix, Table A1 and Table A3), showing that the minima found by the regression are very close to the simulated values (cf. Appendix, Table A1 – Table A4). Therefore, the resulting parameters can be used for the thermodynamic description of the unfolding process.[4,31]

For the determination of the best fitting model and the oligomeric state, the lowest root mean square error of the regression (*RMSE*) is used as the criterion.[40] The *RMSE* of the regression depends on the model employed to describe the unfolding curves (Figure 3). Strikingly, the minimum of the averaged *RMSE* is always found at

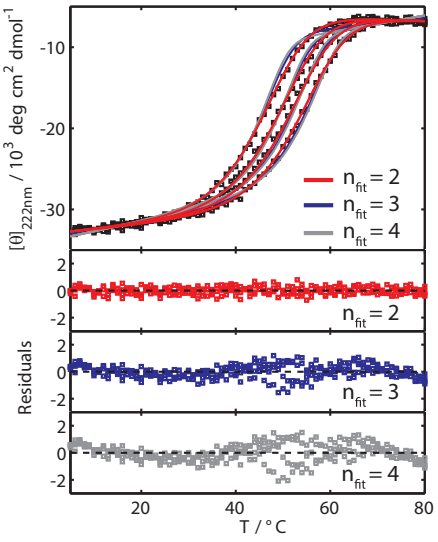

Figure 2. Simulated dataset of GCN4-bzip thermal unfolding (squares) and best fitting models (lines) with molecularities n_{sim} = 2; 3; 4. Residuals in the lower panels show the data is best described by the model with the expected oligomeric number n_{fit} = 2.

the simulated model (n_{fit} - n_{sim} = *0*), showing that the unique model-dependent curve shape can be used to identify the oligomeric state. The accuracy was calculated as the percentage of correctly identified *n*, based on the fitted model (n_{fit}) with the lowest *RMSE* (Figure 4). The accuracy in our simulations was found to be > 99% for n_{sim} < *4*. The accuracy decreases for higher *n* because there is an increasing similarity between the curves (see also Appendix, Figure A1). At higher *n* the minima in the average *RMSE* curves become shallower, which leads to an over-lapping of the confidence intervals of adjacent data points (Figure 3). The lower difference between the average *RMSE* of the correct *n* (n_{fit} - n_{sim} = *0*) and neighboring false *n* (n_{fit} - n_{sim} = *+1; -1*) indicate that the *RMSE* of a wrong model can be lower than at the correct model, which leaded to erroneous determinations of oligomeric numbers in some cases (Figure 3). However, the accuracy for *n* ≥ *4* can be increased if additional data is available. In simulations with 8 melting curves at different concentrations, the minima become sharper compared to simulations with 4 melting curves (cf. Appendix, Figure A2). The accuracy was increased to > 98% for

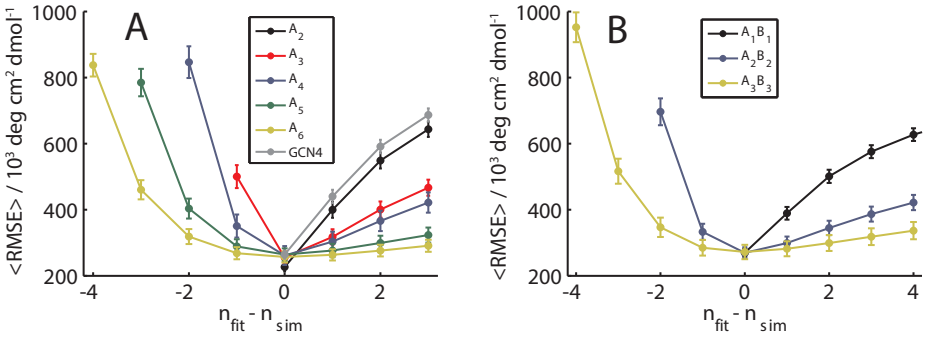

Figure 3. Average of root mean square errors (*<RMSE>*) of model fits to 100 simulated data sets of (A) homomeric peptide complexes (n_{sim} = 2…6, strong) and (B) heteromeric peptide complexes ($v_{1,sim} = v_{2,sim}$; n_{sim} = 2…6, strong) show minima for the expected molecularities $n_{fit} = n_{sim}$.

the A_4 models (cf. Appendix, Table A3). Of course, increasing the amount of data will always be a simple way to improve the outcome of a fitting routine. In practice, the number of used melting curves will depend on the signal quality and the system under study and a careful analysis of the fit results will be indispensable.

Another source of additional information to increase the accuracy can be, for heteromeric complexes, the stoichiometric ratio $v_1 : v_2$:… which is easily obtainable using Jobs method with CD spectroscopy.[41,42] For the simulated datasets with an A_2B_2 stoichiometry, the knowledge of the correct stoichiometric ratio led to an accuracy of 100% while for A_3B_3 the accuracy was significantly increased to 92-96% (cf. Appendix, Table A1). Taken together, the results of the simulations prove that the suggested approach is suited to determining the correct oligomeric state, whereas the number of datasets is an important factor to consider in the experimental planning.

PEPTIDE EXAMPLES

The behavior of real life peptide complexes can be more intricate than idealized simulations. Transitions can occur in multiple steps, or involve different oligomeric states, leading to equation (1) being non-applicable.[4,43] Naturally, the number of possible pathways increases with the oligomeric number *n*. Therefore, the relevance of equation (1) has to be determined individually for every dataset, which can be done based on the derivatives of the melting curves. For the peptide employed here, in general the first derivatives of the measured unfolding curves showed single peaks in good agreement with the derivatives of the best-fitting models (cf. Appendix, Figure A3 – Figure A7), indicative of predominantly cooperative two state unfolding.

To evaluate the proposed approach practically, several well-studied, homo- and heteromeric coiled-coil forming peptide complexes of known oligomeric state in the range *n = 2; 3; 4* were synthesized (*n = 4*: Zheng, T.; Manuscript in preparation).[13,19] Their thermal unfolding was examined using CD spectroscopy (Figure 1a, cf. Appendix, Figure A3 – Figure A7) and the analysis was performed using *FitDis!* (cf. Appendix, Table A5).

During the fitting procedures, it was necessary to determine the baseline parameters (θ_{F0}, θ_{u0}, m_F and m_U) to obtain more reliable fitting results. However, apparent slopes of the baselines of the folded states (m_F) can be caused by pre-transitions, or fraying of the ends of coiled-coil complexes, and an extrapolation of the initial slope might not be useful.[43] A consideration of such a transition in the fitting model would not be possible without additional calorimetric data. Therefore, the folded baseline parameters were initially determined from the overlapping parts of the transition curves at low temperatures and left to vary freely in the final

iteration steps. This procedure is thought to qualitatively model the influence of a possible pre-transition on the shape of the transition curve.

The thermodynamic parameters obtained by regression are in the range that is typical for short-chain, coiled-coil complexes (Table 1).[4,10] As expected, the heterodimer E_{GW}/K_{GW}, the homotrimer CC-Tri-N13, and the heterotetramer $_{WG}K/_{YG}rE$, all show relatively high folding constants K_F at 25°C (Table 1). For a coiled coil pair similar to E_{GW}/K_{GW} missing only the C-terminal glycine and tryptophan residues, Litowski and Hodges measured a K_F of ~1.4 x 10^7 M^{-1} at 20°C, which is in good agreement with the value we found which was ~ 1.8 x 10^7 M^{-1} at 25°C.[13] Positive ΔC_p values as found for all studied peptide complexes (Table 1), generally indicate that hydrophobic amino acid side chains are exposed to water upon the unfolding transition, as it is expected for a dissociation of coiled coils.[44] The increasing values for $\Delta H°$ for higher oligomeric states indicate steeper melting curves and can be expected due to the increasing number of residues in the oligomers.[4]

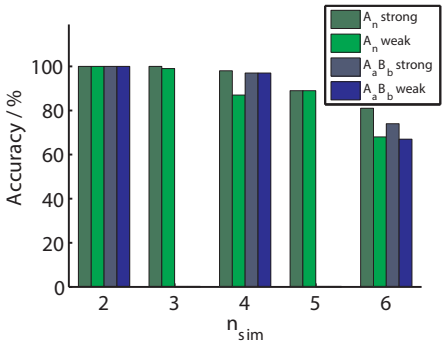

Figure 4. Results of oligomeric number determination of simulated unfolding curves. The accuracy for homomeric (A_n) and heteromeric (A_aB_b) complexes decrease with n_{sim}, but can be increased by additional data. The attributes 'weak' and 'strong' denote weaker or stronger $K_{F\ 25}$ with respect to each other. Parameters for simulation and fit results are given in Supplementary Tables 1-4.

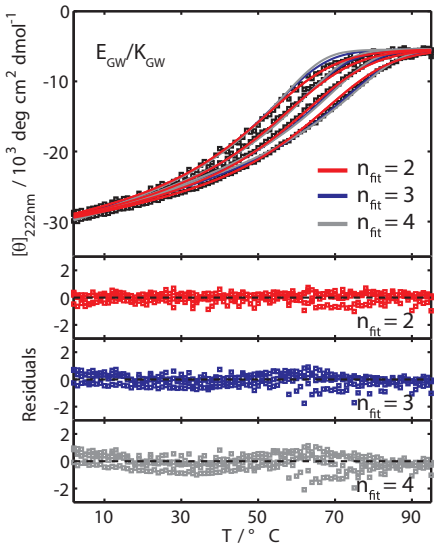

Figure 5. Thermal unfolding of hetero dimer E_{GW}/K_{GW} (squares) and best fitting models (lines) with molecularities n = 2; 3; 4. Residuals in the lower panels show the data is best described by the model with the oligomeric number n_{fit} = 2.

As an example, the measured $[\theta]_{222nm}$ for the heterodimer E_{GW}/K_{GW} and the fitted models with n_{fit} = *2; 3; 4* are shown in Figure 5. The residual analysis indicates that the best fitting model is, as expected, n_{fit} = *2*. In general the residual analysis of the fitting models of all used peptides (cf. Appendix, Figure A3 Figure A7) did not yield results that differed from the results of the *RMSE* analysis (Figure 6).

The oligomeric numbers of the heterodimer E_{GW}/K_{GW} (n = *2*) and the

Table 1. Results of peptide thermal unfolding experiments

Coiled Coil Complex	E_{GW}	K_{GW}	E_{GW} / K_{GW}	*CC-Tri-N13*	$_{WG}K$ / $_{YG}rE$
$P_{T\,min}$…$P_{T\,max}$ / µmol l^{-1} [a]	27…220	22…178	3…25	16…34	2…9
Found υ_1, υ_2, υ_3, …[b]	2	2	1, 1	3	2, 2
Δc_p / kJ mol^{-1} K^{-1}	0.29	1.46	1.06	0.64	4.95
$\Delta H°$ / kJ mol^{-1}	103.4	162.5	215.0	322.5	720.8
$T°$ / °C	83.9	91.6	143.6	138.0	164.9
K_F (25 °C)	5.31 10^2 M^{-1}	3.42 10^3 M^{-1}	1.77 10^7 M^{-1}	3.89 10^{13} M^{-2}	2.91 10^{18} M^{-3}

[a] Range of total peptide complex concentration used in experiment. [b] Stoichiometric factors of best fitting model.

homotrimer CC-Tri-N13 (n = 3) directly coincide with the minimal values in the *RMSE* plots (Figure 6A-B). Thus, for both peptide complexes the expected oligomeric state in solution was confirmed from the best fitting models with the minimal error.

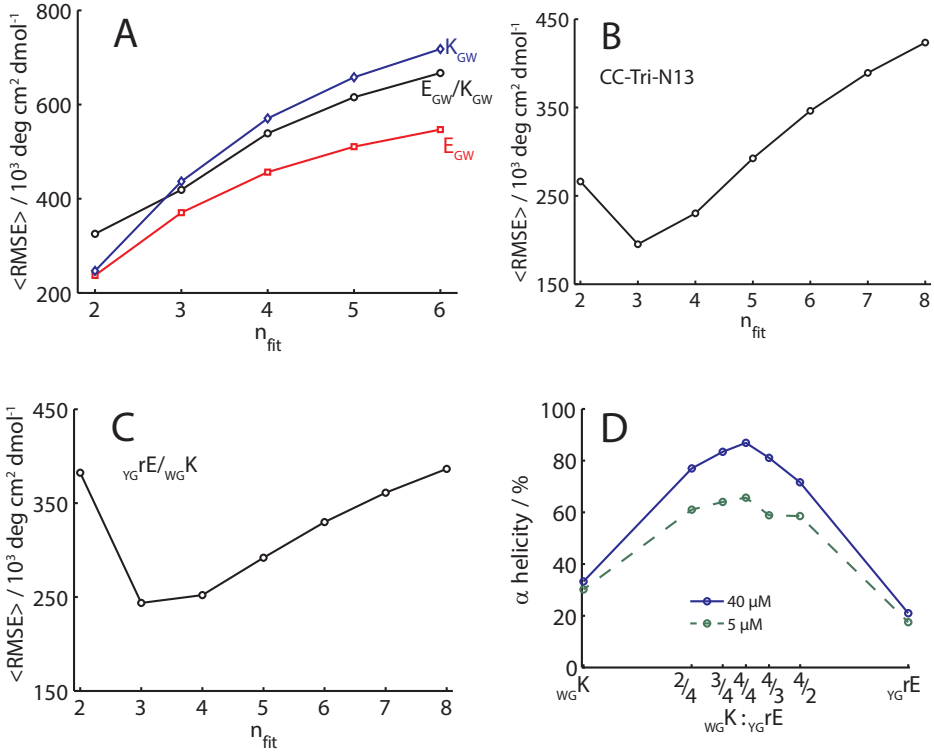

Figure 6. Root mean square errors of best fits with different models (n_{fit} = 2…8) for (A) the dimers E_{GW}/K_{GW}, E_{GW}, and K_{GW}; (B) the homo trimer CC-Tri-N13, and (C) the hetero tetramer ($\upsilon_1 = \upsilon_2 = 2$) $_{YG}rE/_{WG}K$. (D) Job plot of the tetramer $_{YG}rE/_{WG}K$ at constant total monomer concentrations 5; 40 µM confirms stoichiometric ratio υ_1:υ_2 = 1:1.

For the heterotetramer $_{WG}$K/$_{YG}$rE, the results of the residual analysis and the *RMSE* minima were less clear. As shown in the *RMSE* plot in Figure 6C, well-fitting models were obtained with both $n = 3$ ($v_1 = 1$; $v_2 = 2$) and $n = 4$ ($v_1 = v_2 = 2$) (cf. Appendix, Figure A7). A clear decision on a single oligomeric state cannot be drawn based on this data only. Possible co-existing oligomeric states during the unfolding might explain this result. To gain additional information about the state at 25°C *Jobs* method was applied.[41,42] The measurement of the dependency of α-helicity on the molar ratio of the two interacting peptide chains shown in Figure 6D yielded a stoichiometric ratio of $v_1 : v_2 = 1 : 1$. Together with the fitting results, this confirms that for $_{WG}$K/$_{YG}$rE at this temperature the predominant species is the teramer ($n = 4$), with the stoichiometry $v_1 = v_2 = 2$.

Additionally, the behavior of the isolated peptides K_{GW} and E_{GW} was studied. These showed concentration-dependent unfolding curves at relatively high concentrations (cf. Appendix, Figure A3 Figure A4), which give best-fitting results to a homomeric binding model with $n = 2$ (Figure 6A, Table 1). This indicates that, in isolation, both peptides form dimeric homocoils with relatively weak folding constants at 25 °C in the range ~10^2-10^3 M^1.

CONCLUSIONS

Here we have demonstrated a facile way to expand the information gained from thermal unfolding curves of oligomeric peptide complexes above the thermodynamics of folding to the oligomeric state. This method can be easily applied by means of *FitDis!* an easy-to-use program for the determination of thermodynamic parameters, which is available online (http://sbc.lic.leidenuniv.nl/software/fitdis). We showed, via simulations that concentration-dependent unfolding curves can be used to identify the oligomeric state of these complexes. Furthermore the results of the simulations show that depending on the data quality for higher oligomeric states, more datasets or more information is necessary for a reliable result. This is reinforced by experimental findings.

The oligomeric state of several synthesized dimeric, trimeric and tetrameric coiled-coil complexes could be determined from CD thermal unfolding curves. Despite the fact that for higher oligomeric states ($n \geq 4$) the results of the proposed approach become less explicit, the ease and the little additional effort of this method justifies its application. We therefore propose that this facile and accessible method can be used as an additional characterization tool for such oligomers, the study of which is often hampered by experimental problems or the availability of the necessary instrumentation.

MATERIALS AND METHODS

Fmoc-protected amino acids and Sieber Amide resin were purchased from Novabiochem. All other reagents and solvents were obtained at the highest purity available from Sigma-Aldrich or BioSolve Ltd. and used without further purification. Milli-Q water with a resistance more than 18.2 MQ cm^{-1} was provided by a Millipore Milli-Q filtering system.

The amino acid sequences of the peptides used in this study are:

K_{GW}: Ac-$(KIAALKE)_3$GW-NH_2; E_{GW}: Ac-$(EIAALEK)_3$GW-NH_2;[13]

CC-Tri-N13: Ac-GEIAAIKQ EIAANKK EIAAIKW EIAAIKQ GYG-NH_2;[19]

$_{WG}$K: Ac-WG$(KIAALKE)_3$-NH_2; $_{YG}$rE: Ac-YG$(KELAAIE)_3$-NH_2.[45]

PEPTIDE SYNTHESIS

Automated solid phase peptide synthesis was performed using standard protocols via the Fmoc-strategy. Purification was performed by RP-HPLC with a Gemini 5µ C18 reversed phase column. Identity of the peptides was determined by LC-MS or MALDI-MS. The purity was determined by means of analytical RP-HPLC.

CIRCULAR DICHROISM SPECTROSCOPY

Peptide stock solutions of ~1 mg / ml in phosphate buffered saline (PBS, 5 mM KH_2PO4, 15 mM K_2HPO_4, 150 mM NaCl, pH 7.4) were prepared, further diluted for the measurements and stored at 5 °C. Molar peptide concentrations were measured by UV absorbance at 280 nm using molar extinction coefficients of ε = 5500 M^1cm^{-1} per tryptophan and ε = 1490 $M^{-1}cm^{-1}$ per tyrosine residue. For Job plot solutions were prepared at constant monomer concentrations of 5 and 40 µM and varying molar ratios [$_{WG}$K] : [$_{YG}$rE]. The relative α helicity (*rh)* was calculated from $[\theta]_{222nm}$, the mean residue ellipticity at 222 nm and *N* the number of amino acids per peptide by:

$$rh = \frac{[\theta]_{222nm}}{-40\ 10^3\ \mathrm{deg\,cm^2\ dmol^{-1}}\ \left(1 - \frac{4.6}{N}\right)}\ 100\% \qquad (6)$$

The used complex concentrations P_T depended on the peptide used and were in the ranges between 2-34 µM for systems with high K_F and in the ranges 22…220 µM for the complexes with low K_F (Supplementary Table S5). CD measurements were performed on a Jasco J815 CD spectrometer equipped with a Jasco PTC 123 peltier temperature controller. The elipticity at 222 nm $[\theta]_{222}$ was measured as a criterion for α-helicity. The mean residue ellipticity $[\theta]$ was calculated from the measured ellipticity θ, the pathlength l, the molar monomer concentration c_M and the number of amino acids per peptide N by:

$$[\theta] = \frac{\theta}{l\, c_M\, N} \tag{7}$$

Samples were heated in 2 mm quartz cuvettes at a rate of 40 °C h^{-1} in the range 2 - 95 °C. CD spectra between 190 - 260 nm were collected at T = 5, 25 and 80 °C. Spectra taken at 5 °C before and directly after a full heating cycle were found to be fully reproducible for all used peptides except CC-Tri-N13, which showed reduced $[\theta]_{222nm}$. In this case total recovery of the spectrum was achieved after incubation at 5°C for > 12h.

GENERAL DATA TREATMENT

Melting curves of different peptide concentrations are interpreted by means of the formalism described in detail in the appendix. The data can be fitted to eq. A(13) by means of a graphical user interface programmed in MatLab®, called *FitDis!* (http://sbc.lic.leidenuniv.nl/software/fitdis). This application applies global, nonlinear curve fitting using a Trust-Region algorithm with the parameters $\Delta H°$, $T°$, ΔC_P, θ_F, θ_U, m_F and m_U set as global parameters. Analytical solutions for equation (3) can be found for $n < 5$ only. Instead, numerical solutions are calculated using a *zeroin* algorithm (MatLab function: *fzero*). For comparison of the fit results $\boldsymbol{\alpha}_{25}$ at 25 °C as well as $K_{F/U\,25}$ and ΔG_{25} and ΔS_{25} are calculated by equations A(1) and A(2) as well as ΔH_{25} by:

$$\Delta H_T = \Delta H° + \Delta C_P (T - T°) \tag{8}$$

SIMULATION OF UNFOLDING CURVES

For testing of the *FitDis!* fitting procedure a MatLab® script was written to simulate and subsequently fit datasets using equations A2 – A13 (Appendix) with the simulation parameters ($\Delta H°_{sim}$, $T°_{sim}$, $\Delta C_{P,\mathrm{sim}}$) and the baseline parameters ($\theta_{F0,sim}$, $\theta_{U0,sim}$, $m_{F,sim}$ and $m_{U,sim}$) shown in Table A1 – Table **A4** . Models of different n and stoichiometry A_n and $A_{\upsilon 1}B_{\upsilon 2}$ with n = 2…6 and $\upsilon_1 = \upsilon_2 = 1…3$ were used. For every model two different parameter sets denoted 'weak' and 'strong' were assumed. The attributes weak and strong thereby refer to a weaker or stronger folding (i.e. a lower folding constant) at 25 °C with respect to each other. Additionally the thermodynamic parameters of the leucine zipper (GCN4-bzip)[10] were used for simulation. For each model 100 datasets with 4 concentrations in the range $[P_{T\,min} \ldots P_{T\,max}]$ were simulated (Supplementary Table A1 Table A2). Additionally for A_4 – A_6 100 datasets with 8 concentrations were simulated (cf. Appendix, Table A3 Table A4). Normal distributed noise (standard deviation 5%) was added to the concentrations and the simulated θ to simulate measurement error.

Each simulated dataset was fitted assuming different oligomeric models from $n_{fit} = 2…n_{sim}…n_{sim} + 3$ for homomeric models ($A_{n_{sim}}$) and $n_{fit} = 2…n_{sim}…n_{sim} + 4$ for heteromeric models ($A_{v1}B_{v2}$) using the *FitDis!* global fitting algorithm. Starting values for the automated fitting procedure were $\Delta H°_{sim}=-n_{fit}$ *350 kJ/mol,* $T°=100$ °C *and* $\Delta C_{P,sim} = 0$ *kJ / (mol K)*, the starting baseline parameter were the minimal and maximal ellipticity for θ_{F0} *and* θ_{U0} respectively and $m_F = m_U = 0\ K^{-1}$. All parameters were left to vary freely during the regression. The accuracy for each model was calculated after the simulations as the ratio of correctly determined oligomeric numbers to total number of simulated datasets.

DATA INTERPRETATION

FitDis! was used to globally fit thermal denaturation curves of the peptides shown in (cf. Appendix, Table A5). The procedure started with the finding of the baseline parameters (θ_{F0}, θ_{U0}, m_F and m_U) while ignoring data values in the transition part of the curves. For the baselines of the folded states (θ_{F0}, m_F), data points from the initial overlapping parts of the transition curves were fitted. For the unfolding of isolated K_{GW} and E_{GW} no initial overlapping parts were found, due to their low K_F. Therefore the slope m_f was kept constant at 0 during all fits.

The baselines of the unfolded states (θ_{U0}, m_U) were determined from melting curves of comparable peptides in less stable states (cf. Appendix, Table A5) and kept constant while fitting with different models. These were for the heteromeric complexes (E_{GW}/K_{GW} and WGK + $_{YG}$rE) one of the binding partners (E_{GW} or $_{YG}$rE respectively) in the temperature range above 70°C. For CC-Tri-N13 θ_U and m_U were determined from unfolding curves at low monomer concentrations (Supporting Table A5). After convergence, the found solution was tested for robustness. For every dataset several stochiometric models were tested until stable solutions and convergence was reached. For peptides that were expected to be homomerics the tested models were: $v_1 = n = 2; 3; …8$. For peptides that were expected to be heteromerics the tested models were: $v_1 = v_2 = n / 2$ for even n and $v_1 = (n - 1) / 2$; $v_2 = v_1 + 1$ for odd n, with $n = 2; 3; …8$. The resulting best fits for every model can be compared by their root mean square error (RMSE) as the number of fitting parameters is equal in all models.[40,46]

REFERENCES

(1) Matthews, J.; Sunde, M. In *Protein Dimerization and Oligomerization in Biology*; Matthews, J. M., Ed.; Springer New York: 2012; Vol. 747, p 1.

(2) Goodsell, D. S.; Olson, A. J., Structural symmetry and protein function. *Annu Rev Biophys Biomol Struct* **2000**, *29*, 105.

(3) Mason, J. M.; Arndt, K. M., Coiled coil domains: stability, specificity, and biological implications. *Chembiochem* **2004**, *5*, 170.

(4) Doyle, C. M.; Rumfeldt, J. A.; Broom, H. R.; Broom, A.; Stathopulos, P. B.; Vassall, K. A.; Almey, J. J.; Meiering, E. M., Energetics of oligomeric protein folding and association. *Arch. Biochem. Biophys.* **2013**, *531*, 44.

(5) Apostolovic, B.; Danial, M.; Klok, H. A., Coiled coils: attractive protein folding motifs for the fabrication of self-assembled, responsive and bioactive materials. *Chem. Soc. Rev.* **2010**, *39*, 3541.

(6) Woolfson, D. N.; Bartlett, G. J.; Bruning, M.; Thomson, A. R., New currency for old rope: from coiled-coil assemblies to alpha-helical barrels. *Curr. Opin. Struct. Biol.* **2012**, *22*, 432.

(7) Walters, K. J.; Dayie, K. T.; Reece, R. J.; Ptashne, M.; Wagner, G., Structure and mobility of the PUT3 dimer. *Nature Structural Biology* **1997**, *4*, 744.

(8) Glover, J. N. M.; Harrison, S. C., Crystal structure of the heterodimeric bZIP transcription factor c-Fos-c-Jun bound to DNA. *Nature* **1995**, *373*, 257.

(9) Lavigne, P.; Crump, M. P.; Gagné, S. M.; Hodges, R. S.; Kay, C. M.; Sykes, B. D., Insights into the mechanism of heterodimerization from the 1H-NMR solution structure of the c-Myc-Max heterodimeric leucine zipper. *J. Mol. Biol.* **1998**, *281*, 165.

(10) Thompson, K. S.; Vinson, C. R.; Freire, E., Thermodynamic characterization of the structural stability of the coiled-coil region of the bZIP transcription factor GCN4. *Biochemistry* **1993**, *32*, 5491.

(11) Lunin, V. V.; Dobrovetsky, E.; Khutoreskaya, G.; Zhang, R.; Joachimiak, A.; Doyle, D. A.; Bochkarev, A.; Maguire, M. E.; Edwards, A. M.; Koth, C. M., Crystal structure of the CorA Mg^{2+} transporter. *Nature* **2006**, *440*, 833.

(12) Eshaghi, S.; Niegowski, D.; Kohl, A.; Molina, D. M.; Lesley, S. A.; Nordlund, P., Crystal Structure of a Divalent Metal Ion Transporter CorA at 2.9 Angstrom Resolution. *Science* **2006**, *313*, 354.

(13) Litowski, J. R.; Hodges, R. S., Designing heterodimeric two-stranded alpha-helical coiled-coils. Effects of hydrophobicity and alpha-helical propensity on protein folding, stability, and specificity. *J. Biol. Chem.* **2002**, *277*, 37272.

(14) Chan, D. C.; Fass, D.; Berger, J. M.; Kim, P. S., Core Structure of gp41 from the HIV Envelope Glycoprotein. *Cell* **1997**, *89*, 263.

(15) Bullough, P. A.; Hughson, F. M.; Skehel, J. J.; Wiley, D. C., Structure of influenza haemagglutinin at the pH of membrane fusion. *Nature* **1994**, *371*, 37.

(16) Sutton, R. B.; Fasshauer, D.; Jahn, R.; Brunger, A. T., Crystal structure of a SNARE complex involved in synaptic exocytosis at 2.4A resolution. *Nature* **1998**, *395*, 347.

(17) Gradišar, H.; Božič, S.; Doles, T.; Vengust, D.; Hafner-Bratkovič, I.; Mertelj, A.; Webb, B.; Šali, A.; Klavžar, S.; Jerala, R., Design of a single-chain polypeptide tetrahedron assembled from coiled-coil segments. *Nat Chem Biol* **2013**, *9*, 362.

(18) Zaccai, N. R.; Chi, B.; Thomson, A. R.; Boyle, A. L.; Bartlett, G. J.; Bruning, M.; Linden, N.; Sessions, R. B.; Booth, P. J.; Brady, R. L.; Woolfson, D. N., A de novo peptide hexamer with a mutable channel. *Nat Chem Biol* **2011**, *7*, 935.

(19) Fletcher, J. M.; Boyle, A. L.; Bruning, M.; Bartlett, G. J.; Vincent, T. L.; Zaccai, N. R.; Armstrong, C. T.; Bromley, E. H.; Booth, P. J.; Brady, R. L.; Thomson, A. R.; Woolfson, D. N., A basis set of de novo coiled-coil peptide oligomers for rational protein design and synthetic biology. *ACS Synth Biol* **2012**, *1*, 240.

(20) Marsden, H. R.; Korobko, A. V.; van Leeuwen, E. N. M.; Pouget, E. M.; Veen, S. J.; Sommerdijk, N. A. J. M.; Kros, A., Noncovalent Triblock Copolymers Based on a Coiled-Coil Peptide Motif. *J. Am. Chem. Soc.* **2008**, *130*, 9386.

(21) Martelli, G.; Zope, H. R.; Brovia Capell, M.; Kros, A., Coiled-coil peptide motifs as thermoresponsive valves for mesoporous silica nanoparticles. *Chem. Commun.* **2013**, *49*, 9932.

(22) Robson Marsden, H.; Elbers, Nina A.; Bomans, Paul H. H.; Sommerdijk, Nico A. J. M.; Kros, A., A Reduced SNARE Model for Membrane Fusion. *Angew. Chem. Int. Ed.* **2009**, *48*, 2330.

(23) Gonzalez, L.; Plecs, J. J.; Alber, T., An engineered allosteric switch in leucine-zipper oligomerization. *Nature Structural Biology* **1996**, *3*, 510.

(24) Woolfson, D. N. In *Adv. Protein Chem.*; David, A. D. P., John, M. S., Eds.; Academic Press: 2005; Vol. Volume 70, p 79.

(25) Boice, J. A.; Dieckmann, G. R.; DeGrado, W. F.; Fairman, R., Thermodynamic Analysis of a Designed Three-Stranded Coiled Coil. *Biochemistry* **1996**, *35*, 14480.

(26) Schuck, P. In *Protein Interactions*; Schuck, P., Ed.; Springer US: 2007; Vol. 5, p 289.

(27) Gell, D. A.; Grant, R. P.; Mackay, J. P. In *Protein Dimerization and Oligomerization in Biology*; Matthews, J. M., Ed.; Springer New York: 2012; Vol. 747, p 19.

(28) Greenfield, N. J., Analysis of the kinetics of folding of proteins and peptides using circular dichroism. *Nat Protoc* **2006**, *1*, 2891.

(29) Greenfield, N. J., Using circular dichroism spectra to estimate protein secondary structure. *Nat Protoc* **2006**, *1*, 2876.

(30) Greenfield, N. J., Determination of the folding of proteins as a function of denaturants, osmolytes or ligands using circular dichroism. *Nat Protoc* **2006**, *1*, 2733.

(31) Greenfield, N. J., Using circular dichroism collected as a function of temperature to determine the thermodynamics of protein unfolding and binding interactions. *Nat Protoc* **2006**, *1*, 2527.

(32) Greenfield, N. J. In *Methods Enzymol.*; Ludwig, B., Michael, L. J., Eds.; Academic Press: 2004; Vol. Volume 383, p 282.

(33) Johnson, C. R.; Morin, P. E.; Arrowsmith, C. H.; Freire, E., Thermodynamic analysis of the structural stability of the tetrameric oligomerization domain of p53 tumor suppressor. *Biochemistry* **1995**, *34*, 5309.

(34) Chan, H. S.; Shimizu, S.; Kaya, H. In *Methods Enzymol.*; Jo M. Holt, M. L. J., Gary, K. A., Eds.; Academic Press: 2004; Vol. Volume 380, p 350.

(35) Breslauer, K. J. In *Methods Enzymol.*; Michael L. Johnson, G. K. A., Ed.; Academic Press: 1995; Vol. Volume 259, p 221.

(36) Marky, L. A.; Breslauer, K. J., Calculating thermodynamic data for transitions of any molecularity from equilibrium melting curves. *Biopolymers* **1987**, *26*, 1601.

(37) LiCata, V. J.; Liu, C.-C. In *Methods Enzymol.*; Michael L. Johnson, J. M. H., Gary, K. A., Eds.; Academic Press: 2011; Vol. Volume 488, p 219.

(38) Brent, R. P., Algorithm with Guaranteed Convergence for Finding a Zero of a Function. *Comput J* **1971**, *14*, 422.

(39) Brent, R. P. *Algorithms for Minimization Without Derivatives*; Courier Dover Publications, 1973.

(40) Beechem, J. M. In *Methods Enzymol.*; Ludwig Brand, M. L. J., Ed.; Academic Press: 1992; Vol. Volume 210, p 37.

(41) Job, P., Recherches sur la formation de complexes mineraux en solution, et sur le stabilite. *Ann. Chim.-Paris* **1928**, *9*, 113.

(42) Gil, V. M. S.; Oliveira, N. C., On the use of the method of continuous variations. *J. Chem. Educ.* **1990**, *67*, 473.

(43) Dragan, A. I.; Privalov, P. L., Unfolding of a Leucine zipper is not a Simple Two-state Transition. *J. Mol. Biol.* **2002**, *321*, 891.

(44) Schellman, J. A., Temperature, stability, and the hydrophobic interaction. *Biophys. J.* **1997**, *73*, 2960.

(45) Zheng, T.; Manuscript in preparation.

(46) Straume, M.; Johnson, M. L. In *Methods Enzymol.*; Ludwig Brand, M. L. J., Ed.; Academic Press: 1992; Vol. Volume 210, p 87.

APPENDIX

THERMODYNAMIC FORMALISM

The dimensionless equilibrium constant of unfolding $[K_U]$ can be determined from the change of Gibbs free energy upon unfolding ΔG, the gas constant R=8.314 J / (mol K) and the absolute temperature T:

$$[K_U] = e^{\frac{-\Delta G}{RT}} \quad \text{A(1)}$$

The Gibbs-Helmholtz equation gives access to ΔG in the form:

$$\Delta G = \Delta H° + \Delta C_P(T - T°) - T\left(\frac{\Delta H°}{T°} + \Delta C_P \ln\left(\frac{T}{T°}\right)\right) \quad \text{A(2)}$$

Here $T°$ is the temperature, where the unfolding constant $[K_U] = 1$, $\Delta H°$ is the change of enthalpy upon unfolding at $T°$ and ΔC_p is the change in heat capacity upon unfolding, which is assumed to be independent of the temperature in the applied range.

The formalism described by Breslauer[35] gives the formulae necessary for a thermodynamic description of transition equilibria of polymeric oligomers of any molecularity *n*. Here this approach is extended to a formalism that also covers equilibria of any stochiometric ratio $\upsilon_1 : \upsilon_2$ ... and a form is reported that enables the numerical solution of these formulae. For a general reaction of *n* peptide chains forming an *n*-meric folded complex the unfolding and folding constants K_U and K_F can be defined by:

$$A1_{\upsilon_1}A2_{\upsilon_2} \ldots \overset{K_U/K_F}{\longleftrightarrow} \upsilon_1 A1 + \upsilon_2 A2 + \ldots \quad \text{A(3)}$$

$$K_U = \frac{1}{K_F} = \frac{[A1]^{\upsilon_1}[A2]^{\upsilon_2} \ldots}{\left[A1_{\upsilon_1}A2_{\upsilon_2} \ldots\right]} \quad \text{A(4)}$$

$$n = \sum_i \upsilon_i \quad \text{A(5)}$$

In a solution containing all chains in the molar ratios $\upsilon_1 : \upsilon_2$:... the total peptide complex concentration P_T and the concentrations and are connected to the folded fraction α or the unfolded fraction β via:

$$\alpha = 1 - \beta \quad \text{A(6)}$$

$$P_T = \left[A1_{\upsilon_1}A2_{\upsilon_2} \ldots\right]_{\alpha=1} = \frac{1}{\upsilon_i}[Ai]_{\alpha=0} \quad \text{A(7)}$$

$$\left[A1_{\upsilon_1}A2_{\upsilon_2} \ldots\right] = P_T\alpha = P_T(1 - \beta) \quad \text{A(8)}$$

$$\frac{1}{\upsilon_i}[Ai] = P_T(1 - \alpha) = P_T\beta \quad \text{A(9)}$$

Inserting equations A(8) and A(9) in equation A(4), using equations A(5) and A(6) gives:

$$K_F = \frac{\alpha}{\prod_i v_i^{v_i} P_T{}^{n-1}(1-\alpha)^n} = \frac{(1-\beta)}{\prod_i v_i^{v_i} P_T{}^{n-1}\beta^n} \quad \text{A(10)}$$

$$\prod_i v_i^{v_i} K_F P_T{}^{n-1}(1-\alpha)^n - \alpha = 0 \quad \text{A(11)}$$

$$\alpha\beta^n + \beta - 1 = 0 \quad \text{A(12)}$$

Equation A(12) has always one real solution for $0 < \beta < 1$ as the first derivative of the left side is always positive for $\alpha \geq 0$ and the left and right limiting values are -1 and α. Therefore, explicit expressions for the solutions can be found for $n \leq 4$. Furthermore numerical values for any n can be determined by the *zeroin* algorithm.[38] The solutions provide α by application of equation A(6). Equations A(3) – A(12) can also be applied to the special cases of homomeric complex formation and folding of a single chain if one interprets $0^0 = 1$.

Under the assumption that the measured signal $[\theta]$ is proportional to the folded fraction of the peptide complex (which is true for α-helical species when $[\theta]$ is measured at 222 nm) the data can be fitted by:

$$[\theta] = \alpha(\theta_F - \theta_U) + \theta_U \quad \text{A(13)}$$

Here θ_F and θ_U stand for the ellipticities of the fully folded and unfolded peptides, respectively. An additional correction for temperature-dependent linear changes in the observed ellipticity can be applied by:

$$\theta_{F/U} = \theta_{F0/U0} + m_{F/U}\tau \quad \text{A(14)}$$

The parameters θ_{F0} and θ_{U0} stand for the ellipticities at 0°C, m_F and m_U is the slope and τ is the temperature in °C.

A consequence of solving equation A(12) is that the unfolded fraction β depends on K_F by the n^{th} root. This leads to a distinct increase in steepness of the melting curves at high temperatures, upon increase in n (Figure A1). Furthermore, at constant temperature, K_F depends on concentration by the $(n - 1)^{\text{th}}$ root (equation A(12)), leading to a unique concentration dependency of a set of unfolding curves for a distinct n (Figure A1). For $n = 1$ the folding constant K_F becomes independent of the concentration, i.e. the denaturation curves at different concentrations overlap. This feature can be used to prove complex formation.

TABLES AND FIGURES

Table A1. Accuracy, simulated thermodynamic parameters and averaged fitting results of all simulated datasets for $n_{fit} = n_{sim}$ of simulations with 4 melting curves of different concentration. Hitrate under consideration of the stoichiometric ratio $\upsilon_1 : \upsilon_2$ in square brackets Values in parenthesis are the last two digits of the standard deviations of all fitted datasets.

	accuracy %	ΔH_{sim} kJ/mol	$<\Delta H_{fit}>$ kJ/mol	T_{sim} °C	$<T_{fit}>$ °C	$\Delta C_{P\,sim}$ kJ/(mol K)	$<\Delta C_{P\,fit}>$ kJ/(mol K)
GCN4	100	293	294 (14)	94,2	94,1 (14)	1,1	1,16 (34)
A_2 s	100	300	300 (11)	110,0	110,0 (11)	1,2	1,20 (28)
A_2 w	100	250	249 (6)	85,0	85,1 (9)	2,8	2,79 (14)
A_1B_1 s	100 [100]	300	302 (9)	120,0	119,6 (13)	1,5	1,51 (19)
A_1B_1 w	100 [100]	250	250 (6)	95,0	95,0 (11)	2,5	2,51 (14)
A_3 s	100	550	550 (13)	125,0	125,0 (11)	3,5	3,52 (30)
A_3 w	99	480	480 (10)	110,0	110,0 (14)	4,7	4,71 (21)
A_4 s	98	780	781 (23)	130,0	129,9 (18)	5,5	5,51 (45)
A_4 w	87	640	640 (21)	105,0	105,0 (21)	5,8	5,81 (43)
A_2B_2 s	97 [100]	800	803 (28)	130,0	129,8 (22)	5,4	5,45 (49)
A_2B_2 w	97 [100]	640	639 (22)	115,0	115,1 (24)	5,2	5,19 (42)
A_5 s	89	975	973 (39)	135,0	135,2 (25)	6,3	6,26 (69)
A_5 w	89	900	895 (31)	110,0	110,4 (23)	7,8	7,71 (62)
A_6 s	81	1200	1205 (33)	145,0	144,8 (21)	7,9	7,99 (55)
A_6 w	68	1080	1077 (35)	115,0	115,3 (24)	9,0	8,96 (67)
A_3B_3 s	74 [96]	1350	1339 (80)	135,0	135,4 (30)	7,6	7,42 (150)
A_3B_3 w	67 [92]	1150	1147 (46)	105,0	105,3 (28)	9,5	9,45 (92)

Table A2. Simulated baseline parameters, concentration range and averaged fitting results of all simulated datasets for $n_{fit} = n_{sim}$ of simulations with 4 melting curves of different concentration. Values in parenthesis are the last two digits of the standard deviations of all fitted datasets.

	$\theta_{F0,sim}$ 10^3	$<\theta_{F0,fit}>$ 10^3	$m_{F,\,sim}$ K^{-1}	$<m_{F,\,fit}>$ K^{-1}	$\theta_{U0,\,sim}$ 10^3	$<\theta_{U0,\,fit}>$ 10^3	$m_{U,\,sim}$ K^{-1}	$<m_{U,\,fit}>$ K^{-1}	$P_{T\,min}…P_{T\,max}$ µmol l^{-1}
GCN4	-33,00	-33,00 (6)	55	55 (5)	-5,10	-5,16 (55)	-20	-19 (7)	1 … 10
A_2 s	-35,00	-35,00 (6)	80	80 (3)	-4,30	-4,34 (95)	-17	-17 (11)	3,125 … 25
A_2 w	-30,00	-30,00 (23)	87	85 (18)	-4,30	-4,28 (22)	-20	-20 (3)	6,25 … 50
A_1B_1 s	-35,50	-35,52 (5)	110	111 (3)	-5,30	-5,75 (111)	-20	-15 (12)	3,125 … 25
A_1B_1 w	-33,00	-33,01 (28)	85	85 (19)	-4,80	-4,81 (36)	-15	-15 (5)	12,5 … 100
A_3 s	-36,00	-36,00 (5)	85	85 (3)	-4,80	-4,78 (101)	-15	-15 (11)	2,5 … 20
A_3 w	-36,00	-36,00 (21)	85	85 (11)	-4,80	-4,82 (52)	-15	-15 (7)	5 … 40
A_4 s	-34,00	-34,01 (7)	20	21 (4)	-4,60	-4,71 (69)	-15	-14 (8)	1,875 … 15
A_4 w	-33,00	-33,02 (31)	85	85 (18)	-4,60	-4,58 (19)	-20	-20 (3)	3,75 … 30
A_2B_2 s	-34,00	-34,01 (8)	75	75 (4)	-5,10	-5,12 (51)	-20	-20 (6)	1,875 … 15
A_2B_2 w	-34,00	-33,99 (27)	50	50 (14)	-4,60	-4,60 (29)	-22	-22 (4)	7,5 … 60
A_5 s	-32,00	-32,00 (7)	86	86 (4)	-4,80	-4,83 (47)	-15	-15 (5)	1,25 … 10
A_5 w	-33,00	-32,97 (22)	95	94 (12)	-4,80	-4,82 (15)	-10	-10 (2)	2,5 … 20
A_6 s	-31,00	-31,01 (7)	80	80 (3)	-4,85	-4,90 (61)	-20	-19 (7)	1,25 ⋯ 10
A_6 w	-32,00	-32,00 (19)	85	84 (10)	-4,80	-4,80 (13)	-20	-20 (2)	2,5 ⋯ 20
A_3B_3 s	-32,00	-32,00 (5)	42	42 (3)	-5,00	-5,10 (63)	-15	-14 (7)	1,25 ⋯ 10
A_3B_3 w	-30,00	-30,00 (20)	84	84 (14)	-5,00	-5,01 (9)	-21	-21 (1)	1,25 ⋯ 10

Table A3. Accuracy, simulated thermodynamic parameters and averaged fitting results of all simulated datasets for $n_{fit} = n_{sim}$ of simulations with 8 melting curves of different concentration. Values in parenthesis are the last two digits of the standard deviations of all fitted datasets.

	accuracy %	ΔH_{sim} kJ/mol	$\langle\Delta H_{fit}\rangle$ kJ/mol	T_{sim} °C	$\langle T_{fit}\rangle$ °C	$\Delta C_{P\,sim}$ kJ/(mol K)	$\langle\Delta C_{P\,fit}\rangle$ kJ/(mol K)
A_4 s	100	780	778 (15)	130,0	130,1 (11)	1,1	1,16 (34)
A_4 w	98	640	638 (13)	105,0	105,2 (13)	1,2	1,20 (28)
A_5 s	93	975	972 (23)	135,0	135,2 (15)	2,8	2,79 (14)
A_5 w	95	900	899 (20)	110,0	110,1 (14)	1,5	1,51 (19)
A_6 s	87	1200	1194 (29)	145,0	145,3 (17)	2,5	2,51 (14)
A_6 w	79	1080	1076 (24)	115,0	115,3 (16)	3,5	3,52 (30)

Table A4. Simulated baseline parameters and averaged fitting results of all simulated datasets for $n_{fit} = n_{sim}$ of simulations with 8 melting curves of different concentration. Values in parenthesis are the last two digits of the standard deviations of 100 fitted datasets.

	$\theta_{F0,sim}$ 10^3	$\langle\theta_{F0,fit}\rangle$ 10^3	$m_{F,\,sim}$ K^{-1}	$\langle m_{F,\,fit}\rangle$ K^{-1}	$\theta_{U0,\,sim}$ 10^3	$\langle\theta_{U0,\,fit}\rangle$ 10^3	$m_{U,\,sim}$ K^{-1}	$\langle m_{U,\,fit}\rangle$ K^{-1}	$P_{T\,min}\ldots P_{T\,max}$ $\mu mol\ l^{-1}$
A_4 s	-34	-34,00 (6)	20,0	19,8 (22)	-4,6	-4,62 (29)	-20	-19 (7)	1 … 10
A_4 w	-33	-33,00 (18)	85,0	84,2 (96)	-4,6	-4,59 (14)	-17	-17 (11)	3,125 … 25
A_5 s	-32	-32,00 (4)	86,0	86,1 (26)	-4,8	-4,77 (37)	-20	-20 (3)	6,25 … 50
A_5 w	-33	-33,00 (13)	95,0	94,8 (69)	-4,8	-4,79 (9)	-20	-15 (12)	3,125 … 25
A_6 s	-31	-30,99 (5)	80,0	79,9 (20)	-4,85	-4,88 (44)	-15	-15 (5)	12,5 … 100
A_6 w	-32	-31,99 (13)	85,0	83,9 (65)	-4,8	-4,81 (8)	-15	-15 (11)	2,5 ⋯ 20

Table A5. Fit results of best fitting models to thermal unfolding curves

Coiled Coil system	E_{GW}	K_{GW}[13]	K_{GW} / E_{GW}[13]	CC-Tri-N13[19]	$_{WG}K$ / $_{YG}rE$[44]
$P_{T\,min}\ldots P_{T\,max}$ / µmol l^{-1}	27…220	22…178	3…25	16…34	2…9
Found $\upsilon_1, \upsilon_2, \upsilon_3, \ldots$	2	2	1, 1	3	2, 2
$\Delta H°$ / kJ mol^{-1}	103.4	162.5	215.0	322.5	720.8
$T°$/ °C	83.9	91.6	143.6	138.0	164.9
Δc_p /kJ mol^{-1} K^{-1}	0.29	1.46	1.06	0.64	4.95
θ_{F0} / 10^3	-22.531	-27.833	-29.940	-28.684	-32.411
m_{F0}	(0)	(0)	94.5	70.0	115.5
θ_{U0} / 10^3	-4.640	-3.868	(-5.837)[a]	(-4.765)[b]	-6.196
m_{U0}	5.06	-10.34	(4.32)[a]	(-3.04)[b]	(0.89)[c]
$K_{F\,25}$	5.31×10^2	3.42×10^3	1.77×10^7	3.89×10^{13}	2.91×10^{18}
ΔG_{25} / kJ mol^{-1}	15.6	20.2	41.4	77.6	105.4
ΔH_{25} / kJ mol^{-1}	86.1	65.0	89.7	249.8	27.6
ΔS_{25} / J $mol^{-1}K^{-1}$	237	150	162	578	-261

Values in parenthesis were fixed during all fitting procedures. Determined from thermal CD measurement of: [a] [E_{GW}] = 50 µM; T=75…95°C; [b] [CC-Tri-N13] =6.25; 12.5 µM; T=75…95°C; [c] [$_{YG}rE$] = 40 µM; T=70…95°C.

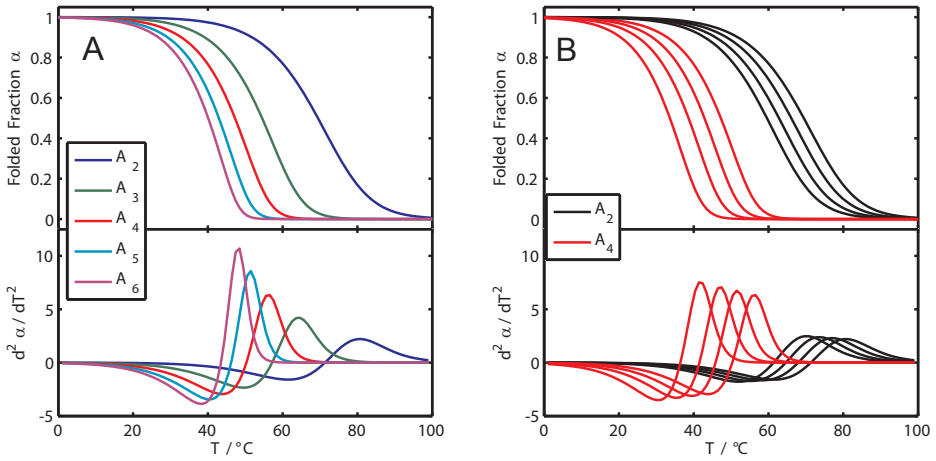

Figure A1. Simulated thermal denaturation curves and their second derivatives. (a) The shape changes with increasing oligomeric model (n = 2…6) i.e. the steepness above the inflection point increases stronger then below it. (b) The distance between concentration dependent melting curves increases with higher oligomeric model. Simulation parameters: monomer standard Enthalpy ($\Delta H° / n$) = 100 kJ / mol; ΔC_p = 0; T° = 120°C ; monomer concentration (n P_T): (a): 120 µM ; (b): 120; 60; 30; 15 µM.

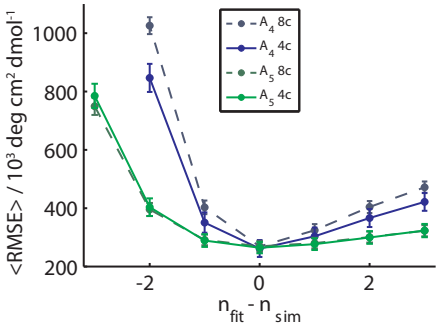

Figure A2. RMSE of fitted simulations with n = 4; 5 with 4 (4c) or 8 (8c) melting curves. For A_4 a more narrow minimum in the RMSE and a higher hitrate was obtained (Table S4).

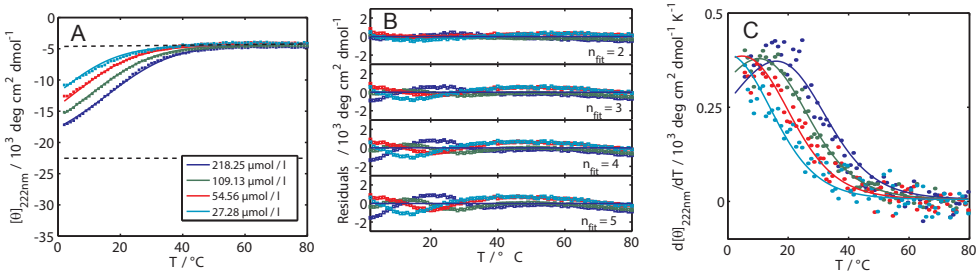

Figure A3. (a) Thermal unfolding data (squares) and best fitting model (υ_1= n = 2; straight lines) with baselines (broken lines) of E_{GW}. (b) Residuals of best fit. (c) First derivative of data (circles) and best fitting model (straight lines). Concentration of the complex (P_T) given in the key.

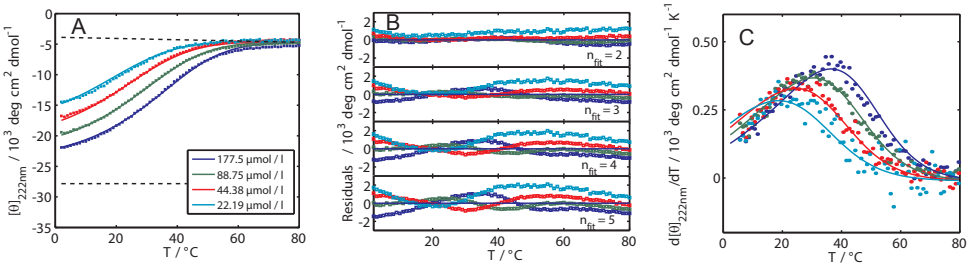

Figure A4. (a) Thermal unfolding data (squares) and best fitting model (v_1= n = 2; straight lines) with baselines (broken lines) of K_{GW}. (b) Residuals of best fit. (c) First derivative of data (circles) and best fitting model (straight lines). P_T given in the key.

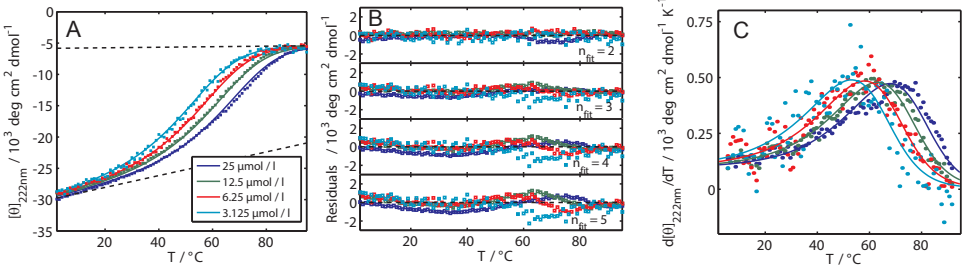

Figure A5. (a) Thermal denaturation data (squares) and best fitting model ($v_1 = v_2 = 1$; straight lines) with baselines (broken lines) of E_{GW}/K_{GW}. (b) Residuals of best fitting models with n_{fit} = 2; 3; 4; 5. (c) First derivative of data (circles) and best fitting model (straight lines). P_T given in the key.

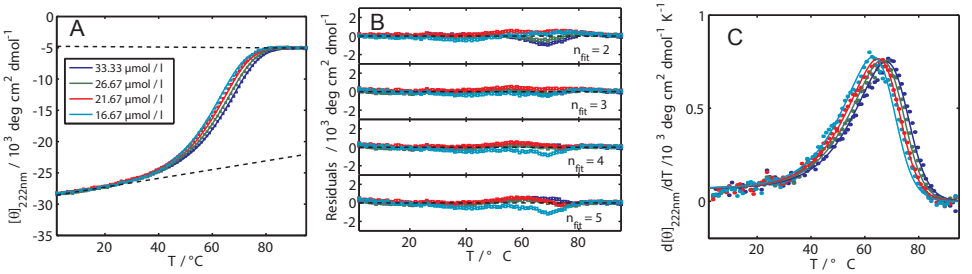

Figure A6. (a) Thermal denaturation data (squares) and best fitting model (n = v_1 = 3; straight lines) with baselines (broken lines) of CC-Tri-N13. (b) Residuals of best fit. (c) First derivative of data (circles) and best fitting model (straight lines). P_T given in the key.

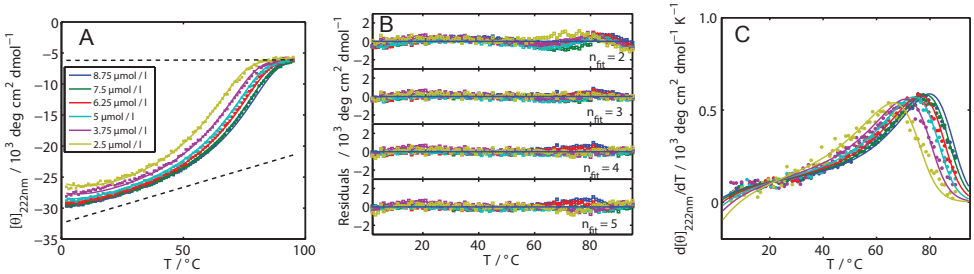

Figure A7. (a) Thermal denaturation data (squares) and best fitting model (($\upsilon_1 = \upsilon_2 = 2$; straight lines) with baselines (broken lines) of $_{WG}K/_{YG}rE$. (b) Residuals of best fit. (c) First derivative of data (circles) and best fitting model (straight lines). P_T given in the key.

Chapter III

Interactions of Fusogenic Coiled-Coil Lipopeptides with Zwitterionic Lipid Monolayers: Implications for Lipopeptide Mediated Vesicle Fusion

ABSTRACT

Fusion of lipid membranes is an important natural process for the intra- and intercellular exchange of molecules. However, little is known about the actual fusion mechanism at the molecular level. In this study we examine a system that models the key features of this process. For the molecular recognition between opposing membranes two membrane anchored heterodimer coiled-coil forming peptides called E: $(EIAALEK)_3$ and K: $(KIAALKE)_3$ were used. Lipid monolayers and IR reflection absorbtion spectroscopy (IRRAS) revealed the interactions of the peptides E, K and their parallel coiled-coil complex E/K with the phospholipid membranes and thereby mimicked the pre- and post-fusion state, respectively. The peptides adopted α-helical structures and incorporated into the monolayers with parallel orientation. The strength of binding to the monolayer differed for the peptides and tethering them to the membrane increased the interactions even further. Remarkably, these interactions played a role even in the post fusion state. These findings shed light on important mechanistic details of the membrane fusion process in this model system. Furthermore, their implications will help to improve the rational design of new artificial membrane fusion systems, which have a wide range of potential applications in supramolecular chemistry and biomedicine.

INTRODUCTION

The fusion of lipid membranes has been in the focus of research for many years. One area of particular interest has been the merging of neuronal vesicles with the plasma membrane. This process is mediated by SNARE (soluble *N*-ethylmaleimide-sensitive factor attachment protein receptor) proteins which cooperatively fold to form a stable 4 helical coiled-coil bundle.[1] Beyond that, *in vivo* membrane fusion shows a broad variety, from synaptic to viral and extracellular fusion and was found to be highly specific, controllable and efficient, which is achieved by a complex interplay of different functional proteins.[2] Apart from the creation of close proximity of the merging membranes, the generation of local curvature is thought to be a common feature in natural fusion machineries.[3] The attempt to mimic these key features of biological fusion processes has led to the development of different synthetic membrane fusion 'machineries'.[4-12]

Inspired by SNARE proteins, we developed a model system using a set of complementary synthetic lipopeptides, which have shown to efficiently trigger *in vitro* membrane fusion.[5] The specificity in these systems is based on the efficient molecular recognition between two parallel coiled–coil forming peptides[13] denoted peptide K: $(\mathbf{K}IAAL\mathbf{KE})_3$ and peptide E: $(\mathbf{E}IAAL\mathbf{EK})_3$. The conjugation of a membrane anchor via a flexible spacer to these peptides resulted in lipopeptide derivatives inserting efficiently into membrane model systems such as vesicles and supported lipid bilayers both *ex situ*[5,14-18] and *in situ*[19,20]. In a typical fusion experiment the formation of E/K complexes is thought to be the first necessary step, bringing two vesicles into close proximity, which is followed by an efficient merging of the membranes.

In recent years several successful attempts have been made to enable membrane fusion in synthetic model systems. Compared to other approaches such as DNA based[7,11] and models based on covalent[8] or hydrogen bonding[9] motifs, membrane fusion triggered by the lipopeptides LPE and LPK was found to be highly effective, specific and leakage free.[5,15] Therefore the E/K induced fusion inspired similar approaches using SNARE trans membrane domains[16] or the *in situ* coupling to the membrane prior to fusion.[20] Additionally the lipopeptide approach allows for further optimization and study by redesigning the different functionalities such as spacer length, binding properties[14,17] and membrane anchors.[19] Recent advances show this model system can even be used to target living cells and can lead to novel applications *in vivo*.[21] Furthermore, a complex influence of several factors including lipopeptide– and lipid concentration on lipopeptide induced membrane fusion was revealed, showing that the underlying mechanism of fusion is not well understood and a simple docking model is not sufficient for its description.[15]

For a more effective enhancement of the fusion specificity and efficiency of these systems, a detailed understanding of the molecular processes occurring on the lipid interface is necessary. Several aspects influencing the properties and binding behaviour of the E/K pair on the interface of model membranes should be taken into account. So far, it has been hypothesized the formation of homo coils (K/K or E/E), might occur due to relative high local peptide concentration at the membrane.[5,14,15,18,19] Another possibility, addressed here, is the direct interaction of peptides E and K with the lipid membrane which can occur due to the amphipathic nature of the coiled–coil binding motif.[22] Using CD spectroscopy it was observed that the peptides show increased α–helicity if they are tethered to the surface of lipid vesicles,[5,14,15,18,19] an observation that might be explained by either homo-coil formation or peptide-membrane interaction. Either way, this would have a direct impact on the mechanism of lipopeptide mediated fusion. Also, in comparable systems peptide clusters have been made responsible for reduced fusion efficiency.[23] This uncertainty about the actual state of the peptides when tethered to lipid membranes shows the necessity to investigate it in more detail and to implement the findings into a precise model of lipopeptide induced membrane fusion.

In the present work we study the interactions between peptides E, K and their coiled–coil complex E/K with lipid model membranes composed of DOPC : DOPE : Cholesterol (2 : 1 : 1). A lipid composition commonly used in fusion model experiments.[6] Monolayer insertion as well as monolayer compression-expansion experiments were performed using the Langmuir film balance technique and were combined with surface sensitive infrared reflection absorption spectroscopy (IRRAS). This allows us to probe the interactions of the peptides with the opposing membrane during fusion as well as the interactions of peptides with the membrane they are tethered to. The molecular structures of the compounds used in this study are shown in Chart 1.

We find that the free peptides as well as the monolayer tethered peptides interact with the monolayers and incorporate with their molecular axis parallel to the lipid interface. The experimental findings will be further discussed within the scope of their implications for lipopeptide induced membrane fusion.

RESULTS AND DISCUSSION

PEPTIDE INCORPORATION

The interactions of the monomeric peptides E and K and their complex E/K with membranes were investigated by incorporation experiments into DOPC : DOPE : Cholesterol (molar ratio 2 : 1 : 1) monolayers. Initially, injection

experiments with varying concentrations of the E/K complex were performed (Figure A1). An E/K concentration of 0.3 μM in the subphase, led to a maximum change in the surface pressure, π, which did not increase upon further addition of the peptide. This peptide concentration was therefore chosen for the further measurements. Monolayers were prepared on PBS in a trough with a constant area and the surface pressure was measured. When the initial surface pressure (π_0) was reached, a peptide solution was injected into the subphase, resulting in a surface pressure change ($\Delta\pi$) due to peptide incorporation into the monolayer. The measured $\Delta\pi$ values are plotted against π_0 for E,K, and E/K in Figure 1.

Chart 1. Amino acid sequence and chemical structures of compounds used in this study.

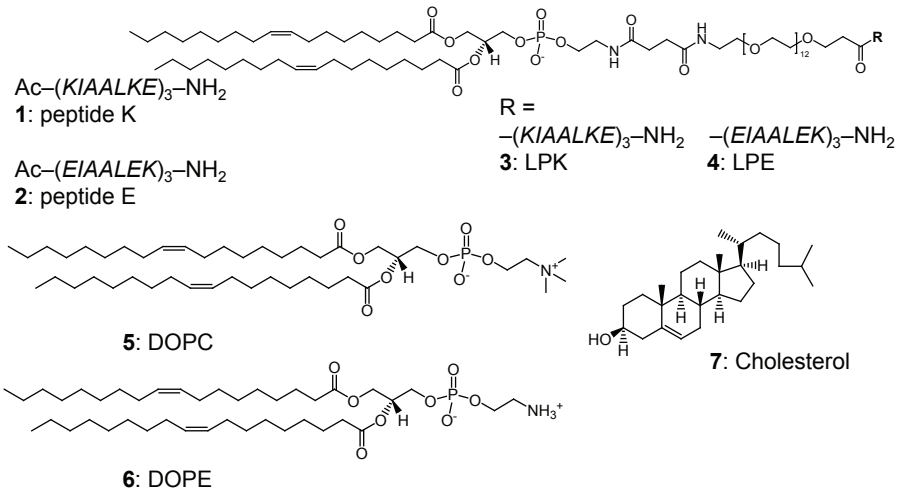

The observed peptide incorporations into the lipid monolayer were fast, reaching their maximal π values within one hour after injection. In all performed experiments, $\Delta\pi$ decreases with increasing π_0, showing a decreasing incorporation tendency of the peptides into the monolayer. The experimental data was fitted with linear functions, while the values of $\Delta\pi^0$ (at $\pi_0 = 0$), namely the surface activity of the pure peptides were excluded. Extrapolation of the resulting linear functions to $\Delta\pi = 0$ yields the maximum insertion pressure π_{mip} at the intercept, which is an indication of the peptide affinity to insert into lipid membranes.[24,25]

The low π_{mip} of ~13 mN / m for peptide E is indicative for a low binding affinity to the monolayer. Both peptide K and the coiled-coil complex E/K show a similar π_{mip} of approximately 25 mN / m. For comparison, the monolayer bilayer equilibrium pressure is 30-35 mN / m.[25-27] Therefore it can be concluded peptide E does not interact with a lipid bilayer. The higher π_{mip} values for K and E/K implicate a higher affinity to the membrane, albeit no or only weak interactions would be expected with bilayers in liposomes of the same composition.

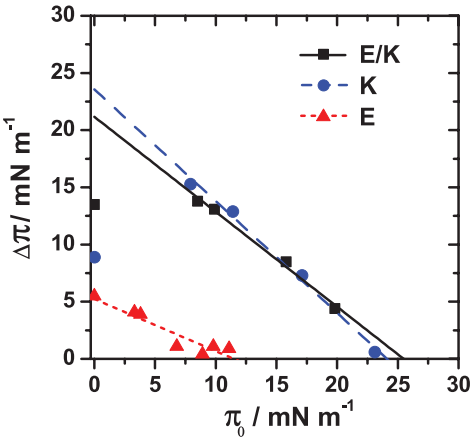

Figure 1. Change in surface pressure Δπ after injection of peptides K (blue circle), E (red triangle) and the complex E/K (black square) under spread DOPE : DOPE : Cholesterol 2 : 1 : 1 monolayers of the initial surface pressure π_0. All experiments were done in PBS with E, K and E/K concentrations in the trough of 0.3 µM. Values $\Delta\pi^0$ at π_0 = 0 mN / m are the surface activity of the peptide without lipid monolayers. Straight lines: linear fit of the data under exclusion of $\Delta\pi^0$. The interpolation of these regression curves gives the maximum insertion pressures π_{mip}: K: 24.5 mN / m; E: 12.5 mN / m; E/K: 25,9 mN / m.

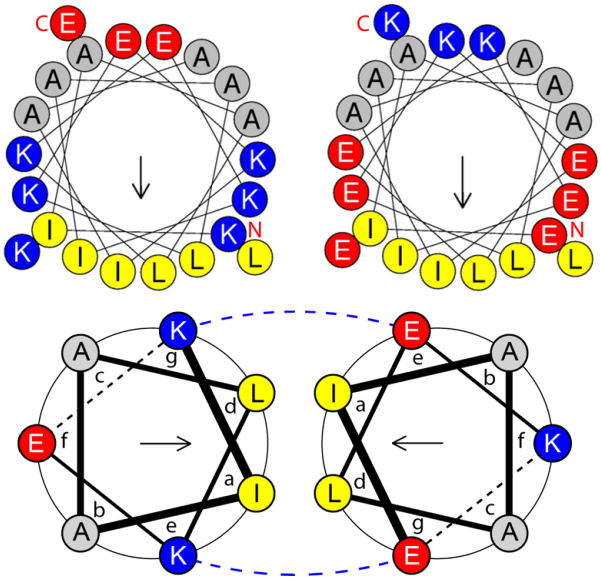

Figure 2. Helical wheel projections of K (top left) and E (top right) peptide assuming a monomeric α - Helical conformation (helical angle/AA = 100°, image prepared with 'HeliQuest 2'[36]) the arrow indicates the direction of the hydrophobic moment. Helical wheel projection assuming coiled-coil interaction (bottom, image prepared by means of 'DrawCoil 1.0'[37]), blue dashed lines indicate supporting electrostatic interactions.

The intercept of the linear regression functions with the Δπ axis can also be interpreted in terms of membrane binding affinity.[25] In the case of peptide E this value is similar to the surface activity of the pure peptide at $\Delta\pi^0$ ~5 mN / m. This shows that the observed pressure increase is the result of a competitive adsorption process to free interface spots of the hydrophobic-hydrophilic air-water interface rather than an active peptide-membrane binding interaction. Peptide K and coiled-

coil E/K, with $\Delta\pi$ intercepts of 21–23 mN / m, were significantly higher compared to their respective $\Delta\pi^0$ values (9 and 13.5 mN / m). This indicates a specific interaction between the lipid molecules and the peptides to be responsible for the increase of the monolayer surface pressure.

Figure 1 reveals the similarity of π_0 dependent peptide K and coiled coil E/K membrane incorporation, the data points overlap considerably. To interpret this result, first the secondary structure of the complex as well as of monomers binding to the monolayer has to be taken into account. A helical wheel projection of the E/K coiled-coil complex as well as a hypothetical ahelical monomeric species is given in Figure 2.[28,29] The main force leading to the coiled-coil formation is a hydrophobic knob-into-holes interaction between isoleucine and leucine moieties resulting in the formation of a hydrophobic core.[30] The distinct arrangement of the charged lysine and glutamic acid residues on the solvent-exposed side of the coiled-coils is designed to preferentially obtain a hetero complex over homo coiled-coil formation (i.e. E/E, K/K).[13] The left handed twist of 20° every two turns in coiled coils, leads to a maximal contact area between the hydrophobic residues and their shielding from the bulk solvent. A hydrophobic insertion of the E/K complex into the monolayer would therefore not be expected but electrostatic interactions of the polar surface of the E/K complex with the lipid head groups is possible.[31]

Alternatively an interaction of unbound K might cause the overlap of the $\Delta\pi$–π_0 curves for peptide K and E/K. The dissociation constant of the complex in water at 20 °C was estimated to be $7x10^{-8}$ M,[13] which means under the chosen experimental conditions ~60 % of the peptides are folded as a coiled-coil complex and unbound peptide K is in equilibrium with the E/K complex. This equilibrium might be further shifted to the side of the monomeric species due to the monolayer binding of the peptides.

The binding of peptide K to the monolayer would also involve hydrophobic interactions, because its specific peptide design leads to another unintended structural motif that can be found from the top images of Figure 2. If an α-helical structure with an average helical turn of 100° per amino acid is assumed, a prominent hydrophobic moment can be found (denoted by arrows in Figure 2). In this conformation peptide K has its positively charged lysine residues in a position perpendicular to the hydrophobic moment and its negatively charged glutamic acid residues central on the polar face. Amphiphatic helices with this charge distribution pattern were classified as amphipathic helices of class A_1.[22,32] This structural motif is often found in apolipoproteins and is known to interact with zwitterionic lipids. Lysine residues in this specific position are thought to enhance the hydrophobic interactions by a 'snorkel' mechanism.[32,33] This phenomenon manifests as a bending of the relatively long lysine side chains towards the polar-apolar

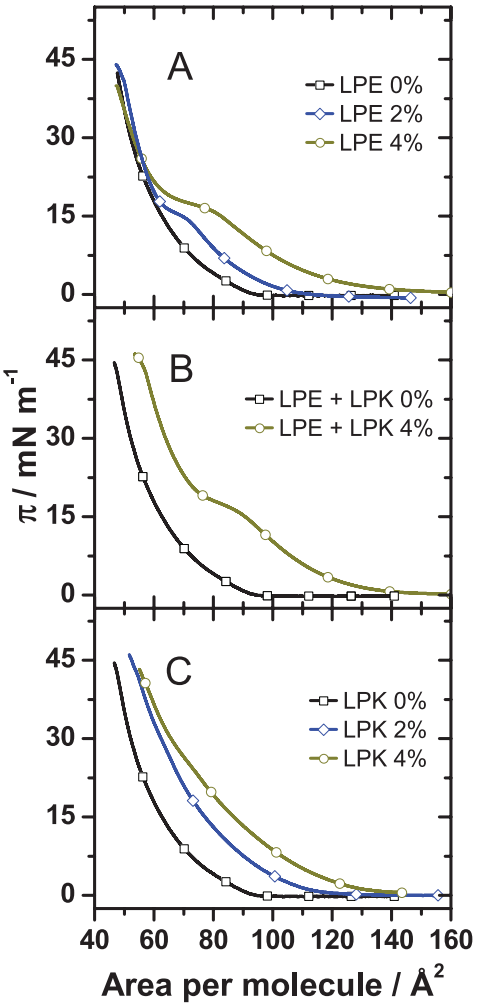

Figure 3. π-A compression isotherms of DOPE : DOPE : Cholesterol (2 : 1 : 1) monolayers containing different amounts of lipopeptides (A) LPE, (B) LPE+LPK, and (C) LPK on PBS.

interface upon membrane insertion, which enhances the apolar surface of the peptide due to an exposure of the lysine hydrocarbon chains. The charge distribution in the corresponding hypothetical α-helical peptide E is exactly the opposite of K. Such a motif is not expected to have distinct interactions with lipid membranes.[34] The results of our lipid monolayer in-sertion experiments correlate well to these expectations, which suggests an interaction of peptide K with the mono-layer might be enhanced via a snorkeling of the lysine side chains.

MONOLAYER COMPRESSION-EXPANSION

The incorporation of free peptides E, K and E/K into monolayers is only partially mimicking the situation found in vesicle fusion studies, in which these peptides are tethered to the lipids by means of a PEG spacer and a lipid anchor. In these cases the spacer groups and the close proximity of the peptides to the membrane as well as to neighboring peptides might influence the interactions of these molecules with the membrane.

In order to examine the interactions of lipid bound peptides (LPE/LPK) with the monolayers containing them, DOPE : DOPE : Cholesterol (2 : 1 : 1) monolayers containing LPE and/or LPK at concentrations in the range (0, 2, 4 mol%) as applied in typical vesicle fusion experiments were studied.[5,15] π-A compression isotherms of these systems were determined and stable monolayers up to 4045 mN / m were observed (Figure 3).

Isotherms of the pure lipid mixture showed no distinct features such as plateaus or break points, which is consistent with monolayers in a liquid expanded state without phase transitions. With lipopeptides in the monolayer, all isotherms showed higher molecular areas at low pressures (0-10 mN / m) as compared to the pure lipid

systems. Upon further compression a distinct plateau at intermediate surface pressures (1520 mN / m) is observed, when LPE is present (Figure 3A). Its size ΔA increases with increasing LPE content in the monolayers. Further compression above these plateaus (> 20 mN / m) led to isotherms comparable to those of the pure lipid film. In contrast, a compression of a 2 mol % LPK monolayer resulted in an isotherm with a shift to higher molecular areas over the entire pressure regime (Figure 3C). In case of a monolayer containing 4 mol% LPK a slight plateau at 2530 mN / m was observed.

The compression of a lipid monolayer containing LPE and LPK in equimolar amounts resulted in an isotherm combining the properties of the isotherms containing either solely LPE or solely LPK, i.e. the isotherm is shifted to higher areas in the entire recorded pressure regime and contains a plateau at 1520 mN / m.

Next the monolayers were studied by means of compressionexpansion cycles in the regions 035 mN / m. During compression-expansion cycles which lasted several hours, slight irreversible loss of monolayer material into the subphase was observed. It was found to be more pronounced in experiments using E or LPE than K or LPK and was increased with higher concentrations of peptides or lipopeptides. Therefore, the data was compared and analyzed by means of the shape of the isotherms which is reflected in their compressibility $C_S = (-1 / A) (\delta\pi / \delta A)_T$, a measure for the mechanical properties of the film. In Figure 4 the compressibilities of the second compression expansion cycles are plotted as function of the surface pressure. At low surface pressures (< 5 mN) all films show comparably high compressibilities. The peaks in the Cs – π plots are equivalent to the plateaus observed in the π-A isotherms.[35] For LPE containing monolayers (Figure 4A) the observed maxima in the compressibility are almost fully reversible upon expansion (Figure 4A). Furthermore, the area under the peaks increases with increasing lipopeptide content, which is accompanied by a slight upshift of the maximum in CS by 0.4 mN / m. The monolayers containing 2 % LPK (Figure 4B) showed no change in the compressibility compared to the pure lipid system. If the LPK content is increased to 4 mol% a slight increased compressibility at higher pressures (> 15 mN) as well as a small and broad peak in C_S was observed, both observations reoccur upon expansion.

For comparison the pure lipid films were spread on a subphase containing different concentrations of free peptides E or K (Figure 4C-D). Here, prominent maxima were found at comparable but lower pressures than the peaks found for the lipopeptides. A higher peptide concentration also led to a higher maximum and a higher area under the peak. However, the peaks in C_S did not reappear upon immediate expansion which shows a compressibility curve that appears as the pure lipid mixture (dashed lines in Figure 4C-D). Also the size of the plateaus increases with increasing peptide concentration (see SI), comparable to the lipopeptides.

We interpret the maxima in compressibilities, i.e. the observed plateaus in the π - A isotherms, to be caused by an exclusion of peptide from the monolayer into the subphase. Similar behaviour was, for instance, described for the amphiphatic helix of neuropeptide y (NPY).[36,37] In this context an increased plateau size upon higher peptide concentration stands for an increased exclusion of material from the lipid interface. An increase of peptide concentration in the trough also leads to an increase in the compressibility maximum which corresponds to a lower slope of the π - A isotherm indicating the exclusion of an increasing amount of peptide material. The π_{mip} of the free peptides found in the incorporation experiments (vertical line in Figure 4) can be compared with the maxima in the C_S – π curves. It can be seen that for the free peptides E and K, the complete area of the peaks lies below the corresponding π_{mip}.This correlates well with the interpretation that a peptide squeeze out is completed at π_{mip}.

The implications of these observations are summarized in a model shown in Figure 5. Compression of monolayers containing free E, K or monolayer-tethered LPE, LPK leads to the squeeze out of peptide at a certain surface pressure π_{SO} (Figure 5A-B). Upon expansion of the monolayer the free peptides do not immediately readsorb (Figure 5C), which leads to the disappearance of the C_S maxima upon expansion. Instead the peptides readsorb slowly, while the films remain at low pressures Figure 5D leading to a reappearance upon the next compression.

With the lipopeptides LPE and LPK comparable results were obtained with minor but important qualitative differences. First, all observed plateaus are reversible upon monolayer expansion and second the plateaus shift to higher surface pressures as compared to the free peptides E and K. With LPK in the monolayer, only at higher lipopeptide concentrations (4 mol%) reversible plateaus are observable. Furthermore, the molecular area of LPK containing monolayers is shifted to higher areas with increasing lipopeptide concentrations at all pressures. This shows at all pressures the peptide part of LPK can be expected to be incorporated in the monolayer (Figure 3). After the plateau at higher concentrations the molecular area of the monolayer is increased, which indicates the peptides are only partially squeezed out. This might be either caused by a squeeze out of parts of the peptide molecules, or due to the complete squeeze out of some peptide molecules. The fact that at lower molar fraction no squeeze out was observed indicates the latter explanation is more plausible.

For an estimation of the incorporated amount of peptide K we assume a simple model for its helix of a stiff rod (diameter 10 Å, length 32 Å) which is incorporated in a stiff monolayer of low compressibility. The expected molecular area increase if all helices are incorporated would be 6.4 $Å^2$ for 2 mol% and 12.8 $Å^2$ for 4 mol%.

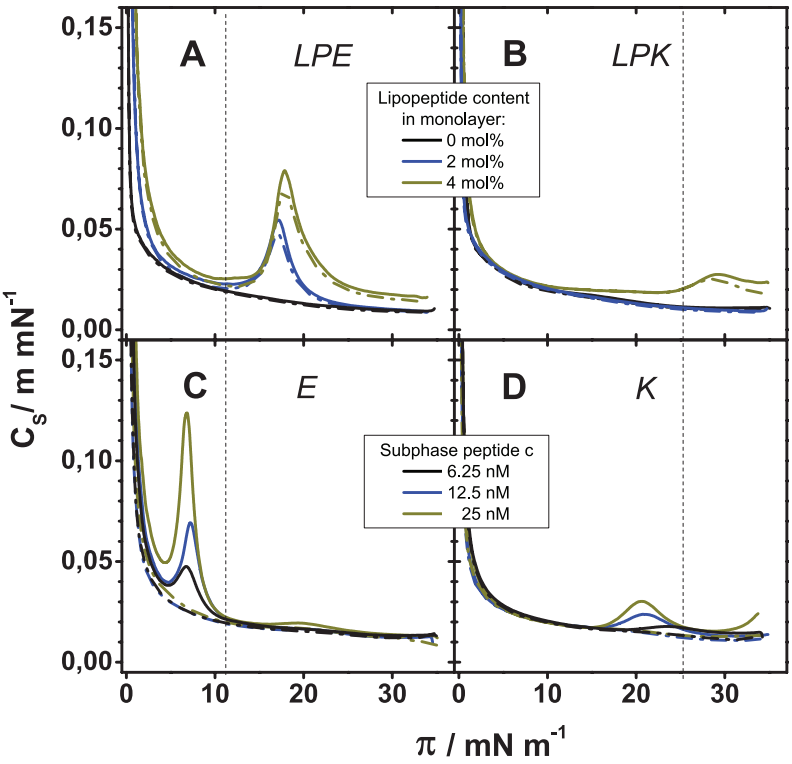

Figure 4. Compressibility (C_S) against surface pressure (π) of second compression-expansion cycles of monolayers with composition DOPE : DOPE : Chol (2 : 1 : 1) containing the tethered lipopeptides LPE (A), LPK (B) at different molar concentrations in the monolayer as well as the free peptides E (A) or K (B) at different subphase concentrations (6.25; 12.5; 25 nM). Vertical dashed lines correspond to π_{mip} as found from peptide incorporation experiments (compare Figure 1).

The molecular area at 40 mN / m was increased by 7.3 Å^2 upon incorporation of 2 mol% LPK as compared to the pure lipid mixture (Figure 3C). This shows, that all the helices are incorporated in the monolayer. At 4 mol% the increase of the molecular area was found to be 9.2 Å^2, impling 72% or less of the helices are incorporated.

The fact that in the case of the monolayer bound lipopeptides, LPE and LPK, the peaks in the compressibilities become reversible upon expansion also correlates with a peptide squeeze out. The bound peptides cannot diffuse into the subphase after they are expelled and therefore are able to immediately reincorporate into the monolayer upon decreasing pressure as the diffusion into interface proximity is not necessary Figure 5C).

To mimic the state after vesicle fusion, monolayers were prepared containing both LPE and LPK. As control an experiment with the coiled-coil complex E/K in the subphase was performed. Figure 6 shows the comparison of the compressibilities of both experiments. The monolayer on the E/K containing subphase shows

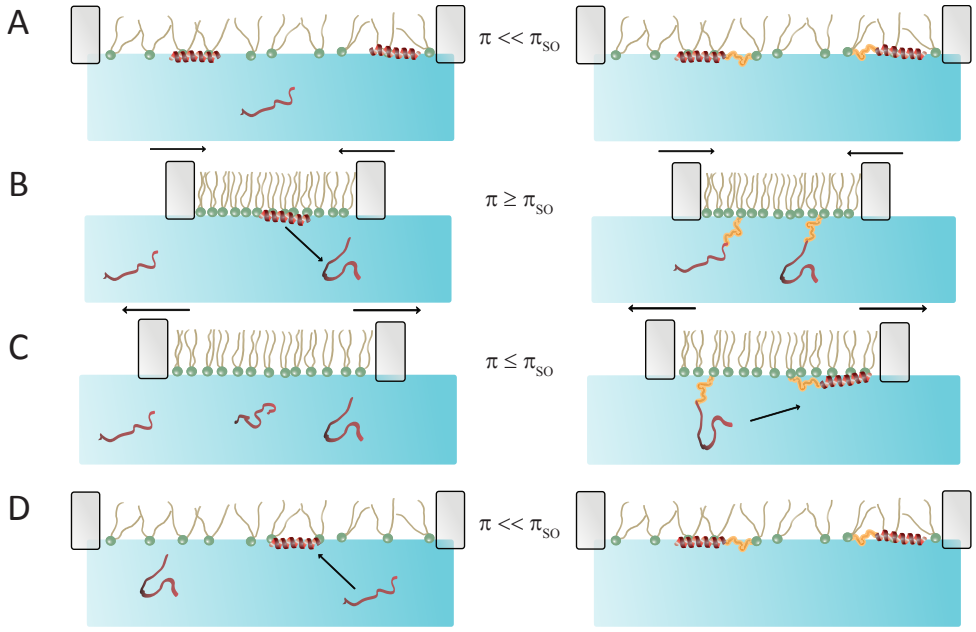

Figure 5. Model of processes upon compression and expansion in lipid monolayers containing free peptides E and K in the subphase (left) or monolayer tethered lipopeptides LPE and LPK (right). (A) Before compression peptides and lipopeptides are in the monolayer. (B) Upon compression above the π_{SO} peptides and lipopeptides are squeezed out from the monolayer. (C) Upon expansion below the π_{SO} lipopeptides are readsorbed into the monolayer while adsorption of free peptides is not immediately observed. (D) At low pressures free peptides readsorb within one hour to the monolayers.

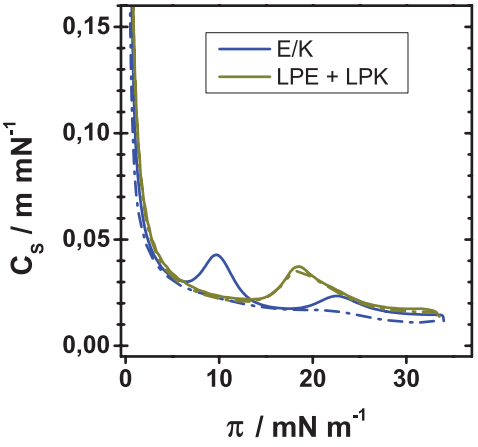

Figure 6. Compressibility (C_s) against surface pressure (π) of second compression-expansion cycles of monolayers with composition DOPE : DOPE : Chol (2 : 1 : 1) containing the complex E/K at a subphase concentration of 12.5 nM as well as the monolayer tethered lipopeptides LPE and LPK at equimolar proportions (total amount of lipopeptide in the monolayer 4 mol%)

two maxima in the compressibility curve, both irreversible upon expansion. The pressure at which the maximal compressibilities are recorded are slightly increased compared to free isolated E and free isolated peptide K at 9.7 and 22.5 mN / m. The interaction of the individual peptides with the membrane seems to be slightly influenced by the presence of the potential binding partner in the monolayer or

subphase. In the case of the monolayer bound LPE and LPK, one maximum which is also reversible upon expansion can be found at 18.4 mN / m as it is found for a monolayer containing LPE only. Additionally, a small shoulder around 22.5 mN / m might indicate another peptide species is expelled from the monolayer or the squeeze out occurs in two different steps. As stated earlier we do not expect the E/K complex to interact with the membrane due to the shielding of the hydrophobic residues of the individual peptides (compare Figure 2). In the context of E/K complex formation, this finding suggests that the interaction of the peptides with the monolayer stands in concurrence to the E/K coiled–coil complex formation because peaks in the compressibility C_S can be found that imply the presence of monomeric peptides in the monolayers.

IRRAS

We performed angle and polarization dependent infrared reflection absorption spectroscopy (IRRAS) measurements of the described monolayers at the air-water interface, in order to further study the origin of the occurring plateaus in the π - A isotherms, and to study the properties of the peptides and lipopeptides when interacting with the lipid monolayers. In a first series of experiments lipid monolayers were spread on d-PBS containing E, K or the complex E/K ([peptide] = 28 nM). In a second series, lipid monolayers were prepared containing 4 mol% LPE and/or LPK lipopeptides. IRRA spectra with varying angle of incidence and polarization were recorded at different constant surface pressures below and above the observed pressures π_{SO}. For a qualitative comparison of the results, spectra recorded in s-polarization were averaged over all angles of incidence. The band intensities of these averaged spectra are sensitive to the surface concentration, provided that the orientation of the absorbing moieties is comparable.

Here, we discuss the spectral region between 1800 and 1600 cm^{-1} (Figure 7), comprising the peptide amide I' band and the lipid C=O stretching vibrational band, being centered at 1640 and 1735 cm^{-1}, respectively. In all experiments the intensities of the C=O band increase upon monolayer compression due to the increasing lipid density in the IR-spot. Equally, the integral intensity of the amide I' band is a measure for the quantity of peptides within the IR spot. Therefore, the ratio $RA_{Amide\ I'}/RA_{C=O}$ (short: AI/CO) was determined in order to quantify the peptide binding to the lipid monolayer (Table 1).

With free peptide E, the amide I' band completely disappeared at pressures above the plateaus (i.e. ≥ 18 mN/m), proving a complete peptide squeeze out from the monolayer within the plateau region. For peptide K AI/CO drops from 1.4 to 0.5 upon compression from 12 to 30 mN / m, indicating a partial peptide squeeze out. (Figure 4). In the case of the complex E/K the AI/CO ratio at the pressure

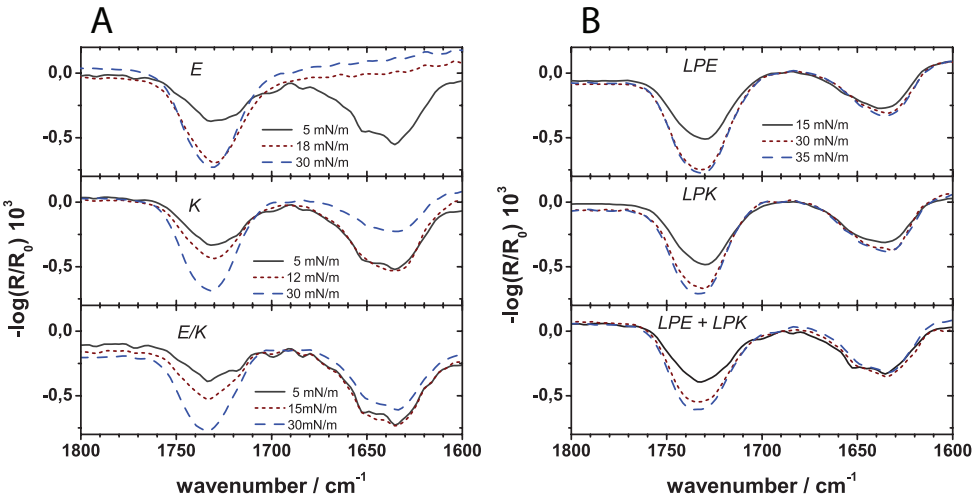

Figure 7. Averaged s-polarized IRRA spectra of monolayers of composition DOPE : DOPE : Chol (2 : 1 : 1) containing the free peptides (A) E, K and the complex E/K as well as the monolayer tethered lipopeptides (B) LPE, LPK and an equimolar mixture LPE + LPK at different surface pressures in the region between 1800 cm^{-1} and 1600 cm^{-1}.

below the plateau (5 mN/m) is higher as compared to the peptides E or K, indicative of a higher peptide concentration at the monolayer. AI/CO decreased from 2.6 to 1.7 upon compression from 5 to 15 mN / m, i.e. above the first plateau. A further decrease to 0.96 occurred upon further compression to 30 mN / m. This shows the squeeze out is accomplished in two steps. The remaining amide I' intensity shows that still some peptide remains bound in the monolayer.

The lipopeptides LPE and LPK are tethered to the monolayer and are therefore confined close to the air-water interface even when the peptidic part of the lipopeptide is expelled from the monolayer. Due to this proximity the peptides are still detected by the IR beam, even after a peptide squeeze out (Table 1). The ratio AI/CO decreased by 25% for LPE, while for LPK only a small decrease was measured. For LPE this indicates an orientation and/or secondary structure change of the peptide, due to the peptide squeeze out. This is expected because the orientation of the peptides when squeezed out in the aqueous bulk should be more random compared to its orientation within a liquid crystalline lipid monolayer. Equally, the secondary structure should be less ordered, because an amphipathic organization is not favorable in aqueous bulk.

Upon compression above the plateau of a monolayer containing LPE and LPK in equal amounts, a decrease of AI/CO from 0.87 to 0.62 was observed. This decrease is comparable to that of monolayers containing only LPE, again indicative of a change in orientation and/or secondary structure of the peptides.

Table 1. Squeeze out pressures π_{SO} from compression expansion experiments and spectroscopic results of IRRAS experiments.

Monolayer[1] +	π_{SO} (mN/m)	π (mN/m)	AI/ CO[4]	S[5]	θ (°) [5]
E[2]	7.0	5	1.40	-0.50	89
		18	0.00	-	-
		30	0.00	-	-
K[2]	20.5	5	1.50	-0.50	89
		12	1.40	-0.50	90
		30	0.46	-0.46	80
E/K[2]	9.7 22.5	5	2.68	-0.50	88
		15	1.71	-0.50	89
		30	0.96	-0.46	80
LPE[3]	17.9	15	0.70	-0.47	82
		30	0.52	0.05	53
		35	0.54	0.04	53
LPK[3]	29.5	15	0.77	-0.47	83
		30	0.76	-0.49	85
		35	0.72	-0.44	78
LPK + LPE[3]	18.4	15	0.87	-0.47	82
		30	0.62	-0.15	61
		35	0.60	-0.18	62

[1]Monolayers composition was DOPC:DOPE:Cholesterol 2:1:1 spread on PBS. [2]Subphase contained [pep] = 28 nM. [3]Monolayer contained total Lipopeptide 4 mol %. [4]Ratio of integrated absorbance of amide I' to integrated absorbance of C=O stretching vibration of s-polarized spectra averaged over all measured angles of incidence. [5]Order parameter S and tilt angle θ of best fit of angle and polarization dependant amide I' band between 1620-1670 cm^{-1} with the model described in the text; detailed fitting results can be found in SI.

AMIDE I' BAND SHAPE

The position of the amide I' band is highly dependent on the peptide secondary structure and therefore often used to estimate relative abundances of secondary structure elements in proteins.[38] Furthermore, the solvent accessibility strongly influences the amide I' band position for short peptide α-helices.[39,40]

The position and shape analysis of amide I' bands obtained by IRRAS at intermediate surface pressures and a transmission FT-IR spectrum of the E/K complex, reveals these amide I' band contours are asymmetrical. They consist of a maximum around 1634 cm^{-1} and a shoulder around 1651 cm^{-1} (Figure 8). Similar spectral shapes were observed for peptides E and K tethered to lipid bilayers by ATR FT-IR.[20] At least two bands are commonly found for coiled-coil forming peptides, caused by differences in the hydrogen bonding of carbonyls buried in the hydrophobic core and solvent accessible carbonyls.[39-43] The transmission FT–IR spectrum of the coiled-coil complex E/K shows a comparable shape and the second derivative revealed two major peaks around 1631 and 1651 cm^{-1} and a small peak around 1672 cm^{-1} (Figure 8). The spectral shape was modeled with two major and one minor gaussian functions in these positions. We therefore conclude the presence of C=O bonds with two different solvent accessibilities in the E and K peptides, when they interact with lipid monolayers. The water accessible amide bonds absorbing at lower wavenumbers (1631 cm^{-1}) then the water inaccessible ones (1651 cm^{-1}). The third minor contribution around 1672 cm^{-1} was assigned to residual trifluoracetic acid from HPLC purification of the lipopeptides.[44]

The finding of the distinct asymmetric band shape, which is typical for interacting helices is surprising, as we do not expect an interaction of oligomers of E/E, K/K or E/K with the membrane. Homo-coil formation of single LPE and single LPK, which would be a possible explanation for these spectra was hypothesized earlier as reason for the increased α-helicity of the peptides at the interface of lipid

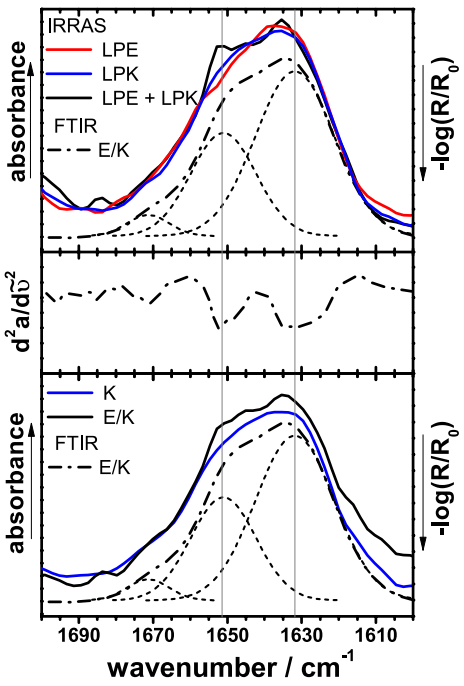

Figure 8. Comparison of amide I' band shape found in averaged s-polarized IRRA spectra of lipopeptides/peptides with DOPE : DOPE : Chol (2 : 1 : 1) monolayers at π = 15 mN / m (K: π = 12 mN / m) at these surface pressures peptide E is already squeezed out. For comparison a transmission spectrum of E/K at 1 mM in d-PBS and its band fit with 3 gauss peaks is shown as black dashed lines in the top and bottom panel. The second derivative of the E/K transmission spectrum is shown in the middle panel. Top panel: Monolayer tethered lipopeptides LPE, LPK and equimolar mixture LPE + LPK (total lipopeptides 4 mol%); bottom panel: free K and complex E/K ([pep] = 28 nM). Spectra were normalized for clarity.

vesicles.[5,15] However, we would expect homo-coils to have their hydrophobic binding site inaccessible and therefore not to incorporate into the monolayers, which contradicts the results of the monolayer compression experiments.

An explanation would be the coexistence of the peptides in different states. A fraction of the peptides bound to the membrane explains the results of monolayer compression experiments while coexisting non-bound homo-coils could explain the two spectral components. However, this model would only explain the spectral shapes of the monolayer tethered peptides. Untethered peptides that are expelled from the monolayer diffuse into the subphase and do not contribute to the amide I' absorption as can be seen from the AI/CO ratios of the free E peptide (Table 1). As a homo-coil is not expected to incorporate into the monolayers the appearance of two spectral components cannot be explained by this model in the case of free peptides E and K.

Another possibility is the assumption that the different solvent accessibilities of the amide C=O bonds, is caused by the alignment of single amphipathic helices at the hydrophobic/hydrophilic interface and a partial insertion of hydrophobic side chains into the hydrophobic part of the monolayer. Designed and natural amphipathic helices are known to incorporate into lipid bilayers with their center on the level of the lipid glycerol backbone[45,46] which can be expected to result in a different solvent accessibility of their carbonyl groups depending on their position with respect to the monolayer interface. Similar FTIR amide I' band splittings have been reported for the interactions of amphipathic helices with inverse micelles, which are thought to mimic the properties of water at the interface of lipid

bilayers.[47,48] We therefore propose the observed two spectral components originate from different water accessibilities of the amide C=O bonds in an amphipathic helix that penetrates the hydrophobic part of the monolayer with its hydrophobic residues and is oriented with its helical axes parallel to the monolayer plane.

For a more detailed analysis of changes in the amide I' band shapes upon monolayer compression principal component analysis (PCA) was applied to the IRRA spectra of LPE and LPK.[49] This approach allows the determination of the spectral components necessary to describe the deviations from the mean of all analyzed spectra and to sort the spectra by their degree of similarity (Figure A3 and Supporting Discussion).

The PCA is discussed in detail in the appendix and revealed details of the squeeze out model:

I) For LPE and LPK the amide I' bands above π_{SO} are red shifted compared to spectra below the squeeze out.This implies the secondary structure of most peptide molecules changes from helical to a more unstructured state upon squeeze out (Figure 5).

II) Above π_{SO} the amide I' bands of LPE are a red shifted compared to LPK, which is in common with a squeeze out of more peptide molecules in case of LPE while only a partial squeeze out of LPK occurs.

ANGLE DEPENDENCE OF IRRA SPECTRA

The orientation and order of molecules can be estimated from angle dependent IRRAS measurements. As described in detail by Schwieger et al.[50] and in the supporting information molecular order parameters S can be obtained from fitting of the angle dependent reflectance absorbance spectra under certain conditions. The order parameter S can have values between -0.5 and +1, standing for an orientation of all molecules parallel or perpendicular to the monolayer, respectively. It can be used to calculate the averaged molecular tilt angles θ with respect to the membrane normal, under the assumption of an unimodal distribution of θ.

Fitting of the angle dependent s- and p-polarized amide I' bands was performed assuming two spectral components that can be assigned to solvent exposed (~1631 cm^{-1}) and buried (~1651 cm^{-1}) amide bonds (see appendix for fitting results, routine and experimental amide I' bands). Figure 9 summarizes the fitting results. It shows a comparison of the integrated experimental band intensities with those of the best fitting simulated ones. In all cases the spectra in p-polarization showed negative band intensities below and positive band intensities above the Brewster angle (~53°). In general, the modeled amide I' bands gave good overlap with the shape of the experimental bands in the regions 1620-1670 cm^{-1} and with models

assuming helix order parameters $S \leq 0$ (Figure A4-9). Peptides E and K as well as E/K showed values for S close to -0.5 at low surface pressures up to 15 mN / m, indicative of an orientation of the helices parallel to the membrane plane, i.e. a tilt of ~90° with respect to the monolayer normal (Table 1). Peptide K and E/K showed amide I' bands at higher pressures and here S slightly increased to ~ -0.46 upon compression above the squeeze out at 30 mN / m. Thus, the peptide molecules on the interface are either on average slightly more tilted towards the membrane normal ($\theta \sim 80°$) or their structure is less ordered compared to the lower surface pressures. A possible explanation might be a partial squeeze out of the peptide molecules leading to a situation where the ends of the peptide chains reach into the aqueous phase.

The monolayer tethered LPK, LPE and mixtures of both also showed order parameters close to -0.5 at intermediate pressures below π_{SO}. This again indicates a predominantly parallel orientation of the peptides with respect to the membrane ($\theta \sim 82\text{-}87°$).

Above the squeeze out pressure the order parameters increased in all cases. The values of S close to 0 in case of LPE above the π_{SO} are probably caused by random distributions of the amide bonds. That means in this situation are either randomly distributed helices or non-ordered structures present. Alternatively, but unlikely an order parameter of 0 can indicate an orientation of the helices around ~54°. For the LPE containing monolayers this result is in line with a squeeze out of peptides leading to non-ordered structure of the peptides in the aqueous phase.

The order parameters increased slightly from -0.49 to -0.44 for LPK above π_{SO}. This can be caused by a change of the mean angle of all helices ($\theta \sim 78°$). However this observation is also in common with a partial squeeze out of peptide molecules as was concluded from the π-A isotherms and the PCA.

The order parameter S also increases strongly for monolayers containing both LPK and LPE above the squeeze out pressure. The multiple possible states of LPE and LPK peptides in this case complicate the interpretation of this result. A slightly negative value of ~ -0.15 might be due to the coexistence of squeezed out E and/or K peptides and remaining monomeric α helical peptides interacting with the monolayer.

Taken together the PCA and fitting results of the angle dependent IRRAS measurements confirm important details of the model depicted in Figure 5. Peptides and lipopeptides interact with the monolayer in an α-helical conformation, inserted parallel to the monolayer plane and loose structure when they are squeezed out.

IMPLICATIONS FOR LIPOPEPTIDE MEDIATED FUSION.

A lipid monolayer is a simple yet a useful model system for the outer leaflet of a vesicle lipid bilayer.[24,25] In this study we mimicked the prefusion state of liposomes

with monolayers containing the individual peptides E and K and the postfusion

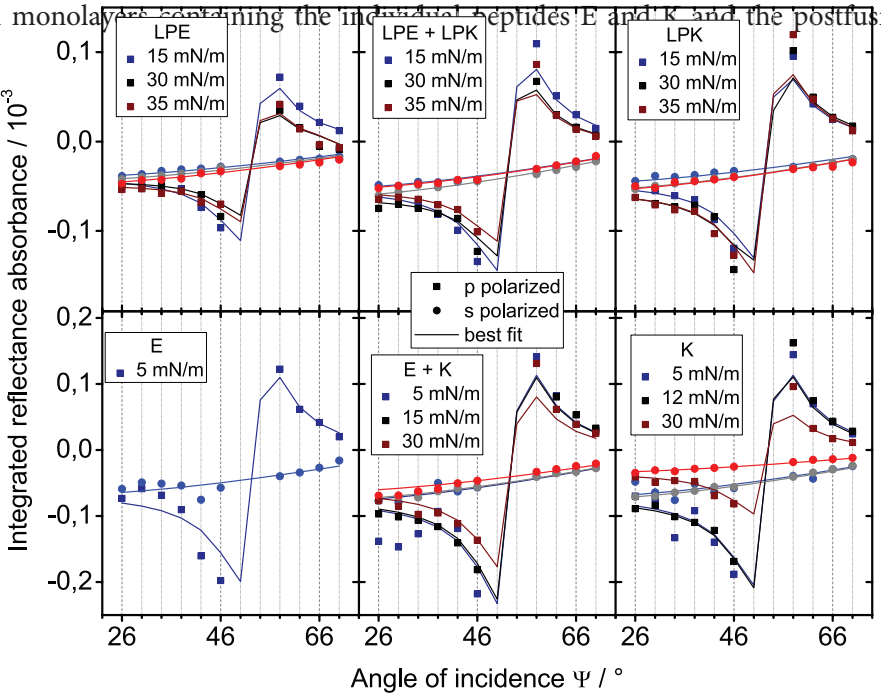

Figure 9. Amide I' band (1620-1670 cm^{-1}) intensities in p-(squares) and s-(circles) polarized angle of incidence dependent IRRAS experiments. Best fitting models are shown as solid lines, the corresponding tilt angles are given in Table 1. Monolayer composition: DOPE : DOPE : Cholesterol (2 : 1 : 1); Lipopeptides LPE, LPK and LPE + LPK in the monolayer (4 mol%; top panels); Peptides E, K or the complex E/K in the subphase ([pep] = 28 nM, lower panels).

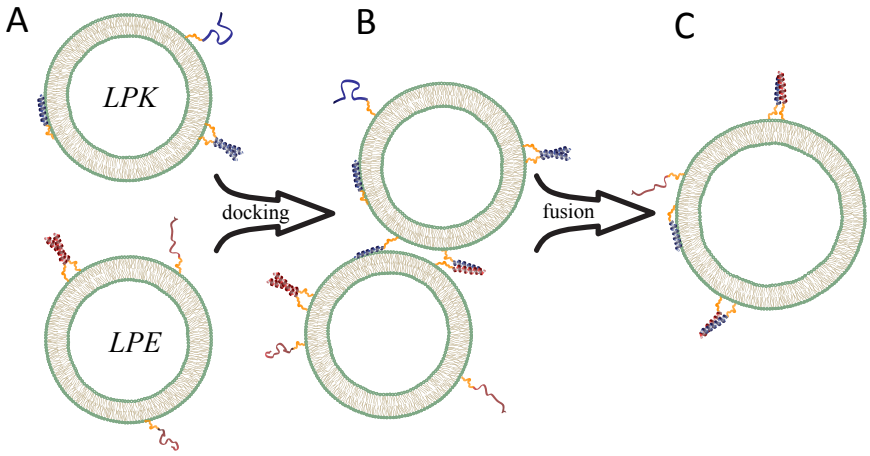

Figure 10. Possible states of peptides on vesicles. (A) On isolated vesicles, (B) on vesicles in close proximity (C) on a fused vesicle.

state with monolayers containing the coiled-coil complex E/K. Due to the relatively high amount of hydrophilic charged amino acids in the sequence of E and K a complete incorporation into the hydrophobic interior of a bilayer is not expected and is furthermore, sterically hindered by the tether to the monolayer in the case of LPE and LPK. The found angles θ displayed in Table 1, and the observed reversible squeeze out, clearly indicate a parallel incorporation of the helical peptide at the hydrophilic/hydrophobic interface of the lipids, with the hydrophobic leucine and isoleucine residues being directed towards the hydrophobic core of the monolayer.

However, it remains the question for the peptide state on the vesicle surface. By means of circular dichroism spectroscopy it is generally observed that vesicle tethered peptides have a certain degree of helicity, which was also interpreted as a sign for E/E and K/K homo-coiling (Figure 10A, B).[5,14,15,17,18] We assume these homo-coils are in equilibrium with an unbound (probably unstructured) state which makes it accessible for the hetero-coil formation necessary for fusion. However, an inter-vesicular homo-coil formation that leads to vesicle fusion was not found.

Another possible explanation for the helicity of the peptides in the prefusion state is revealed in the present study. Monolayers at π = 30-35 mN / m are generally accepted to mimic the conditions found in bilayers.[26,27] The presented data show the incorporation of both monolayer tethered and free peptide K in this pressure regime, implying the same behavior to occur in vesicles. Therefore, we hypothesize the tethered K peptides can interact with both, the membrane they are tethered to and an opposing membrane in close proximity, i.e. an approaching vesicle during fusion (Figure 10A, B). In contrast, free or tethered peptide E incorporates into monolayers only at pressures < 20 mN/m and IRRAS confirmed a less ordered state on the membrane. Thus E does not interact with vesicles even when it is monolayer tethered (Figure 10A - C).

The experiments with monolayers containing either peptides E and K or both lipopeptides LPE and LPK give results indicating the E/K complex is not the only species on the monolayer. We conclude the peptides still interact with the monolayer in a monomeric way. For our fusion model this implies that in the post fusion state the monolayer bound form of the K peptide exists in a dynamic equilibrium with the E/K hetero complex (Figure 10C). The membrane bound K might contribute to the efficacy of the ongoing fusion process, because it might be an intermediate for an effective 'recycling', i.e. a dissociation of the E/K complex and a reuse of the monomeric E and K peptide in a new fusion process. It was concluded earlier by Marsden et al that the fusion with the LPE/LPK systems can go through multiple rounds.[15]

Another possible influence is that the interaction of peptide K initiates distortion of the membranes, necessary for merging of the lipid bilayers.[3,51,52] Because

it has been shown in several studies that the shallow insertion of amphipathic helices into one leaflet of a bilayer can effectively create curvature.[53-55]

CONCLUSIONS

The data presented here on the spontaneous monolayer incorporation of peptides, IRRAS and compression-expansion cycles of lipid monolayers containing the free peptides E, K and the tethered peptides LPK, LPE prove the direct interactions of these peptides with lipids used in numerous vesicle fusion assays. These peptides incorporate as monomers with their helical axis parallel to the lipid monolayer plane, can be expelled by applied lateral pressure, can readsorb if the pressure is lowered and can again be squeezed out upon subsequent compression. It was found that the squeeze out of peptide K is only partial, whereas peptide E is completely squeezed out of the monolayer upon compression. Based on the determined π_{mip} and π_{SO} values the strength of the peptide monolayer interactions can be estimated to be rather weak for negatively charged E peptides and moderate in the case of positively charged peptide K.

The tethering of the peptides has two major effects. First, the initial step in peptide adsorption to the monolayer i.e. the diffusion of peptides in close proximity of the monolayer is not necessary anymore, which results in expansion reversible plateaus in the π-A isotherms. Second, the π_{SO} are increased, which indicates an increase in the strength of the interactions, this effect cannot be solely explained by increased local proximity. One possible effect contributing to this might be the physical and chemical properties of the spacer, which was polyethylene glycol in this study.

In systems intended to mimic the post fusion state the peptides also interact as monomers with the monolayers i.e. they exist in more states than solely the E/K complex.

Based on these result we developed a more precise model for the lipopeptide mediated vesicle fusion. We assume the stronger interaction of the LPK, as opposed to the LPE, with the lipid interface play an important role in the mechanism of this process. Additional to the function of vesicle docking, LPK might be responsible for the creation of local curvature, disruption of the membrane interface, efficient complex dissociation after fusion, or all of these. This multi functionality would be a unique feature of the lipopeptide mediated vesicle fusion and provide a handle for its rational improvement.

MATERIALS AND METHODS

MATERIALS

DOPC, DOPE and cholesterol were purchased from Avanti Polar Lipids. Chloroform, methanol (both HPLC grade), D_2O (99.9 % deuterium content), buffer salts and HCl and DCl (99% deuterium content) for pH/pD adjustment, were purchased from Sigma-Aldrich. All water was ultrapure with resistance ≥ 18 MΩ and TOC ≤ 2 ppm produced from a MilliQ Reference A+ purification system. All monolayer and IR experiments were carried out in phosphate buffered saline of the following composition: 150 mM NaCl, 20 mM PO_4^{3-} in H_2O (PBS) or D_2O (d-PBS) at pH / pD 7.4, respectively.

PEPTIDE SYNTHESIS

The free peptides E: Ac-$(EIAALEK)_3$-NH_2 and K: Ac-$(KIAALKE)_3$-NH_2 were synthesized using standard Fmoc-chemistry on a Biotage Syro I and purified by RP-HPLC to yield a purity > 95% based on LC-MS. The lipopeptides were synthesized and purified as described elsewhere.[19] Purified peptides and lipopeptides (2-5 mg / ml) in aqueous HCl (20 mM) were lyophilized three times in order to replace trifluoracetate with chloride anions.

MONOLAYER PREPARATION

Lipid solutions of DOPE : DOPE : Cholesterol 2 : 1 : 1 (c = 1 mM) with varying amounts of lipopeptides of 0, 2 and 4 mol% were prepared in $CHCl_3$/CH_3OH 3:1 vol%. For the preparation of a lipid monolayer a distinct volume of these solutions was spread on PBS buffer at 25 °C by means of a microliter syringe, the solvent was allowed to evaporate and the film to equilibrate for at least 15 minutes. A microbalance was used for surface pressure measurements using a platinum plate.

Peptide monolayer incorporation studies were performed in a home built round Teflon trough (diameter 50 mm, volume 61.4 ml) equipped with an injection hole to enable injections of peptide solutions into the bulk without disturbance of the monolayer. Compression-expansion cycles were performed in a KSV Minitrough 2 (365 x 74 mm^2), equipped with hydrophilic barriers made from Delrin. For p-A compression isotherms, the prepared monolayers were compressed with 3 $Å^2$ / (molecule min) until monolayer collapse.

Initial cleaning of the troughs was achieved by means of diluted detergent solution (2% Hellmanex (Hellma Analytics, Müllheim, Germany) in H_2O), followed by extensive rinsing with ~50°C Milli-Q water, wiping with $CHCl_3$/MeOH and final multiple rinsing with Milli-Q water. All Langmuir trough setups were hold constant at 25 °C by means of a circulating water bath and were isolated from the environment by plastic covers.

PEPTIDE INCORPORATION.

After monolayer equilibration, when a constant surface pressure was reached (typically 30 minutes), a peptide solution of peptide E, K or the coiled-coil complex E/K (1 mM) in PBS was injected. The final concentration in the subphase was 0.3 μM. The injections were performed without disturbing the monolayer by means of an injection hole, while gently stirring the bulk phase to assure a fast distribution within the subphase. The increase of surface pressure due to peptide incorporation into the monolayers was measured until a constant surface pressure was reached. The peptide surface activity was determined at a PBS/air interface.

COMPRESSION-EXPANSION CYCLES

For compression-expansion cycles of lipid monolayers containing the free peptides E and K or the coiled-coil complex E/K, peptide solutions with a final [peptide] = 6.25; 12.5 and 25 nM in PBS were prepared, placed in the Langmuir trough and a lipid monolayer was spread on top. After equilibration, compressionexpansion cycles of the monolayer were performed with a compression/expansion speed of 3 $Å^2$ / (molecule min). After each cycle an one hour waiting time allowed the peptides to readsorb from the subphase at a constant surface pressure of 1 mN / m. Experiments were repeated at least twice to enssure reproducibility of the isotherm shape, while differences in the absolute areas in the range of $\pm 5A^2$ / molecule were found due to instabilities of the films over extended periods. For the determination of the compressibility, isotherms of the second compression-expansion cycle were smoothed by means of a 60 point adjacent average method and subsequently compressibilities were calculated as:
$C_S = (-1 / A) (\delta\pi / \delta A)_T$, with the molecular Area A and the surface pressure π.

IRRAS

IRRAS measurements were performed on a BRUKER Vector 70 FT–IR spectrometer equipped with a nitrogen cooled MCT detector and an A511 reflection unit (Bruker Optics, Germany), placed over the Langmuir trough setup (Riegler & Kierstein, Germany). The sample trough (30 x 6 cm^2) was equipped with a Wilhelmy balance using a filter paper as pressure probe. A circular reference trough (r = 3 cm) placed next to the sample trough can be brought into the focus of the IR beam by means of a shuttle. The filling levels of both troughs were kept equal and constant by means of an automated, laser reflection controlled, pumping system connected to reservoirs of D_2O.

Lipid monolayers containing the free peptides or lipopeptides were prepared as described above. d-PBS was used as subphase. The pD was set to 7.4 by adding

0.4 to the read-out of a standard pH-meter.[56] In experiments with the free peptides E, K or the coiled-coil complex E/K the final peptide concentration in the subphase was 28 nM. After the first compression-expansion cycle was finished, peptides were allowed to readsorb to the monolayer for one hour before the following compression was started which was accompanied by IRRA spectra measurements. IRRA spectra were recorded at constant surface pressures above and below the expected squeeze out pressure of the peptides. Details of the recorded spectra can be found in th SI.

SIMULATION OF IRRA SPECTRA

Angle and polarization dependent IRRA spectra were used to determine the orientation of membrane bound peptide helices. For this simulations and fiting of IRRA spectra was performed using MATLAB software (The MathWorks, Inc., USA). The optical model of Kuzmin and Mikhailov[57-59] was adopted to simulate spectra with multiple and overlapping bands. Details of this model are given in Schwieger et al.[50] The optical constants of the D_2O subphase were taken from Bertie et al.[60] Simulations were fitted to the experimental spectra by means of a non-linear least-square fit in the amide I' region (1620-1670 cm^{-1}). Details of the fitting procedure and parameters are given in the SI.

TRANSMISSION FT–IR

Transmission FT–IR spectra of the peptide complex E/K (1 mM) in PBS were measured using a Bio-Rad Excalibur spectrometer equipped with a nitrogen cooled MCT detector. A temperature controlled liquid transmission cell with CaF_2 windows and a fixed nominal path length of 50 μm was used. Sample spectra of peptide in d-PBS and reference spectra of dPBS at 25 °C were measured at a resolution of 2 cm^{-1} with a zero filling factor of 1. For each spectrum 1000 scans were averaged. The final absorbance spectra were calculated by $A = -lg(I / I_0)$ and corrected by manual subtraction of a water vapor spectrum.

REFERENCES

(1) Südhof, T. C.; Rothman, J. E., Membrane fusion: grappling with SNARE and SM proteins. *Science* **2009**, *323*, 474.

(2) Jahn, R.; Lang, T.; Südhof, T. C., Membrane Fusion. *Cell* **2003**, *112*, 519.

(3) Martens, S.; McMahon, H. T., Mechanisms of membrane fusion: disparate players and common principles. *Nat. Rev. Mol. Cell Biol.* **2008**, *9*, 543.

(4) Ma, M. M.; Bong, D., Controlled Fusion of Synthetic Lipid Membrane Vesicles. *Acc. Chem. Res.* **2013**, *46*, 2988.

(5) Robson Marsden, H.; Elbers, Nina A.; Bomans, Paul H. H.; Sommerdijk, Nico A. J. M.; Kros, A., A Reduced SNARE Model for Membrane Fusion. *Angew. Chem. Int. Ed.* **2009**, *48*, 2330.

(6) Marsden, H. R.; Tomatsu, I.; Kros, A., Model systems for membrane fusion. *Chem. Soc. Rev.* **2011**, *40*, 1572.

(7) Stengel, G.; Zahn, R.; Höök, F., DNA-Induced Programmable Fusion of Phospholipid Vesicles. *J. Am. Chem. Soc.* **2007**, *129*, 9584.

(8) Kashiwada, A.; Tsuboi, M.; Matsuda, K., Target-selective vesicle fusion induced by molecular recognition on lipid bilayers. *Chem. Commun.* **2009**, 695.

(9) Ma, M.; Paredes, A.; Bong, D., Intra- and Intermembrane Pairwise Molecular Recognition between Synthetic Hydrogen-Bonding Phospholipids. *J. Am. Chem. Soc.* **2008**, *130*, 14456.

(10) Ravoo, B. J.; Weringa, W. D.; Engberts, J. B. F. N., Membrane Fusion in Vesicles of Oligomerizable Lipids. *Biophys. J.* **1999**, *76*, 374.

(11) Chan, Y.-H. M.; van Lengerich, B.; Boxer, S. G., Effects of linker sequences on vesicle fusion mediated by lipid-anchored DNA oligonucleotides. *Proceedings of the National Academy of Sciences* **2009**, *106*, 979.

(12) Lygina, A. S.; Meyenberg, K.; Jahn, R.; Diederichsen, U., Transmembrane Domain Peptide/Peptide Nucleic Acid Hybrid as a Model of a SNARE Protein in Vesicle Fusion. *Angew Chem Int Edit* **2011**, *50*, 8597.

(13) Litowski, J. R.; Hodges, R. S., Designing heterodimeric two-stranded alpha-helical coiled-coils. Effects of hydrophobicity and alpha-helical propensity on protein folding, stability, and specificity. *J. Biol. Chem.* **2002**, *277*, 37272.

(14) Zheng, T. T.; Voskuhl, J.; Versluis, F.; Zope, H. R.; Tomatsu, I.; Marsden, H. R.; Kros, A., Controlling the rate of coiled coil driven membrane fusion. *Chem. Commun.* **2013**, *49*, 3649.

(15) Robson Marsden, H.; Korobko, A. V.; Zheng, T.; Voskuhl, J.; Kros, A., Controlled liposome fusion mediated by SNARE protein mimics. *Biomaterials Science* **2013**, *1*, 1046.

(16) Meyenberg, K.; Lygina, A. S.; van den Bogaart, G.; Jahn, R.; Diederichsen, U., SNARE derived peptide mimic inducing membrane fusion. *Chem. Commun.* **2011**, *47*, 9405.

(17) Versluis, F.; Dominguez, J.; Voskuhl, J.; Kros, A., Coiled-coil driven membrane fusion: zipper-like vs. non-zipper-like peptide orientation. *Faraday Discuss.* **2013**, *166*, 349.

(18) Tomatsu, I.; Marsden, H. R.; Rabe, M.; Versluis, F.; Zheng, T.; Zope, H.; Kros, A., Influence of pegylation on peptide-mediated liposome fusion. *J. Mater. Chem.* **2011**, *21*, 18927.

(19) Versluis, F.; Voskuhl, J.; van Kolck, B.; Zope, H.; Bremmer, M.; Albregtse, T.; Kros, A., In Situ Modification of Plain Liposomes with Lipidated Coiled Coil Forming Peptides Induces Membrane Fusion. *J. Am. Chem. Soc.* **2013**, *135*, 8057.

(20) Pahler, G.; Panse, C.; Diederichsen, U.; Janshoff, A., Coiled-Coil Formation on Lipid Bilayers-Implications for Docking and Fusion Efficiency. *Biophys. J.* **2012**, *103*, 2295.

(21) Zope, H. R.; Versluis, F.; Ordas, A.; Voskuhl, J.; Spaink, H. P.; Kros, A., In vitro and in vivo supramolecular modification of biomembranes using a lipidated coiled-coil motif. *Angew Chem Int Ed Engl* **2013**, *52*, 14247.

(22) Segrest, J. P.; De Loof, H.; Dohlman, J. G.; Brouillette, C. G.; Anantharamaiah, G. M., Amphipathic helix motif: Classes and properties. *Proteins: Structure, Function, and Bioinformatics* **1990**, *8*, 103.

(23) Pahler, G.; Lorenz, B.; Janshoff, A., Impact of peptide clustering on unbinding forces in the context of fusion mimetics. *Biochem. Biophys. Res. Commun.* **2013**, *430*, 938.

(24) Brockman, H., Lipid monolayers: why use half a membrane to characterize protein-membrane interactions? *Curr. Opin. Struct. Biol.* **1999**, *9*, 438.

(25) Calvez, P.; Bussières, S.; Éric, D.; Salesse, C., Parameters modulating the maximum insertion pressure of proteins and peptides in lipid monolayers. *Biochimie* **2009**, *91*, 718.

(26) Blume, A., A comparative study of the phase transitions of phospholipid bilayers and monolayers. *Biochim. Biophys. Acta* **1979**, *557*, 32.

(27) Marsh, D., Lateral pressure in membranes. *Biochim. Biophys. Acta* **1996**, *1286*, 183.

(28) Gautier, R.; Douguet, D.; Antonny, B.; Drin, G., HELIQUEST: a web server to screen sequences with specific α-helical properties. *Bioinformatics* **2008**, *24*, 2101.

(29) Grigoryan, G.; Keating, A. E., Structural specificity in coiled-coil interactions. *Curr. Opin. Struct. Biol.* **2008**, *18*, 477.

(30) Lindhout, D. A.; Litowski, J. R.; Mercier, P.; Hodges, R. S.; Sykes, B. D., NMR solution structure of a highly stable de novo heterodimeric coiled-coil. *Biopolymers* **2004**, *75*, 367.

(31) Vagt, T.; Zschörnig, O.; Huster, D.; Koksch, B., Membrane Binding and Structure of De Novo Designed α-Helical Cationic Coiled-Coil-Forming Peptides. *ChemPhysChem* **2006**, *7*, 1361.

(32) Mishra, V. K.; Palgunachari, M. N., Interaction of Model Class A1, Class A2, and Class Y Amphipathic Helical Peptides with Membranes. *Biochemistry* **1996**, *35*, 11210.

(33) Mishra, V. K.; Palgunachari, M. N.; Segrest, J. P.; Anantharamaiah, G. M., Interactions of synthetic peptide analogs of the class A amphipathic helix with lipids. Evidence for the snorkel hypothesis. *J. Biol. Chem.* **1994**, *269*, 7185.

(34) Jensen, M. B.; Bhatia, V. K.; Jao, C. C.; Rasmussen, J. E.; Pedersen, S. L.; Jensen, K. J.; Langen, R.; Stamou, D., Membrane Curvature Sensing by Amphipathic Helices a Single Liposome Study Using alpha-Synuclein and Annexin B12. *J. Biol. Chem.* **2011**, *286*, 42603.

(35) Yu, Z.-W.; Jin, J.; Cao, Y., Characterization of the Liquid-Expanded to Liquid-Condensed Phase Transition of Monolayers by Means of Compressibility. *Langmuir* **2002**, *18*, 4530.

(36) Dyck, M.; Lösche, M., Interaction of the Neurotransmitter, Neuropeptide Y, with Phospholipid Membranes: Film Balance and Fluorescence Microscopy Studies. *J. Phys. Chem. B* **2006**, *110*, 22143.

(37) Dyck, M.; Kerth, A.; Blume, A.; Losche, M., Interaction of the neurotransmitter, neuropeptide Y, with phospholipid membranes: Infrared spectroscopic characterization at the air/water interface. *J. Phys. Chem. B* **2006**, *110*, 22152.

(38) Barth, A., Infrared spectroscopy of proteins. *Biochim. Biophys. Acta* **2007**, *1767*, 1073.

(39) Manas, E. S.; Getahun, Z.; Wright, W. W.; DeGrado, W. F.; Vanderkooi, J. M., Infrared Spectra of Amide Groups in a-Helical Proteins: Evidence for Hydrogen Bonding between Helices and Water. *J. Am. Chem. Soc.* **2000**, *122*, 9883.

(40) Walsh, S. T.; Cheng, R. P.; Wright, W. W.; Alonso, D. O.; Daggett, V.; Vanderkooi, J. M.; DeGrado, W. F., The hydration of amides in helices; a comprehensive picture from molecular dynamics, IR, and NMR. *Protein Sci.* **2003**, *12*, 520.

(41) Brewer, S. H.; Tang, Y.; Vu, D. M.; Gnanakaran, S.; Raleigh, D. P.; Dyer, R. B., Temperature dependence of water interactions with the amide carbonyls of alpha-helices. *Biochemistry* **2012**, *51*, 5293.

(42) Wang, T.; Lau, W. L.; DeGrado, W. F.; Gai, F., T-Jump Infrared Study of the Folding Mechanism of Coiled-Coil GCN4-p1. *Biophys. J.* **2005**, *89*, 4180.

(43) Heimburg, T.; Schünemann, J.; Weber, K.; Geisler, N., FTIR-Spectroscopy of Multistranded Coiled Coil Proteins. *Biochemistry* **1999**, *38*, 12727.

(44) Andrushchenko, V. V.; Vogel, H. J.; Prenner, E. J., Optimization of the hydrochloric acid concentration used for trifluoroacetate removal from synthetic peptides. *J. Pept. Sci.* **2007**, *13*, 37.

(45) Hristova, K.; Wimley, W. C.; Mishra, V. K.; Anantharamiah, G. M.; Segrest, J. P.; White, S. H., An amphipathic α-helix at a membrane interface: a structural study using a novel X-ray diffraction method. *J. Mol. Biol.* **1999**, *290*, 99.

(46) Hristova, K.; Dempsey, C. E.; White, S. H., Structure, Location, and Lipid Perturbations of Melittin at the Membrane Interface. *Biophys. J.* **2001**, *80*, 801.

(47) Mukherjee, S.; Chowdhury, P.; Gai, F., Infrared Study of the Effect of Hydration on the Amide I Band and Aggregation Properties of Helical Peptides. *J. Phys. Chem. B* **2007**, *111*, 4596.

(48) Mukherjee, S.; Chowdhury, P.; DeGrado, W. F.; Gai, F., Site-specific hydration status of an amphipathic peptide in AOT reverse micelles. *Langmuir* **2007**, *23*, 11174.

(49) Jolliffe, I. T. *Principal Component Analysis*, 2002.

(50) Schwieger, C.; Chen, B.; Tschierske, C.; Kressler, J.; Blume, A., Organization of T-Shaped Facial Amphiphiles at the Air/Water Interface Studied by Infrared Reflection Absorption Spectroscopy. *J. Phys. Chem. B* **2012**, *116*, 12245.

(51) McMahon, H. T.; Kozlov, M. M.; Martens, S., Membrane Curvature in Synaptic Vesicle Fusion and Beyond. *Cell* **2010**, *140*, 601.

(52) Chernomordik, L. V.; Kozlov, M. M., Protein-lipid interplay in fusion and fission of biological membranes. *Annu. Rev. Biochem.* **2003**, *72*, 175.

(53) Campelo, F.; McMahon, H. T.; Kozlov, M. M., The hydrophobic insertion mechanism of membrane curvature generation by proteins. *Biophys. J.* **2008**, *95*, 2325.

(54) Varkey, J.; Isas, J. M.; Mizuno, N.; Jensen, M. B.; Bhatia, V. K.; Jao, C. C.; Petrlova, J.; Voss, J. C.; Stamou, D. G.; Steven, A. C.; Langen, R., Membrane Curvature Induction and Tubulation Are Common Features of Synucleins and Apolipoproteins. *J. Biol. Chem.* **2010**, *285*, 32486.

(55) Kozlov, M. M.; McMahon, H. T.; Chernomordik, L. V., Protein-driven membrane stresses in fusion and fission. *Trends Biochem. Sci.* **2010**, *35*, 699.

(56) Glasoe, P. K.; Long, F. A., Use of glass electrodes to measure acidities in deuterium oxide. *J. Phys. Chem.* **1960**, *64*, 188.

(57) Kuzmin, V. L.; Mikhailov, A. V., Molecular theory of light reflection and applicability limits of the macroscopic approach. *Opt. Spectrosc. (USSR)* **1981**, *51*, 383.

(58) Kuzmin, V. L.; Romanov, V. P.; Mikhailov, A. V., Reflection of light at the boundary of liquid systems and structure of the surface layer: A review. *Opt. Spectrosc. (USSR)* **1992**, *73*, 1.

(59) Flach, C. R.; Gericke, A.; Mendelsohn, R., Quantitative Determination of Molecular Chain Tilt Angles in Monolayer Films at the Air/Water Interface: Infrared Reflection/Absorption Spectroscopy of Behenic Acid Methyl Ester. *J. Phys. Chem. B* **1997**, *101*, 58.

(60) Bertie, J. E.; Ahmed, M. K.; Eysel, H. H., Infrared intensities of liquids. 5. Optical and dielectric constants, integrated intensities, and dipole moment derivatives of water and water-d2 at 22 degree C. *J. Phys. Chem.* **1989**, *93*, 2210.

(61) Marsh, D.; Müller, M.; Schmitt, F.-J., Orientation of the Infrared Transition Moments for an α-Helix. *Biophys. J.* **2000**, *78*, 2499.

APPENDIX

CONCENTRATION DEPENDENCY OF E/K-MONOLAYER INTERACTION

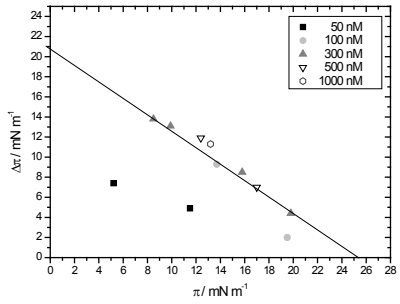

Figure A1. Change in surface pressure Δπ after injection of peptide mixture E/K under spread DOPE : DOPE : Cholesterol 2 : 1 : 1 monolayers of the initial surface pressure p_0. All experiments were done in PBS with varying E/K concentration in the trough of (0.05; 0.1; 0.3; 0.5 and 1 μM). Data points at trough concentrations > 0.1 μM coincide on a straight line. Therefore a trough concentration of 0.3 μM was chosen for further incorporation experiments.

SIZE OF PLATEAUS IN MONOLAYER COMPRESSION EXPANSION ABOVE E AND K

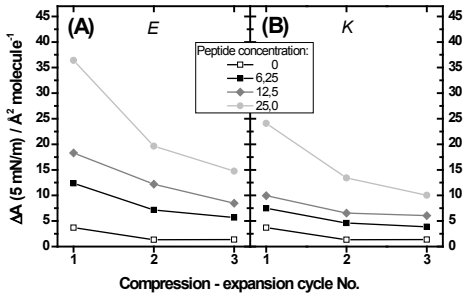

Figure A2. Differences in molecular areas (ΔA) at 5 mN/m against compression expansion cycle number of monolayers with composition DOPE : DOPE : Chol (2 : 1 : 1) containing the free peptides E (A) or K (B) at different subphase concentrations (6.25; 12.5; 25 nM). Plateaus decrease in size at repeated compression and increases with increasing peptide concentration.

DETAILS OF IRRA SPECTRA MEASUREMENTS

Monolayers were prepared as described in the materials and methods section. IRRA spectra were recorded at constant surface pressures above and below the expected squeeze out pressure of the peptides. At each pressure at least 3 cycles of angle dependent IRRA spectra were recorded. For each spectral cycle s- and p-polarized spectra were recorded at incident angles varying from 26° to 70° with an increment of 4°, while spectra close to the Brewster angle (50° and 54°) were discarded. For each sample reflectance spectrum (R) a total number of 2000 scans at a resolution of 4 cm^{-1} and a zero filling factor of 2 were averaged. Reference reflectance spectra (R_0) were recorded at the same experimental conditions at an identical subphase without monolayer. The reflectance absorbance spectra were calculated as $RA = lg(R / R_0)$.

RA spectra recorded at identical polarization and angles of incidence were averaged prior to data evaluation in order to minimize spectral contributions of water vapour absorptions and to improve the signal to noise (S/N) ratio. All spectra obtained in s-polarization were averaged for obtaining spectra with good S/N ratio being interpretable in terms of secondary structure and for the quantification of the amount of peptide present.

PRINCIPAL COMPONENT ANALYSIS OF IRRAS AMIDE I' BANDS

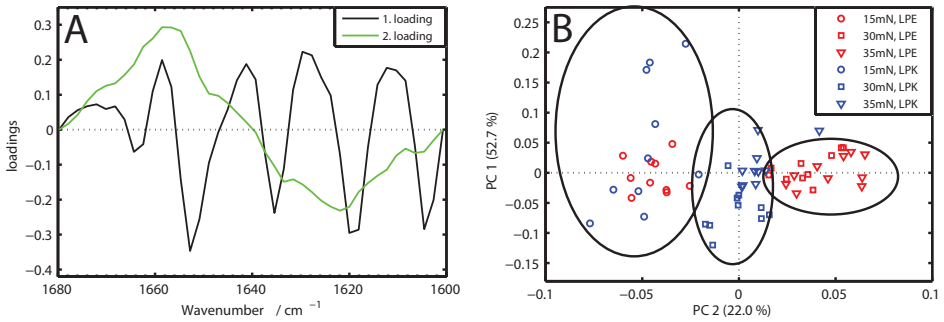

Figure A3. Results of PCA of normalized s-polarized IRRA spectra in the amide I' region of LPE and LPK containing monolayers at 15, 30, and 35 mN / m. A) Loadings of 1st (black) and 2nd (green) PC. B) Scores of 1st PC (PC 1) plotted over score of 2nd PC (PC 2), data points are colored according to used lipopeptide (LPE – red; LPK – blue). Symbol types represent the surface pressure during measurement (15 mN / m < π_{SO} – circle, 30 mN / m > π_{SO} – square, 35 mN / m > π_{SO} – triangle).

IRRA spectra were evaluated by a principal component analysis (PCA) performed by the MATLAB *princomp* function (statistics toolbox), on s-polarized spectra in the range of 1600 – 1680 cm^{-1}, after subtraction of a linear baseline. The intensity values of spectra recorded at various angles of incidence, surface pressure and film composition were written as row vectors and divided by their norm. Spectra recorded at the same experimental conditions were averaged before baseline subtraction and normalization. The normalized intensity vectors were then arranged in the rows of the matrix, which was analysed by PCA.

The PCA was performed on a set of spectra being recorded at monolayers containing LPE and monolayers containing LPK, at surface pressures of 15, 30 and 35 mN/m respectively and at different angles of incidence. This approach allows the determination of the spectral components that are necessary to describe the deviations from the mean of all analyzed spectra and to sort the spectra by their degree of similarity. The loadings of the first two principal components (PC 1 and PC 2) are shown in Figure A3. PC 1 contains mainly contributions of water vapor absorbtions while component 2 with its single positive maximum around 1659 cm^{-1} and a single negative maximum at 1622 cm^{-1} can be assigned to a spectral shift. Together both components account for ~75% of the spectral deviations from the mean. The analysis shows that the major difference between the spectra is their content in water vapor absorptions. This is due to the experimental difficulties to maintain constant ambient moisture above reference and sample trough and over the long time of the experiment. Furthermore, it explains that the spectra cannot be analyzed by more straight forward methods as second derivative spectroscopy or Fourier self deconvolution. The advantage of PCA is that it separates changes that are independent from each other. Thus in this case it reveals the more interesting variations in PC 2.

The graph shown in Figure A3 depicts the scores of PC 1 plotted against the scores of PC 2. It can be seen, that the points separate into three different groups with respect to their scores of the second principal component.

The first group, at score values for PC 2 < 0, contains all spectra that were taken at 15 mN / m with LPE or LPK in the monolayer, i.e. all spectra below the squeeze out pressures. In this group the score of component 1 scatters the most due to a less stable water vapor atmosphere in the beginning of the experiments. The negative score values of PC 2 show that these spectra below the squeeze out have more (negative) intensity around 1659 cm^{-1} and less (negative) intensity around 1622 cm^{-1} compared to the mean of all spectra. This means the spectra above π_{SO} are red shifted compared to spectra below the squeeze out.

This red shift shows that the band at 1653 cm^{-1} decreases in intensity upon squeeze out, which can be explained by the presence of less water-inaccessible amide bonds. The intensity increase at lower wavenumbers can be explained analogously by presence of more unstructured peptides or water accessible amide bonds. This shift therefore suggests that the secondary structure of most peptide molecules changes from helical to a more unstructured state upon squeeze out.

The points in the score plot in Figure A3 belonging to spectra above the squeeze out pressure clearly split up depending on the type of lipopeptide used. The scores of PC 2 with LPE containing monolayers are higher than the scores of PC 2 for LPK. This shows a higher (negative) intensity around 1622 cm^{-1} and a lower (negative) intensity around 1659 cm^{-1} (i.e. a red shift) in the LPE amide I' bands compared to the LPK amide I' bands. This difference shows that for LPE more amide C=O go from a hydrophobic shielded to a water accessible state and is therefore in common with a squeeze out of more peptide molecules in case of LPE compared to only a partial squeeze out of LPK.

DETAILED FITTING PROCEDURE OF AMIDE I' IRRAS BAND

The intensities of IRRAS bands strongly depend on the angle of incidence and the polarization (parallel – p or perpendicular – s to the plane of incidence) of the incident IR beam. These dependencies contain detailed information about the orientation of the transition dipole moment (TDM) of the absorbing moieties with respect to the monolayer normal. Fitting of the angle dependent absorbance can be achieved and yields molecular order parameters S, if additionally the angle α between the molecular axis and the transition dipole moment can be estimated.[59] Here, an extension of this approach was applied to calculate and fit the reflectance absorbance bands consisting of multiple overlapping spectral components as reported by Schwieger et al.[50]

The IRRAS band intensities and shapes are simulated assuming lorentzian absorption bands with the vibrational frequency n_0, the full width at half height

fwhh and the absorption coefficient *k*. Depending on the orientation of the transition dipole moment (TDM) within the molecule *α,* the tilt angle of the molecule with respect to the layer normal *θ*, the intensity varies with experimental parameters angle of incidence (AoI) and polarization (p or s) of the IR beam. Furthermore, the refractive index of the film *n* and the film thickness as well as the polarizer quality *Γ* have to be known to simulate complete reflectance-absorbance spectra. *Γ* was determined from independent measurements and set to 0.009 for all simulations. The frequency dependent refractive indices and absorption coefficients of the D_2O subphase are taken from Bertie et al.[60]

The parameters *n* and *d* were determined for each measurement by a fit of the D_2O absorption in the spectral range of 2300 - 2800 cm^{-1}. The spectra were then simulated with three bands: one C=O stretching vibrational band in the range of 1710 - 1752 cm^{-1} and two amide I' components at υ_1 = 1631 and υ_2 = 1651 cm^{-1}, accounting for amide bonds in hydrophilic and hydrophobic environment, respectively. For both components α was set to 38°.[61]

Prior to the fit of simulated spectra to the experimental data in the amide I' range, all spectra were offset at 1690 cm^{-1}. Next, the lipid C=O band intensity was estimated by adjusting the respective k value. Finally, the amide I' band of s- and p-polarized spectra and all measured AoI (see experimental section; total: 20 spectra) were fitted by means of a global non-linear least square method using a Levenberg-Marquardt algorithm, in the wavenumber range of 1620 – 1670 cm^{-1}. The helix tilt angle *θ*, as well as the absorption coefficients k_1 and k_2, and $fwhh_1$ and $fwhh_2$ of both amide I' components were free fitting parameters. To yield reliable and reproducible fits different starting values for the fitting parameters were tested. The resulting best fitting spectra are displayed together with the experimental data in Figure A4 to Figure A9.

Within the applied model[50,59] the tilt angle *θ* is calculated from the order parameter *S* under the assumption of a unimodal and small tilt angle distribution, according to: $S = \frac{3\langle \cos^2 \theta \rangle - 1}{2}$ In the result section of the paper both values are listed and discussed.

BEST FITTING MODELS AND EXPERIMENTAL AMIDE I' BANDS

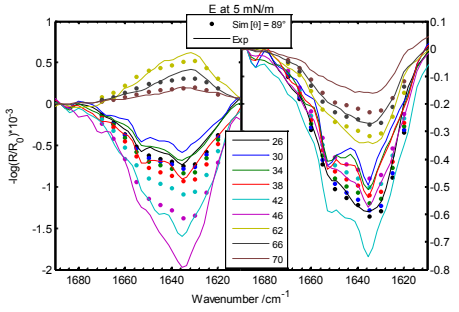

Figure A4. Experimental IRRAS amide I' bands (straight lines) and best fitting models (dots) of a DOPC, DOPE, Cholesterol (molar ratio 2 : 1 : 1) monolayer at 5 mN / m prepared on a PBS subphase containing 28 nM E peptide.

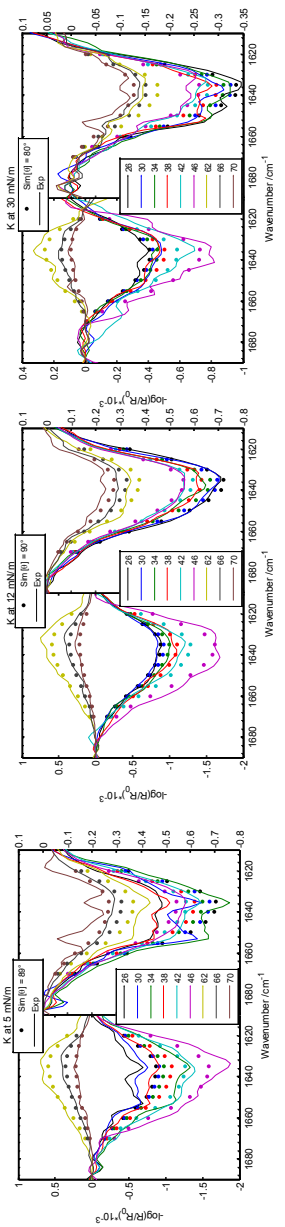

Figure A5. Experimental IRRAS amide I' bands (straight lines) and best fitting models (dots) of a DOPC, DOPE, Cholesterol (molar ratio 2 : 1 : 1) monolayer at 5 mN/m (left), 12 mN / m (middle) and 30mN/m (right) prepared on a PBS subphase containing 28 nM K peptide.

Figure A6. Experimental IRRAS amide I' bands (straight lines) and best fitting models (dots) of a DOPC, DOPE, Cholesterol (molar ratio 2 : 1 : 1) monolayer at 5 mN / m (left), 15 mN / m (middle) and 30 mN / m (right) prepared on a PBS subphase containing 28 nM E/K complex.

Figure A7. Experimental IRRAS amide I' bands (straight lines) and best fitting models (dots) of a DOPC, DOPE, Cholesterol (molar ratio 2 : 1 : 1) monolayer containing 4 mol% LPE at 15 mN / m (left), 30 mN / m (middle) and 35 mN / m (right).

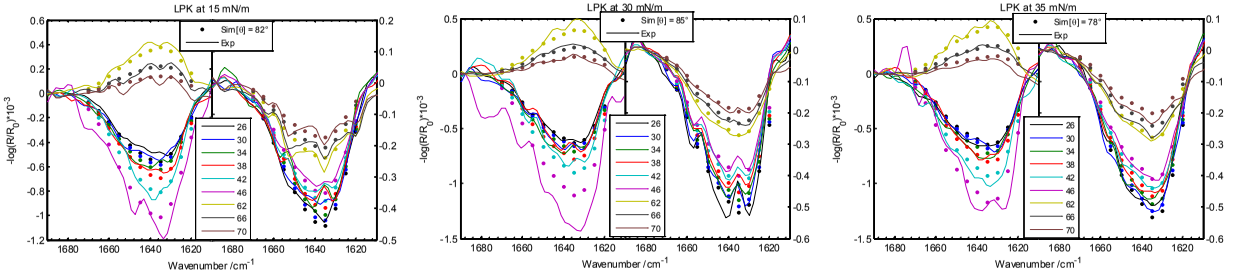

Figure A8. Experimental IRRAS amide I' bands (straight lines) and best fitting models (dots) of a DOPC, DOPE, Cholesterol (molar ratio 2 : 1 : 1) monolayer containing 4 mol% LPK at 15 mN / m (left), 30 mN / m (middle) and 35 mN / m (right).

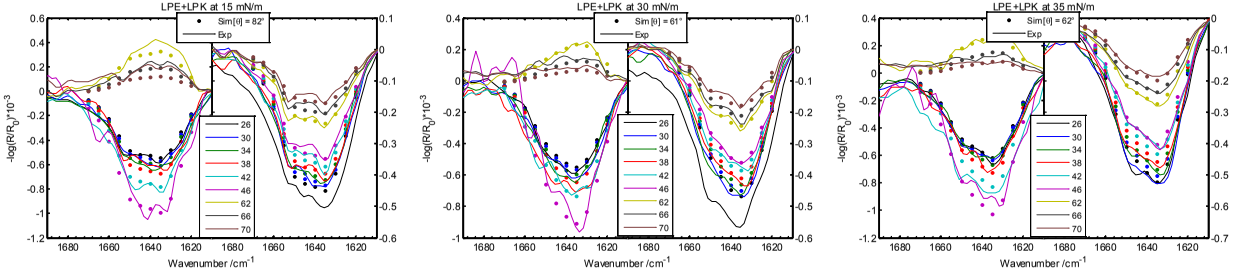

Figure A9. Experimental IRRAS amide I' bands (straight lines) and best fitting models (dots) of a DOPC, DOPE, Cholesterol (molar ratio 2 : 1 : 1) monolayer containing 2 mol% LPE and 2 mol% LPK at 15 mN / m (left), 30 mN / m (middle) and 35 mN / m (right).

Chapter IV

Insertion of an amphipathic coiled-coil peptide in lipid vesicles: Molecular details revealed by tryptophan fluorescence spectroscopy

ABSTRACT

Biological membrane fusion is achieved by complex mechanisms that involve concerted protein-protein and protein-membrane interactions. The synthetic model fusion system based on lipidated coiled-coil forming peptides LPE and LPK was proposed initially to be a minimal system that enables fusion of vesicles exclusively by peptide-peptide interactions. However, in a recent lipid monolayer study, evidence for additional interactions of the coiled-coil forming peptides with the membrane was found. The aim of this chapter is to study these peptide membrane interactions in a bilayer model system to gain insight into the interplay of peptide-peptide and peptide-membrane interactions. For this reason fluorescence emission and quenching as well as circular dichroism spectroscopy of tryptophan labeled E and K variants in the absence and presence of vesicles was examined. The positively charged K peptide is found to incorporate into the bilayers while E shows no interaction. The coiled coil formation is found to be in an equilibrium with this interaction. Interestingly, it is found that anchoring the peptide in the membrane strongly reduces the availability of K for coiled coil formation. These results support the hypothesis of an asymmetric behavior of the two peptides during fusion and raises new important questions for the mechanism of fusion which appears to be more complex than initially proposed.

INTRODUCTION

The ability to induce vesicle fusion of lipopeptides of the LPE/LPK type has been shown in numerous papers.[2-12] In these studies the formation of a coiled-coil complex between the outer membrane peptide moieties E: $(EIAALEK)_3$ and K: $(KIAALKE)_3$ is thought to be the main contribution that facilitates the merging of the bilayers. Variations of lipid anchors[8,11] and spacer lengths[13] were used, and were found to have different influences on the molecules ability to induce fusion. So far, the variation of the amino acid sequence led to fusogenic molecules only in the case of an increase of the number of heptad repeats of E and K,[9] which indicates that the specific sequence has a function other than simply facilitating coiled-coil formation that leads to vesicle docking.

It was shown in *Chapter III*, that the untethered free peptides E and K as well as the tethered lipopeptides LPE and LPK interact as helices with lipid monolayers of the composition commonly used in these vesicle fusion experiments.[14] In addition, the orientation of the helix parallel to the monolayer surface could be proven. The amphipathic moment in the helices is expected to orient in such a way that the hydrophobic face is directed towards the hydrophobic part of the monolayer. Peptide K, or the tethered LPK, was shown to interact much more strongly with the monolayers than E or LPE, which led to the hypothesis that in bilayer systems the peptides would be in different states compared to each other. Free or tethered K is expected to show a predominantly membrane bound helical state, whereas the weaker monolayer binding peptide E is expected to remain in the aqueous phase in an unordered state.

Different states of the peptides on the lipid interface would have a direct impact on the mechanistic details of lipopeptide mediated vesicle fusion. The direct interactions might lead to distortion of the bilayers and increased local curvature which is thought to promote the merging of lipid bilayers.[15-17] Furthermore, it would raise the question of the accessibility of the membrane bound peptide for the coiled-coil binding partner. This molecular recognition is thought to be responsible for the initial docking of vesicles prior to bilayer merging.[2,4,6,8,9] Another possibility is an inhibiting effect. A strong interaction of K with the membrane and burying of the hydrophobic side chains in the hydrophobic core of the bilayer might reduce the peptide's propensity to form coiled coils and to dock vesicles together. On the other hand the proposed asymmetric behavior of LPK and LPE might also provide a handle for the rational improvement of this fusion system, which therefore should be studied in detail in bilayer systems.

In most fusion studies using the LPE/LPK type lipopeptides or similar systems, circular dichroism spectroscopy (CD) is used to study the formation of the coiled coil complex. Homo coil formation (K/K, E/E) was usually made responsible for the helical content of the lipopeptides at the membrane prior to fusion. However

the proposed interaction of peptides with the bilayers is also accompanied by an increase in helical content. Therefore additional analytical methods are employed here in order to distinguish between these processes.

To test the hypothesis of the different states in lipid bilayers, variants of E, K, LPE and LPK that contain tryptophan residues are synthesized here, named E_{GW}, K_{GW}, LPE_{GW}, and LPK_{GW}. These variations allow the measurement of the tryptophan fluorescence emission for probing of the polarity of the environment, as well as measurement of the accessibility to quenchers in the aqueous environment.[18,19] The specific utilization of coiled-coil complexes containing the tryptophan label on just one binding partner allows the investigation of the equilibria between membrane binding and coiled-coil complex formation. Together with CD spectroscopy these data allow the confirmation of the asymmetric interaction hypothesis. Beyond that, the penetration depth of the free and tethered peptide K into the bilayer is estimated, by means of depth dependent fluorescence quenching using brominated lipids as quenchers.

RESULTS AND DISCUSSION

PEPTIDE DESIGN

A glycine and a tryptophan residue were added on the C-terminus of the original sequences of the peptides E and K, published by Litowski and Hodges[20] as they are used in numerous membrane fusion studies.[2,4-10] This yielded the peptide variants EGW: (Ac-(EIAALEK)$_3$-GW-NH$_2$) and KGW: (Ac-(KIAALKE)$_3$-GW-NH$_2$). Assuming a fully helical state this elongation does not break the hydrophobic moment and the tryptophan is located on the hydrophobic face (Figure 1). Fluorescence spectroscopy can be used to monitor changes in the polarity of the micro environment of the tryptophan as well as its accessibility to quenchers. These properties are expected to change upon coiled coil complex formation for hydrophobic residues in the center of the sequence. Therefore in order to probe changes originating from membrane binding events rather than from coiled complex formation the C-terminus was elongated and the tryptophan was placed at the end of the extended peptide chain. Thus the tryptophan is not expected to be on the hydrophobic binding site in the coiled coil complex. The C-terminus was chosen over the N-terminus to avoid possible effects arising from potential interactions with the PEG spacer or steric effects in the lipopeptides.

COILED COIL BINDING

The binding between E_{GW} and K_{GW} was studied using CD spectroscopy. The UV-CD spectrum of E_{GW}/K_{GW} at 25 °C is typical for peptides with high α-helical content,

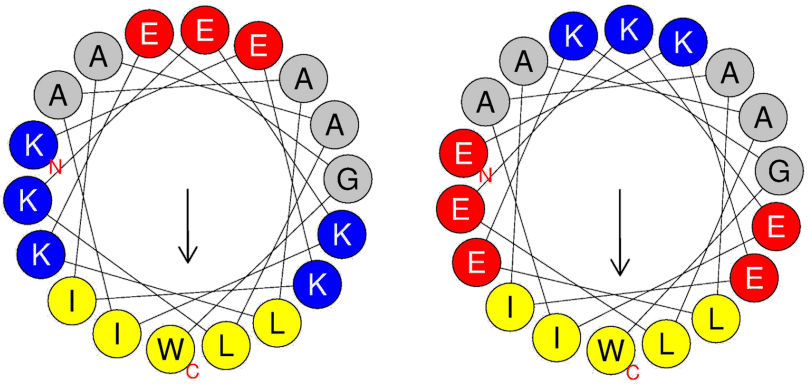

Figure 1. Helical wheel projection of the 18 C-terminal amino acids of K_{GW} (left) and E_{GW} (right).[1]

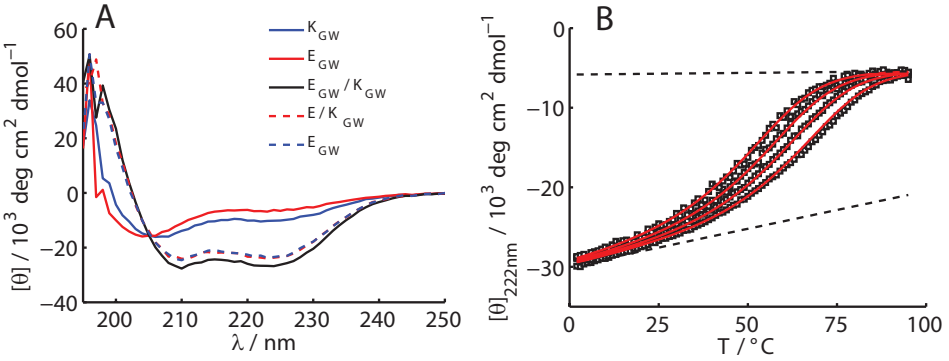

Figure 2. (A) CD spectra of E_{GW}, K_{GW}, and, the coiled coil complexes E_{GW}/K_{GW}, E/K_{GW} and K_{GW}/E at 50 µM total peptide concentrations and 25°C. Values in parenthesis are the helicities calculated from $[\theta]_{222nm}$ (B) CD thermal denaturation curves of E_{GW}/K_{GW} at [50 µM; 25 µM; 12.5 µM; 6.25 µM] total peptide concentrations (squares) and best fitting binding model (straight lines) and its baselines (dashed lines). The apparent T_M increases with the total peptide concentration.

showing two minima around 208 and 222 nm, while the spectra of the isolated peptides E_{GW} and K_{GW} show spectra typical for less helical structures (Figure 2A).[21-23] The helical content can be estimated from the ellipticity at 222 nm ($[\theta]_{222nm}$).[21,22] The helicity was found to increase from 21% and 33% for E_{GW} and K_{GW} respectively, to 83% for the E_{GW}/K_{GW} complex (Table 1). Also the formation of E_{GW}/K and K_{GW}/E complexes could be observed based on spectra representing high helical content with 74% and 75%, respectively (Figure 2A). Under the same conditions E, K, and E/K showed helicities of 21%, 23%, and 72% respectively (Table 1, spectra not shown). The increasing helical contents prove the interactions between the peptide chains that are accompanied by folding into more helical structures, i.e. formation of the coiled-coil complexes.

Table 1. Helicities of studied peptides and peptide mixtures

K_{GW}	33 %	E/K_{GW}	75 %
E_{GW}	21 %	E_{GW}/K	74 %
K	23 %	E_{GW}/K_{GW}	83 %
E	21 %	E/K	72 %

[total Peptide]=50 μM

The thermodynamics of folding for the E_{GW}/K_{GW} complex were studied by measuring the temperature and concentration dependencies of $[\theta]_{222nm}$ (Figure 2B). With increasing temperature $[\theta]_{222nm}$ increases, indicating that the coiled-coil complex unfolds. The shift of the apparent melting temperature T_M with increasing peptide concentration proves that the unfolding process involves more than one peptide chain (*Chapter II*).[24,25] The data was fitted by a dimeric A_1B_1 binding model as described in *Chapter II* and the folding constant K_f at 20 °C was found to be ~3.2 10^7 M^{-1} which is slightly higher than K_f = 5.5 10^6 M^{-1} of the unlabeled complex E/K (*Chapter VI*). In terms of Gibbs energy of folding (ΔG_f) this corresponds to -42.1 and -37.8 kJ / mol respectively. Litowski and Hodges reported ΔG_f = -40.2 kJ / mol for the original sequence of E/K, which is in line with the results reported here.[20] The slightly higher folding constant of E_{GW}/K_{GW}, might be caused by the increase of hydrophobic interactions due to an extended hydrophobic face or π-π- stacking of the C-terminal tryptophan residues.

Taken together these results show, that the C-terminal elongation of the peptides E and K by a glycine and a tryptophan residue did not perturb the oligomeric state of the coiled coil complex and had little influence on the binding strength between the two peptides. For the further investigation of the interactions of the peptides with lipid vesicles these small changes are considered to be negligible.

LIPID VESICLE BINDING

The binding of tryptophan labeled peptides K_{GW} and E_{GW} to vesicles was probed by their tryptophan fluorescence emission which strongly depends on the microenvironment of this residue.[18,19] In PBS buffer both, K_{GW} and E_{GW} show similar fluorescence emission spectra with the maxima of their emission (λ_{max}) at 345 nm. As was intended, the formation of the complexes E_{GW}/K and E/K_{GW} by addition of the respective binding partner in equimolar concentrations caused no significant changes in the spectra (Figure 3). Thus, the C-terminus of the peptides is not involved in the hydrophobic binding of the E_{GW}/K and K_{GW}/E coiled-coil complexes. Next, the lipid to peptide ratio was varied by addition of vesicles of the composition DOPE : DOPE : Cholesterol (2 : 1 : 1), as generally used in multiple vesicle fusion studies.[2-10] The concentration of the tryptophan labeled peptide [X_{GW}] was kept constant. The intensity of the emission of K_{GW} alone and bound in the complex E/K_{GW} increased with increasing lipid concentration, while λmax was blue

shifted (Figure 4) leading to the spectra at maximum lipid concentration shown in Figure 3. The emission spectra of E_{GW} and the complex E_{GW}/K were not affected significantly by vesicle addition. The blue shift and the intensity increase for K_{GW} and E/K_{GW} increase with increasing lipid to peptide ratios (Figure 4) and are an indication for a change of the environment of the tryptophan residue to a more apolar environment,[18,19] showing that the C-terminal tryptophan residue of K_{GW} gets inserted in the hydrophobic part of the lipid bilayer.

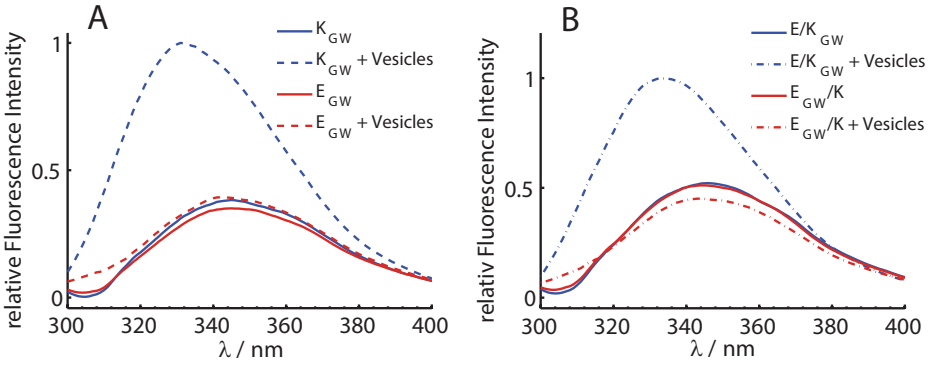

Figure 3. Fluorescence emission spectra of (A) peptides K_{GW} and E_{GW} in absence and presence of lipid vesicles and of (B) the peptide complexes E/K_{GW} and E_{GW}/K. Spectra with vesicles at [Lipid] : [X_{GW}]=2000:1 .

The fact that both an intensity increase and a blue shift of the spectra are also observed for E/K_{GW} but not for E_{GW}/K shows that there is no hydrophobic interaction of the peptide complex with the membrane but rather a competition between coiled-coil complex formation and K membrane interaction. The intensity increase is reduced for E/K_{GW} compared to K_{GW}, showing that the active concentration of K_{GW} available for membrane binding is reduced, due to E/K_{GW} complex formation. The binding of K_{GW} to the vesicles appears to be saturated at a [Lipid] : [X_{GW}] ratio of 1000:1 (Figure 4). Therefore for further measurements at constant lipid concentrations this ratio was chosen. For measurements with LPE_{GW} and LPK_{GW} a ratio of 100:1 was chosen because this is in the range of typical vesicle fusion experiments.[2-10]

The increase in fluorescence intensity was used to calculate the partition coefficient K_p between the bilayer and the aqueous environment according to equation (2) (Figure 5). The partition coefficient of K_{GW} was found to be ~6.2 10^3 M^{-1}, which is in range of partition coefficients found for amphipathic A helices binding to POPC membranes.[26] The apparent partition coefficient of K_{GW}/E is 1.7 10^3 M^{-1} and is therefore significantly lower than that found for K_{GW}. The binding of K_{GW} in the

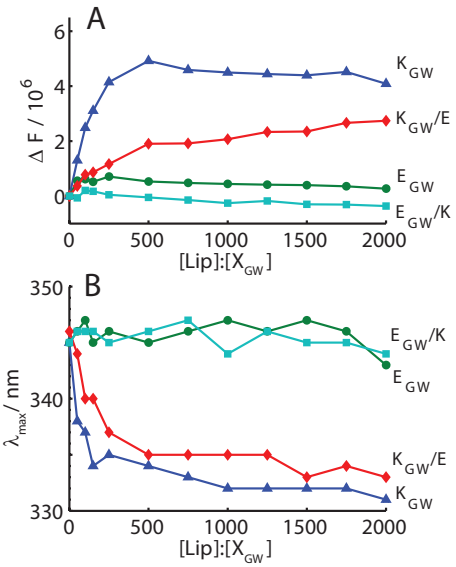

Figure 4. Increase of fluorecence intensity ΔF (A) and maximum of fluorescence emission λ_{max} (B) versus lipid to peptide ratio for peptides E_{GW}, K_{GW} and the complexes E_{GW}/K, E/K_{GW} mixed with vesicles.

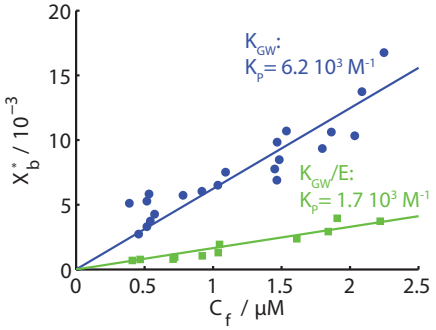

Figure 5. Apparent binding isotherms of K_{GW} and K_{GW}/E binding to DOPE : DOPE : Chol (2 : 1 : 1). X_b^* is the molar ratio of bound peptide per 60% total lipid and C_f the concentration of free peptide. Straight lines are linear fits of the data yielding as slope the displayed apparent partition coefficients K_p.

coiled-coil complex therefore reduces the amount of free peptide available for membrane binding, leading to a lower apparent partition coefficient.

FLUORESCENCE QUENCHING

The accessibility of the tryptophan side chain for the polar uncharged quencher acrylamide was measured. Acrylamide has good access to tryptophans that are not strongly hydrophobic shielded. The Stern-Vollmer plots show that acrylamide readily quenches the fluorescence of the peptides K_{GW} and E_{GW} when they are free in solution (Figure 6A & B). Similar Stern-Vollmer constants (K_{SV}) around 30 M^{-1} confirm good accessibilities of the aromatic side chains in E_{GW}, K_{GW}, E_{GW}/K, and E/K_{GW} in buffer (Table 2). When the untethered peptide K_{GW} was mixed with vesicles or when vesicle tethered lipopeptides LPK_{GW} were used, the quenching was less effective (Figure 6B) and the Stern Vollmer constants were significantly lowered (Table 2 & 3), which confirms that the tryptophan is incorporated into the membrane. Similarly, CD spectra of comparable systems revealed increased α-helical content at low lipid to peptide ratios of 100 : 1 (Table 2 & 3, Figure 6D). Thus, the membrane binding of peptide K_{GW} is associated with a folding of the peptide into a helical state.

Different states were found for E_{GW} mixed with vesicles, and for membrane tethered LPE_{GW}. The tryptophan moieties in both systems were readily water accessible as shown by effective quenching and high values for K_{SV} (Table 2 & 3, Figure 6A). Meanwhile the helical contents found

by CD spectroscopy were low for untethered E_{GW}, while they were increased for the tethered LPE_{GW} (Figure 6C). Thus, E_{GW} stays out of the lipid membrane and has unordered peptide chains. The increased helicity and relative good acrylamide accessibility of LPE_{GW} can be interpreted as a membrane unbound homo coiled-coil (cf. *Chapter V*).

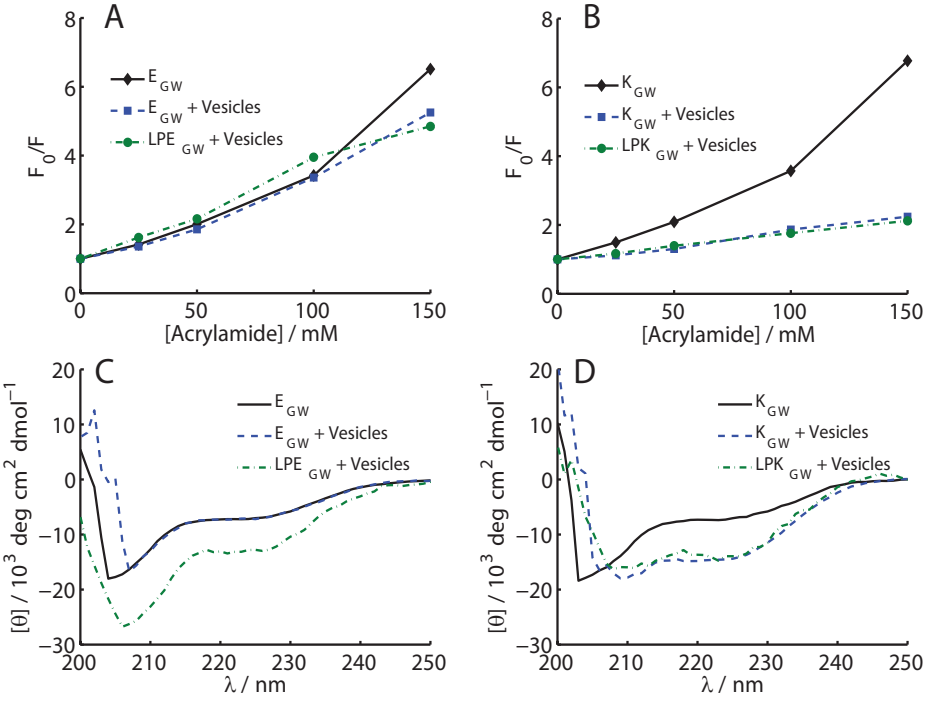

Figure 6. Tryptophan fluorescence quenching by acrylamide and CD spectra. Comparison of E_{GW}, with E_{GW} mixture with vesicles and vesicle tethered LPE_{GW} (A & C). Comparison of E_{GW} with E_{GW} mixture with vesicles and vesicle tethered LPE_{GW} (A & C). Comparison of K_{GW}, with K_{GW} mixture with vesicles and vesicle tethered LPK_{GW} (B & D). Fluorescence quenching experiments (A & B) were done at [Lipid] : $[X_{GW}]$ = 1000 : 1, [Lipid] : $[LPX_{GW}]$ = 100 : 1). CD experiments (C & D) were done at [Lipid] : $[X_{GW}]$ = [Lipid] : $[LPX_{GW}]$ = 100 : 1. Vesicles in all experiments are composed of DOPE : DOPE : Cholesterol (2 : 1 : 1).

Table 2. Stern Vollmer constants K_{SV} and helicities of peptides.

	K_{SV} / M^{-1}		Helicity / %	
	PBS[a]	Vesicles[a, b]	PBS[c]	Vesicles[c, d]
K_{GW}	33,4	8,2	23,0	45,7
K_{GW}/E	30,1	12,5	63,4	64,0
E_{GW}	31,7	26,0	22,5	22,6
E_{GW}/K	28,0	27,7	60,9	59,4

[a]$[X_{GW}]$=2.5 µM;[b] [Lipid]:$[X_{GW}]$=1000:1; [c][total Peptide]=5 µM; [d][Lipid]:[Peptide]=100:1

Table 3. Stern Vollmer constants and helicities of lipopeptides.

	K_{SV}/M^{-1} [a]	Helicity / %[a]
LPK_{GW}	7,5	44,1
LPK_{GW}/ E	8,0	42,0
LPE_{GW}	26,5	41,1
LPE_{GW}/K	23,2	52,8

[a]$[LPX_{GW}]$=2,5 µM, [Lipid]:$[LPX_{GW}]$= 100:1

Additionally fluorescence quenching and CD experiments were performed with E/K_{GW} and E_{GW}/K whose results are also summarized in Table 2 & 3. Both E/K_{GW} and E_{GW}/K show significant increases in helicity, in both the absence and presence of vesicles. Additionally, the accessibility of the tryptophan is increased for K_{GW}/E, while it is rather constant for E_{GW}/K. This is in common with an increased amount of membrane unbound peptide K_{GW} due to the coiled coil complex formation in the solution, while the accessibility for the tryptophan in E_{GW} does not change upon complex formation, because it is already fairly accessible, beforehand.

The addition of the binding partners K or E to the tethered lipopeptides LPE_{GW} and LPK_{GW} however, resulted in relatively little changes in the Stern Vollmer constants (Table 2), indicating that the state of the tryptophan labeled peptides does not change significantly. For the membrane unbound peptide LPE_{GW}, indeed no change in the acrylamide accessibility upon coiled complex formation is expected. However for LPK_{GW} this is an unexpected result, because a LPK_{GW}/E complex formation is expected to be accompanied by higher accessibility of the tryptophan, as it was the case for K_{GW}/E. Simultaneously, the helicity for LPK_{GW} is not changed significantly, while for LPE_{GW} it is increased when the binding partner is added (Table 2). Whether this increase is predominantly caused by K - membrane binding, coiled coil formation, or both cannot be answered with the current data.

The K_{GW}/E coiled coil complex formation in presence of vesicles clearly led to an increased accessibility of the tryptophan i.e. a significantly increased K_{SV} and a strong increase in α - helicity (Table 2). Furthermore the apparent K_P was reduced (Figure 5). The absence of these effects for LPK_{GW}/E in the presence of vesicles therefore indicates that the tethering to the membrane makes an increasing portion of the LPK_{GW} lipopetides inaccessible to coiled-coil formation.

To further test this, excess amounts of binding partners were added to K_{GW} and LPK_{GW} mixtures with vesicles, which yielded the fluorescence spectra shown in Figure 7. Increasing red shifts of the emission spectra were observed for untethered K_{GW}, while for tethered LPK_{GW} very subtle shifts were found. The red shift shows that fewer K_{GW} molecules are membrane bound upon higher E concentration, while many LPK_{GW} molecules stay in the membrane bound state. This increased inaccessibility for the binding partner might be caused by the simple fact that a portion of the lipopeptides is situated in the inner leaflet of the vesicles. Additionally, interactions of the peptide with the membrane might be enhanced by the tethering to the membrane interface as it was found while studying the interactions of LPK and LPE with lipid monolayers (*Chapter III*).

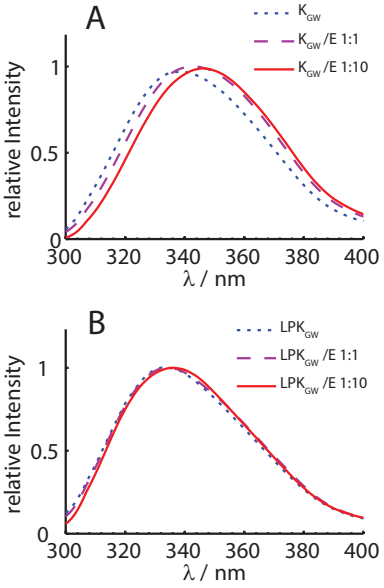

Figure 7. Fluorescence emission spectra of K_{GW} mixed with vesicles (A) and vesicle tethered LPK_{GW} (B) upon increasing concnetration of binding partner E. [Lipid] : [K_{GW}] = [Lipid] : [LPK_{GW}] = 100 : 1.

MEMBRANE BOUND QUENCHERS

To determine the penetration depth of K_{GW} and LPK_{GW} into the lipid bilayer, depth dependent fluorescence quenching experiments were performed, using the bromine modified 1-palmitoyl-2-(dibromo)stearoyl-PC lipids with bromine moieties at different positions on the acetyl chain (6, 7-; 9, 10-;11, 12-diBrPC). Both LPK_{GW} and K_{GW} are quenched most efficiently by bilayers containing the bromine lipids with the bromine incorporated at a relatively shallow position - 6,7-diBrPC (Figure 8A), which indicates that the tryptophan moieties are incorporated closest to this position. As a control, quenching of tryptophan in E_{GW} by the diBr-PCs was found to be minor which is as expected, because this peptide does not incorporate into the membrane as shown earlier.

Based on the known depth of the bromine labels in the used lipids,[27] two different methods can be used to estimate the distance of the tryptophan indole ring from the bilayer center.[28-30] It has to be assumed that the distance of the bromine moieties from the center of the bilayer is the same in the lipid bilayers used in the

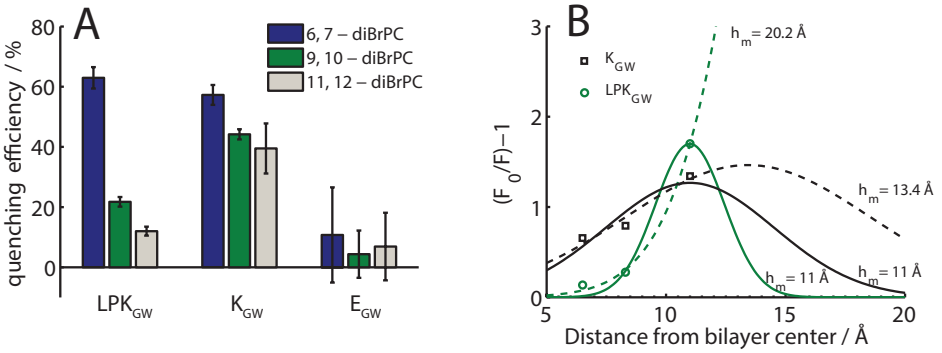

Figure 8. Tryptophan quenching efficiency of LPK_{GW}, K_{GW} and E_{GW} mixed with vesicles containing di-BrPC (A) Depth dependent quenching profiles of K_{GW} and LPK_{GW} with modeled profiles with the parameters displayed in Table 3. (B) Error bars represent 95% confidence intervals. Quenching vesicles were of the composition DOPE : di-BrPC : DOPE : Ch 1 : 1 : 1 : 1, the fluorescence without quencher F_0 was determined with vesicles of the composition DOPE : DOPE : Ch 2 : 1 : 1. [Lipid] : [K_{GW}] = 1000 : 1; [Lipid] : [LPK_{GW}] = 100 : 1.

present study as in pure di-BrPC bilayers, which were used for determination of the depth of the bromine labels. However precise determination of the bilayer thickness requires diffraction experiments and the available data in the literature is limited. McIntosh and Holloway determined, by x-ray diffraction, the headgroup distance in pure di-BrPC bilayers by x-ray diffraction to be ~40 Å for 6, 7- and 11, 12 – diBrPC.[27,28] Hung *et. al.* studied bilayers of a DOPE : Cholesterol (3:1) mixture in a fluid state, which is comparable to the mixture used in the present study and determined the distance between the phosphate groups to be ~40 Å as well,[31] showing that the assumption of equal thicknesses is reasonable. To determine the penetration depth of the tryptophan residues the parallax method (PM) can be applied using the fluorescence intensities of the strongest quenchers close to the fluorophore.[26,28,32,33] Using the results of 6,7- and 9, 10-diBrPC, PM yields distances of 12.4 Å and 20.2 Å of the indole ring of K_{GW} and LPK_{GW} from the center of the bilayer.

The second method, the distribution analysis (DA), is generally considered to better reflect the physics of the quenching, due to the disordered nature of the lipid bilayer. Also, it can be applied for quenchers with higher distances to the fluorophore as well as in cases of incomplete binding.[29,30,33-35] The depth dependent quenching profiles (QP) of LPK_{GW} and K_{GW} are depicted in Figure 8B and analyzed with Gaussian profiles. The parameters of these profiles are the most probable penetration depth of the fluorophore (h_m) i.e. the peak position, the transversal deviation (σ) reflected in the width, and the quenching efficiency (S) reflected in the area of the quenching profile. However, the data for depth dependent LPK_{GW} and K_{GW} quenching would be overfitted if all parameters were set free during regression, because the few available data points appear to be on the same flank of one Gaussian. Instead, the parameters h_m were fixed at different values to assess the influence on the fitted profiles and to evaluate the implications of the resulting models (Table 4). In this way reasonable simulations of the quenching profiles were obtained for $h_m \geq 11$ Å, the position of the most shallow quencher (Figure 8B). Therefore it can be concluded that the most probable depth of the tryptophans in the bilayer is not deeper than 11 Å from the bilayer center.

Fixing the parameter h_m at the values obtained from PM yielded a reasonable fit of the quenching profile for K_{GW}, while for LPK_{GW} a very large profile that appears unlikely if compared to profiles found in comparable quenching experiments was obtained.[29,30,33-35] However, if one directly compares the quenching profiles for K_{GW} and LPK_{GW} and their fits with $h_m = 11$ Å it becomes clear that the profile for LPK_{GW} must be more narrow than for K_{GW} i.e. σ must be significantly smaller, which might indicate less conformational freedom of the peptide.[33]

A shallow membrane incorporation of the tryptophan above 11 Å from the center is in line with the model of an insertion of the helical peptide parallel to the membrane

Table 4. Parameters used for distribution analysis.

	h_m / Å	σ/ Å	S / Å
K_{GW}	11,0[a]	3,5	11,2
	13,4[b]	5,1	18,8
LPK_{GW}	11,0[a]	1,4	6,1
	20,2[b]	4,1	222,3

[a]distance to the bilayer center of shallowest quencher; [b] Z_{cf} calculated by parallax method with F_1 and F_2 of the quenchers closest to the fluorophore

surface and with the hydrophobic face penetrating into the hydrophobic core of the bilayer. This can be conceived based on simple geometrical considerations as outlined in Figure 9. Assuming an α helical structure with a distance of the indole ring to the helical axis of ~8 Å the helix would be centered at a distance of 19 Å from the bilayer centre.[33] Based on the estimated phosphate to phosphate distance for the bilayer under study of 40 Å this means the helix center is close to the glycerol and phosphate groups of the lipids.

However, this estimation neglects the influence of the relative high conformational freedom of the C-terminal tryptophan. End fraying might lead to a distribution of different conformations in the membrane including deeper penetrations of a less ordered peptide. In a comparable study Mishra and Palgunachari studied amphiphatic mo-del peptides of class A_1, A_2 and Y with tryptophan moieties in the centre of the peptide sequence and on the hydro-phobic face and found relatively shallow incorporations as in the present study.[26] London and Ladhokin revised this quenching data using the DA method and determined $h_m = 9.0 - 9.4$ Å[33] which also implies a shallow in-corporation with the helical axis in the vicinity of the lipid glycerol backbone. Interestingly the A_1 helix, which most closely resembles the structure of peptide K_{GW} was found to incorporate the shallowest with $h_m = 9.4$ Å. The data was found to be in good agreement with x-ray diffraction data for another model peptide of class A incorporated into DOPC bilayers by Hristova et al.[36] The data found in the present study correlates well with these results and confirms that peptide K_{GW} exhibits interactions with the lipid bilayers as it is expected for the amphipathic class A helix.

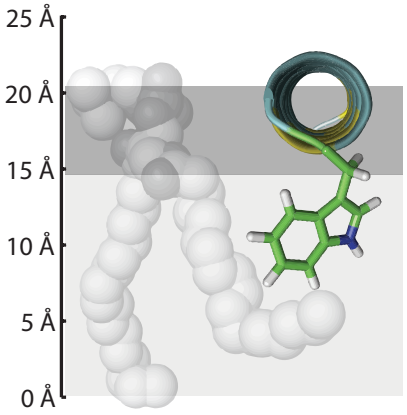

Figure 9. Simple model of K_{GW} in hypothtical fully helical state, incorporated in one mono-layer of the lipid membrane with hydrophobic face (yellow) towards acyl chain region. Pene-tration depth of tryptophan side chain is 11 Å as estimated from depth dependent fluorescence quenching experiments. View along the helix axis. Membrane structure with polar headgroup region (dark gray area) and acyl chain area (light gray area) based on DOPC x-ray diffraction data.[36] The orientation of lipids in the monolayer is illustrated for clarity.

CONCLUSIONS

The data reported here on the fluorescence emission of tryptophan for K_{GW} and LPK_{GW}, i.e. the shift of λ_{max}, the intensity increase, the reduced accessibility for quenchers in the aqueous phase, the quenching by membrane bound bromine and additionally the increase in α - helicity clearly prove the incorporation of K_{GW} and LPK_{GW} into the bilayers of vesicles. Conversely, the same data for E_{GW} and LPE_{GW} show that these peptides do not interact with the lipids. The fusion of vesicles as mediated by these lipopeptides is therefore an asymmetric process, because the involved peptides behave differently.

As expected the coiled-coil complex was not found to incorporate as a dimer into the bilayer and the formation of the complex was found to be able to compete with the membrane binding of untethered K_{GW}. Surprisingly, this was drastically reduced in case of the tethered LPK_{GW}, whose accessibility for the binding partner seemed to be very low. The binding of the peptide part of LPK_{GW} seems to be strengthened by the tethering to the lipid interface as was found in the monolayer experiments in *Chapter III*. This would imply that for vesicle docking prior to fusion of the membranes only low amounts of binding peptides are necessary.

The helix of K_{GW} incorporates to a relatively shallow depth into one leaflet of the lipid bilayer as shown by the depth dependent quenching. Together with snorkeling of the lateral lysine side chains as was proposed for amphiphatic A helices,[26,37-39] such a wedge-like incorporation can create high local curvatures in membranes which is a common mechanism to lower the energy barriers during the merging of lipid bilayers.[15-17]

This raises the question of whether the interaction of peptide K with the lipid is a critical element necessary for the membrane fusion. Conversely, it might be just a side effect that has no, or even an inhibiting, influence. One way to address this question would be targeted inhibition of the peptide membrane interaction by varying the amino acid sequence, as will be studied in *Chapter VI*. Finally, its answer will heavily improve our fundamental understanding of the lipopeptide mediated fusion process and open new possibilities to further improve this system.

EXPERIMENTAL SECTION

MATERIALS

Fmoc-protected amino acids and Sieber Amide resin for peptide synthesis were purchased from Novabiochem. DOPC (1, 2-dioleoyl-sn-glycero-3-phosphocholine), DOPE (1, 2-dioleoyl-sn-glycero-3-phosphoethanolamine), the di-BrPCs (1-palmitoyl-2-(m,n-dibromo)stearoyl-sn-glycero-3-phosphocholine with m, n = 6, 7; 9, 10; 11, 12) and cholesterol were purchased from Avanti Polar Lipids. Solvents, buffer salts

and acrylamide were purchased from Sigma-Aldrich. All water was ultrapure with resistance ≥ 18 MΘ cm^{-1} and TOC ≤ 2 ppm produced from a MilliQ Reference A+ purification system. All experiments were carried out in phosphate buffered saline (PBS) of the following composition: 150 mM NaCl, 20 mM PO_4^{3-} in H_2O at pH 7.4.

PEPTIDE SYNTHESIS

The peptides E: Ac-$(EIAALEK)_3$-NH_2, E_{GW}: Ac-$(EIAALEK)_3$GW-NH_2, K: Ac-$(KIAALKE)_3$-NH_2, and K_{GW}: Ac-$(KIAALKE)GW_3$-NH_2 were synthesized using standard Fmoc-chemistry on a Biotage Syro I and purified by RP-HPLC to yield a purity > 95% based on HPLC. Identity of the peptides was determined by LC-MS. The lipopeptides were synthesized and purified as described elsewhere.[2,8] Peptide stock solutions in PBS were prepared ~2 mg/ml and the concentration was determined by UV absorbance at 280 nm, for peptides without tryptophan the concentration was based on the mass. Lipopeptide stock solutions were prepared in $CHCl_3$:MeOH 3:1 solution and added to the lipids prior to solvent evaporation.

VESICLE PREPARATION.

Lipid stock solutions of the compositions DOPE : DOPE : Cholesterol (2 : 1 : 1) and DOPE : di-BrPC : DOPE : Cholesterol (1 : 1 : 1 : 1) were prepared in $CHCl_3$: MeOH 3 : 1. For experiments with lipopeptides stock solutions were mixed with LPX_{GW} stock solutions to yield mixtures with 1 mol% LPX_{GW}. Lipid films were created by slow evaporation of the solvents under N_2 stream and kept under vacuum overnight. The films were rehydrated with PBS yielding final lipid concentrations of typically 1 mM or 10 mM for vesicle titration experiments. Large unilamellar vesicles (LUVs) were formed by sonication at 55 °C for ~ 15 min. The size of the vesicles was tested by DLS using a Malvern Zetasizer nano-s and was typically found to be ~100 nm.

FLUORESCENCE SPECTROSCOPY

Tryptophan fluorescence emission was measured using a Tecan infinite M1000 pro plate reader. Excitation was 280 nm and emission was recorded in the range 300 - 450 nm using steps of 1 nm and bandwidths of 5 and 10 nm for excitation and emission. For each measurement 3 scans at 25 °C were averaged and corrected for scattering. Black Greiner 96 well plates were used.

For experiments with increasing lipid to peptide ratio mixtures of peptides at constant concentrations of tryptophan containing peptides $[X_{GW}]$ = 2.5 μM and increasing concentrations of lipid up to 5 mM were prepared with constant

volume of 200 µl. The complexes E_{GW}/K and E/K_{GW} where used at molar ratios 1 : 1 with [X_{GW}] = 2.5 µM. For determination of the highest partition coefficient of [K_{GW}] additional data points were collected with lipid concentrations up to 1.25 mM. The maxima of the emission λ_{max} were determined from adjacent average smoothed spectra. The data was interpreted as partition equilibrium.[26,40-42] The fluorescence intensities F in presence of vesicles were used to calculate the fraction of membrane bound peptide P_b by:

$$P_b = [X_{GW}] \frac{F - F_0}{F_\infty - F_0} \tag{1}$$

with the concentration of the tryptophan containing peptide [X_{GW}], F_0 the fluorescence intensity without vesicles. The fluorescence intensity when all peptide is membrane bound was obtained from extrapolation of a double reciprocal plot of F vs the lipid concentration [Lipid] to 1 / [Lipid] = 0. To obtain the partition coefficient K_p the data was linearly fitted to:

$$X_b^* = K_p C_f \tag{2}$$

where X_b^* is the molar ratio of bound peptide per accessible (outer leaflet ~60%) lipid and C_f the concentration of free (unbound) peptide.

For acrylamide quenching, peptides in absence or presence of vesicles [Lipid] : [X_{GW}] = 1000:1, were mixed with increasing concentrations of quencher yielding constant concentrations [X_{GW}] = 2.5 µM and V = 200 µl and increasing [Acrylamide] = 0…150 µM in each well. In quenching experiments with LPK_{GW} and LPE_{GW} concentrations were [LPX_{GW}] = 2.5 µM and [Lipid] : [LPX_{GW}] = 100:1. The fluorescence emission in presence F and in absence F_0 of quencher was fitted to yield the Stern-Vollmer constants K_{SV} by:

$$\frac{F_0}{F} = K_{SV}[Q] + 1. \tag{3}$$

For quenching with brominated lipids vesicles were composed of DOPE : diBr-PC:DOPE : Cholesterol 1 : 1 : 1 : 1, for the fluorescence intensity in absence of quencher F_0 DOPE : DOPE : Cholesterol 2 : 1 : 1 was used. Experiments were done at [LPX_{GW}] = 10 µM, [Lipid]:[LPX_{GW}] = 100:1 and [X_{GW}] = 2.5 µM [Lipid] : [X_{GW}] = 1000 : 1. The quenching efficiency QE was calculated by:

$$QE = \left(1 - \frac{F}{F_0}\right) \times 100\%. \tag{4}$$

To estimate the distance of the fluorophore from the center of the bilayer Z_{cf} the parallax method[26,28,32,33] was applied using the fluorescence intensities of shallower F_1 and deeper quencher F_2:

$$Z_{cf} = \frac{-\frac{1}{\pi C}\ln\left(\frac{F_1}{F_2}\right) - L_{21}}{2L_{21}} + L_{c1} \quad (5)$$

where C is the molar fraction per lipid area (~60 Å^2)[31], L_{2l} is the distance between deeper and shallower quencher, and L_{c1} is the distance between shallow quencher and bilayer center. For PM the fluorescence intensities of the two closest quenchers were used only. For application of the distribution analysis method (DA), the quenching profile QP as function of the distance to the bilayer center h was fitted by two symmetric Gaussians:

$$QP = \frac{F_0}{F} - 1 = \frac{S}{\sigma\sqrt{2\pi}} e^{-\frac{(h-h_m)^2}{2\sigma^2}} + \frac{S}{\sigma\sqrt{2\pi}} e^{-\frac{(h+h_m)^2}{2\sigma^2}} \quad (6)$$

the parameter h_m stands for the most probable distance between fluorophore and bilayer center, S is the areas and σ the dispersions of the Gaussians. Due to the limited amount of data values of h_m were fixed at different values, while leaving S and σ vary freely.

CIRCULAR DICHROISM SPECTROSCOPY

CD spectra were measured using a Jasco J815 CD spectrometer equipped with a Jasco PTC 123 peltier temperature controller. Quartz cuvettes with pathlengths l of 1, 2 and 5 mm were used. Peptide stock solutions were diluted with buffer to the desired total peptide concentrations and eventually mixed with vesicles at [Lipid] : [Peptide] = 100 : 1 at 5 µM total peptide concentration. Spectra of the lipopeptides tethered to vesicle were measured at [Lipid] : [LPX_{GW}] = 100 : 1 in 250 µM total lipid concentration and complementary peptide E or K was added [LPX_{GW}] : [Y_{GW}] = 1 : 1. Spectra were baseline corrected and the mean residue ellipticity [θ] was calculated by:

$$[\theta] = \frac{\theta}{l\, c_M\, N} \quad (7)$$

where θ is the observed ellipticity, l the pathlength, c_M the molar total peptide concentration and N the number of amino acids per peptide. The relative α - helicity rh was calculated from the ellipticity at 222nm $[\theta]_{222nm}$ by:[21,22]

$$rh = \frac{[\theta]_{222nm}}{-40\ 10^3\ \mathrm{deg\,cm^2\ dmol^{-1}}\ \left(1 - \frac{4.6}{N}\right)}\ 100\% \quad (8)$$

For temperature dependent unfolding experiments peptide stock solutions were diluted with buffer to the desired total peptide concentrations in the range 6 – 50 µM.

$[\theta]_{222nm}$ was measured as a function of temperature *T* in a 2 mm quartz cuvette at a heating rate of 40 °C / h in the range 2 – 95 °C. Additionally, CD spectra between 190 - 260 nm were collected at *T* = 5, 25 and 80 °C. Spectra taken at 5 °C before and directly after a full heating cycle were found to be fully reproducible. The data was analyzed by means of A_1B_1 binding model using the program *FitDis!* as described in Chapter II.

REFERENCES

(1) Gautier, R.; Douguet, D.; Antonny, B.; Drin, G., HELIQUEST: a web server to screen sequences with specific α-helical properties. *Bioinformatics* **2008**, *24*, 2101.

(2) Robson Marsden, H.; Elbers, Nina A.; Bomans, Paul H. H.; Sommerdijk, Nico A. J. M.; Kros, A., A Reduced SNARE Model for Membrane Fusion. *Angew. Chem. Int. Ed.* **2009**, *48*, 2330.

(3) Marsden, H. R.; Tomatsu, I.; Kros, A., Model systems for membrane fusion. *Chem. Soc. Rev.* **2011**, *40*, 1572.

(4) Tomatsu, I.; Marsden, H. R.; Rabe, M.; Versluis, F.; Zheng, T.; Zope, H.; Kros, A., Influence of pegylation on peptide-mediated liposome fusion. *J. Mater. Chem.* **2011**, *21*, 18927.

(5) Voskuhl, J.; Wendeln, C.; Versluis, F.; Fritz, E. C.; Roling, O.; Zope, H.; Schulz, C.; Rinnen, S.; Arlinghaus, H. F.; Ravoo, B. J.; Kros, A., Immobilization of Liposomes and Vesicles on Patterned Surfaces by a Peptide Coiled-Coil Binding Motif. *Angew Chem Int Edit* **2012**, *51*, 12616.

(6) Robson Marsden, H.; Korobko, A. V.; Zheng, T.; Voskuhl, J.; Kros, A., Controlled liposome fusion mediated by SNARE protein mimics. *Biomaterials Science* **2013**, *1*, 1046.

(7) Versluis, F.; Dominguez, J.; Voskuhl, J.; Kros, A., Coiled-coil driven membrane fusion: zipper-like vs. non-zipper-like peptide orientation. *Faraday Discuss.* **2013**, *166*, 349.

(8) Versluis, F.; Voskuhl, J.; van Kolck, B.; Zope, H.; Bremmer, M.; Albregtse, T.; Kros, A., In Situ Modification of Plain Liposomes with Lipidated Coiled Coil Forming Peptides Induces Membrane Fusion. *J. Am. Chem. Soc.* **2013**, *135*, 8057.

(9) Zheng, T. T.; Voskuhl, J.; Versluis, F.; Zope, H. R.; Tomatsu, I.; Marsden, H. R.; Kros, A., Controlling the rate of coiled coil driven membrane fusion. *Chem. Commun.* **2013**, *49*, 3649.

(10) Zope, H. R.; Versluis, F.; Ordas, A.; Voskuhl, J.; Spaink, H. P.; Kros, A., In vitro and in vivo supramolecular modification of biomembranes using a lipidated coiled-coil motif. *Angew Chem Int Ed Engl* **2013**, *52*, 14247.

(11) Meyenberg, K.; Lygina, A. S.; van den Bogaart, G.; Jahn, R.; Diederichsen, U., SNARE derived peptide mimic inducing membrane fusion. *Chem. Commun.* **2011**, *47*, 9405.

(12) Pahler, G.; Panse, C.; Diederichsen, U.; Janshoff, A., Coiled-Coil Formation on Lipid Bilayers-Implications for Docking and Fusion Efficiency. *Biophys. J.* **2012**, *103*, 2295.

(13) H. Zope, unpublished results

(14) Rabe, M.; Schwieger, C.; Zope, H. R.; Versluis, F.; Kros, A., Membrane Interactions of Fusogenic Coiled-Coil Peptides: Implications for Lipopeptide Mediated Vesicle Fusion. *Langmuir* **2014**, *30*, 7724.

(15) Campelo, F.; McMahon, H. T.; Kozlov, M. M., The hydrophobic insertion mechanism of membrane curvature generation by proteins. *Biophys. J.* **2008**, *95*, 2325.

(16) Kozlov, M. M.; McMahon, H. T.; Chernomordik, L. V., Protein-driven membrane stresses in fusion and fission. *Trends Biochem. Sci.* **2010**, *35*, 699.

(17) McMahon, H. T.; Kozlov, M. M.; Martens, S., Membrane Curvature in Synaptic Vesicle Fusion and Beyond. *Cell* **2010**, *140*, 601.

(18) Eftink, M. R. In *Methods Biochem. Anal.*; John Wiley & Sons, Inc.: 2006, p 127.

(19) Lakowicz, J. R. *Principles of Fluorescence Spectroscopy*; Springer, 2007.

(20) Litowski, J. R.; Hodges, R. S., Designing heterodimeric two-stranded alpha-helical coiled-coils. Effects of hydrophobicity and alpha-helical propensity on protein folding, stability, and specificity. *J. Biol. Chem.* **2002**, *277*, 37272.

(21) Chen, Y.-H.; Yang, J. T.; Chau, K. H., Determination of the helix and β form of proteins in aqueous solution by circular dichroism. *Biochemistry* **1974**, *13*, 3350.

(22) Gans, P. J.; Lyu, P. C.; Manning, M. C.; Woody, R. W.; Kallenbach, N. R., The helix–coil transition in heterogeneous peptides with specific side-chain interactions: Theory and comparison with CD spectral data. *Biopolymers* **1991**, *31*, 1605.

(23) Greenfield, N. J., Using circular dichroism spectra to estimate protein secondary structure. *Nat Protoc* **2006**, *1*, 2876.

(24) Breslauer, K. J. In *Methods Enzymol.*; Michael L. Johnson, G. K. A., Ed.; Academic Press: 1995; Vol. Volume 259, p 221.

(25) Doyle, C. M.; Rumfeldt, J. A.; Broom, H. R.; Broom, A.; Stathopulos, P. B.; Vassall, K. A.; Almey, J. J.; Meiering, E. M., Energetics of oligomeric protein folding and association. *Arch. Biochem. Biophys.* **2013**, *531*, 44.

(26) Mishra, V. K.; Palgunachari, M. N., Interaction of Model Class A1, Class A2, and Class Y Amphipathic Helical Peptides with Membranes. *Biochemistry* **1996**, *35*, 11210.

(27) McIntosh, T. O.; Holloway, P. W., Determination of the depth of bromine atoms in bilayers formed from bromolipid probes. *Biochemistry* **1987**, *26*, 1783.

(28) Chattopadhyay, A.; London, E., Parallax method for direct measurement of membrane penetration depth utilizing fluorescence quenching by spin-labeled phospholipids. *Biochemistry* **1987**, *26*, 39.

(29) Ladokhin, A.; Holloway, P. W.; Kostrzhevska, E. G., Distribution analysis of membrane penetration of proteins by depth-dependent fluorescence quenching. *J Fluoresc* **1993**, *3*, 195.

(30) Ladokhin, A. S. In *Methods Enzymol.*; Ludwig Brand, M. L. J., Ed.; Academic Press: 1997; Vol. Volume 278, p 462.

(31) Hung, W.-C.; Lee, M.-T.; Chen, F.-Y.; Huang, H. W., The Condensing Effect of Cholesterol in Lipid Bilayers. *Biophys. J.* **2007**, *92*, 3960.

(32) Killian, J. A.; Keller, R. C. A.; Struyve, M.; De Kroon, A. I. P. M.; Tommassen, J.; De Kruijff, B., Tryptophan fluorescence study on the interaction of the signal peptide of the Escherichia coli outer membrane protein PhoE with model membranes. *Biochemistry* **1990**, *29*, 8131.

(33) London, E.; Ladokhin, A. S. In *Curr. Top. Membr.*; Sidney A. Simon, T. J. M., Ed.; Academic Press: 2002; Vol. Volume 52, p 89.

(34) Ladokhin, A. S.; Holloway, P. W., Fluorescence of membrane-bound tryptophan octyl ester: a model for studying intrinsic fluorescence of protein-membrane interactions. *Biophys. J.* **1995**, *69*, 506.

(35) Ladokhin, A. S., Measuring membrane penetration with depth-dependent fluorescence quenching: Distribution analysis is coming of age. *Biochimica et Biophysica Acta (BBA) - Biomembranes* **2014**, *1838*, 2289.

(36) Hristova, K.; Wimley, W. C.; Mishra, V. K.; Anantharamiah, G. M.; Segrest, J. P.; White, S. H., An amphipathic α-helix at a membrane interface: a structural study using a novel X-ray diffraction method. *J. Mol. Biol.* **1999**, *290*, 99.

(37) Varkey, J.; Isas, J. M.; Mizuno, N.; Jensen, M. B.; Bhatia, V. K.; Jao, C. C.; Petrlova, J.; Voss, J. C.; Stamou, D. G.; Steven, A. C.; Langen, R., Membrane Curvature Induction and Tubulation Are Common Features of Synucleins and Apolipoproteins. *J. Biol. Chem.* **2010**, *285*, 32486.

(38) Segrest, J. P.; Deloof, H.; Dohlman, J. G.; Brouillette, C. G.; Anantharamaiah, G. M., Amphipathic Helix Motif - Classes and Properties. *Proteins* **1990**, *8*, 103.

(39) Mishra, V. K.; Palgunachari, M. N.; Segrest, J. P.; Anantharamaiah, G. M., Interactions of synthetic peptide analogs of the class A amphipathic helix with lipids. Evidence for the snorkel hypothesis. *J. Biol. Chem.* **1994**, *269*, 7185.

(40) Schwarz, G.; Stankowski, S.; Rizzo, V., Thermodynamic analysis of incorporation and aggregation in a membrane: Application to the pore-forming peptide alamethicin. *Biochimica et Biophysica Acta (BBA) - Biomembranes* **1986**, *861*, 141.

(41) Beschiaschvili, G.; Seelig, J., Melittin binding to mixed phosphatidylglycerol/phosphatidylcholine membranes. *Biochemistry* **1990**, *29*, 52.

(42) Gazit, E.; Boman, A.; Boman, H. G.; Shai, Y., Interaction of the Mammalian Antibacterial Peptide Cecropin P1 with Phospholipid Vesicles. *Biochemistry* **1995**, *34*, 11479.

Chapter V

The interplay between membrane interaction and homo-coiling of coiled-coil peptides on the membrane studied by temperature dependent FTIR and CD spectroscopy

ABSTRACT

Knowledge of the structure of the fusogenic membrane tethered peptides E and K is a key element in the understanding of their role in membrane fusion. Special conditions can be found at the interface of the membrane, where the peptides are confined in close proximity to other peptide molecules as well as to the lipid interface. Consequently, different possible structural states were proposed for the peptides when tethered to this interface. Due to the multitude of possible states, the determination of the structure solely on the basis of circular dichroism spectra at a single temperature can be misleading. Also it has not been possible so far to unambiguously distinguish between the membrane bound and the coiled-coil state of these peptides by means of infrared spectroscopy (IR) using IR reflection absorbtion spectroscopy, due to very similar amide I' bands. Here, the molecular basis of this similarity is investigated by means of site-specific ^{13}C labeled FTIR spectroscopy. Structural similarities between the amphipathic membrane interacting helix of K and the amphipathic coiled-coil forming helix of E are shown to cause the similar spectroscopic properties. Furthermore the peptide structure is investigated using temperature dependent CD and IR spectroscopy and it is shown that the different states can be distinguished on the basis of their thermal behavior. These results will prove useful in further investigation of the membrane fusing lipopeptides as they form the basis for an unequivocal determination of the peptide state by easy spectroscopic methods.

INTRODUCTION

Membrane tethered coiled-coil forming lipopeptides have been examined extensively in different studies[1-12] and in the previous chapters due to their ability to induce lipid membrane fusion. The systems apparent simplicity and possible applications[8,9] have raised a particular interest to conceive the mechanism of lipopeptide mediated fusion. The binding state and secondary structure of the peptide molecular recognition units E: $(EIAALEK)_3$-NH_2 and K: $(KIAALKE)_3$-NH_2 when tethered to the membrane are crucial for understanding of this mechanism.

Circular dichroism (CD) spectroscopy is often used in fusion studies to estimate the helical content of the peptides. Generally, the vesicle tethered lipopeptides exhibit increased helical contents compared to their untethered equivalents E and K (*Chapter IV*).[1-8] The increased helical content has often been attributed to the formation of homo-coils EE and KK at the membrane, but is without distinct experimental proof. However, it has been shown in *Chapters III* & *IV* that the helical content of membrane tethered peptide K can be explained by its interactions with the membrane which induces the formation of a monomeric amphipathic A helix.[13] This shows the ambiguity of the CD method in the case of complex systems and demonstrates the necessity of further analytical methods to study them.

Typical CD spectra of α-helices exhibit two minima around 208 and 222nm (cf. *Chapter II* & *IV*). Due to the low absolute ellipticity of other secondary structure elements at this position, the mean residual ellipticity at 222 nm ($[\theta]_{222nm}$) is a convenient measure for helical content.[14,15] However by using $[\theta]_{222nm}$ only, it is not possible to distinguish whether the origin of this helicity is due to coiled-coil complex formation or folding into a single α helix. A second criterion which is commonly used in the characterization of coiled-coil complexes by CD is the ratio $[\theta]_{222nm}$ / $[\theta]_{208nm}$.[16,17] However $[\theta]_{208nm}$ is often perturbed in experiments with vesicles, due to light scattering in this wavelength region. Also, the ratio $[\theta]_{222nm}/[\theta]_{208nm}$ might lead to inconclusive results in systems with coexisting unordered peptide chains. However, the monitoring of peptide melting curves by means of CD spectroscopy was proven to allow for distinctive conclusions on the molecularity of peptide unfolding processes (*Chapter II*) and therefore poses a promising approach to distinguish coiled-coil formation from peptide membrane interaction.

An additional convenient method for the study of peptide and protein structures is Fourier transform infra-red (FTIR) spectroscopy. The position of the amide I band which mainly originates from the carbonyl stretching vibration of the peptide bond is known to strongly depend on its secondary structure.[18] In D_2O this band is usually referred to as amide I'. Coiled-coils have been shown to

exhibit characteristic amide I' bands with two main components, which are not observed for single helices.[19-23] This pattern is caused by the different accessibility of the amide carbonyls for the solvent. Coiled-coils are amphipathic helices, due to the arrangement of hydrophobic (h) and polar (*p*) amino acids in the so called heptad repeat: *hpphppp*. The positions in this pattern are denoted *abcdefg* (Chart 1). The carbonyls on the hydrophilic face, especially in the *b*, *c*, and *f* position of the heptad repeat can form additional hydrogen bonds with the solvent and absorb ~20 cm^{-1} lower than the amides on the hydrophobic face.[22,23] Surprisingly, a similar pattern was also found in amide I' bands of peptide K interacting with lipid monolayers using infrared reflection absorption spectroscopy (IRRAS, *Chapter III*). As an interaction of the peptide as the homomeric coiled-coil complex with the membrane seems unlikely, it was hypothesized that the pattern arises from a different accessibility of the carbonyls to water, caused by the shallow insertion of the single amphipathic A helix. This hypothesis allowed fitting of the angle dependency of the IRRA spectra, yielding the model of the helix insertion parallel to the membrane interface. Although a coherent bigger picture resulted from this approach, the origin of the two band pattern in the lipid bound form of K remains questionable, also due to sparse reports of comparable effects in literature.[24-27] Therefore, further investigations towards the IR spectroscopic properties of the membrane incorporated

Chart 1. Chemical structures of CPK and CPE lipopeptides used in this study and helical wheel profection of E/K coiled-coil complex.

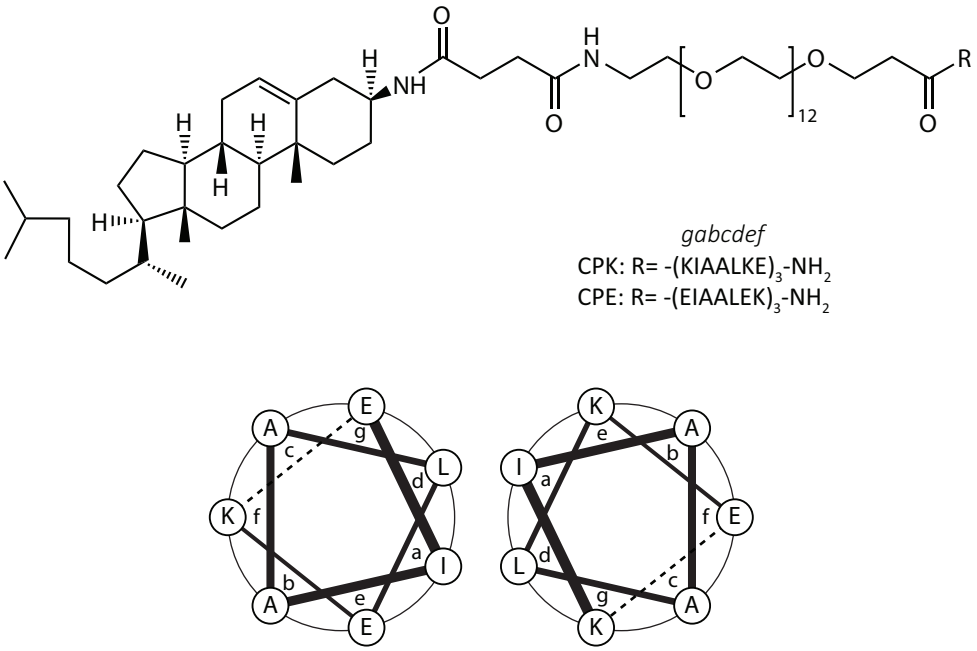

state of K together with an unequivocal band assignment are necessary to substantiate the helix insertion model. The latter can be done by site specific labeling of the amide with ^{13}C, which is a convenient way to gain structural information for peptides at the residue level.[22,28-34]

In this chapter a combination of CD melting curves and temperature dependent IR spectra is applied to the coiled-coil forming peptides E, K and their lipid tethered equivalents. The lipid tethers in this study are made by cholesterol connected via a polyethylene glycol (PEG_{12}) spacer to the peptide moieties (lipopeptides CPE, CPK; Chart 1). It is shown that a detailed analysis by means of singular value decomposition (SVD)[35-37] of these temperature dependencies can shed light on the intrinsic temperature dependencies of the amide I' two band pattern and reveals structural properties of the peptides. Additional evidence is presented to support the model of the homo-coiling of peptide E on the membrane surface. Furthermore, the origin of the low absorbing amide I' component is determined by studying ^{13}C labeled peptide K.

RESULTS AND DISCUSSION

CD OF FREE PEPTIDES AND VESICLE TETHERED LIPOPEPTIDES

Melting curves of peptides, monitored by CD spectroscopy have been shown to contain relevant information about the molecularity of the peptide unfolding (*Chapter II*). The CD unfolding curves of untethered peptides E and K in the absence and presence of vesicles and tethered to the vesicle interface were measured (Figure 1). In these and all further experiments the lipid composition was DOPE : DOPE : Cholesterol (2 : 1 : 1), and the buffer was phosphate buffered saline (PBS, pH 7.4). It is shown in *Chapter VI* that the free peptides E and K exhibit shifts of the melting curves towards lower temperatures with decreasing peptide concentration, showing that the observed process is the unfolding of a homomeric coiled-coil complex.[38,39]

In a mixture with vesicles the $[\theta]_{222nm}$ of K was significantly lower over the complete temperature regime, i.e. the helical content was increased (Figure 1A). This is caused by the interaction of the peptide with the lipid bilayer which is accompanied with its folding into an amphipathic helix. Compared to the experiment without vesicles, the shape of the curve appears almost linear with a shallower, uniform slope. In peptide folding studies similar linear increases of folded coiled-coils are often considered as an intrinsic temperature induced change of the optical properties of the helix that does not relate to significant structural change.[40] Another possibility is that it is caused by non-cooperative changes such as end fraying of helices.[41,42]

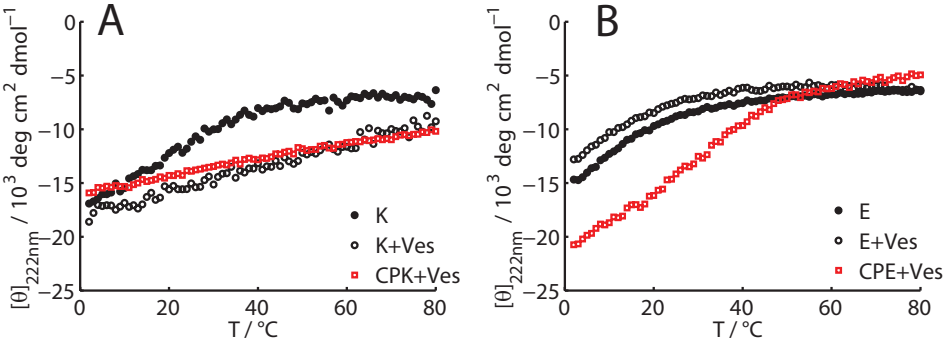

Figure 1. Temperature dependency of ellipticity at 222 nm for (A) K in buffer, K mixed with vesicles, and CPK tethered to vesicles, and for (B) E in buffer, E mixed with vesicles, and CPE tethered to vesicles. Experimental conditions: total peptide concentrations [E] = [K] = 40 μM; [CPE] = [CPK] = 20 μM; [lipid] : [peptide] = [lipid] : [lipopeptide] = 50 : 1. All measurements in PBS.

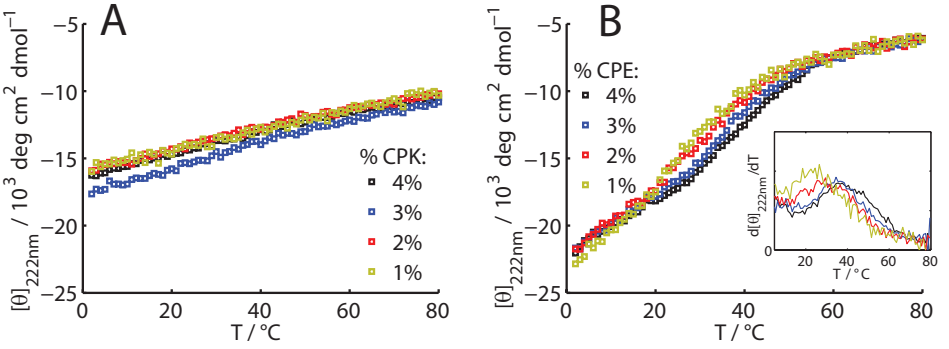

Figure 2. Temperature dependecy of ellipticity at 222nm for (A) CPK and (B) CPE tethered to lipid vesicles at varying molar fractions (total lipid concentration in all experiments 1 mM, in PBS).

In contrast, E in a mixture with vesicles shows a very similar $[\theta]_{222nm}$ curve to the lipid free solution (Figure 1B). The slight shift to higher values is attributed to an artifact caused by light scattering by the vesicles. Thus, the untethered E shows no interactions with the vesicles that induce the formation of a helix.

The membrane tethered CPK also shows decreased $[\theta]_{222nm}$ over the measured temperature range and closely resembles K mixed with vesicles indicating similarities in the structures and binding states of the peptides (Figure 1A). Based on $[\theta]_{222nm}$ at 25 °C the helicity was found to be 45% and 48% for K and CPK respectively. Assuming that all peptides are membrane bound this would imply that the peptides are only partially folded as a helix. However, from this data one cannot determine whether the observed helicity originates from a single state, populated by all peptide molecules or multiple states, differently populated.

CPE, in contrast, shows a $[\theta]_{222nm}$ curve that differs from its untethered equivalents (Figure 1B). A lower ellipticity was found that increases up to ~50 °C where the curve approaches those of the untethered peptides. This increase in helical content is generally attributed to the homo-coiling of the peptides (*Chapter IV*).[1-8] To scrutinize this, further experiments were performed by varying the lipopeptide concentration (Figure 2). CPK showed no significant changes in the temperature dependent $[\theta]_{222nm}$ with concentration change. In contrast, the $[\theta]_{222nm}$ curves of CPE shifted slightly to lower temperatures with decreasing concentration. The derivatives do not consist of a single peak indicating that the observed transition is not a simple two state unfolding. Consequently, fitting the data with several cooperative melting models with molecularities in the range $n = 2…5$ as described in *Chapter II* yielded insufficient results (data not shown). The maxima in the first derivative also illustrates the shift of the apparent melting temperature T_m (Figure 2B, inset). Therefore it shows that the unfolding of the peptide on the membrane is of a molecularity bigger than 1, meaning it is a coiled-coil complex.

The folded fraction (α) of peptide can be determined from the ellipticities at fully folded (θ_F) and fully unfolded (θ_u) states. Assuming values for a coiled coil with high helical content[15] of θ_F = 32,000 deg cm^2 dmol^{-1}, and θ_u = -5,000 deg cm^2 dmol^{-1} the value of $[\theta]_{222nm}$ at 25 °C of CPE 1 mol% suggests that more than 37% of the CPE molecules are folded as homo coils in a standard vesicle fusion experiment.

The melting of the untethered peptides E and K in buffer proved, that they are able to form homo coils at relatively low folding constants K_F compared to the E/K hetero coil (cf. *Chapter II* & *VI*). However, when tethered to the interface of the vesicles the local peptide concentration is drastically increased, leading to a dramatically increased T_m of CPE compared to the untethered E, despite the fact that the overall concentration is lower (Figure 1B). Using the experimental conditions of the melting curves in Figure 1B this effect can be illustrated: the mean molecular density in a 40 µM solution of untethered E is ~24000 molecules / µm^3, which is slightly less than the number of peptides that are confined to the lipid bilayer interface (~33000 molecules / µm^2) at 2% lipopeptide concentration and an average area of 60 Å^2 per lipid. Considering that one lipid leaflet including its direct aqueous periphery is only ~5 nm thick, it is clear that this corresponds to an immense agglomeration of molecules and thus to a high local concentration. This explains the substantial amount of homo coiling of CPE on the vesicles.

IR SPECTROSCOPY OF PEPTIDES IN SOLUTIONS

FTIR spectroscopy is a common technique to estimate the secondary structure of peptides and proteins, because the position of the amide I' band is strongly

influenced by its secondary structure and hydrogen bond formation. Also, the melting processes that were followed by CD spectroscopy are expected to manifest in this band.[33,37,43]

First, the IR spectra of E, K and EK in PBS prepared from D_2O (d-PBS) were measured at 5 °C. At a total peptide concentration of 1 mM these peptides are expected to predominantly exist in the coiled-coil state at low temperatures. Accordingly, the amide I' bands of the peptides are all dominated by two main components at ~1630 cm^{-1} and ~1649 cm^{-1}, which is a typical pattern for coiled-coils (Figure 3, Table 1). The origin of the additional small component at 1668 cm^{-1} is most probably residual trifluoroacetic acid (TFA) from the peptide purification. Additionally at 1564 cm^{-1} the carbonyl stretching mode of the glutamic acid side chains can be found.

The positions of the underlying components in the amide I' band were determined from the maxima in the smoothed second derivative and the shape of the bands could be adequately fitted with three Gaussians in these positions (Figure 3, Table 1). Unless otherwise stated all band fitting procedures yielded well separated peaks according to the 95% confidence intervals (Table 1 and Table 2). The lower relative absorbance ratios of the two main components at 1630 cm^{-1} and 1649 cm^{-1} (A_1 / A_2, Table 1) of E and K compared to E/K might arise from contributions of unordered structures. These are expected to overlap as a broad band centered at ~1645 cm^{-1} (see below) and cannot be resolved in this manner. The addition of more than three bands will also result in an adequate description of the band shape and underlying hidden contributions cannot be excluded. For instance Pähler et. al. used five strongly overlapping bands to describe the amide I' band of an E/K variant tethered to a supported lipid bilayer.[12] However these bands appear overfitted and the authors state no rationale for this model. Since the simpler pattern with two main bands reported here can be explained with a consistent physical model, this interpretation is used in the following.

The two main components of the amide I' band originate from the heterogeneous environment of the helix in the coiled coil.[19-23,26,44] The frequency of the amide I' band is known to shift down by ~20 cm^{-1} per hydrogen bond to the amide carbonyl. The carbonyls on the hydrophobic face of the coiled-coil form exclusively intra-molecular hydrogen bonds in the common i to i + 4 manner. On the other side, carbonyls on the hydrophilic face are available for one additional hydrogen bond from the solvent, which lowers their frequency.

To test this model, a variant of K was synthesized with the alanine residues situated in the b and c position of the heptad repeat containing ^{13}C labeled carbonyls (^{13}CK). The isotope effect is known to specifically lower the amide I' position of the

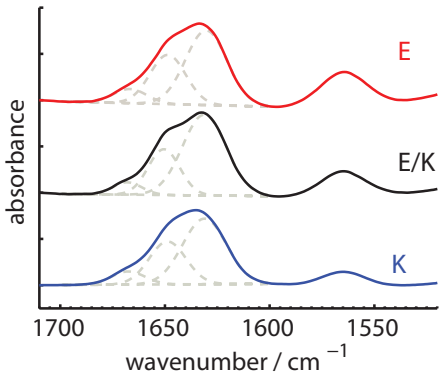

Figure 3. FTIR spectra of E, EK and, K at 5°C (solid lines) and fits of the amide I' bands with gaussians (broken lines) [peptide]= 1 mM, in d-PBS.

labeled residue by 35 - 40 cm^{-1}.[22,28-34] The IR spectra of ^{13}CK and E/^{13}CK at 5 °C showed strongly reduced intensities at 1630 cm^{-1} compared to their unlabeled equivalents K and E/K (Figure 4). Additionally a band at ~1592 cm^{-1} arised, the amide I' band of the ^{13}C labeled carbonyls. The amide I' bands of ^{13}CK and E/^{13}CK could be fitted with 4 Gaussian bands. The carbonyl band of glutamic acid was additionally included in the fit at 1564 cm^{-1}, to enhance the band shape modeling at low frequencies. The fit of E/^{13}CK yielded $A_1 / A_2 = 1.24$, which is smaller than the value for E/K of 2.45 showing that the absorbance at 1630 cm^{-1} is significantly reduced (Table 1, Figure 4B). It is

Table 1. Peak positions and absorbance ratio of peptides determined from band fitting.. Values in parenthesis are 95% confidence intervall with respect to the last two digits.

	$\tilde{\nu}_1$ (cm^{-1})	$\tilde{\nu}_2$ (cm^{-1})	$\tilde{\nu}_3$ (cm^{-1})	$\tilde{\nu}_{13C}$ (cm^{-1})	A_1/A_2[a]
E	1630.3 (4)	1648.6 (3)	1666.7 (11)	-	1.75
K	1631.1 (5)	1648.8 (4)	1667.6 (9)	-	1.82
E/K	1631.2 (2)	1650.5 (1)	1668.0 (5)	-	2.45
^{13}CK	1628.0[b]	1645.0 [b]	1666.4 (5)	1593.3 (1)	1.05
E/^{13}CK	1631.0 (11)	1649.5 (6)	1669.5 (7)	1592.6 (3)	1.24

[a] Absorbance ratio: $Abs(\tilde{\nu}_1)/ Abs(\tilde{\nu}_2)$, determined from area of fitted Gaussians.
[b]Value fixed during band fitting procedure.

Table 2. Peak positions and absorbance ratio of vesicle tethered lipopeptides and peptides mixed with vesicles determined from band fitting. Values in parenthesis are 95% confidence intervall with respect to the last two digits.

	$\tilde{\nu}_1$ (cm^{-1})	$\tilde{\nu}_2$ (cm^{-1})	$\tilde{\nu}_3$ (cm^{-1})	$\tilde{\nu}_{13C}$ (cm^{-1})	A_1/A_2[a]
E	1630.3 (4)	1648.6 (3)	1666.7 (11)	-	1.75
K	1631.1 (5)	1648.8 (4)	1667.6 (9)	-	1.82
E/K	1631.2 (2)	1650.5 (1)	1668.0 (5)	-	2.45
^{13}CK	1628.0[b]	1645.0 [b]	1666.4 (5)	1593.3 (1)	1.05
E/^{13}CK	1631.0 (11)	1649.5 (6)	1669.5 (7)	1592.6 (3)	1.24

[a] Absorbance ratio: $Abs(\tilde{\nu}_1)/ Abs(\tilde{\nu}_2)$, determined from area of fitted Gaussians.
[b]Value fixed during band fitting procedure.

expected that some absorbance remains at 1630 cm^{-1} because the amide I' bands of amino acids in the *f* position is expected at this wavenumber.[22] The amide I' band of the *e* and *g* positions have not been studied in detail yet. However for ^{13}CK no specific, narrow band for the remaining ^{12}C carbonyls on the hydrophilic face at ~1630 cm^{-1} could be resolved. Instead, band fitting yielded a relatively broad band at ~1628 cm^{-1}, which might be the result of an overlap of the expected hydrogen bound ^{12}C carbonyl and contributions from coexisting random structures. Nevertheless the reduction of the water exposed helix band in this position is obvious (Figure 4A).

The reduced absorbance shows that the 1630 cm^{-1} component consists mainly of contributions from the alanine residues, which are situated on the hydrophilic face of the amphipathic helix in the *b* and *c* positions of the heptad repeat. This is further strengthened by the position of the ^{13}C amide I' at ~1592 cm^{-1} the isotope shift is ~38 cm^{-1} which is in range of the typical values of 35-40 cm^{-1} reported for different model peptides independent of their secondary structure and hydrogen bonding.[22,28-34] Manas et. al. reported the position of ^{13}C-Ala in the *b* and *f* position of a GCN4-p1' leucine zipper with 1587 cm^{-1} whereas a ^{13}C-Leu in the d-position, i.e. the hydrophobic face of the same peptide absorbed at 1607 cm^{-1}.[22] Thus, the position found in the present study reflects the expectation for a water accessible helical ^{13}C amide I' band.

IR OF LIPOPEPTIDES

Next, the spectra of the lipopeptides CPE and CPK tethered to lipid vesicles were measured (Figure 5A). Just as for the untethered E and K, the amide I' bands were dominated by 2 main components. Under consideration of the strong absorbance of the lipid C=O stretching band at ~1740 cm^{-1} the amide I' bands were fitted by Gaussians yielding A_1/A_2 values of 1.52 and 1.03 for CPE and CPK respectively (Table 2). For CPE this result is in line with the assumption of homo coiling of the peptide on the vesicle interface. For CPK this band shape is similar to amide I' bands found in IRRA spectra from lipid monolayers containing the lipopeptide LPK (*Chapter III*).[13] Although the peptide moieties in these molecules are thought to interact as monomers with the lipid bilayers, they show the typical amide I' band shape of multimeric coiled-coils. However K is thought to insert as an amphipathic A helix into one leaflet of the lipid bilayer with its helical axis parallel to the membrane interface (*Chapter III* & *IV*). This would also result in a shielding of the hydrophobic face from water. The water density in DOPC bilayers is known to drop significantly below the lipid phosphate group.[45] This can explain the appearance of two amide I' components that can be attributed to solvent accessible and inaccessible carbonyls.

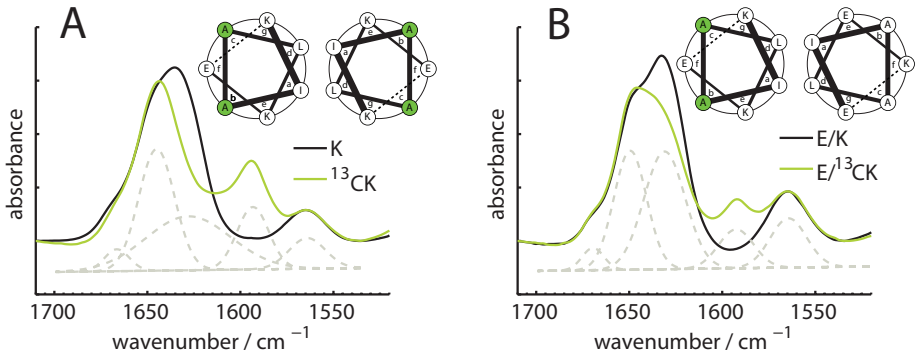

Figure 4. Normalized IR spectra (continuous lines) of (A) K, ^{13}CK, (B) E/K, and E/^{13}CK at 5°C and Gaussian fits of ^{13}C peptide spectra (broken lines). Spectra were normalized with respect to the C=O stretching band of glutamic acid at 1565 cm^{-1}. Fitted curves are offset for clarity. [peptide] = 1 mM, in d-PBS. Insets show helical wheel projections of dimeric coiled-coils with the position of the ^{13}C labeled alanine residues highlighted in green.

Although the assignment of water accessible and buried amide I' helical bands in coiled-coils is a well-studied phenomenon in solution,[19-23,31,37,44,46,47] the related effect in a lipid membrane is reported only scarcely by other groups. A variable two band pattern was reported by Bi et al. for S-palmitoylated N-terminal peptide of pulmonary surfactant peptide SP-C interacting with DPPC monolayers.[24] The authors interpreted a change of the relative band intensities with respect to each other as the expelling of helical fragments of the peptides from the monolayer, leading to a variation in hydration of the helix. Mukerjhee et. al. found amide I' bands with solvent accessible and buried components for alanine rich helical peptides, and amphipathic helices in reverse micelles that mimic membrane water interfaces.[26,27]

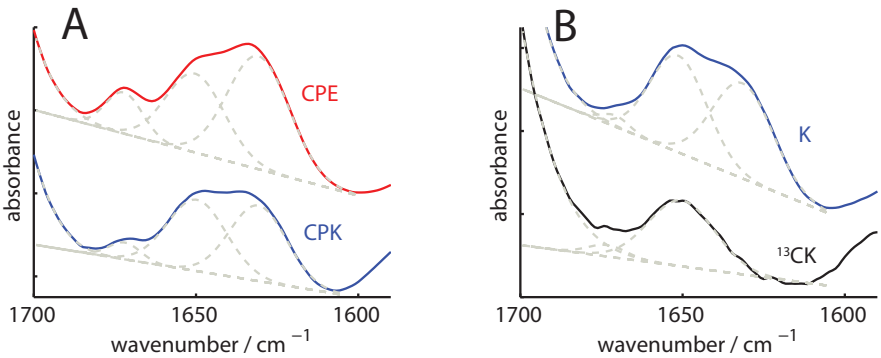

Figure 5. FTIR spectra (continuous lines) of vesicle tethered (A) CPE and CPK; (B) K at 5 °C and ^{13}CK at 10 °C mixed with vesicles at [lipid] : [peptide] = 200 : 1; [peptide] = 100 µM and fits of the amide I' bands with Gaussians (broken lines). All measurements in d-PBS.

To verify the assignment of the two main bands to water exposed and buried helices, the IR spectra of untethered peptides K and ^{13}CK when interacting with vesicles were measured. Due to the need of a relatively high [lipid] : [peptide] ratio (200 : 1) the peptide concentration is relatively low in these experiments and the spectra are markedly affected by residual H_2O below 1600 cm^{-1} and the strong lipid C=O band above 1700 cm^{-1}. While the influence of the lipid C=O could be modeled by fitting additional large Gaussian bands, contributions below 1600 cm^{-1} could hardly be resolved. Despite that, the distinct two band pattern described above can be found in the amide I' band of K in the membrane, with A_1/A_2 similar to CPK of 1.05 (Figure 5B, Table 2). Strikingly, the amide I' band of ^{13}CK in the membrane showed a strongly reduced absorbance at 1630 cm^{-1} and no contribution at this position was necessary to fit the band shape. Remaining bands in this position could not be resolved due to the relatively low peptide signal. The reduced absorbance at 1630 cm^{-1} implies a high structural similarity of the membrane bound and the homo-coiled state of K, in both helices the alanine amide carbonyls are accessible for hydrogen bonds from water. In the monomeric amphipathic A helix that was proposed as the membrane interacting species of K in *Chapter III*, the alanine residues are also expected to be situated on the hydrophilic face, which is in common with their ^{12}C amide I' absorbance at ~1630 cm^{-1}. The remaining peak, mainly centered at 1650 cm^{-1}, is also in common with remaining absorbance of mostly buried ^{12}C amides of the hydrophobic face.

The relatively low A_1 / A_2 ratios of CPK and K interacting with vesicles, compared to CPE or the homo coils of E, K and E/K might be caused by higher amounts of unordered structures (Table 1 and 2). This correlates well with the helicity values found by CD spectroscopy. However, it is difficult to distinguish if unstructured contributions are caused by unfolded domains within individual chains with all peptides being membrane bound or by the existence of different peptide populations, i.e. helical and unstructured. Certain arguments speak for the former. An unstructured form would be expected to be in equilibrium with a homomeric coiled coil and would result in concentration dependent temperature profiles. The absence of this concentration dependence (Figure 2A), therefore might be interpreted as the absence of different populations and supports the model of partially unfolded peptide chains. Short peptides tend to fray at their termini[34] and these ends might reach out of the membrane staying unfolded. In this perspective also the slight positive slope of the temperature dependent $[\theta]_{222nm}$ might indicate an increasing non-cooperative end fraying, leading to a less folded state at higher temperatures.[42]

TEMPERATURE DEPENDENCIES OF PEPTIDES

The temperature dependent unfolding of coiled-coils as measured by CD spectroscopy is also reflected in the temperature dependent amide I' bands. Deconvolution of the amide I' bands of the unfolded peptides E and K at 75 °C yielded broad single bands centered at ~1645 cm^{-1} with the TFA shoulder around ~1668 cm^{-1} (data not shown). Thus, the unfolded band overlaps strongly with the two helical bands. In order to clarify the changes in the amide I' band upon unfolding, difference spectra of the molar absorbance per amino acid residue ($\Delta\varepsilon = \varepsilon_T - \varepsilon_{5°C}$) are interpreted in the following (Figure 6 - Figure 9). These are also sometimes referred to as 'fingerprints' of a conformational change because they can be analyzed in terms of their magnitude, shape, and temperature dependence and classified according to their similarity.[48]

However, the straightforward interpretation of the difference spectra is hampered by the intrinsic temperature dependence of the amide I' band components and artefacts from residual H_2O in the case of low peptide signals (see below). For instance the temperature dependent difference amide I' bands of E/K clearly show no isosbestic point, which shows that more than one process affects the absorbance band (Figure 6A). The overlapping spectral changes can be separated by means of singular value decomposition (SVD) in combination with a global fitting routine.[35-37] For instance a band can show an intensity decrease, due to a reaction or a structural transition, at the same time this band can shift its position, due to changes in the strength of hydrogen bonds with temperature. These two spectral components overlap in the resulting difference spectra, both having their own temperature dependency. Under the assumption that the single spectral components have a temperature dependency of a sigmoidal shape, the different components that overlap in the spectrum can be distinguished. The results of this linear algebra procedure are the separated spectral components $D_1 \ldots D_n$ and their temperature dependencies $F_1 \ldots F_n$ (Figure 6B, D, F) which all together model the original temperature dependent difference spectra. The resulting *D* components can be interpreted to reveal molecular details of the temperature dependent processes. The *F* components yield the midpoints of the transitions $T_{m1} \ldots T_{m2}$ and their widths and describe the physics of the underlying process more precisely than measuring the absorbance at a single frequency.[37]

For the untethered peptides E, K and E/K one transition is assumed to be the unfolding of the coiled-coils, which is modeled in the F_1 component with the thermodynamic parameters ($\Delta H°, \Delta C_p, T°$) known from CD measurements (*Chapter VI*). The corresponding D_1 components of all peptides show a striking similarity with a strong and broad negative component centered at ~1630 cm^{-1} and a positive feature at 1660 cm^{-1} (Figure 6B, D, F). The corresponding F_1 thermal components are all ≥ 0,

which means that the unfolding of the coiled-coils is always accompanied by a vanishing of the band at 1630 cm^{-1}. In K and E/K the D_2 components are very similar with a positive feature at ~1624 cm^{-1} and negative intensity in the region 1640 cm^{-1}-1660 cm^{-1} (Figure 6B, D). Taking into account the negative values of F_2 over the whole temperature regime this corresponds to a blue shift of the water exposed band of the coiled-coil spectrum. The midpoint of this transition (T_{m2}) is below the melting temperature of the peptides which shows that the process influences the spectra less while the coiled coils melt. This blue shift is a known phenomenon for the water exposed amide I' band of coiled-coils. Manas et. al. reported that amide I' bands of water exposed carbonyls show stronger blue shifts at increasing temperature than buried ones, probably due to the weakening of the additional hydrogen bonds.[22]

The D_2 and F_2 components of E mainly overlap with its D_1 and F_1 components, i.e. in this case the SVD global fitting routine could not resolve additional information (Figure 6F). Due to the lower tendency of E to form homo coils (compare *Chapter VI*) there is less influence of the blue shift of the 1630 cm^{-1} band on the difference spectra.

While the water accessible amide I' band vanishes upon melting, the influence of melting on the solvent buried amide I' band is found in the difference spectra of ^{13}CK (Figure 7). The D_1 component indicates a broadening of the band at ~1650 cm^{-1}, resulting from the rising of the band of unstructured peptide chains. The negative feature at 1590 cm^{-1} corresponds to the disappearing of the water exposed ^{13}C amide I' due to melting and is accordingly observed only in difference spectra ^{13}CK and E/^{13}CK (Figure 7, Figure A1). The temperature dependent difference spectra of E/^{13}CK were found to be rather complex due to the multitude of bands. Thus it is not discussed in detail; however these spectra did not contradict the results described before (Figure A1).

Taken together the analysis of the temperature dependent IR difference spectra of E, K, ^{13}CK and E/K revealed that the thermal unfolding of the coiled-coils can be retrieved in these spectra by a specific 'fingerprint' difference spectrum, which is dominated by a strong absorbance decrease at 1630 cm^{-1} and an increase at 1650 cm^{-1}. This overlaps with a more subtle shift of the water accessible helical band of the coiled-coil at 1630 cm^{-1} to higher frequencies, which occurs at temperatures below the cooperative melt of the complex.

Strikingly, the thermal difference spectra of membrane tethered CPE are also dominated by this pattern as can be seen in its D_1 component (Figure 8A-B). The T_{m1} of the corresponding sigmoidal F_1 component is at 38 °C, which lies well in the range of T_m found in the CD unfolding curves (Figure 2). Furthermore, the D_2 component indicates a slight blue shift of the 1630 cm^{-1} band as was found for the untethered coiled-coils. Thus this data strongly suggests that membrane tethered E is in a homomeric coiled-coil state, which unfolds upon heating (Figure 10A).

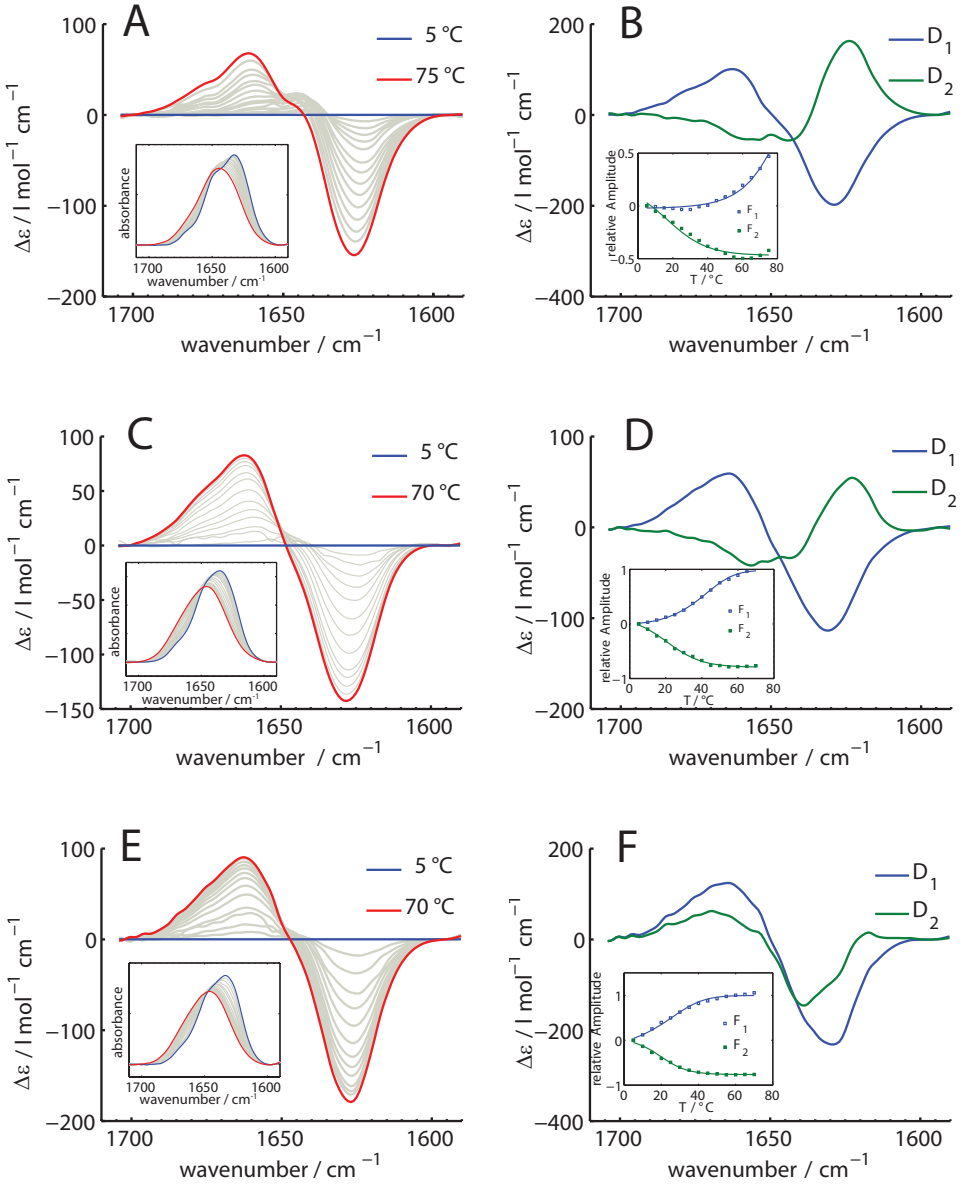

Figure 6. Temperature dependency and singular value decomposition of amide I' bands for (A-B) E/K T = 5 - 75°C, (C-D) K T = 5 - 70°C, and (E-F) E T = 5 - 70°C (A, C, E) Temperature dependent difference spectra in the amide I' region with amide I' bands in the insets in 5 °C steps (B, D, F) Results of singular value decomposition D_1 and D_2 spectral components and F_1, F_2 temperature profiles (squares) and fit results (lines) in the insets; [peptide] = 1 mM, in d-PBS.

Conversely, the difference spectra of the membrane tethered CPK and K mixed with vesicles show both D_1 components with a broad absorbance increase at ~1650 cm^{-1} but only a small decrease at 1623 cm^{-1} (Figure 8C-D, Figure 9). These spectral components

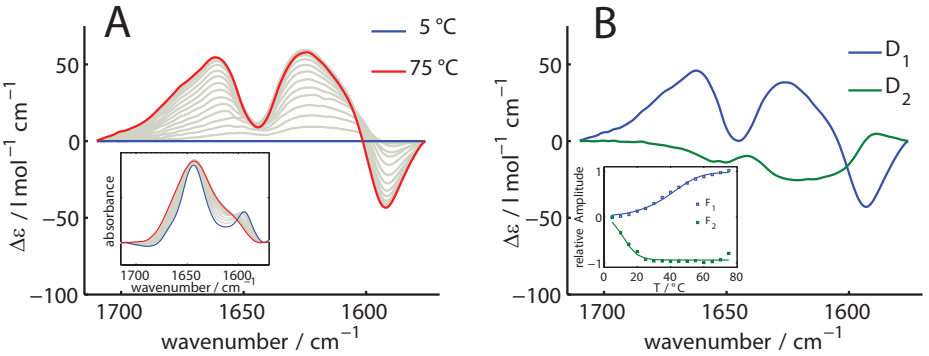

Figure 7. (A) Temperature dependent difference spectra in the amide I' region with amide I' bands in the insets in 5 °C steps of ^{13}CK in d-PBS; (B) Results of singular value decomposition D_1 and D_2 spectral components and F_1, F_2 temperature profiles (squares) and fit results (lines) in the insets, T = 5 - 75°C.

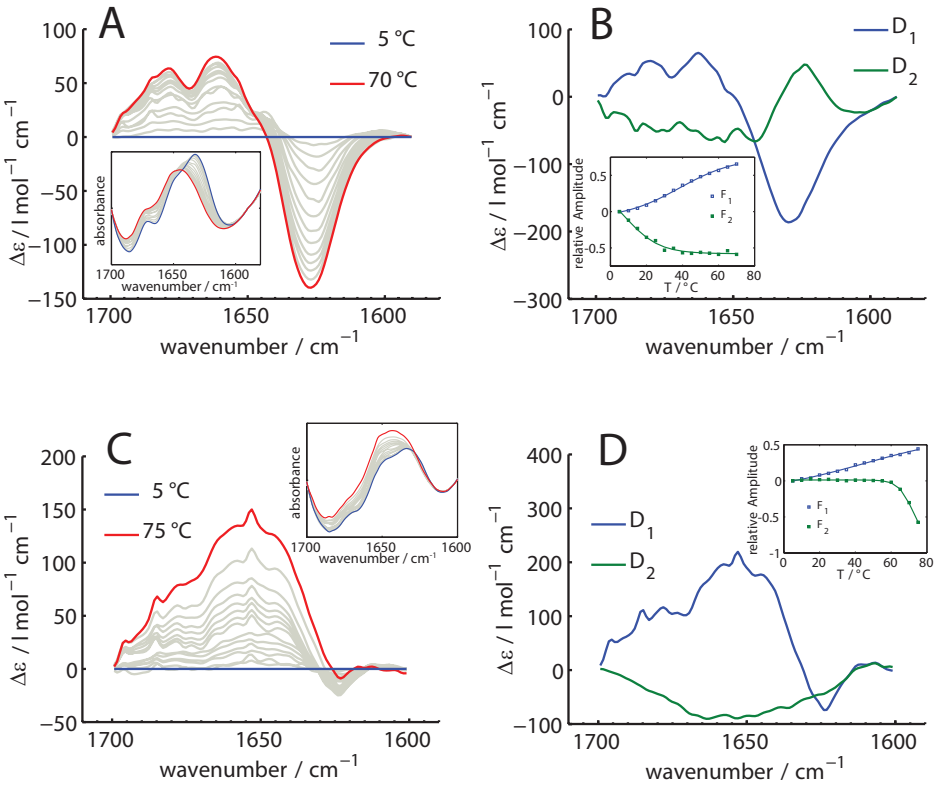

Figure 8. Temperature dependency and singular value decomposition of amide I' bands for lipopeptides tethered to vesicles in d-PBS (A, B) CPE 1 mol% T = 5 - 70°C and (C, D) CPK T = 5 - 75°C; (A, C) Temperature dependent difference spectra in the amide I' region with amide I' bands in the insets in 5 °C steps (B, D) Results of singular value decomposition D_1 and D_2 spectral components and F_1, F_2 temperature profiles (squares) and fit results (lines).

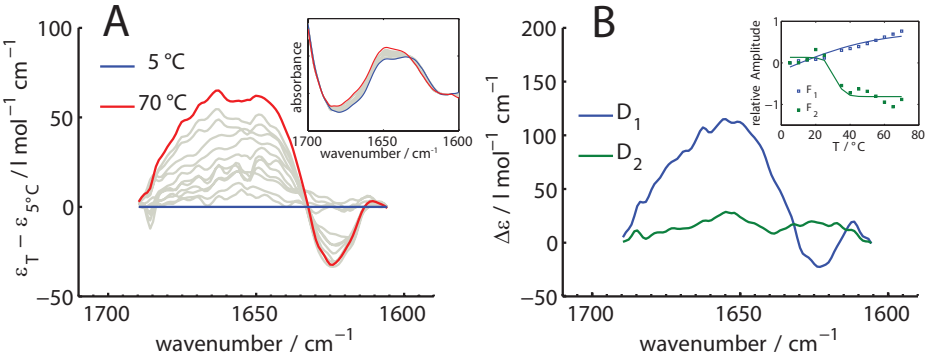

Figure 9. (A) Temperature dependent difference spectra in the amide I' region with amide I' bands in the insets in 5 °C steps of K mixed with vesicles; (B) Results of singular value decomposition D_1 and D_2 spectral components and F_1, F_2 temperature profiles (squares) and fit results (lines) in the insets ([K] = 100 µM; [Lipid]:[K] = 200 : 1, in d-PBS) T = 5 - 70°C.

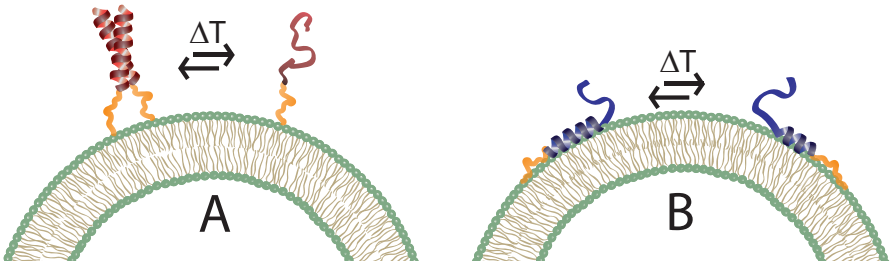

Figure 10. Schematic drawing of temperature dependent changes of peptide states when tethered to membranes. (A) CPE is predominantly folded in an E/E coiled coil which unfolds and dissociates upon heating. (B) CPK is predominantly bound to the membrane in a helical state and stays bound upon heating.

differ substantially from the D_1 component of CPE and therefore indicate a different transition. The increase at 1650 cm^{-1} was also apparent in the D_1 component of ^{13}CK mixed with vesicles (Figure A2). The decrease at 1623 cm^{-1} appears to arise from the temperature dependent blue shift of the water exposed band. It has to be noted that the components found in the D_2 component of these measurements appear to be artefacts arising from variations in the residual H_2O concentration in the sample. Band fitting of the spectra at 75 °C revealed that these amide I' bands still consist of two main components of a similar area at 1635 cm^{-1} and 1652 cm^{-1} (Figure A3). Interestingly, the corresponding F_1 components are relatively shallow and almost linear, indicating that the observed D_1 spectral component does not relate to a cooperative transition, which is in line with the almost linear shapes of the $[\theta]_{222nm}$ curves of CPK and K mixed with vesicles (Figure 1).

This discussed data show that membrane bound K exhibits a fundamental different temperature dependency from an unfolding coiled-coil. Despite the expected blue shift of the water accessible band, the amide I' retains its two main components up to 75 °C. Thus the peptide does not unfold cooperatively and stays bound to the membrane even

at temperatures as high as 75 °C (Figure 10B). However the intermediate helical content, decreasing with temperature found by CD (Figure 1 and Figure 2) and the relatively low absorbance ratio A_1 / A_2 (Table 2) indicate a certain contribution of unordered structure in the peptide chains which might, upon heating, increase in a non-cooperative way.

CONCLUSIONS

The temperature dependent unfolding of the coiled-coil forming peptides E and K in solution and tethered to lipid vesicles could be followed by CD and difference IR spectroscopy and yielded comparable temperature profiles. Membrane tethered CPE showed concentration dependent temperature profiles in CD, typical for an unfolding transition and the IR spectral changes exhibit the characteristics of coiled-coil unfolding. In contrast, CPK on membranes exhibits no transition, remaining in its membrane bound state up to 75 °C. The membrane bound CPK also exhibits a considerable amount of unordered structures, which indicate a partially folded helix in the membrane bound state.

The IR spectra of membrane tethered homo-coiled CPE and membrane incorporated, monomeric CPK show remarkable similarities, despite their different states. This is caused by similar accessibilities of the amide carbonyls for water in the coiled-coil and the amphipathic A helix which are both partially hydrophobically buried. These results contribute further to the model of lipopeptide mediated fusion as they provide additional support for the hypothesis of the asymmetric process. The two recognizing units behave fundamentally differently in the prefusion state. These results show, that the special conditions at the membrane interface have different influence on the state of membrane tethered peptides, depending on their individual properties. This influence is difficult to predict and has to be studied for each peptide individually.

It was proposed earlier (*Chapter III*) that the interaction of K with the membrane induces curvature which helps overcoming the highly curved intermediate states of lipid reorganistion during fusion. Thus, a specific manipulation of the membrane affinity of K appears to be a promising handle to influence the fusion mechanism.

EXPERIMENTAL SECTION

MATERIALS

Fmoc-protected amino acids and Sieber amide resin for peptide synthesis were purchased from Novabiochem, Fmoc-protected (1-^{13}C, 99%) L-alanine was purchased from Cambridge Isotope Laboratories. DOPC (1,2-dioleoyl-sn-glycero-3-phosphocholine), DOPE (1,2-dioleoyl-sn-glycero-3-phosphoethanolamine), and cholesterol were purchased from Avanti Polar Lipids. Solvents, buffer salts, D_2O and DCl (deuterium content ≥ 99.9%) were purchased from Sigma-Aldrich. All

water was ultrapure with resistance ≥ 18 MΩ cm^{-1} and TOC ≤ 2 ppm produced from a MilliQ Reference A+ purification system. All experiments were carried out in phosphate buffered saline prepared in water (PBS) or D_2O (d-PBS) of the composition: 150 mM NaCl, 20 mM PO_4^{3-} at pH/pD 7.4.[49]

PEPTIDE SYNTHESIS

The peptides E: Ac-$(EIAALEK)_3$-NH_2, K: Ac-$(KIAALKE)_3$-NH_2, and ^{13}CK with the same sequence as K and a ^{13}C amide labelled alanine residue were synthesized using standard Fmoc-chemistry on a Biotage Syro I and purified by RP-HPLC to yield a purity > 95% based on HPLC. Identity of the peptides was determined by LC-MS. The lipopeptides were synthesized and purified as described elsewhere.[3,6] Peptides were solved in 10 mM HCl and lyophilized three times to remove TFA.[50] Peptide stock solutions in d-PBS were prepared at ~2 mg/ml and diluted accordingly for the measurements. Lipopeptide stock solutions were prepared in a $CHCl_3$: MeOH; 3 : 1 solution and added to the lipids prior to solvent evaporation.

VESICLE PREPARATION

Lipid stock solutions of the composition DOPE : DOPE : Cholesterol (2 : 1 : 1) were prepared in $CHCl_3$: MeOH 3 : 1. For experiments with lipopeptides, lipid stock solutions were mixed with CPK and CPE stock solutions to yield mixtures with the desired molar ratio. Lipid films were created by slow evaporation of the solvents under N_2 stream and kept under vacuum overnight. The films were rehydrated with PBS or d-PBS yielding final lipid concentrations of typically 1 - 2 mM for CD or 20 mM for IR measurements. For measurements with untethered peptides, the lipid films were directly hydrated with solutions of the peptides. Large unilamellar vesicles (LUVs) were formed by sonication at 55 °C for ~15 min. The size of the vesicles was tested by DLS using a Malvern Zetasizer nano-s and was typically found to be ~100 nm.

CIRCULAR DICHROISM SPECTROSCOPY

Thermal unfolding of peptides and lipid tethered peptides were measured as described in *Chapters II* & *IV*. The mean residual ellipticity *[θ]* and the relative helicity *rh* were calculated as described in the aforementioned chapters. The fraction of folded peptide α is calculated, using the ellipticity when all molecules are folded or unfolded (θ_F, θ_u) by:

$$\alpha = \frac{[\theta] - \theta_U}{\theta_F - \theta_U} \quad (1)$$

TRANSMISSION FT–IR SPECTROSCOPY

Transmission FT–IR spectra were measured using a Bio-Rad Excalibur spectrometer equipped with a nitrogen cooled MCT detector. A temperature controlled liquid transmission cell with CaF_2 windows and a fixed nominal path length of 50 mm was used. The precise pathlength (d) was determined by the interference fringe method. Sample spectra in d-PBS and reference spectra of dPBS at 25 °C were measured at a resolution of 2 cm^{-1} with a zero filling factor of 1. Spectra were recorded between 5 and 75 °C in steps of 5 °C. The temperature of the cell was measured and kept constant during measurement at ± 0.2 °C. For each spectrum 128 scans were averaged. Several spectra were averaged and corrected by manual subtraction of a water vapor spectrum. The molar absorptivity per residue (ε) was calculated from the absorbance (A), the peptide concentration (c) and the number of amino acid residues per peptide chain according to Beer-Lambert law:

$$\varepsilon = \frac{A}{ncd}. \tag{2}$$

For band fitting[51] of the amide I' the second derivative of the spectra were smoothed for determination of the position of underlying bands. The positions found were used as input for fitting of the band shape with Gaussian peaks on a linear baseline by means of a trust-region-reflective algorithm.

SINGULAR VALUE DECOMPOSITION AND GLOBAL FITTING

For analysis of difference spectra from baseline corrected molar absorptivity spectra (ε_T - $\varepsilon_{5°C}$) singular value decomposition (SVD) in combination with global curve fitting was applied.[35-37] The data matrix $\mathrm{A}(\tilde{\nu}, T)$ was created by ordering the difference spectra in such a way that each column corresponds to a temperature. SVD is applied to the data matrix (MatLab function: *svd*) yielding three matrices U, S, and V^T:

$$\mathrm{A}(\tilde{\nu}, T) = USV^T, \tag{3}$$

corresponding to the basis spectra (U), the singular values (S), and the transposed of the temperature development of the basis spectra (V^T). From these matrices components above a rank (r) of 2 were omitted as they mainly contained noise. To describe the data matrix based on overlapping physical transitions it is assumed that these matrices can be described by a matrix D containing the spectral components of the overlapping components and F^T containing their temperature dependencies:

$$USV^T = DF^T. \tag{4}$$

Multiplication with the pseudo inverse of F^T (F^{T+}) yields:

$$D = USH \tag{5}$$

with

$$H = V^T F^{T+}. \tag{6}$$

This means the matrix H contains the coefficients determining how the weighted basis spectra (US) must be mixed to yield the spectral component matrix D and these coefficients can be obtained by globally fitting V^T with physical models for each spectral component. The model used for measurements of lipopeptides or peptides with vesicles consisted of two sigmoid functions:

$$f(T)_n = h_{n1}\left(b_1 + \frac{m_1 - b_1}{1 + \exp\left(\frac{T_{m_1} - T}{\delta_1}\right)}\right) + h_{n2}\left(b_2 + \frac{m_2 - b_2}{1 + \exp\left(\frac{T_{m_2} - T}{\delta_2}\right)}\right). \tag{7}$$

In this equation subscript n refers to the n^{th} row of the matrix V^T; h_{n1} and h_{n2} are the corresponding elements of H, while b, m, T_m, and δ are the minimum value, maximum value, midpoint, and width of the two sigmoidal transitions. For fitting a trust-region-reflective algorithm (MatLab function: *lsqcurvefit*) was used, leaving the parameters b, m, T_m, and δ global.

For melting of the coiled-coil peptides E, K, and E/K one transition was assumed to be the thermal peptide unfolding. The parameters $\Delta H°$ and $T°$, the enthalpy and the temperature where the folding constant $K_F = 1$ and ΔC_p, the change in heat capacity upon folding as determined by CD spectroscopy in *Chapter VI* were used and set constant during global fitting. In the applied model, the first sigmoid function was replaced by the temperature dependent fraction of folded peptide $\alpha(T)$:

$$f(T)_n = h_{n1}(\alpha(T)(m_1 - b_1) + b_1) + h_{n2}\left(b_2 + \frac{m_2 - b_2}{1 + \exp\left(\frac{T_{m_2} - T}{\delta_2}\right)}\right). \tag{8}$$

With the unfolded fraction ($\beta = 1 - \alpha$), $\alpha(T)$ was calculated by using the analytical solutions of:

$$a\beta^2 + \beta - 1 = 0, \tag{9}$$

as described in detail in *Chapter II*.
The F matrix was determined from:

$$F^T = H^{-1}V^T. \tag{10}$$

All calculations were performed using MatLab 2013a equipped with curve fitting toolbox.

REFERENCES

(1) Marsden, H. R.; Tomatsu, I.; Kros, A., Model systems for membrane fusion. *Chem. Soc. Rev.* **2011**, *40*, 1572.

(2) Robson Marsden, H.; Korobko, A. V.; Zheng, T.; Voskuhl, J.; Kros, A., Controlled liposome fusion mediated by SNARE protein mimics. *Biomaterials Science* **2013**, *1*, 1046.

(3) Robson Marsden, H.; Elbers, Nina A.; Bomans, Paul H. H.; Sommerdijk, Nico A. J. M.; Kros, A., A Reduced SNARE Model for Membrane Fusion. *Angew. Chem. Int. Ed.* **2009**, *48*, 2330.

(4) Tomatsu, I.; Marsden, H. R.; Rabe, M.; Versluis, F.; Zheng, T.; Zope, H.; Kros, A., Influence of pegylation on peptide-mediated liposome fusion. *J. Mater. Chem.* **2011**, *21*, 18927.

(5) Versluis, F.; Dominguez, J.; Voskuhl, J.; Kros, A., Coiled-coil driven membrane fusion: zipper-like vs. non-zipper-like peptide orientation. *Faraday Discuss.* **2013**, *166*, 349.

(6) Versluis, F.; Voskuhl, J.; van Kolck, B.; Zope, H.; Bremmer, M.; Albregtse, T.; Kros, A., In Situ Modification of Plain Liposomes with Lipidated Coiled Coil Forming Peptides Induces Membrane Fusion. *J. Am. Chem. Soc.* **2013**, *135*, 8057.

(7) Zheng, T. T.; Voskuhl, J.; Versluis, F.; Zope, H. R.; Tomatsu, I.; Marsden, H. R.; Kros, A., Controlling the rate of coiled coil driven membrane fusion. *Chem. Commun.* **2013**, *49*, 3649.

(8) Zope, H. R.; Versluis, F.; Ordas, A.; Voskuhl, J.; Spaink, H. P.; Kros, A., In vitro and in vivo supramolecular modification of biomembranes using a lipidated coiled-coil motif. *Angew Chem Int Ed Engl* **2013**, *52*, 14247.

(9) Voskuhl, J.; Wendeln, C.; Versluis, F.; Fritz, E. C.; Roling, O.; Zope, H.; Schulz, C.; Rinnen, S.; Arlinghaus, H. F.; Ravoo, B. J.; Kros, A., Immobilization of Liposomes and Vesicles on Patterned Surfaces by a Peptide Coiled-Coil Binding Motif. *Angew Chem Int Edit* **2012**, *51*, 12616.

(10) Meyenberg, K.; Lygina, A. S.; van den Bogaart, G.; Jahn, R.; Diederichsen, U., SNARE derived peptide mimic inducing membrane fusion. *Chem. Commun.* **2011**, *47*, 9405.

(11) Pahler, G.; Lorenz, B.; Janshoff, A., Impact of peptide clustering on unbinding forces in the context of fusion mimetics. *Biochem. Biophys. Res. Commun.* **2013**, *430*, 938.

(12) Pahler, G.; Panse, C.; Diederichsen, U.; Janshoff, A., Coiled-Coil Formation on Lipid Bilayers-Implications for Docking and Fusion Efficiency. *Biophys. J.* **2012**, *103*, 2295.

(13) Rabe, M.; Schwieger, C.; Zope, H. R.; Versluis, F.; Kros, A., Membrane Interactions of Fusogenic Coiled-Coil Peptides: Implications for Lipopeptide Mediated Vesicle Fusion. *Langmuir* **2014**, *30*, 7724.

(14) Chen, Y.-H.; Yang, J. T.; Chau, K. H., Determination of the helix and β form of proteins in aqueous solution by circular dichroism. *Biochemistry* **1974**, *13*, 3350.

(15) Gans, P. J.; Lyu, P. C.; Manning, M. C.; Woody, R. W.; Kallenbach, N. R., The helix–coil transition in heterogeneous peptides with specific side-chain interactions: Theory and comparison with CD spectral data. *Biopolymers* **1991**, *31*, 1605.

(16) Cooper, T. M.; Woody, R. W., The Effect of Conformation on the Cd of Interacting Helices - a Theoretical-Study of Tropomyosin. *Biopolymers* **1990**, *30*, 657.

(17) Litowski, J. R.; Hodges, R. S., Designing heterodimeric two-stranded alpha-helical coiled-coils. Effects of hydrophobicity and alpha-helical propensity on protein folding, stability, and specificity. *J. Biol. Chem.* **2002**, *277*, 37272.

(18) Barth, A., Infrared spectroscopy of proteins. *Biochim. Biophys. Acta* **2007**, *1767*, 1073.

(19) Heimburg, T.; Schuenemann, J.; Weber, K.; Geisler, N., Specific Recognition of Coiled Coils by Infrared Spectroscopy: Analysis of the Three Structural Domains of Type III Intermediate Filament Proteins. *Biochemistry* **1996**, *35*, 1375.

(20) Reisdorf, W. C., Jr.; Krimm, S., Infrared amide I' band of the coiled coil. *Biochemistry* **1996**, *35*, 1383.

(21) Heimburg, T.; Schünemann, J.; Weber, K.; Geisler, N., FTIR-Spectroscopy of Multistranded Coiled Coil Proteins. *Biochemistry* **1999**, *38*, 12727.

(22) Manas, E. S.; Getahun, Z.; Wright, W. W.; DeGrado, W. F.; Vanderkooi, J. M., Infrared Spectra of Amide Groups in a-Helical Proteins: Evidence for Hydrogen Bonding between Helices and Water. *J. Am. Chem. Soc.* **2000**, *122*, 9883.

(23) Walsh, S. T.; Cheng, R. P.; Wright, W. W.; Alonso, D. O.; Daggett, V.; Vanderkooi, J. M.; DeGrado, W. F., The hydration of amides in helices; a comprehensive picture from molecular dynamics, IR, and NMR. *Protein Sci.* **2003**, *12*, 520.

(24) Bi, X.; Flach, C. R.; Pérez-Gil, J.; Plasencia, I.; Andreu, D.; Oliveira, E.; Mendelsohn, R., Secondary Structure and Lipid Interactions of the N-Terminal Segment of Pulmonary Surfactant SP-C in Langmuir Films: IR Reflection–Absorption Spectroscopy and Surface Pressure Studies†. *Biochemistry* **2002**, *41*, 8385.

(25) Lewis, R. N. A. H.; Prenner, E. J.; Kondejewski, L. H.; Flach, C. R.; Mendelsohn, R.; Hodges, R. S.; McElhaney, R. N., Fourier Transform Infrared Spectroscopic Studies of the Interaction of the Antimicrobial Peptide Gramicidin S with Lipid Micelles and with Lipid Monolayer and Bilayer Membranesâ€ *Biochemistry* **1999**, *38*, 15193.

(26) Mukherjee, S.; Chowdhury, P.; Gai, F., Infrared Study of the Effect of Hydration on the Amide I Band and Aggregation Properties of Helical Peptides. *J. Phys. Chem. B* **2007**, *111*, 4596.

(27) Mukherjee, S.; Chowdhury, P.; DeGrado, W. F.; Gai, F., Site-specific hydration status of an amphipathic peptide in AOT reverse micelles. *Langmuir* **2007**, *23*, 11174.

(28) Tadesse, L.; Nazarbaghi, R.; Walters, L., Isotopically enhanced infrared spectroscopy: a novel method for examining secondary structure at specific sites in conformationally heterogeneous peptides. *J. Am. Chem. Soc.* **1991**, *113*, 7036.

(29) Decatur, S. M.; Antonic, J., Isotope-Edited Infrared Spectroscopy of Helical Peptides. *J. Am. Chem. Soc.* **1999**, *121*, 11914.

(30) Barber-Armstrong, W.; Donaldson, T.; Wijesooriya, H.; Silva, R. A. G. D.; Decatur, S. M., Empirical Relationships between Isotope-Edited IR Spectra and Helix Geometry in Model Peptides. *J. Am. Chem. Soc.* **2004**, *126*, 2339.

(31) Starzyk, A.; Barber-Armstrong, W.; Sridharan, M.; Decatur, S. M., Spectroscopic evidence for backbone desolvation of helical peptides by 2,2,2-trifluoroethanol: an isotope-edited FTIR study. *Biochemistry* **2005**, *44*, 369.

(32) Decatur, S. M., Elucidation of Residue-Level Structure and Dynamics of Polypeptides via Isotope-Edited Infrared Spectroscopy. *Acc. Chem. Res.* **2006**, *39*, 169.

(33) Kubelka, G. S.; Kubelka, J., Site-Specific Thermodynamic Stability and Unfolding of a de Novo Designed Protein Structural Motif Mapped by 13C Isotopically Edited IR Spectroscopy. *J. Am. Chem. Soc.* **2014**, *136*, 6037.

(34) Fesinmeyer, R. M.; Peterson, E. S.; Dyer, R. B.; Andersen, N. H., Studies of helix fraying and solvation using 13C' isotopomers. *Protein Sci.* **2005**, *14*, 2324.

(35) Hendler, R. W.; Shrager, R. I., Deconvolutions based on singular value decomposition and the pseudoinverse: a guide for beginners. *J. Biochem. Bioph. Methods* **1994**, *28*, 1.

(36) Henry, E. R.; Hofrichter, J. In *Methods Enzymol.*; Ludwig Brand, M. L. J., Ed.; Academic Press: 1992; Vol. Volume 210, p 129.

(37) Brewer, S. H.; Tang, Y.; Vu, D. M.; Gnanakaran, S.; Raleigh, D. P.; Dyer, R. B., Temperature dependence of water interactions with the amide carbonyls of alpha-helices. *Biochemistry* **2012**, *51*, 5293.

(38) Breslauer, K. J. In *Methods Enzymol.*; Michael L. Johnson, G. K. A., Ed.; Academic Press: 1995; Vol. Volume 259, p 221.

(39) Doyle, C. M.; Rumfeldt, J. A.; Broom, H. R.; Broom, A.; Stathopulos, P. B.; Vassall, K. A.; Almey, J. J.; Meiering, E. M., Energetics of oligomeric protein folding and association. *Arch. Biochem. Biophys.* **2013**, *531*, 44.

(40) Greenfield, N. J., Using circular dichroism collected as a function of temperature to determine the thermodynamics of protein unfolding and binding interactions. *Nat Protoc* **2006**, *1*, 2527.

(41) Chan, H. S.; Shimizu, S.; Kaya, H. In *Methods Enzymol.*; Jo M. Holt, M. L. J., Gary, K. A., Eds.; Academic Press: 2004; Vol. Volume 380, p 350.

(42) Dragan, A. I.; Privalov, P. L., Unfolding of a Leucine zipper is not a Simple Two-state Transition. *J. Mol. Biol.* **2002**, *321*, 891.

(43) Kubelka, J., Multivariate Analysis of Spectral Data with Frequency Shifts: Application to Temperature Dependent Infrared Spectra of Peptides and Proteins. *Anal. Chem.* **2013**, *85*, 9588.

(44) Paschek, D.; Puhse, M.; Perez-Goicochea, A.; Gnanakaran, S.; Garcia, A. E.; Winter, R.; Geiger, A., The Solvent-Dependent Shift of the Amide I Band of a Fully Solvated Peptide as a Local Probe for the Solvent Composition in the Peptide/Solvent Interface. *Chemphyschem* **2008**, *9*, 2742.

(45) Ku erka, N.; Gallová, J.; Uhríková, D.; Balgavý, P.; Bulacu, M.; Marrink, S.-J.; Katsaras, J., Areas of Monounsaturated Diacylphosphatidylcholines. *Biophys. J.* **2009**, *97*, 1926.

(46) Wang, T.; Lau, W. L.; DeGrado, W. F.; Gai, F., T-Jump Infrared Study of the Folding Mechanism of Coiled-Coil GCN4-p1. *Biophys. J.* **2005**, *89*, 4180.

(47) Imamura, H.; Isogai, Y.; Takekiyo, T.; Kato, M., Effect of pressure on the secondary structure of coiled coil peptide GCN4-p1. *Biochimica et Biophysica Acta (BBA) - Proteins & Proteomics* **2010**, *1804*, 193.

(48) Barth, A.; Zscherp, C., What vibrations tell about proteins. *Quarterly Reviews of Biophysics* **2002**, *35*, 369.

(49) Glasoe, P. K.; Long, F. A., Use of glass electrodes to measure acidities in deuterium oxide. *J. Phys. Chem.* **1960**, *64*, 188.

(50) Andrushchenko, V. V.; Vogel, H. J.; Prenner, E. J., Optimization of the hydrochloric acid concentration used for trifluoroacetate removal from synthetic peptides. *J. Pept. Sci.* **2007**, *13*, 37.

(51) Meier, R. J., On art and science in curve-fitting vibrational spectra. *Vib. Spectrosc* **2005**, *39*, 266.

APPENDIX

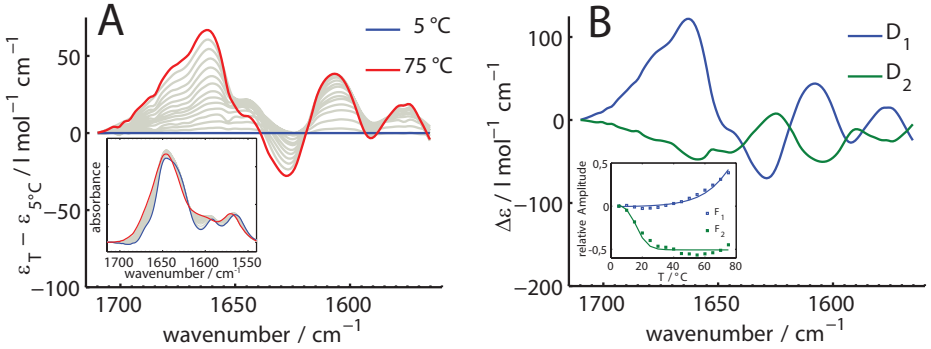

Figure A1. (A) Temperature dependent difference spectra of E/^{13}CK in d-PBS (T = 5 - 75°C) in the amide I' region with amide I' bands in the insets in 5 °C steps; (B) Results of singular value decomposition D_1 and D_2 spectral components and F_1, F_2 temperature profiles (squares) and fit results (lines) in the inset.

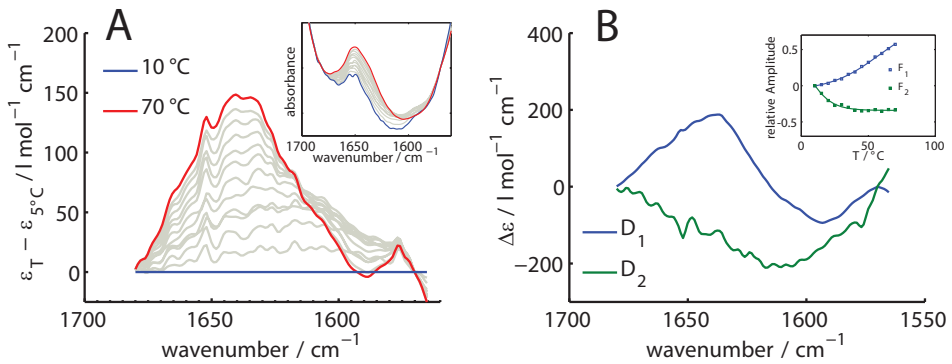

Figure A2. (A) Temperature dependent difference spectra in the amide I' region with amide I' bands in the insets in 5 °C steps; (B) Results of singular value decomposition D_1 and D_2 spectral components and F_1, F_2 temperature profiles (squares) and fit results (lines) in the inset of ^{13}CK mixed with vesicles in d-PBS ([13CK] = 100 µM; [Lipid] : [K] = 200:1) T = 10 - 70°C.

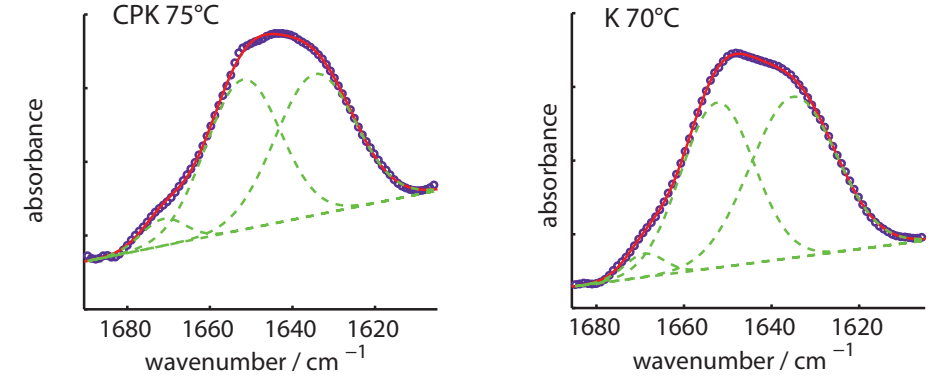

Figure A3. Amide I' bands (circles) of vesicle tethered CPK in d-PBS at 75 °C and K mixed with vesicles in d-PBS at 70 °C; fitted Gaussian bands (broken lines) and resulting band shape (continuous line).

Chapter VI

Can one methylene group make a difference? Influence of lysine snorkeling on the activity of fusogenic coiled-coil peptides

ABSTRACT

The state of the fusogenic coiled coil forming peptides E and K when tethered to lipid membranes was studied in detail in the recent chapters and it was hypothesized that the interaction of K with the membrane plays a significant role in the mechanism of lipopeptide-mediated membrane fusion. In this chapter a proof of this hypothesis is attempted. The membrane interaction of amphipathic helices of the class A type, such as peptide K, is thought to be enhanced by snorkeling of lysine side chains, i.e. their bending towards a more polar environment. It is shown here, that inhibition of this mechanism in K-variants with shortened lysine side chains significantly reduces the membrane affinity of the peptide and its binding affinity to peptide E. However, when tethering these K-homologues in form of lipopeptides to vesicles, membrane fusion with CPE was not inhibited as anticipated due to unexpected changes of the peptides' lipid affinity at the bilayer. Nevertheless, these results allow for important conclusions about the molecular details of the K-membrane and E/K interactions.

INTRODUCTION

The understanding of the mechanism of vesicle fusion mediated by coiled-coil forming lipidated peptides such as LPE, LPK, CPE, and CPK studied in the last chapters and several vesicle fusion studies,[1-6] is thought to allow the specific enhancement of such systems. The initial inspiration for these synthetic membrane-fusion model systems was derived from natural SNARE (soluble NSF attachment protein receptor) proteins. These play a central role in the complex protein machinery that drives specific intracellular membrane fusion, for instance in neuronal release of neurotransmitters.[7-9] The SNARE proteins are known to dock, fusing vesicles to the target membrane by the formation of a 4-helix coiled-coil bundle. Although the molecular players were identified in recent years, the precise sequence of molecular events in neuronal vesicle fusion remains a highly debated topic.[8-12] Despite the differences, a common feature in the various models is that docking of the vesicles to the target membrane is necessary but does not provide sufficient energy to enable full bilayer merging. Instead, mechanisms are under discussion that involve stress generation or destabilization in the prefusion membrane, with this stress or destabilization being released after fusion. This can for instance be a pulling force that arises from the zippering of the spacer region of the SNARE complex into a rigid coiled-coil from the prefusion trans- to the postfusion cis- complex,[8,9] or a specific Ca^{2+}-dependent wedge like incorporation of synaptotagmin into one leaflet of the bilayer.[10-13]

In the synthetic fusogenic lipopeptide systems the coiled-coil forming peptides E and K are tethered to the membrane anchor via a polyethylene glycol spacer. A transfer of a pulling force into the bilayer by such a flexible moiety appears questionable. However, in *Chapters III-IV* evidence was presented that K incorporates into lipid mono- and bilayers with its helical axis parallel to the membrane plane due to its amphipathic character. The amphipathic helix of class A that was proposed as the membrane interacting form might therefore form the necessary peptide wedge that creates sufficient membrane curvature to promote the bilayer merging. A possible approach to prove such a mechanism is the targeted inhibition of the peptide membrane interaction which is anticipated to drastically reduce fusion efficiency. This inhibition could be achieved by varying the lipid composition, aiming for a non-binding composition. The challenge in this approach will be to ensure that the physical properties of the membrane are not changed too drastically allowing fusogenity to be retained. Unpublished results from Martelli et. al. imply the feasibility of this approach.[14]

An alternative strategy that will be followed in this chapter is to use a negative redesign approach, i.e. to inhibit the peptide membrane interaction by varying the peptide primary structure.[15] The challenge with this approach will be to retain

the coiled-coil binding propensity and specificity of K as these properties are anticipated to have an influence on vesicle docking and therefore fusion efficiency.[3,6] A disruption of the amphipathic helix or a change of the overall charge of K should, in principle, inhibit the helical membrane incorporation, although such a strong change will also significantly change the binding properties. Thus, the sequence variation should be relatively subtle.

A characteristic property of the helical wheel of K is its regularity, which is a consequence of its uniform primary structure. The positions of the heptad repeat, (*a*...*g*) which is the typical repeating sequence pattern in coiled-coils, are uniformly filled with the same amino acids (Chart 1).[16,17] This regular primary structure also leads to a very uniform distribution in the standard α-helix with 3.6 residues per turn. This distinct arrangement with the positively charged residues orthogonal to the hydrophobic moment and the negatively charged ones central on the polar face was categorized as a class A amphipathic helix, which is common in apolipoproteins and interacts with lipid interfaces.[18,19]

It was proposed that the relatively long lysine side chains, often found in the orthogonal position of the class A helices, bend towards the polar face which increases the surface of the hydrophobic face and brings the charged tips into a more favorable polar environment (Figure 1).[19-25] This process, called snorkeling, creates a wedge shaped cross section and allows the helix to penetrate more deeply into the hydrophobic interior of the lipid bilayer and thus enhances its membrane affinity. One way to limit the effectiveness of snorkeling is to substitute the lysines with ornithine or 2, 4- diaminobutyric acid, i.e. amino acids whose side chains are, respectively, one or two methylene units shorter than lysine but contain the same terminal amino functionality (Chart 1).[21] However such a relatively subtle change still can have a substantial influence on the binding properties of a coiled coil complex as electrostatic *g/e'* interactions, i.e. between the *g* position of one helix and the *e* position of the subsequent heptad of the other helix, are affected and are known to contribute to the binding energy (Chart 1).[15,26-29]

In this chapter, the design of K homologues with shortened lysine side chains is reported. The coiled coil binding properties in homo- and hetero complexes with E are studied in detail. Furthermore, the membrane interactions of the K-homologues are probed, which substantiates the principle feasibility of the chosen negative design approach and the influence of snorkeling on the membrane interaction of K. From this initial set of K-homologues, the most promising candidates with regard to little membrane and reasonable E binding were chosen and CPK lipopeptide homologues based on these K homologues were synthesized. These CPK homologues were then tested for their ability to induce membrane fusion.

Chart 1. Helical wheel projection of the E/K coiled coil complex, with potential ionic interactions marked as broken lines; chemical structures of lysine, ornithine, and 2, 4 – diaminobutyric acid; helical wheel projection of K as a monomeric α-helix, the arrow indicates the direction of the hydrophobic moment. Images created by means of 'Draw-Coil 1.0' and 'HeliQuest 2'.[16, 17]

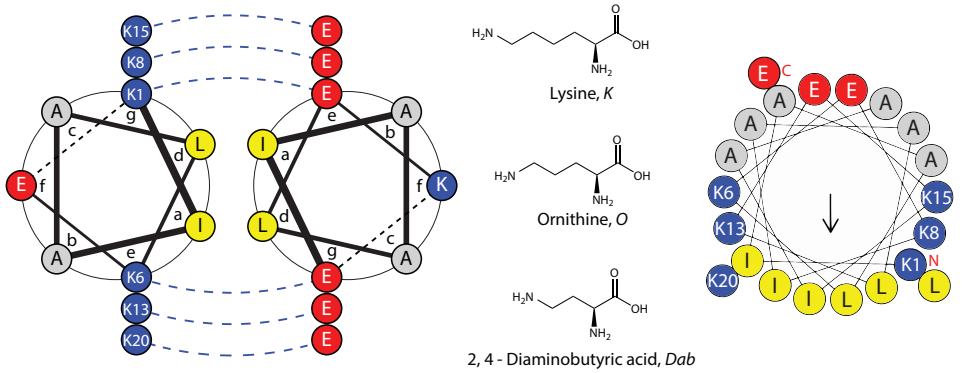

RESULTS AND DISCUSSION

PEPTIDE DESIGN

Peptide K was redesigned using shorter lysine analogues in order to reduce the snorkeling ability of the peptides whilst leaving the overall amphipathic helix and the charge distribution intact as these factors are important for maintaining coiled coil binding and specificity. Ornithine (O) with one methylene unit shorter, and 2, 4 – diaminobutyric acid (Dab) with two methylene units shorter, were used to substitute all lysine residues in the *e* and *g* positions of the heptads which gave the peptides O_6 and Dab_6 (Chart 1 and Table 1). It was found that these substitutions strongly influenced the coiled-coil binding strength (see below). Thus, to obtain a variant of K that more closely resembles the binding properties of the original E/K pair, further derivates were synthesized with partial substitutions of the lysines. The peptides K_3O_3 and O_3K_3 had all *e*, or all *g*, positions substituted with ornithine; and the peptide $K_2O_2K_2$ had the two middle lysines, K8 and K13, substituted with ornithine residues (Table 1). All peptides were synthesized using solid phase peptide synthesis.

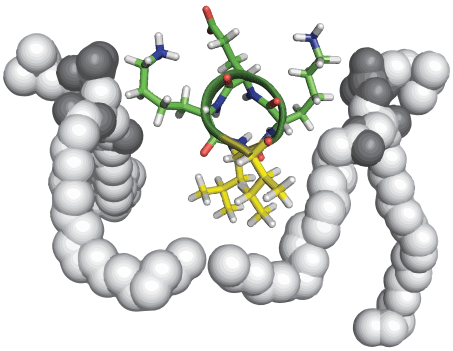

Figure 1. Illustration of the snorkeling mechanism of the *LKEKI* sequence of peptide K. View from the C-terminus. Long chained positively charged lysine residues bend towards the polar face. Carbons of hydrophobic *I* and *L* residues are depicted in yellow, carbons of polar residues *K* or *E* are green. Nitrogen, oxygen, and hydrogen atoms are blue, red and white, respectively.

Table 1. Overview of the studied peptides.

Short name	Substitution[a]	Sequence[a]
E		Ac-(*EIAALEK*)$_3$-NH_2
K		Ac-(*KIAALKE*)$_3$-NH_2
Dab_6	*K1, K6, K8, K13, K15, K20 = Dab*	Ac-(*DabIAALDabE*)$_3$-NH_2
O_6	*K1, K6, K8, K13, K15, K20 = O*	Ac-(*OIAALOE*)$_3$-NH_2
O_3K_3	*K1, K8, K15 = O*	Ac-(*OIAALKE*)$_3$-NH_2
K_3O_3	*K6, K13, K20 = O*	Ac-(*KIAALOE*)$_3$-NH_2
$K_2O_2K_2$	*K8, K13 = O*	Ac-*KIAALKE OIAALOE KIAALKE*-NH_2

[a]Ornithine residues are denoted by *O*; 2, 4 – diaminobutyric acid residues are denoted by *Dab*

COILED-COIL BINDING

Circular dichroism (CD) spectroscopy was used to determine the binding properties of the peptides. First, the tendency of all peptides to form homomeric coiled-coil complexes was tested by means of temperature dependent circular dichroism (CD) spectroscopy. The mean residue ellipticity at 222 nm ($[\theta]_{222nm}$) is a convenient measure for the helical content and melting curves based on this measure yield valuable insight as to the thermodynamics and molecularity of the complex folding (*Chapter II*).[30-33] The $[\theta]_{222nm}$ temperature curves of E and K showed increasing ellipticities reaching a plateau, which indicates a cooperative unfolding of the helical peptides. Similar observations were found for the tryptophan labeled variants E_{GW} and K_{GW} of these peptides in *Chapter II* and can be interpreted as the unfolding of the homomeric coiled coils E/E and K/K (see below). In contrast the $[\theta]_{222nm}$ curves of the peptides containing Orn and Dab displayed no temperature dependent unfolding behavior and their spectra showed the characteristics of unstructured peptides (Figure A1 and Figure A2). Thus, the homo-coil formation is strongly inhibited by the shortened side chains.

The comparison of the behavior of E with O_6 indicates that, despite Orn and Glu having equal side-chain lengths, the carboxylate group of the glutamic acid residues are preferred for homo coil formation over the ammonium groups of ornithine. Both the homo coil inhibition with shorter chain lengths and the preference of the carboxylate in the homo coil were reported by Ryan and Kennan, who studied the chain length influence in the *e* and *g* positions of an acidic and basic coiled-coil pair acid-p1/base-p1.[27] Thus, they appear to be general effects and illustrate the importance of electrostatic interactions between residues in the *g* and *e'* positions. A possible explanation for these effects might be a mechanism similar to the snorkeling of lysine side chains in the amphipathic A helix. In the relatively unstable E/E and K/K homocoils the side chains in the *e* and *g* positions might reduce the

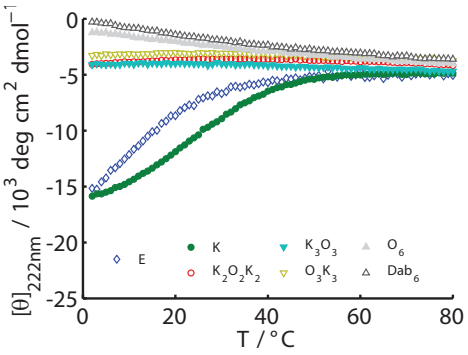

Figure 2. Temperature dependency of mean residue ellipticity at 222 nm of E, K, and K- homologues. Experimental conditions: [peptide] = 100 µM,buffer: PBS, pH 7.4.

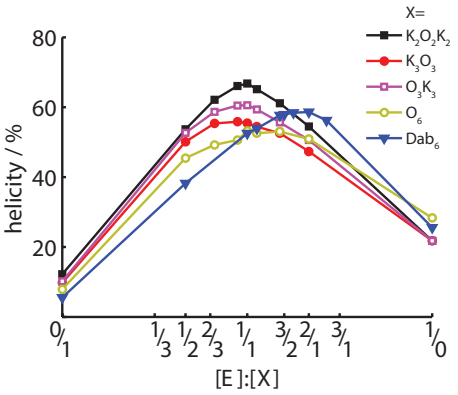

Figure 3. Job plot of the coiled coil complexes composed of E and K homologues (X) at constant total monomer concentrations $[E]+[X]=200\,\mu M$.

repulsive ionic interactions by bending away from the binding partner. The reduction of this ability might therefore explain the inhibited homocoiling in the side-chain shortened K-homologues.

To test if the K derivatives form coiled-coil complexes with E, Jobs method[34,35] was applied, i.e $[\theta]_{222nm}$ was used to determine the helicity as a function of the molar ratio of E to its binding partner X ($[E] : [X]$), while leaving the total peptide concentration ($[E] + [X]$) constant (Figure 3). When E was mixed with the different binding partners, the CD spectra showed the typical shape of helical peptides with minima at 208 nm and 222 nm (Figure A1 and Figure A2). Based on $[\theta]_{222nm}$ all K-variants showed an increased helical content when mixed with E, compared to the peptides alone at $[E] : [X] = 0 / 1$, or 1 / 0 respectively. This shows that E interacts with all the binding partners and forms heteromeric coiled-coil complexes. For the complex E/K, the stoichiometric ratio is known to be 1 : 1.[36]

The peptides K_3O_3, O_3K_3 and $K_2O_2K_2$ showed maximum helical content at $[E] : [X]$ of 1 : 1, which implies that they form a complex with equal numbers of chains of both binding partners, i.e. their stoichiometric ratio ($v_E : u_X$) is also 1 : 1. For Dab_6 the maximum helical content is found at $[E] : [Dab_6] = 2 : 1$, implying this stoichiometric ratio for the coiled-coil complex. The Job plot of O_6 is broader, compared to the others, which might either be caused by several complexes of different stoichiometric ratios or a relatively low binding constant.[37]

Temperature and concentration dependent CD unfolding curves of the peptide complexes were measured, to determine the thermodynamics of un-folding and the molecularity (n) of the unfolding process (Figure A3 - Figure A10). All studied complexes including the homocoils of E/E and K/K showed shifts of the unfolding curves to higher tem-peratures with increasing total peptide concentration, implying that all

observed unfoldings involve more than a single peptide chain (*Chapter II*).[38,39] The data were fitted to thermodynamic unfolding models of different molecularities. The unfolding curves of all peptide complexes except E/Dab_6 were best fitted by models with $n = 2$, based on the minimum root mean square error of the fits (RMSE, Figure 4). This means that these peptides form predominantly dimers in solution. The only exception, E/Dab_6, gave good fitting models with molecularities of 3 and 4. Taking into account the result of Jobs method, which implied a stoichiometric ratio in the complex of 2 : 1, this indicates that the coiled-coil complex is trimeric with two chains of E and one chain of Dab_6.

The best fitting models also yielded the thermodynamics of the unfolding with the parameters ΔH°, T° and ΔCP, which allows the prediction of the complex stability at every temperature (Table A1). These parameters were used to calculate the free enthalpy of unfolding per monomer chain as well as the folding constant at 25 °C (ΔG_{25} / n and K_{F25}), which allows for a comparison of the stability of the different coiled complexes (Figure 5 and Table 2). The original sequence of E/K was found to be the most stable of the studied complexes with the highest ΔG_{25} and K_{F25}. Shortening of the side chains in the e and g positions led, in every case, to a reduction of the free enthalpy per chain. The E/O_6 dimer was found to be the least stable of the heterodimers. Compared to that, the unfolding free enthalpy of E/Dab_6 is increased, showing that the formation of the trimer compensates for the loss of unfolding energy upon shortening of the side chains.

The peptide pairs with mixed ornithine and lysine side chains E/O_3K_3, E/K_3O_3, and E/$K_2O_2K_2$ showed intermediate stabilities and folding constants in the same order of magnitude (Table 2). It appears that the position of substitution in the helix has an influence on the unfolding free enthalpy, although definitive conclusions are difficult due to the low significance of the differences. The unfolding free enthalpy of the homo coils K/K and E/E was found to be the smallest, which is due to the repulsive interactions of identically charged residues in the *e* and *g* position in these complexes.

The general trend of the decreasing dimeric hetero coiled-coil stability with the decreasing chain length of charged residues in the *e* and *g* positions is in line with the results reported by Ryan and Kennan for the homologues of acid-p1/base-p1.[27] In their study the side chain shortened variants were forced into a dimeric state by single buried asparagine residues in the *a* position of the heptad and the shortening of the basic side chains up to 2, 3-diaminopropionic acid resulted in a strong destabilization of these complexes. A comparable effect for the *b* and *c* positions in tetrameric complexes was also reported by Vu et. al.[26] The reason for the effect in the dimers appears to be the ability of the longer side chains in the *e* position to get closer to the oppositely charged residue in the *g'* position of the neighboring peptide,

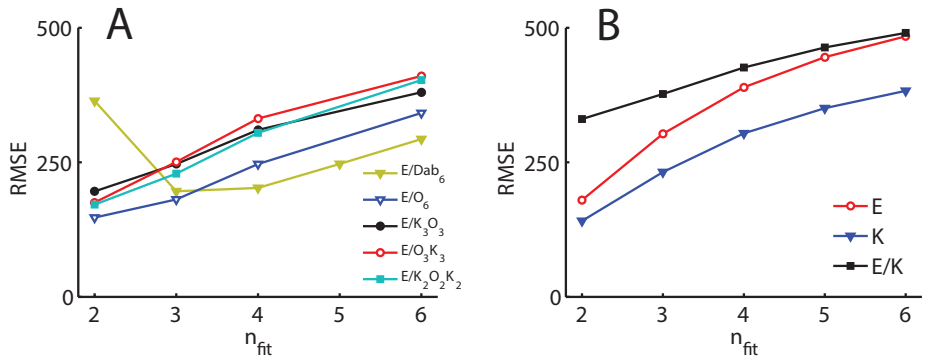

Figure 4. Root mean square errors of best fits with different models (n_{fit} = 2…6) for (A) the coiled coils of E with the K homologues E/X; (B) E, K and E/K. Data was fitted using *FitDis!*. For data, best fitting models, and fit parameters see appendix.

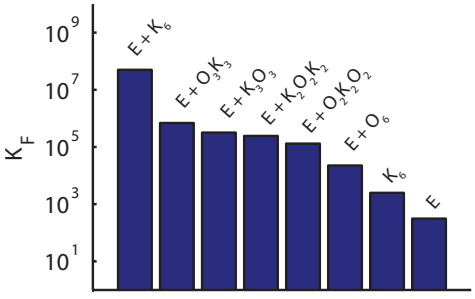

Figure 5. Free enthalpy of peptide folding at 25 °C per chain monomer of all studied peptide complexes.

Table 2. Folding constants of studied coiled coil complexes at 25 °C

Coiled coil	K_{F25}
E/K	3.7 10^6 M^{-1}
E/KDab	1.7 10^9 M^{-2}
E/O3K3	6.9 10^5 M^{-1}
E/K3O3	3.2 10^5 M^{-1}
E/K2O2K2	2.4 10^5 M^{-1}
E/Korn	2.3 10^4 M^{-1}
K/K	2.5 10^3 M^{-1}
E/E	3.1 10^2 M^{-1}

which increases attractive ionic interactions and stabilizes the dimeric state. In a molecular dynamics study, Pendley et al. predicted a drastically reduced coiled-coil binding propensity of E/O_6, due to the reduction of this stabilizing effect,[28] which is in line with the results reported here. This stabilizing effect was even stronger reduced for E/Dab_6, destabilizing the potential dimer so far that the trimer was formed. The trimeric state is thought to be a relatively stable oligomeric default state for coiled-coils, that is adopted in the absence of strong determinants of oligomeric state.[15]

The aim of the present study is to find a homologue for peptide K with suppressed membrane interactions while retaining the oligomeric state and the binding strength as much as possible. Considering these criteria, the variants with mixed lysine and ornithine residues in *e* and *g* positions appeared to be the best candidates for the further studies.

PEPTIDE MEMBRANE INTERACTIONS

To probe if the peptides interact with membranes as the original K, the temperature dependency of $[\theta]_{222nm}$ was measured for the peptides mixed with vesicles of the composition DOPE : DOPE : Cholesterol 2 : 1 : 1 (Figure 6). Strikingly, mixing with vesicles had no significant influence on any of the K homologues, while $[\theta]_{222nm}$ of K mixed with vesicles showed the typical decrease due to its increased helicity over the whole temperature range as known from *Chapter V*.

Thus, the interactions of the K homologues with the membrane are drastically reduced as was intended by the negative peptide design. The chain length of the positively charged side chains placed orthogonally to the amphipathic moment in the A-helix has a strong influence on membrane incorporation, which can be explained by the snorkeling of these chains. The longer lysine side chains are thought to allow a deeper penetration of the amphiphatic A-helix into the lipid bilayer as they can bend further towards the hydrophilic face of the helix.[19,21,25] A deeper possible penetration depth increases the peptides' lipid affinity, due to an increased hydrophobic interaction.

Mishra et. al. showed reduced lipid affinity for a homologue of the model peptide 18A where all 4 lysine residues were substituted by 2, 4–diaminobutyric acid.[21] Interestingly, it is shown here that shortening of only the two central lysine side chains in a helix with 5.8 turns as in $K_2O_2K_2$ significantly decreases the lipid affinity of the helix. Also, shortening on one side of the helix as in K_3O_3 and O_3K_3 gives this effect which shows that the cooperative snorkeling of several lysine side chains is responsible for the relatively high lipid affinity of K.

LIPOPEPTIDE MEDIATED VESICLE FUSION

As all the tested peptides showed a reduced lipid affinity compared to K with no measurable lipid induced helix formation (Figure 6), they all appeared suitable for generating lipopeptide variants of CPK with reduced lipid interaction. Taking the binding properties into account, O_3K_3 and $K_2O_2K_2$ were chosen for further experiments as they were found to form dimeric hetero coils with E and most closely resemble the binding affinity of the original sequence. The lipopeptides CPO_3K_3, $CPK_2O_2K_2$, CPK, and CPE were synthesized using standard methods (Chart 2).[2,5]

To study the lipopeptides ability to mediate membrane fusion, two sets of liposomes of the composition DOPE : DOPE : Cholesterol 2 : 1 : 1 in PBS were prepared. One set contained CPE and the other CPK or its homologues $CPK_2O_2K_2$ and CPO_3K_3, the lipopeptide concentration with respect to the total lipid concentration in all vesicles was 1 mol%. Vesicle fusion can be identified by three hallmarks: aggregation; lipid mixing; and content mixing (Figure 7).[1-6,40] Aggregation

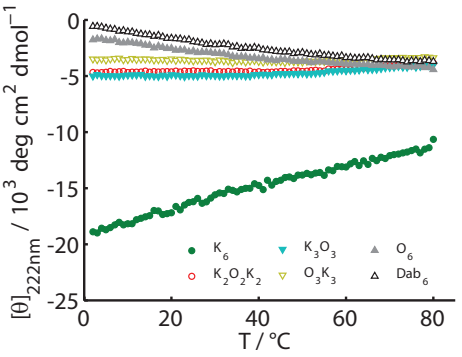

Figure 6. Temperature dependency of mean residue ellipticity at 222 nm of E, K, and K- homologues mixed with DOPE : DOPE : Cholesterol (2 : 1 : 1) vesicles. Experimental conditions [lipid] : [peptide]=25 : 1, [peptide] = 100 μM.

of vesicles can be measured by means of dynamic light scattering. The mixing of lipids within the bilayer is measured by means of lipids fluorescently labeled with lissamine rhodamine B (LR-DOPE) and 7-nitro-2-1,3-benzoxadiazol-4-yl (NBD-DOPE) which are incorporated into the CPE containing liposomes.[40,41] Mixing of this bilayer with a label-free bilayer results in the reduction of Förster resonance energy transfer (FRET) and consequently gives an increase in the FRET donor fluorescence (DOPE-NBD). The 100% reference is the fluorescence of liposomes containing only half of the dyes. Finally, content mixing is measured using the self-quenching fluorescent dye sulforhodamine B, which is encapsulated in CPE containing vesicles.[4,5] Upon content mixing the dye is diluted, which leads to an increase in fluorescence intensity, here the 100% reference was the fluorescence of vesicles lysed by detergent. The 0% reference value in both content and lipid mixing experiments was the fluorescence of CPE vesicles mixed with vesicles lacking the binding partner.

Contrary to expectations, vesicles labeled with CPO_3K_3 and $CPK_2O_2K_2$ showed all three hallmarks of fusion upon mixing with CPE containing vesicles (Figure 7). The hydrodynamic radii (r_h) increased after mixing of the vesicles and the lipid and content mixing assays showed fluorescence increases comparable to the original CPK. Thus, the anticipated inhibition of fusion could not be observed and vesicle fusion is mediated also by the side chain shortened homologues of CPK.

Chart 2. Chemical structure of lipopeptides CPE, CPK, CPO_3K_3, and $CPK_2O_2K_2$. Positions of the amino acids in the heptad repeat are denoted with the letters a…g, Ornithine residue is denoted with O

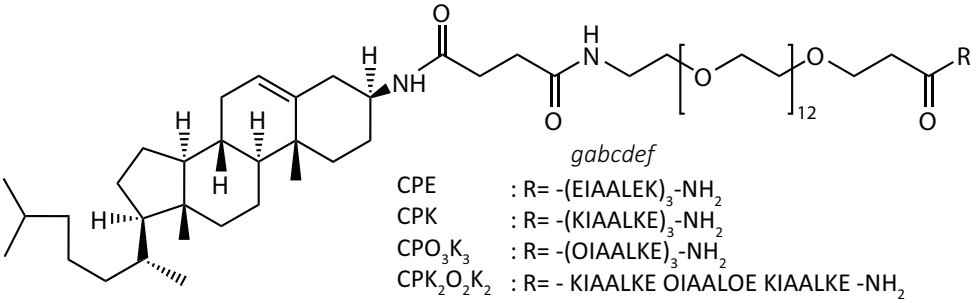

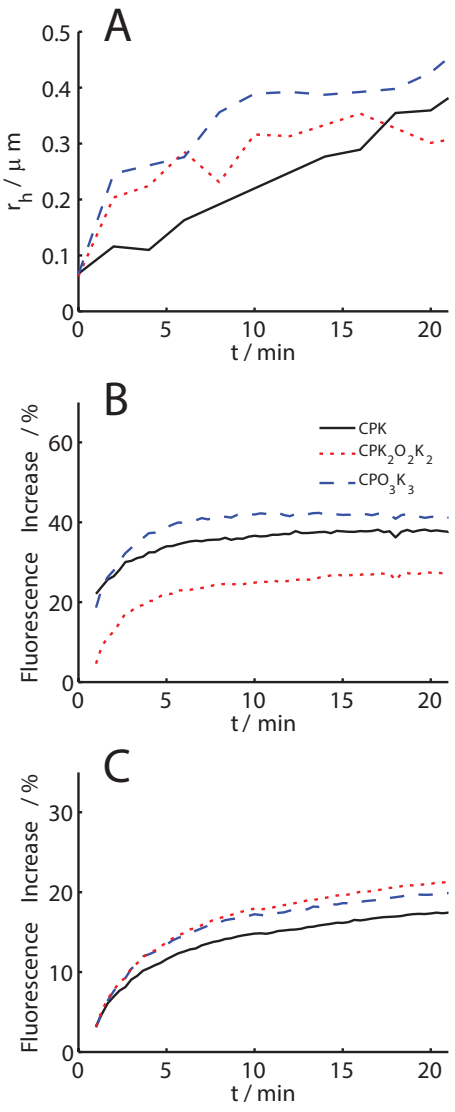

Figure 7. Results of vesicle fusion experiments. Mixing of CPE decorated liposomes with CPK (black line), $CPK_2O_2K_2$ (red line), or CPO_3K_3 (blue line) resulted in (A) increase of hydrodynamic radius as measured by DLS; (B) lipid mixing, measured by increase of DOPE-NBD fluorescence in FRET experiments; and (C) mixing of vesicle contents, measured by increase in sulforhodamine B fluorescence. In all experiments: lipopeptide concentration 1 mol%; [lipid] = 100 µM; buffer: PBS pH 7.4 in (A) and (B); TES pH 7.4 in (C).

To reassess whether the interactions of the lipopeptides with the membrane are indeed inhibited as anticipated, $[\theta]_{222nm}$ of lipopeptide containing vesicles was measured as a function of the temperature (Figure 8). Surprisingly, the membrane tethered $CPK_2O_2K_2$ and CPO_3K_3 showed a reduced mean residual ellipticity compared to the untethered $K_2O_2K_2$ and O_3K_3 in a mixture with vesicles. This shows that the helical content is significantly increased. It is unlikely, that this increased helical content is caused by the formation of homomeric coiled coils on the membrane, because in this case $[\theta]_{222nm}$ would display a typical sigmoidal shape of a cooperative unfolding as was shown for CPE (*Chapter V*). Instead, the $[\theta]_{222nm}$ curves overlap largely with the graphs of vesicle tethered CPK and vesicles mixed K (Figure 8), i.e. they show similar slopes and values of helicity. Thus this data indicates, that the CPK homologues $CPK_2O_2K_2$ and CPO_3K_3 partially fold into α helices and interact with the membrane they are tethered to as was found for membrane tethered K (*Chapters III-V*).

This means that the interaction of these peptides with the membrane is strengthened due to their tethering to the membrane. The full CD spectra at 25 °C of the untethered peptides $K_2O_2K_2$ and O_3K_3 showed only very little effect upon mixing with vesicles (Figure 9). The membrane tethered $CPK_2O_2K_2$ and CPO_3K_3 however, clearly showed spectra with more pronounced minima at 222 nm

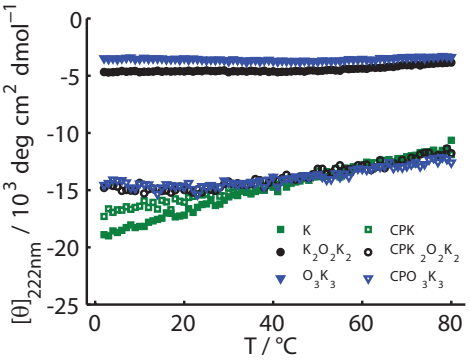

Figure 8. Temperature dependency of mean residue ellipticity at 222 nm of K, $K_2O_2K_2$, and O_3K_3 mixed with vesicles and vesicle tethered CPK, $CPK_2O_2K_2$, and CPO_3K_3. Experimental conditions [lipid] : [peptide] = 25 : 1, [peptide] = 100 µM; [lipid] : [CPX] = 100 : 1, [CPX] = 10 µM, lipid composition DOPE : DOPE : Cholesterol (2 : 1 : 1), in PBS, pH7.4.

and 208 nm, indicative of the formation of helices. A similar increase of the peptide membrane interactions due to membrane tethering was also reported for the lipopeptides LPK in monolayer experiments (*Chapter III*) and LPK_{GW} in tryptophan fluorescence measurements (*Chapter IV*) and appears to be a general property of these systems, although the reasons for this are unclear at this moment. Unfortunately this effect also causes $CPK_2O_2K_2$ and CPO_3K_3 to resemble CPK in their membrane interactions and makes drawing significant conclusions on the effect of these interactions on lipopeptide mediated membrane fusion impossible.

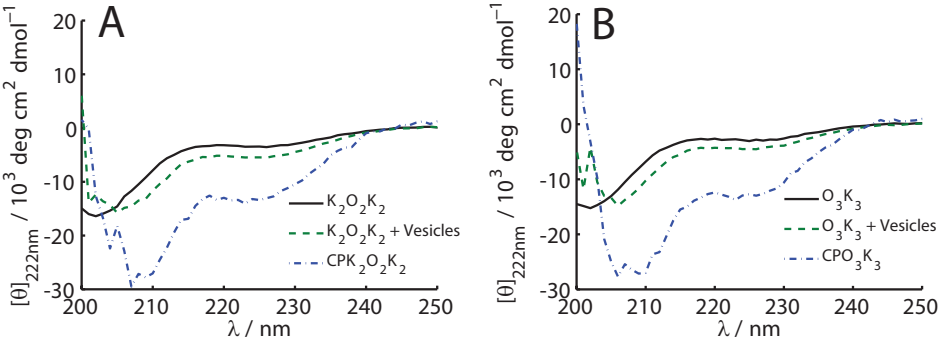

Figure 9. Circular dichroism spectra at 25 °C of (A) $K_2O_2K_2$, $K_2O_2K_2$ mixed with vesicles, and vesicle tethered $CPK_2O_2K_2$; (B) O_3K_3, O_3K_3 mixed with vesicles, and vesicle tethered CPO_3K_3. Experimental conditions are the same as in Figure 9.

CONCLUSIONS

The shortening of the lysine side chains in the *e* and *g* positions of the heptad repeat of peptide K had an inhibiting effect on both its coiled-coil formation with E and its lipid affinity. Both properties are determined by similar structural constraints of K and a targeted inhibition of one without influencing the other remains challenging if not impossible.

A substitution of all six lysines by ornithine led to very weak E binding and a substitution with six 2, 4 - diaminobutyric acid further destabilized the dimer and more stable trimers were the predominant species in solution. Partial substitution

yielded stronger binding that more closely resembles the properties of the original K. None of the K-homologues showed a strong α-helical interaction with lipids used in vesicle fusion experiments. This proves that lysine snorkeling makes a substantial contribution to the lipid affinity of K. However when tethered to the lipid membrane in the form of lipopeptides, $CPK_2O_2K_2$ and CPO_3K_3 resemble CPK in helicity and show an increased membrane interaction. Accordingly, their ability to mediate membrane fusion with CPE labeled vesicles is similar to CPK.

This approach to the study of the influence of the peptide membrane interactions on the lipopeptide mediated fusion by shortening the lysine side chains turned out to be complicated by the multiple effects such a variation causes and has not yet been successful. Furthermore it became apparent that untethered peptides with low lipid affinity can display a different behavior once tethered to the membrane and this was unexpected. In future, this behaviour should be considered when predicting lipopeptide properties on the basis of peptide properties.

EXPERIMENTAL SECTION

MATERIALS

Fmoc-protected amino acids and Sieber Amide resin for peptide synthesis were purchased from Novabiochem. DOPC (1, 2-dioleoyl-sn-glycero-3-phosphocholine), DOPE (1, 2-dioleoyl-sn-glycero-3-phosphoethanolamine), cholesterol, NBD-DOPE (1,2-dioleoyl-sn-glycero-3-phosphoethanolamine-N-(7-nitro-2-1,3-benzoxadiazol-4-yl) (ammonium salt)), and LR-DOPE (1,2-dioleoyl-sn-glycero-3-phosphoethanolamine-N-(lissamine rhodamine B sulfonyl) (ammonium salt)) were purchased from Avanti Polar Lipids. Solvents, sulforhodamine B, and buffer salts were purchased from Sigma-Aldrich. All water was ultrapure with resistance ≥ 18 MΘ cm^{-1} and TOC ≤ 2 ppm produced from a MilliQ Reference A+ purification system. All experiments were carried out in phosphate buffered saline (PBS) of the following composition: 150 mM NaCl, 20 mM PO_4^{3-} in H_2O at pH 7.4.

PEPTIDE SYNTHESIS

The peptides E: Ac-$(EIAALEK)_3$-NH_2, K: Ac-$(KIAALKE)_3$-NH_2, were synthesized using standard Fmoc-chemistry on a Biotage Syro I and purified by RP-HPLC to yield a purity > 95% based on HPLC. Identity of the peptides was determined by LC-MS. The lipopeptides were synthesized and purified as described elsewhere.[2,5] Peptide stock solutions in PBS were prepared at concentrtations of ~2 mg / ml, the concentration was based on the mass. Lipopeptide stock solutions were prepared in a $CHCl_3$: MeOH 3 : 1 solution and added to the lipids prior to solvent evaporation.

VESICLE PREPARATION.

Lipid stock solutions of the compositions DOPE : DOPE : Cholesterol (2 : 1 : 1) and DOPE : DOPE : Cholesterol:NBD-DOPE : LR-DOPE (49.5 : 24.75 : 24.75 : 0.5 : 0.5) were prepared in $CHCl_3$: MeOH 3 : 1. For experiments with lipopeptides, stock solutions were mixed with CPE, CPK, $CPK_2O_2K_2$ or CPO_3K_3 stock solutions in $CHCl_3$/MeOH to yield mixtures with 1 mol% lipopeptide content. Lipid films were created by slow evaporation of the solvent from a precise amount of stock solution under a N_2 stream and kept under vacuum overnight. The films were rehydrated with PBS yielding final lipid concentrations of typically 0.1 – 2.5 mM. Large unilamellar vesicles (LUVs) were formed by sonication at 55°C for ~10 min. The size of the vesicles was tested by DLS using a Malvern Zetasizer nano-s and was typically found to be ~100 nm.

CIRCULAR DICHROISM SPECTROSCOPY

CD spectra were measured using a Jasco J815 CD spectrometer equipped with a Jasco PTC 123 peltier temperature controller. Quartz cuvettes with pathlengths l of 1 or 2 mm were used. Spectra were measured from 190 nm to 250 nm with a bandwith of 1 nm, baseline corrected and the mean residue ellipticity *[θ]* was calculated by:

$$[\theta] = \frac{\theta}{l\, c_M\, N} \tag{1}$$

where θ is the observed ellipticity, l the pathlength, c_M the molar total peptide concentration and N the number of amino acids per peptide.

For Job plots at 25 °C the relative peptide ratio of E to its binding partner *[E] : [X]* was varied between 0 : 10 and 10 : 0 while leaving the total peptide concentration *[E] + [X]* constant at 200 µM. The relative α - helicity (*rh*) was calculated from the ellipticity at 222 nm $[\theta]_{222nm}$ by:[30,31]

$$rh = \frac{[\theta]_{222nm}}{-40\ 10^3\ \mathrm{deg\,cm^2\ dmol^{-1}}\ \left(1 - \frac{4.6}{N}\right)}\ 100\% \tag{2}$$

For probing of peptide-lipid interactions, peptide stock solutions were diluted with buffer to the desired total peptide concentration and eventually mixed with vesicles at [Lipid] : [Peptide] = 25 : 1 at 100 µM total peptide concentration. Spectra of the lipopeptides tethered to vesicles were measured at [Lipid] : [CPX] = 100 : 1 in 1 mM total lipid concentration.

For temperature dependent unfolding experiments, peptide stock solutions were diluted with buffer to the desired total peptide concentrations in the range 5 - 200 µM for the hetero coiled-coil complexes and in the range 100 – 1000 µM for

the weaker binding homo coiled-coil complexes of E and K. $[\theta]_{222nm}$ was measured as a function of temperature T at a heating rate of 40 °C / h in the range 2 – 95 °C. Additionally, CD spectra between 190 - 260 nm were collected at T = 5, 25 and 80 °C. Spectra taken at 5 °C before and directly after a full heating cycle were found to be fully reproducible. The data was analyzed by means of the thermodynamic formalism described in detail *Chapter II* using the program *FitDis!*. The general equilibrium for the 2 state unfolding of an n-meric folded peptide complex into n monomers with the folding and unfolding constants K_F and K_U is:

$$A1_{\upsilon_1}A2_{\upsilon_2} \ldots \overset{K_U/K_F}{\longleftrightarrow} \upsilon_1 A1 + \upsilon_2 A2 + \ldots, \tag{3}$$

where the molecularity n is the sum of the stoichiometric factors υ_i ($n = \Sigma\upsilon_i$). The equilibrium constants give access to the free enthalpy of unfolding (ΔG) by:

$$[K_U] = e^{\frac{-\Delta G}{RT}} \tag{4}$$

with the absolute temperature T and the gas constant R. The temperature dependency of ΔG is determined by the Gibbs-Helmholtz equation with the thermodynamic parameters $\Delta H°$, $T°$, and ΔC_p and connected to the measured signal ($[\theta]_{222nm}$) via the baseline parameters θ_{F0}, θ_{u0}, m_F, and m_U as described in detail in *Chapter II*. These parameters are used to fit the data and stand for the temperature where $\Delta G = 0$ ($T°$), the enthalpy at $T°$ ($\Delta H°$), the change of heat capacity upon unfolding (ΔC_p), the ellipticities of the fully folded and fully unfolded state at 0 °C (θ_{F0} and θ_{u0}), and the temperature slopes of the ellipticities of the fully folded and fully unfolded state (m_F and m_U). The data was fitted by different models from n = 2…6, with $\upsilon_1 = \upsilon_2$ for even n and $\upsilon_1 = \upsilon_2 + 1$ for odd n in the case of hetero coiled coils and $\upsilon_1 = n$ in the case of homo coiled coils of E and K. The fitting procedure is explained in *Chapter II* also. The different models were compared on the basis of the root mean square errors (RMSE) of the fits.

VESICLE FUSION EXPERIMENTS

In all fusion experiments CPE containing vesicles were mixed in a 1 : 1 ratio with vesicles containing CPK, $CPK_2O_2K_2$ or CPO_3K_3, total lipid concentrations were 0.1 mM and lipopeptides in the bilayers were at 1 mol%. Size increase was measured using a Malvern Zetasizer nano-s. Before mixing, vesicle solutions showed only one population with a hydrodynamic radius (r_h) of ~50 nm. After mixing, the size was measured every 2 minutes for 60 minutes and generally two populations were

observed: one at a relatively constant radius of 40 - 80 nm which had decreasing intensity and another with increasing r_h and increasing intensity. The latter population was interpreted as the size increase.

For lipid mixing, CPE containing vesicles contained additionaly 0.5 mol% LR-DOPE and 0.5 mol% NBD-DOPE. After mixing in a black 96 well plate, NBD-DOPE fluorescence emission was measured using a Tecan infinite M1000 pro plate reader. Excitation and emission wavelengths were 460 nm and 535 nm respectively and both bandwidths were 10 nm. The fluorescence increase ΔF was calculated by:

$$\Delta F = \frac{F - F_0}{F_{max} - F_0}, \tag{5}$$

with the fluorescence emission F, and the reference values F_{max} and F_0. In lipid mixing experiments F_0 was the fluorescence emission of CPE labeled vesicles mixed with vesicles containing no lipopeptides and F_{max} was the fluorescence emission of vesicles containing only half the dyes NBD-DOPE and LR-DOPE.

For content mixing experiments CPE labeled liposomes (total lipid concentration 1 mM) were formed in a 20 mM solution of sulforhodamine B in TES buffer. The vesicles were separated from excess dye by means of a sephadex G-50 column. The vesicle containing fraction was collected and diluted to a total volume of 10 ml to reach a final total lipid concentration of ~0.1 mM. After vesicle mixing, sulforhodamine B emission was monitored at 580 nm using an excitation wavelength of 520 nm and bandwidths of 10 nm. The fluorescence increase was calculated using equation (5), with F_0 being the fluorescence intensity of sulphorhodamine B loaded CPE vesicles mixed with empty vesicles and F_{max} being the fluorescence intensity of sulforhodamine B loaded CPE vesicles lysed with 10 vol% Triton X-100.

REFERENCES

(1) Robson Marsden, H.; Korobko, A. V.; Zheng, T.; Voskuhl, J.; Kros, A., Controlled liposome fusion mediated by SNARE protein mimics. *Biomaterials Science* **2013**, *1*, 1046.

(2) Robson Marsden, H.; Elbers, Nina A.; Bomans, Paul H. H.; Sommerdijk, Nico A. J. M.; Kros, A., A Reduced SNARE Model for Membrane Fusion. *Angew. Chem. Int. Ed.* **2009**, *48*, 2330.

(3) Tomatsu, I.; Marsden, H. R.; Rabe, M.; Versluis, F.; Zheng, T.; Zope, H.; Kros, A., Influence of pegylation on peptide-mediated liposome fusion. *J. Mater. Chem.* **2011**, *21*, 18927.

(4) Versluis, F.; Dominguez, J.; Voskuhl, J.; Kros, A., Coiled-coil driven membrane fusion: zipper-like vs. non-zipper-like peptide orientation. *Faraday Discuss.* **2013**, *166*, 349.

(5) Versluis, F.; Voskuhl, J.; van Kolck, B.; Zope, H.; Bremmer, M.; Albregtse, T.; Kros, A., In Situ Modification of Plain Liposomes with Lipidated Coiled Coil Forming Peptides Induces Membrane Fusion. *J. Am. Chem. Soc.* **2013**, *135*, 8057.

(6) Zheng, T. T.; Voskuhl, J.; Versluis, F.; Zope, H. R.; Tomatsu, I.; Marsden, H. R.; Kros, A., Controlling the rate of coiled coil driven membrane fusion. *Chem. Commun.* **2013**, *49*, 3649.

(7) Rothman, J. E., The Principle of Membrane Fusion in the Cell (Nobel Lecture). *Angew. Chem. Int. Ed.* **2014**.

(8) Südhof, T. C.; Rothman, J. E., Membrane fusion: grappling with SNARE and SM proteins. *Science* **2009**, *323*, 474.

(9) Jahn, R.; Fasshauer, D., Molecular machines governing exocytosis of synaptic vesicles. *Nature* **2012**, *490*, 201.

(10) Hui, E.; Johnson, C. P.; Yao, J.; Dunning, F. M.; Chapman, E. R., Synaptotagmin-Mediated Bending of the Target Membrane Is a Critical Step in Ca2+-Regulated Fusion. *Cell* **2009**, *138*, 709.

(11) Kozlov, M. M.; McMahon, H. T.; Chernomordik, L. V., Protein-driven membrane stresses in fusion and fission. *Trends Biochem. Sci.* **2010**, *35*, 699.

(12) McMahon, H. T.; Kozlov, M. M.; Martens, S., Membrane Curvature in Synaptic Vesicle Fusion and Beyond. *Cell* **2010**, *140*, 601.

(13) Campelo, F.; McMahon, H. T.; Kozlov, M. M., The hydrophobic insertion mechanism of membrane curvature generation by proteins. *Biophys. J.* **2008**, *95*, 2325.

(14) Martelli, G.; manuscript in preparation

(15) Woolfson, D. N. In *Adv. Protein Chem.*; David, A. D. P., John, M. S., Eds.; Academic Press: 2005; Vol. Volume 70, p 79.

(16) Grigoryan, G.; Keating, A. E., Structural specificity in coiled-coil interactions. *Curr. Opin. Struct. Biol.* **2008**, *18*, 477.

(17) Gautier, R.; Douguet, D.; Antonny, B.; Drin, G., HELIQUEST: a web server to screen sequences with specific α-helical properties. *Bioinformatics* **2008**, *24*, 2101.

(18) Segrest, J. P.; De Loof, H.; Dohlman, J. G.; Brouillette, C. G.; Anantharamaiah, G. M., Amphipathic helix motif: Classes and properties. *Proteins: Structure, Function, and Bioinformatics* **1990**, *8*, 103.

(19) Segrest, J. P.; Jones, M. K.; Mishra, V. K.; Anantharamaiah, G. M. In *Curr. Top. Membr.*; Sidney A. Simon, T. J. M., Ed.; Academic Press: 2002; Vol. Volume 52, p 397.

(20) Hristova, K.; Wimley, W. C.; Mishra, V. K.; Anantharamiah, G. M.; Segrest, J. P.; White, S. H., An amphipathic α-helix at a membrane interface: a structural study using a novel X-ray diffraction method. *J. Mol. Biol.* **1999**, *290*, 99.

(21) Mishra, V. K.; Palgunachari, M. N.; Segrest, J. P.; Anantharamaiah, G. M., Interactions of synthetic peptide analogs of the class A amphipathic helix with lipids. Evidence for the snorkel hypothesis. *J. Biol. Chem.* **1994**, *269*, 7185.

(22) Segrest, J. P.; Deloof, H.; Dohlman, J. G.; Brouillette, C. G.; Anantharamaiah, G. M., Amphipathic Helix Motif - Classes and Properties. *Proteins* **1990**, *8*, 103.

(23) Segrest, J. P.; Jones, M. K.; De Loof, H.; Brouillette, C. G.; Venkatachalapathi, Y. V.; Anantharamaiah, G. M., The amphipathic helix in the exchangeable apolipoproteins: a review of secondary structure and function. *J. Lipid Res.* **1992**, *33*, 141.

(24) Mishra, V. K.; Palgunachari, M. N., Interaction of Model Class A1, Class A2, and Class Y Amphipathic Helical Peptides with Membranes. *Biochemistry* **1996**, *35*, 11210.

(25) Palgunachari, M. N.; Mishra, V. K.; Lund Katz, S.; Phillips, M. C.; Adeyeye, S. O.; Alluri, S.; Anantharamaiah, G. M.; Segrest, J. P., Only the two end helixes of eight tandem amphipathic helical domains of human apo A-I have significant lipid affinity. Implications for HDL assembly. *Arteriosclerosis, thrombosis, and vascular biology* **1996**, *16*, 328.

(26) Vu, C.; Robblee, J.; Werner, K. M.; Fairman, R., Effects of charged amino acids at b and c heptad positions on specificity and stability of four-chain coiled coils. *Protein Sci.* **2001**, *10*, 631.

(27) Ryan, S. J.; Kennan, A. J., Variable Stability Heterodimeric Coiled-Coils from Manipulation of Electrostatic Interface Residue Chain Length. *J. Am. Chem. Soc.* **2007**, *129*, 10255.

(28) Pendley, S. S.; Yu, Y. B.; Cheatham, T. E., Molecular dynamics guided study of salt bridge length dependence in both fluorinated and non-fluorinated parallel dimeric coiled-coils. *Proteins-Structure Function and Bioinformatics* **2009**, *74*, 612.

(29) Mason, J. M.; Arndt, K. M., Coiled coil domains: stability, specificity, and biological implications. *Chembiochem* **2004**, *5*, 170.

(30) Chen, Y.-H.; Yang, J. T.; Chau, K. H., Determination of the helix and β form of proteins in aqueous solution by circular dichroism. *Biochemistry* **1974**, *13*, 3350.

(31) Gans, P. J.; Lyu, P. C.; Manning, M. C.; Woody, R. W.; Kallenbach, N. R., The helix–coil transition in heterogeneous peptides with specific side-chain interactions: Theory and comparison with CD spectral data. *Biopolymers* **1991**, *31*, 1605.

(32) Greenfield, N. J., Using circular dichroism collected as a function of temperature to determine the thermodynamics of protein unfolding and binding interactions. *Nat Protoc* **2006**, *1*, 2527.

(33) Marky, L. A.; Breslauer, K. J., Calculating thermodynamic data for transitions of any molecularity from equilibrium melting curves. *Biopolymers* **1987**, *26*, 1601.

(34) Job, P., Recherches sur la formation de complexes mineraux en solution, et sur le stabilite. *Ann. Chim.-Paris* **1928**, *9*, 113.

(35) Gil, V. M. S.; Oliveira, N. C., On the use of the method of continuous variations. *J. Chem. Educ.* **1990**, *67*, 473.

(36) Litowski, J. R.; Hodges, R. S., Designing heterodimeric two-stranded alpha-helical coiled-coils. Effects of hydrophobicity and alpha-helical propensity on protein folding, stability, and specificity. *J. Biol. Chem.* **2002**, *277*, 37272.

(37) Olson, E. J.; Bühlmann, P., Getting More out of a Job Plot: Determination of Reactant to Product Stoichiometry in Cases of Displacement Reactions and n:n Complex Formation. *The Journal of Organic Chemistry* **2011**, *76*, 8406.

(38) Breslauer, K. J. In *Methods Enzymol.*; Michael L. Johnson, G. K. A., Ed.; Academic Press: 1995; Vol. Volume 259, p 221.

(39) Doyle, C. M.; Rumfeldt, J. A.; Broom, H. R.; Broom, A.; Stathopulos, P. B.; Vassall, K. A.; Almey, J. J.; Meiering, E. M., Energetics of oligomeric protein folding and association. *Arch. Biochem. Biophys.* **2013**, *531*, 44.

(40) Marsden, H. R.; Tomatsu, I.; Kros, A., Model systems for membrane fusion. *Chem. Soc. Rev.* **2011**, *40*, 1572.

(41) Struck, D. K.; Hoekstra, D.; Pagano, R. E., Use of resonance energy transfer to monitor membrane fusion. *Biochemistry* **1981**, *20*, 4093.

APPENDIX

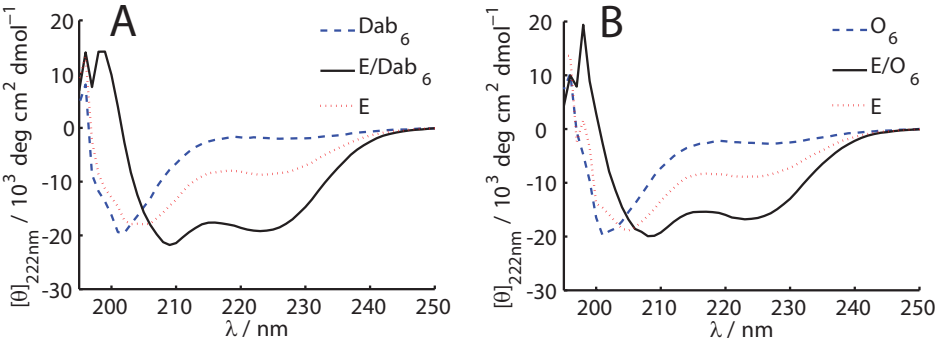

Figure A1. CD spectra of (A) Dab_6, E/Dab_6 [E] : [Dab_6] = 2 : 1, and E (B) O_6, E/O_6 [E] : [O_6] = 1 : 1, and E at total peptide concentrations of 200μM in PBS.

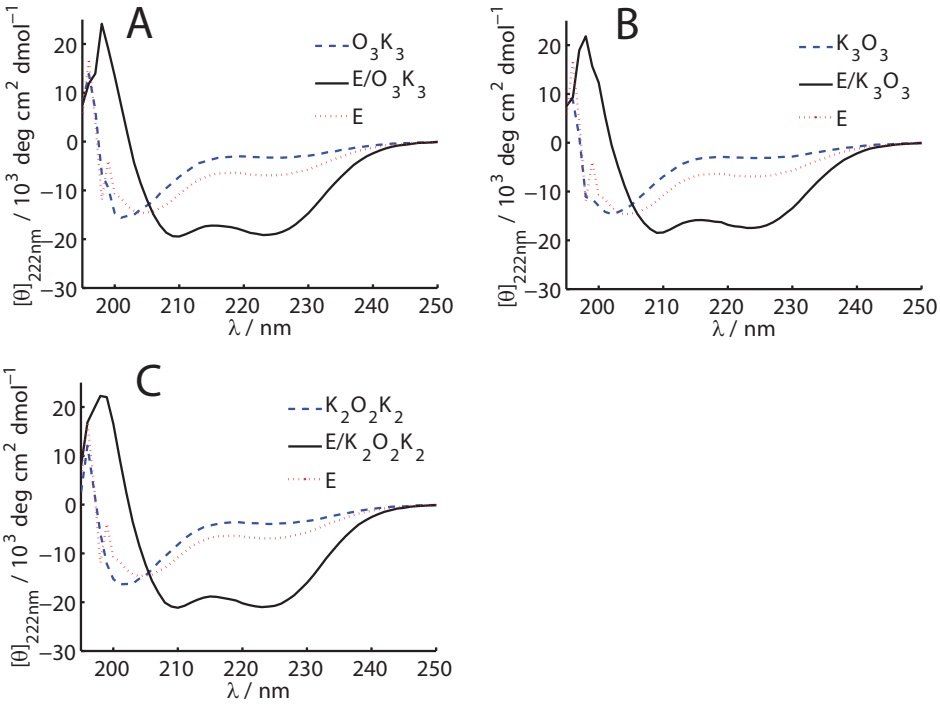

Figure A2. CD spectra of (A) O_3K_3, E/O_3K_3 [E] : [O_3K_3] = 1 : 1, and E (B) K_3O_3, E/ K_3O_3 [E] : [K_3O_3] = 1 : 1, and E (C) $K_2O_2K_2$, E/ $K_2O_2K_2$ [E] : [$K_2O_2K_2$] = 1 : 1, and E at total peptide concentrations of 200 μM in PBS.

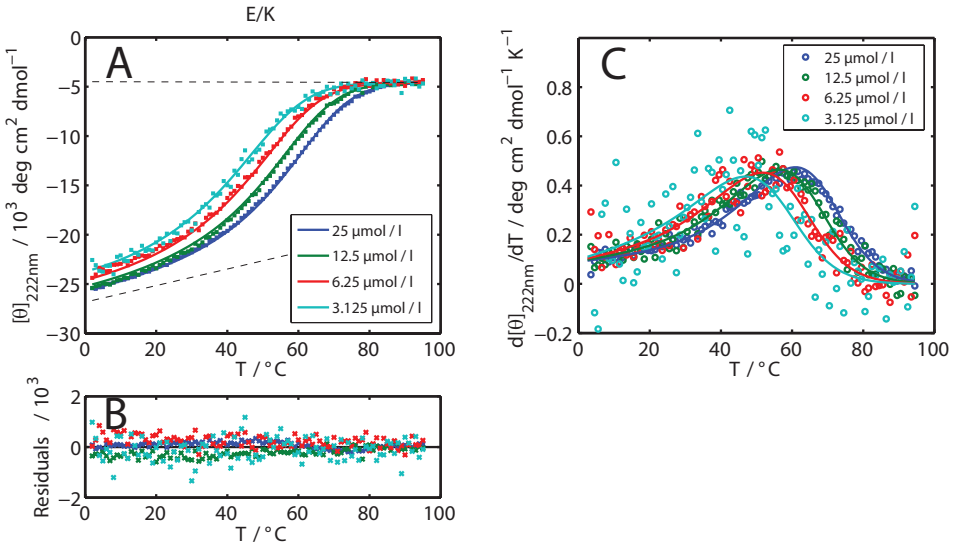

Figure A3. (A) Thermal denaturation data (squares) and best fitting model ($\upsilon_1 = \upsilon_2 = 1$; solid lines) with baselines (broken lines) of E/K. (B) Residuals of best fit. (C) First derivative of data (circles) and best fitting model (solid lines). Concentration of the coiled coil complex given in the key.

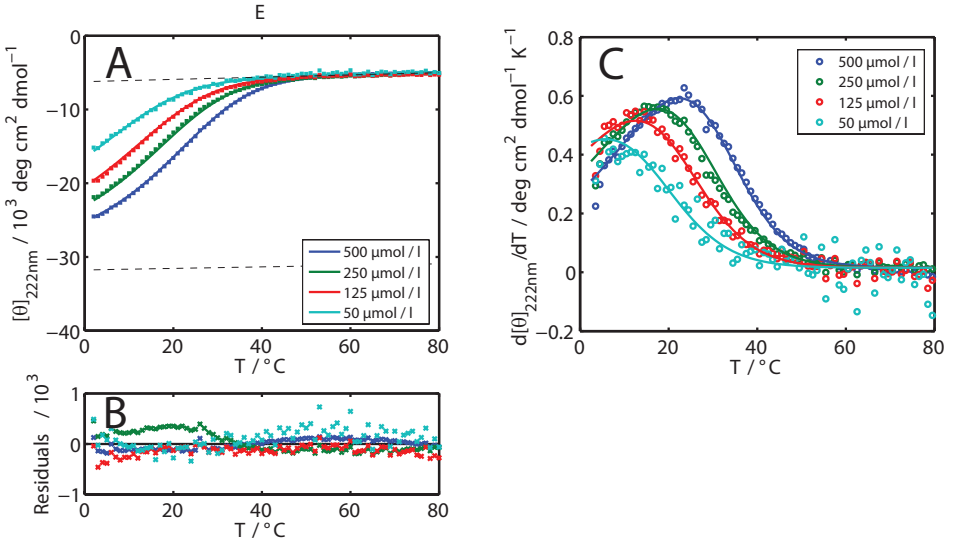

Figure A4. (A) Thermal denaturation data (squares) and best fitting model ($\upsilon_1 = n = 2$; solid lines) with baselines (broken lines) of E. (B) Residuals of best fit. (C) First derivative of data (circles) and best fitting model (solid lines). Concentration of the coiled coil complex given in the key.

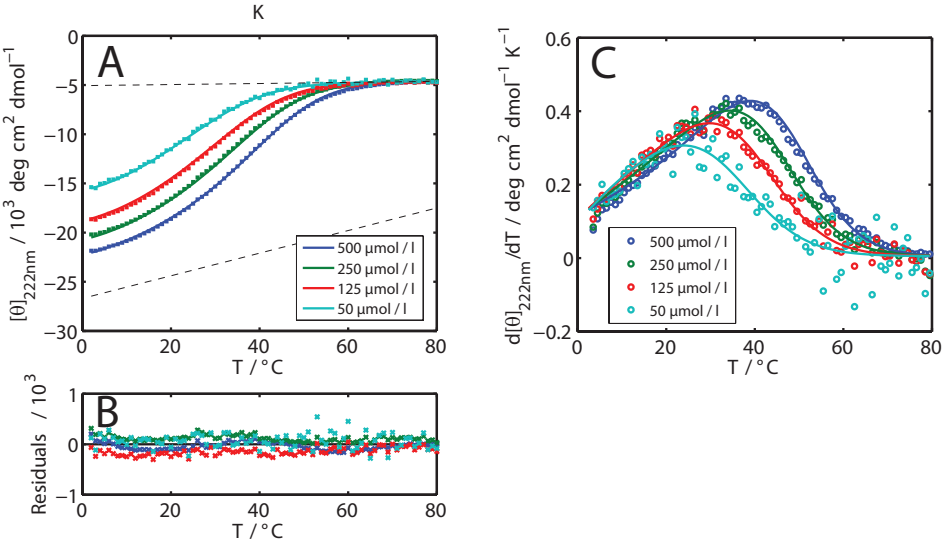

Figure A5. (A) Thermal denaturation data (squares) and best fitting model (υ_1 = n = 2; solid lines) with baselines (broken lines) of K. (B) Residuals of best fit. (C) First derivative of data (circles) and best fitting model (solid lines). Concentration of the coiled coil complex given in the key.

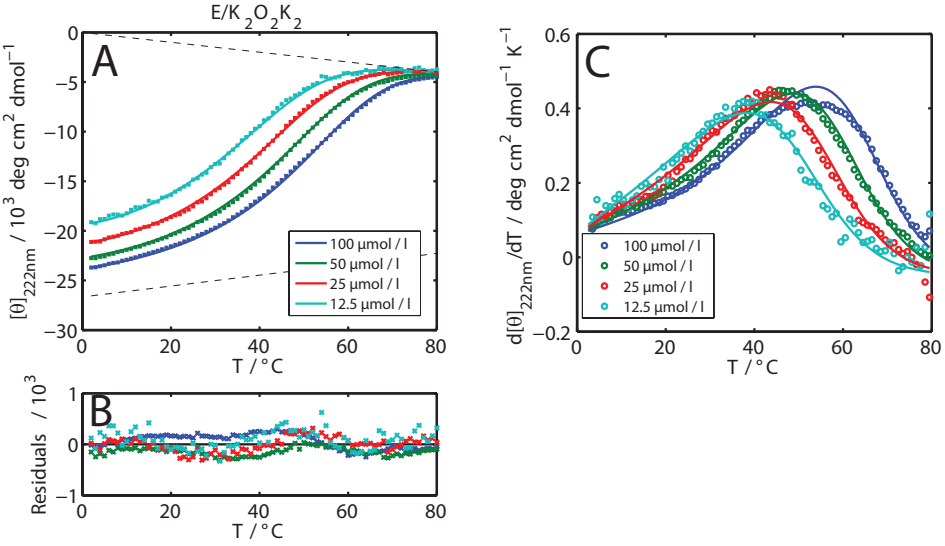

Figure A6. (A) Thermal denaturation data (squares) and best fitting model (υ_1 = n = 2; solid lines) with baselines (broken lines) of $E/K_2O_2K_2$. (B) Residuals of best fit. (C) First derivative of data (circles) and best fitting model (solid lines). Concentration of the coiled coil complex given in the key.

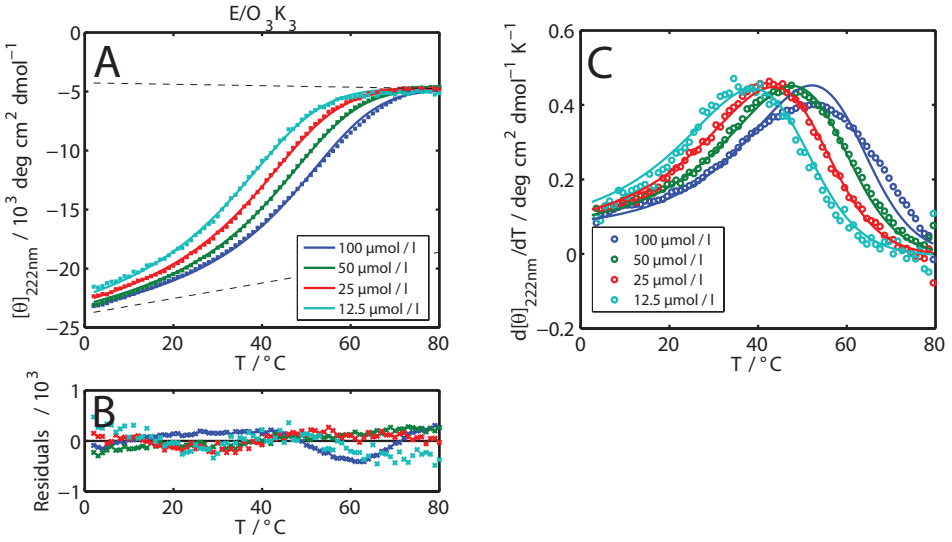

Figure A7. (A) Thermal denaturation data (squares) and best fitting model ($\upsilon_1 = \upsilon_2 = 1$; solid lines) with baselines (broken lines) of E/O_3K_3. (B) Residuals of best fit. (C) First derivative of data (circles) and best fitting model (solid lines). Concentration of the coiled coil complex given in the key.

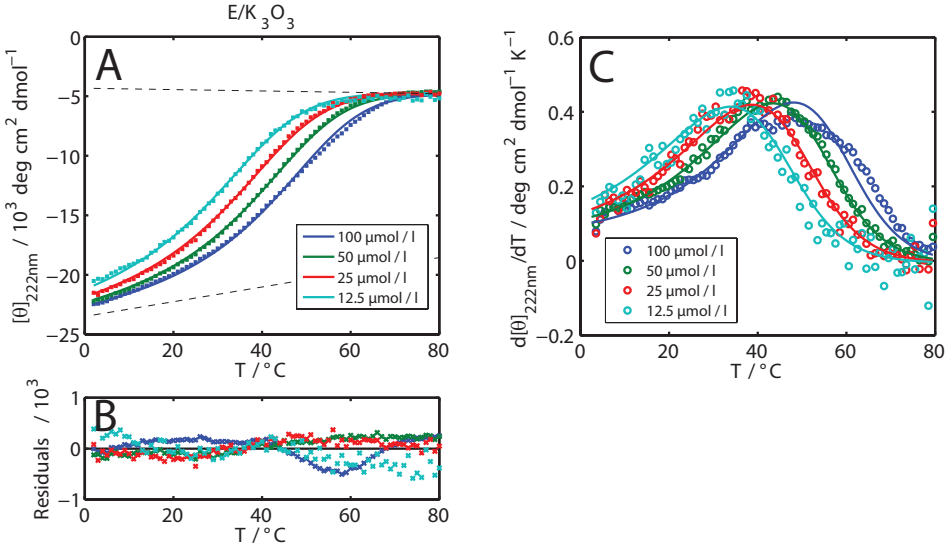

Figure A8. (A) Thermal denaturation data (squares) and best fitting model ($\upsilon_1 = \upsilon_2 = 1$; solid lines) with baselines (broken lines) of E/K_3O_3. (B) Residuals of best fit. (C) First derivative of data (circles) and best fitting model (solid lines). Concentration of the coiled coil complex given in the key.

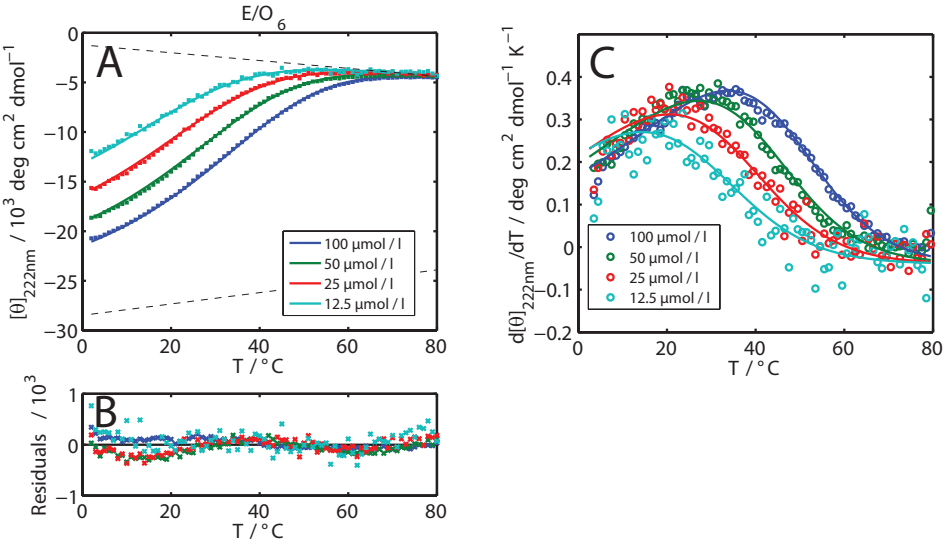

Figure A9. (A) Thermal denaturation data (squares) and best fitting model ($\upsilon_1 = \upsilon_2 = 1$; solid lines) with baselines (broken lines) of E/O_6. (B) Residuals of best fit. (C) First derivative of data (circles) and best fitting model (solid lines). Concentration of the coiled coil complex given in the key.

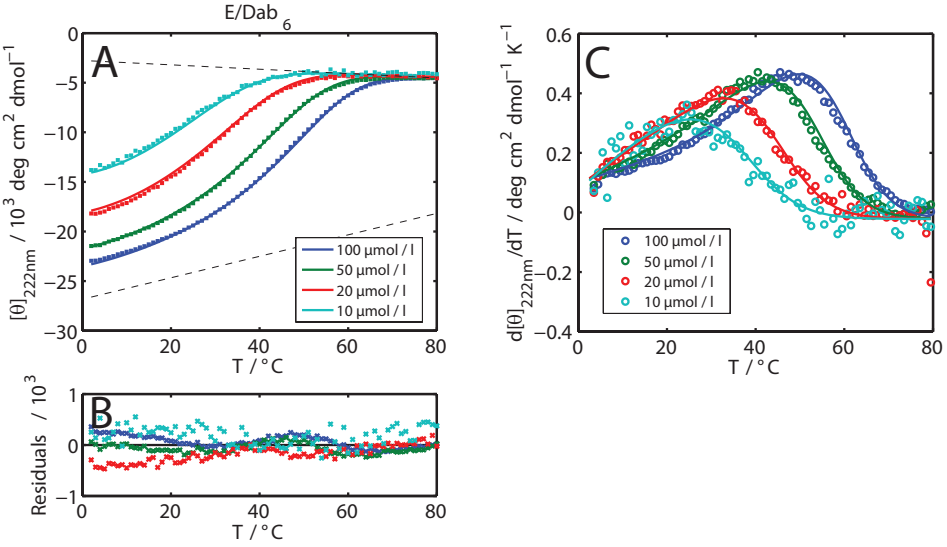

Figure A10. (A) Thermal denaturation data (squares) and best fitting model ($\upsilon_1 = 2, \upsilon_2 = 1$; solid lines) with baselines (broken lines) of E/Dab_6. (B) Residuals of best fit. (C) First derivative of data (circles) and best fitting model (solid lines). Concentration of the coiled coil complex given in the key.

Table A1. Thermodynamic and baseline parameters of best fitting models for the thermal unfolding of coiled coil complexes.

	Model	$\Delta H°$ (kJ mol^{-1})	T° (°C)	ΔC_P (kJ mol^{-1} K^{-1})	θ_{F0} (10^3 deg cm^2 dmol^{-1})	m_F (deg cm^2 dmol^{-1} K^{-1})	θ_{U0} (10^3 deg cm^2 dmol^{-1})	m_U (deg cm^2 dmol^{-1} K^{-1})
E/K	A_1B_1	263.3	120.8	-2.1	-26.838	83.9	-4.491	-0.9
E/KDab	A_2B_1	386.4	116.9	-3.3	-26.617	103.4	-3.582	-12.4
E/O3K3	A_1B_1	221.5	107.1	-1.5	-23.811	64.9	-4.263	-6.1
E/K3O3	A_1B_1	208.5	106.4	-1.4	-23.480	61.7	-4.320	-5.7
E/K2O2K2	A_1B_1	230.6	111.6	-2.0	-26.684	56.1	0	-49.9
E/Korn	A_1B_1	168.4	112.9	-1.2	-28.534	65.9	-1.183	-39.9
K/K	A_2	198.4	77.3	-2.5	-26.764	119.3	-5.036	5.1
E/E	A_2	163.2	61.5	-1.7	-32.022	34.2	-6.202	14.9

Chapter VII

Summary and Perspectives

SUMMARY

For decades a large amount of research has dealt with membrane interactions of peptides and proteins as well as peptide-peptide interactions to understand the mechanisms of essential biological processes such as protein-driven vesicle budding and fission, cell penetration and lysis by peptides, and of course protein-driven membrane fusion. The advance of these fields, in combination with recent progress in cell biology, has inspired chemists to mimic these biological processes with simple model systems. However, it becomes apparent that these model systems are more complex than initially thought and the lessons that were learned from natural systems can also be applied here.

The work reported in this thesis applied and extended classical methods for the study of peptide-peptide and peptide-membrane interactions to study the properties of the fusogenic coiled-coil forming lipopeptides in different membrane model systems or in solution. These lipopeptides comprise coiled-coil forming peptides, called E or K, tethered to a membrane anchor via a polyethylene glycol (PEG_{12}) spacer. The DOPE anchored LPE and LPK, the cholesterol anchored CPE and CPK, the untethered peptides E and K and variants of them with altered amino acid sequences were used. The membrane model systems used were lipid monolayers and vesicles of the composition DOPE : DOPE : cholesterol 2 : 1 : 1. Hypotheses were constructed and tested based on the current biochemical and biophysical models of natural membrane fusion.

Initially, a general introduction of concepts and models important for the thesis was given in *Chapter I*. Peptide-peptide interactions in the form of the thermal unfolding of coiled-coil complexes were the focus of *Chapter II*. A common technique employing unfolding curves measured by circular dichroism (CD) spectroscopy was extended by means of a generalized model that covers the 2-state unfolding of peptide oligomers of any stoichiometry. An easy-to-use program, called '*FitDis!*' was developed to fit experimental, concentration dependent, thermal unfolding curves with these models. It was shown that the comparison of the fit results of different models allows conclusions to be drawn on the oligomeric state of the peptide complex. Simulated datasets showed the feasibility of this approach for dimers and trimers and revealed that for higher oligomeric states more data is necessary for improved reliability. Experimental melting curves from coiled coil peptides of known oligomeric state confirmed the applicability of this approach. This method and the developed program will improve the information gained from oligomeric peptide melting transitions and ease the application of this technique to supramolecular systems such as the membrane bound fusogenic lipopeptides.

These fusogenic lipopeptides were studied in detail in the subsequent chapters. In *Chapter III* the interactions of the free peptides E, K and the lipopeptides LPE and

LPK with lipid monolayers were studied. The untethered peptides E, K, and mixtures of both incorporated spontaneously into these monolayers and showed weak, and medium affinity, respectively, to these lipids. However, the monolayer tethered LPE and LPK showed higher affinities. The peptides E, K, and the lipopeptide LPE could be reversibly squeezed out of the monolayers by application of lateral pressure, i.e. a compression of the monolayers. Upon release of the pressure i.e. an expansion of the monolayers LPE immediately reincorporated into the monolayers, while the untethered peptides E and K reincorporated slowly. LPK mostly resisted this squeeze out, indicating higher membrane affinity. Data gained from surface sensitive infrared reflection absorption spectroscopy confirmed the squeeze out of peptide and furthermore supported the model of the peptides being α-helical and incorporated with their helical axis parallel to the monolayer interface. The observed interactions were also found in monolayers containing both LPE and LPK which indicated that these peptides do not interact as a complex with the membrane. It was anticipated that monomeric amphipathic helices of E and K are the monolayer interacting species, and that the stronger interactions of LPK compared to LPE will play a role in lipid bilayer systems such as vesicles.

This prediction was tested in *Chapter IV*, by means of the peptides E_{GW}, K_{GW}, and the lipopeptides LPE_{GW}, LPK_{GW} which were designed, based on the original sequences of E and K. The variation in the peptide sequence was shown to only slightly influence coiled-coil formation and the obtained tryptophan fluorescence emission could be used to probe the polarity of the microenvironment. The microenvironment of K_{GW} and LPK_{GW} became more hydrophobic upon vesicle addition accompanied by an increased helicity as measured by CD spectroscopy, proving the interaction of these peptides with the vesicles. Contrary to this, the complementary E_{GW} and LPE_{GW} showed no change of its microenvironment polarity, although LPE_{GW} showed increased helicity on vesicles. The coiled coil complex formation in solution was found to reduce but not to completely inhibit the K_{GW} – membrane interaction. Surprisingly, the membrane tethered LPK_{GW} could not be readily pulled out of the membrane by coiled coil complex formation, thus it showed an increased membrane affinity compared to K_{GW}. Furthermore, fluorescence quenching experiments with water soluble and membrane bound quenchers supported these conclusions and allowed for the estimation of the penetration depth of K_{GW}. It was found that the peptide incorporates rather shallowly into the membrane, which is in common with an insertion of an α-helix centered close to the glycerol and phosphate groups of the lipids.

A close-up image of the secondary structures of the membrane tethered CPE, CPK and untethered, membrane bound K could be obtained in *Chapter V* using temperature dependent infrared (IR) and circular dichroism spectroscopy. Vesicle

tethered CPE showed CD unfolding curves and temperature dependency of its IR amide I' bands that indicate unfolding of homomeric coiled coil complexes. In contrast, vesicle bound K and membrane tethered CPK showed no cooperative unfolding and stable IR amide I' bands. This showed that the membrane bound helix was rather stable and might fray on the termini. Furthermore the amide I' band shape of the membrane bound K, homo coiled K, and the coiled coil complex EK was investigated by means of the isotopically labeled variant ^{13}CK. It was found that in all these spectra, the amide I' band two band pattern which was observed is caused by amphipathic helices, and thus the membrane bound structure shows high similarities to the coiled-coil bound structure of K.

Taken together all the data and conclusions from *Chapters III – V* drew the image of an asynchronous behavior of the membrane tethered lipopeptides. Tethered K incorporated as a helix, with a parallel orientation to the membranes, while tethered E formed significant amounts of α-helical homo coils on the membrane surface. Both states were also expected in the post fusion membranes. Hence an asymmetric mechanism was proposed in which the K interaction is the membrane curvature-inducing or membrane distorting process that promotes fusion.

To test this hypothesis, K variants with shortened lysine side chains were designed in *Chapter VI*, with the aim being to suppress the membrane interaction. It was anticipated that the long lysine side chains snorkel, i.e. bend towards the polar interface to have a more favourable conformation in the membrane. The sequence variations strongly reduced the membrane affinity of the untethered K variants, hence the snorkeling contributed strongly to the membrane binding. However, the variations also strongly influenced the coiled-coil binding propensity, which strongly reduced the number of reasonable sequences for lipopeptide synthesis. Finally, two cholesterol anchored lysine shortened lipopeptides CPO_3K_3 and $CPK_2O_2K_2$ were synthesized. However, vesicles decorated with these molecules still showed the hallmarks of full fusion with CPE decorated liposomes, and an α-helical interaction of CPO_3K_3 and $CPK_2O_2K_2$ with the membrane was found by CD. Thus, the outcome of the fusion experiments was not sufficient to disprove the hypothesis, that K-membrane interaction is necessary to promote the vesicle fusion.

Taken together, the work reported here led to a new perspective on lipopeptide mediated vesicle fusion and one important general insight: an alleged easy model system such as the fusogenic lipopeptides can reveal complex interdependent interactions and equilibria in a close-up view. Also, finding the right magnifying glass can be a challenging and time-consuming task.

PERSPECTIVES

Within this thesis several important aspects that need to be focused on were revealed and these indicate the direction further research should pursue. It might turn out to be a challenging task to find definite proof for the hypothesis that peptide K induces the necessary membrane disruption to enable lipid reorganization during fusion. However, experimentally testable predictions based on this hypothesis can be made, which might deliver indirect proof or disproof. For instance, different systems based on coiled-coil forming lipopeptides are currently designed to be tested in fusion experiments. If a system is found that efficiently docks liposomes but does not fuse them, full fusion should be triggered by the addition of untethered peptide K. The wanted system does not necessarily need to be based on coiled-coil forming peptides; other molecular recognition systems might suffice for that purpose. Another approach to deliver indirect proof is to attempt to suppress the peptide membrane interaction by variation of the lipid composition. Incorporation of charged lipids, variation of the acyl chains or variation of cholesterol concentration will influence the membrane binding of K and maybe even E. The challenge of this approach will be the preservation of the intrinsic ability of the lipids to fuse, which is why this approach might not deliver a definite proof.

From a mechanistic point of view the effect of the K incorporation on the membrane structure is very important. The central question is whether the incorporation causes curvature in the membrane and if this is positive or negative curvature. A detailed NMR study is being undertaken at the moment and calorimetric studies and X-ray or neutron scattering experiments are further possible ways to approach this. For instance DSC studies can reveal the influence of peptide K on the phase transition of PE lipids from the fluid L_{α} to the inverse hexagonal H_{II} phase, which contains negative curvature. A reduction of this transition temperature would indicate negative curvature creation, and increased promotion of positive curvature. These insights might feed back into the peptide design with the aim of specifically influencing the curvature creation by the helical membrane insertion. In such studies also molecular dynamics simulations will be helpful to test the rationality of the developed models.

Plenty of possibilities appear concerning the new design of fusogenic lipopeptides. One might use databases or rational design to find sequences that are able to form similar amphipathic helices as K, i.e. that can form coiled-coils and bind to membranes; one could try to find heterotrimeric sequences, which allow for triggering of fusion by addition of a free binding partner; or one could employ curvature-sensing amphipathic helices to specifically recognize and fuse small vesicles.

From the possible routes mentioned here it becomes apparent that much potential is seen in a combined approach of biophysical studies, coupled with targeted peptide design, because this will open exciting opportunities for the understanding and thus the rational improvement of artificial membrane fusion systems.

SAMENVATTING

Al tientallen jaren wordt er onderzoek verricht aan peptide-peptide interacties en de interactie van membranen met peptiden en eiwitten. Dit wordt gedaan om het mechanisme te doorgronden van essentiële biologische processen zoals bijvoorbeeld de uitstulping en splitsing van vesikels, membraanfusie en de werking van antimicrobiele peptiden. De recente vooruitgang in de celbiologie heeft chemici geïnspireerd om deze biologische processen na te bootsen met simpele modelsystemen. Het is duidelijk geworden dat deze modelsystemen complexer zijn dan aanvankelijk werd aangenomen en dat de lessen die we hebben geleerd van biologische systemen ook hier toepasbaar zijn.

Dit proefschrift beschrijft de toepassing en uitbreiding van de klassieke methodes in het onderzoek aan peptide-peptide interacties en peptide-membraan-interacties met als doel de eigenschappen van fusogene coiled-coil-vormende lipopeptiden in oplossing en in diverse modelsystemen van membranen te bestuderen. Deze lipopeptiden bevatten coiled-coil peptiden, de zogenaamde peptiden E en K, die via polyethyleenglycol (PEG_{12}) verbonden zijn met een anker in het membraan. De DOPE-verankerde LPE en LPK werden gebruikt, alsmede de cholesterol verankerde CPE en CPK, de peptiden E en K zonder fosfolipide anker, alsmede variaties hierop door middel van gewijzigde aminozuursequenties. De gebruikte modelsystemen waren monolagen en vesikels met de samenstelling DOPC : DOPE : cholesterol (2 : 1 : 1). Hypotheses werden opgesteld en getest op basis van hedendaagse biochemische en biofysische modellen van natuurlijke membraanfusie.

In *Hoofdstuk I* wordt een algemene introductie van de concepten en modellen gegeven die van belang zijn voor de opvolgende hoofdstukken. Peptide-peptide interacties in de vorm van temperatuur-geïnduceerde ontvouwing van coiled-coil-complexen zijn het onderwerp van *Hoofdstuk II*. Een algemene techniek, die gebruik maakt van ontvouwingscurves die door circulair dichroïsmespectroscopie gemeten worden, is verbetered om het aantal ketens in oligomere peptidecomplexen te bepalen. Ook wordt de ontwikkeling van het gebruikersvriendelijke programma '*FitDis!*' beschreven waarmee deze methode kan worden toegepast. De methode en het programma zullen de informatie, die wordt verkregen uit de smeltovergangen van oligomere peptide verbeteren en zullen het gemakkelijker maken om deze techniek ook toe te passen op supramoleculaire systemen zoals fusogene lipopeptides die aan membranen gebonden zijn.

De volgende hoofdstukken beschrijven een gedetailleerde studie van de fusogene lipopeptiden. In *Hoofdstuk III* wordt de interactie van lipide monolagen

met de vrije peptiden E en K bestudeerd en met de lipopeptiden LPE en LPK. Er wordt voorgesteld dat waneer peptides E en K gevouwen zijn als amfipatische helixen zij interacties aangaan met de monolaag. Vergeleken met LPE wordt een sterkere interactie gevonden tussen de monolaag en LPK. Er wordt verwacht dat die interacties een rol spelen in systemen van dubbellagen lipide membranen. Deze voorspelling wordt getest in *Hoofdstuk IV* waarbij gebruik wordt gemaakt van de peptiden E_{GW}, K_{GW} en de lipopeptiden LPE_{GW}, LPK_{GW} die ontworpen zijn op basis van de originele aminozuur sequenties van E en K. Het blijkt, dat peptide K_{GW} relatief ondiep in het membraan bindt, waarbij de α-helix die dichtbij de glycerol en de fosfaatgroepen van de lipiden gecentreerd is. Een close-up-weergave van de secundaire structuren van CPE, CPK en de direct aan het membraan gebonden peptide K wordt verkregen in *Hoofdstuk V* met behulp van temperatuurafhankelijke infrarood- en circulair dichroïsmespectroscopie.

In *Hoofdstukken III* t/m *V* wordt duidelijk dat de membraangebonden lipopeptiden asynchroon gedrag vertonen. Peptide K is als een helix geïncorporeerd met een paralelle oriëntatie aan de membranen, terwijl een significant deel van peptide E homocoils vormt op het membraanoppervlak. Beide toestanden zijn zeer waarschijnlijk ook na de fusie aanwezig in de membranen. Een asymmetrisch mechanisme wordt voorgesteld waarin de peptide K membraanfusie bevordert door de oppervlaktekromming van het membraan te verstoren.

Om deze hypothese in *Hoofdstuk VI* te testen worden variaties op peptide K met kortere lysine-zijketens ontworpen met als doel de interactie met het membraan te onderdrukken. Hoewel een sluitend bewijs voor de hypothese nog ontbreekt, wordt wel aangetoond dat de lysine-zijgroepen significant bijdragen aan de membraanbinding van peptide K door middel van een zogenaamd snorkelmechanisme.

Het complete werk dat in dit proefschrift beschreven is heeft geleid tot een nieuw perspectief op de door lipopeptiden gefaciliteerde membraanfusie. Het heeft tot een belangrijk algemeen inzicht geleid: een gemakkelijk modelsysteem zoals dat van de fusogene lipopeptiden kan in close-up-weergave de complexe en onderling afhankelijke interacties en evenwichten aan het licht brengen. Bovendien is ondervonden dat het opsporen van het juiste vergrootglas een uitdagende en tijdrovende taak is.

ZUSAMMENFASSUNG

Seit Jahrzenten werden Peptid-Membran- und Peptid-Peptid-Wechselwirkungen umfangreich erforscht um die Mechanismen von essenziellen biologischen Prozessen, wie proteingesteuerte Vesikelknospung und –abspaltung, Zellpenetration und –lyse durch Peptide und natürlich proteingesteuerte Lipidmembranfusion, zu verstehen. Zusammen mit den jüngsten Erkenntnissen aus der Zellbiologie haben die Fortschritte in diesen Gebieten Chemiker inspiriert solche biologische Prozesse mit einfachen Modelsystemen zu imitieren. Es stellt sich jedoch heraus, dass diese Modelsysteme komplexer sind als bisher angenommen und dass man die Lektionen die von natürlichen Systemen gelernt wurden, auch hier anwenden kann.

Die in dieser Dissertation beschriebenen Studien benutzten und erweiterten klassische Methoden für die Untersuchung von Peptid-Peptid- und Peptid-Membran-Wechselwirkungen um die Eigenschaften fusiogener, Coiled-coil bildender Lipopeptide in verschiedenen Modellmembranen oder in Lösung zu studieren. Diese Lipopeptide bestehen aus Coiled-coil bildenden Peptiden, namens E und K, die mittels einer Polethylenglykolkette (PEG_{12}) an einen Membrananker gebunden sind. Sowohl die DOPE-verankerten Moleküle LPE und LPK, die cholesterolverankerten CPE und CPK, als auch die unverankerten, freien Peptide E, K und Varianten von diesen mit veränderten Aminosäuresequenzen wurden untersucht. Als Membranmodellsysteme wurden Lipidmonoschichten und Vesikel der Zusammensetzung DOPC : DOPE : Cholesterol 2 : 1 : 1 benutzt. Auf der Basis von aktuellen biochemischen und biophysikalischen Modellen der natürlichen Membranfusion wurden Hypothesen erstellt und getestet.

Zunächst wurde in *Kapitel I* eine generelle Einleitung über Konzepte und Modelle gegeben, die für die Dissertation von Belang sind. Peptid-Peptid-Wechselwirkungen in der Gestalt von temperaturabhängigen Entfaltungen von Coiled-coil Komplexen wurden in *Kapitel II* fokussiert. Eine weit verbreitete Methode, die auf Circulardichroismus (CD)-spektroskopischen Schmelzkurven basiert, wurde erweitert um die Anzahl der Ketten in oligomeren Peptidkomplexen zu bestimmen. Ein benutzerfreundliches Programm namens ‚FitDis!' wurde entwickelt das die Anwendung dieser Methode vereinfacht. Diese Methode sowie das entwickelte Programm werden die Informationen, die aus Schmelzkurven oligomerer Peptide erhältlich sind, erweitern und die Anwendung dieser Technik auf supramolekulare Systeme, wie zum Beispiel die membrangebundenen Lipopeptide, vereinfachen.

Diese fusiogenen Lipopeptide wurden in den folgenden Kapiteln detailliert untersucht. In *Kapitel III* wurden die Wechselwirkungen der freien Peptide E, K

und der Lipopeptide LPE und LPK mit Lipidmonoschichten untersucht. Es wurde vorgeschlagen, dass E und K als amphipathische Helices mit den Monoschichten wechselwirken. Eine stärkere Wechselwirkung mit der Monoschicht wurde für LPK im Vergleich zu LPE festgestellt und es wurde angenommen, dass diese Wechselwirkungen auch in Bischichten wie z.B. Vesikeln von Bedeutung sein werden.

Diese Voraussage wurde in *Kapitel IV*, mithilfe der Peptide E_{GW}, K_{GW} und der Lipopeptide LPE_{GW} und LPK_{GW} die auf Grundlage der Originalsequenzen von E und K entworfen wurden, getestet. Es wurde entdeckt, dass das Peptid K_{GW} relativ flach in der Lipidmembran liegt, was mit dem Modell des Einbaus einer α-Helix in der Nähe der Lipidglycerol und phosphatgruppen einhergeht. Eine Nahaufnahme der Sekundärstrukturen von membranverankertem CPE, CPK und unverankertem, membrangebundenen K konnte in *Kapitel V*, mithilfe von temperaturabhängiger Infrarot (IR)- und CD-Spektroskopie, erhalten werden.

Zusammengefasst implizierten die Daten und Schlussfolgerungen der *Kapitel III – V* das Bild eines asynchronen Verhaltens der membranverankerten Lipopeptide. Das verankerte K baut sich als Helix mit paralleler Orientierung in die Membran ein, während ein beträchtlicher Teil des verankerten E auf der Membranoberfläche α-helicale homomere Coiled-coils bildet. Beide Zustände werden auch nach der Fusion in der Membran erwartet. Dementsprechend wurde ein asymmetrischer Mechanismus vorgeschlagen der besagt, dass diese Wechselwirkung von K eine Krümmung oder Deformation der Membran verursacht und somit den Fusionsprozess begünstigt. Mit dem Ziel diese Hypothese zu testen, wurden in *Kapitel VI* Varianten von K entworfen, die gekürzte Lysin-Seitenketten aufweisen. Obwohl ein eindeutiger Beweis für die Hypothese nicht erbracht werden konnte, konnte gezeigt werden, dass die basischen Lysine-Seitenketten durch einen Schnorchelmechanismus stark zur Bindung des Peptides an die Membran beitragen.

Zusammengenommen haben die Studien in dieser Dissertation zu einer neuen Sichtweise auf die lipopeptidgesteuerte Vesikelfusion geführt und zu einer wichtigen allgemeineren Einsicht: Ein vermeintlich einfaches Modellsystem, wie die fusiogenen Lipopeptide können von Nahem betrachtet komplexe und gegenseitig abhängige Wechselwirkungen und Gleichgewichte offenbaren und die richtige Lupe zu finden, kann sich als eine herausfordernde und zeitaufwendige Aufgabe herausstellen.

LIST OF SYMBOLS

A	area per molecule
Ai, A1, A2, …	monomeric peptide chain
AI/CO	ratio of absorbances of amide I' to carbonyl stretch
C_S	monolayer compressibility
C_f	concentration of membrane unbound peptide
c_M	monomer concentration
d	film thickness
F	fluorescence intensity
h_m	most probable penetration depth of the fluorophore
fwhh	full width at half height
k	absorption coefficient
K_F	equilibrium constant of folding
K_U	equilibrium constant of unfolding
K_P	partition coefficient
K_{SV}	Stern Vollmer constant
L_{xy}	distance between depth of quencher x and y
l	path length
M	molar mass
m_F, m_U	temperature slope of ellipticity of fully folded, fully unfolded state
N	number of amino acids per chain
n	in Chapter III: refractive index, else: oligomeric number
P_b	fraction of membrane bound peptide
P_T	concentration of complex
QE	quenching efficiency
R	in Chapter III: reflectance, else: universal gas constant
rh	relative helicity
r_h	hydrodynamic radius
RA	reflectance absorbance
RMSE	root of mean square error
S	in Chapter III: order parameter, in Chapter IV: area of Gaussian
T	absolute temperature
T°	reference temperature where $\Delta G=0$
T_m	apparent melting temperature
X_b^*	molar ratio of bound peptide per accessible lipid
Z_{cf}	distance of fluorophore to centre of lipid bilayer

α	in Chapter III: angle between molecular axis and transition dipole moment, else: folded fraction
β	unfolded fraction
Γ	polarizer quality
ΔC_P	heat capacity change of unfolding
ΔG	free enthalpy of unfolding
$\Delta H°$	enthalpy of unfolding at reference temperature T°
$\Delta\pi$	change in surface pressure
$\Delta\pi^0$	change in surface pressure at π_i=0
e	molar absorbance
θ	in Chapter III: molecular tilt angle, else: ellipticity
$[\theta]$	mean residual ellipticity
θ_F, θ_U	ellipticity of fully folded (F) and fully unfolded (U) state
θ_{F0}, θ_{U0}	ellipticity of fully folded (F) and fully unfolded (U) state at 0 °C
λ	wavelength
$\tilde{\nu}$	wavenumber
π	surface pressure
π_0	initial surface pressure
π_{mip}	maximum insertion surface pressure
π_{SO}	surface pressure of squeeze out
σ	width of Gaussian
υ_i, υ_1, υ_2, …	stoichiometric coefficient
Δ…	change in …
[...]	concentration of …
<...>	mean value of …
$..._{25}$	… value at 25 °C
$\cdots_{fit}$	value obtained from curve fitting
$\cdots_{max}$	maximal value
$\cdots_{min}$	minimal value
$..._{sim}$	value used for simulation
$...^T$	transpose of matrix

LIST OF ABBREVIATIONS

A	alanine
Ac	acetyl
AH	amphipathic α-helix
ALPS	ArfGAP1 lipid packing sensor
AoI	angle of incidence
ATR	attenuated total reflection
AUC	analytical ultracentrifugation
bZip	basic leucine zipper domain
CD	circular dichroism
DA	distribution analysis
Dab	2, 4 - diaminobutyric acid
di-BrPC	1-palmitoyl-2-(dibromo)stearoyl- sn-glycero-3-phosphocholine
DLS	dynamic light scattering
DOPC	1, 2-dioleoyl-sn-glycero-3-phosphocholine
DOPE	1, 2-dioleoyl-sn-glycero-3-phosphoethanolamine
d-PBS	deuterated phosphate buffered saline
DPPC	1, 2-dipalmytoyl-sn-glycero-3-phosphocholine
E	glutamic acid
Fmoc	fluorenylmethoxycarbonyl
FRET	Förster resonance energy transfer
FTIR	Fourier transform infrared
G	glycine
GCN4	eukaryotic transcriptional activator protein
GUV	giant unilamellar vesicle
h	hydrophobic amino acid residue
HPLC	high pressure liquid chromatography
I	isoleucine
IRRAS	infrared reflection absorption spectroscopy
K	lysine
L	leucine
LC	liquid chromatography
LR-DOPE	1,2-dioleoyl-sn-glycero-3-phosphoethanolamine-N-(lissamine rhodamine B sulfonyl) (ammonium salt)
LUV	large unilamellar vesicle
MALDI	matrix assisted laser desorption ionization
MCT	mercury cadmium tellurid

MeOH	methanol
MS	mass spectrometry
NBD-DOPE	1,2-dioleoyl-sn-glycero-3-phosphoethanolamine-N-(7-nitro-2-1,3-benzoxadiazol-4-yl
NPY	neuropeptide y
O	ornithine
p	polar amino acid residue
PC	principal component
PCA	principal component analysis
PEG	polyethylene glycol
PM	parallax method
QP	depth dependent quenching profile
RP	reverse phase
SEC MALS	size exclusion chromatography with multi angle laser scattering
SM	Sec1/Munc18-like
S/N	ratio signal to noise
SNAP	synaptosomal-associated protein
SNARE	soluble NSF attachment protein receptor
SUV	small unilamellar vesicle
SVD	singular value decomposition
TDM	transition dipole moment
TFA	trifluoroacetic acid
TOC	total organic carbon
UV	ultra violet
W	tryptophan

CURRICULUM VITAE

Martin Rabe was born on 9th April, 1984 in Jena, Germany. After finishing high school, he started to study chemistry at the Martin-Luther-University Halle-Wittenberg, Germany in 2004. He started his search for a scientific field with different research internships in bioorganic synthesis and physical chemistry. He then chose a specialization in physical chemistry and conducted his diploma project as well as subsequent research projects in the Biophysical Chemistry group, under the guidance of Prof. Alfred Blume. There, he studied the interactions of protein therapeutic solutions, with nonionic polymeric detergents in the bulk and at the air-water interface. His curiosity for the physical chemistry of biomolecules originates from this experience. In 2009 he graduated with a diploma (MSc) in chemistry.

In 2010 Martin joined the Supramolecular and Biomaterials Chemistry (SBC) group of Dr. Alexander Kros at Leiden University in the Netherlands as a PhD student. There, he studied the biophysical properties of peptides and lipopeptides that are used in artificial membrane fusion systems, as it is reported in this thesis. Currently he works in the SBC group with Dr. Gregory Schneider on the characterization of lipid functionalized graphene monolayers.

LIST OF PUBLICATIONS

Tomatsu, I.; Marsden, H. R.; Rabe, M.; Versluis, F.; Zheng, T.; Zope, H.; Kros, A., Influence of pegylation on peptide-mediated liposome fusion. *J. Mater. Chem.* **2011**, *21*, 18927.

Bahreman, A.; Rabe, M.; Kros, A.; Bruylants, G.; Bonnet, S., Binding of a Ruthenium Complex to a Thioether Ligand Embedded in a Negatively Charged Lipid Bilayer: A Two-Step Mechanism. *Chemistry – A European Journal* **2014**, *20*, 7429.

Rabe, M.; Schwieger, C.; Zope, H. R.; Versluis, F.; Kros, A., Membrane Interactions of Fusogenic Coiled-Coil Peptides: Implications for Lipopeptide Mediated Vesicle Fusion. *Langmuir* **2014**, *30*, 7724.

Rabe, M.; Boyle, A.; Zope, H. R; Versluis, F.; Kros, A., Determination of peptide oligomeric states from thermal unfolding by CDspectroscopy. *Pep. Sci.***2014,** accepted.

Rabe, M.; Aisenbrey, C.; de Wert, V.; Bruggeman, D.; Raap J.; Bechinger, B.; Kros, A.; Insertion of an amphipathic coiled-coil peptide in lipid bilayers: Molecular details revealed by tryptophan fluorescence spectroscopy and ^{31}P-NMR. Manuscript in preparation.

Rabe, M.; Zope, H. R.; Kros, A., The interplay between membrane interaction and homo-coiling of membrane tethered coiled-coil peptides. Manuscript in preparation.

Rabe, M.; Rudge, R.; Zope, H. R.; Kros, A., Can one methylene group make a difference? Influence of lysine snorkeling on the activity of fusogenic coiled-coil peptides. Manuscript in preparation.